

THE ANALYSIS AND OPTIMIZATION OF ELECTROSTATIC ELECTRON OPTICAL  
LENSES WITH ROTATIONAL SYMMETRY, THROUGH THE USE OF ORTHOGONAL  
FUNCTIONS.

by

JOHANNES PETRUS VAN DER MERWE

Submitted in partial fulfilment of the requirements for the degree of  
Doctor of Philosophy, in the department of Physics, University of Natal.

Durban.

1978

## P R E F A C E

An interest in the emission electron microscope some years ago provided the author with a stimulus to study electrostatic electron optics, and the desire to carry out high precision electron optical calculations on the relatively small computers that he had access to during the initial stages of the study, led to the investigation of the possibility of using orthogonal functions in electron optical analysis and design.

Prof. N.D. Clarence, then head of the department of Physics at Natal University (Durban) was approached by me with a proposal of a Ph. D. project in electron optics, and – although no research was undertaken in his department in this branch of physics – he was kind enough to accept me as a student. I shall always remain grateful to him for this trust in me.

Dr. P.W. Hawkes of Cavendish Laboratory, Cambridge, was requested to evaluate the proposal, and thanks to his encouraging comments this study was undertaken. Dr. Hawkes has also been kind enough to read and comment on some of the publications listed below, and I want to assure him of my appreciation for his assistance.

Prof. A.D.M. Walker and Dr. D. Spalding were appointed as my supervisors, and I want to express my appreciation for the courteous and helpful way in which they responded to my queries over the years. Prof. Walker is also thanked for reading and commenting on this manuscript as well as some of the publications listed below.

In view of the rapid development of electron optics I decided to publish

results as they became available. In this way the following chapters were published, or were submitted for publication in virtually their present forms, except for minor modifications and editing :

Chapter (2) was published as : "Electron Optical Properties of some Fourier-Bessel Electrostatic Fields with Rotational Symmetry. I, Basis Fields." University of Zululand Publications, Series III, no. 23 (1978).

Chapter (3) was published as : "Electron Optical Properties of some Fourier-Bessel Electrostatic Fields with Rotational Symmetry. II, An Analytical Study of Weak Fields". University of Zululand Publications, Series III, no. 24 (1978).

Chapter (4) was published as : "Electron Optical Properties of some Fourier-Bessel Electrostatic Fields with Rotational Symmetry. III, Computed Properties of Synthesized Fields". University of Zululand Publications, Series III, no. 25 (1978).

Chapter (5) was published as "A Fourier-Bessel Solution of an Einzel Type Electrostatic Field with Rotational Symmetry". J. Appl. Phys. 49, 4335 (1978).

Chapter (6) will be published as : "Fourier-Bessel Series Solution for Potential and Intensity Field of Open Electron Optical Systems with Rotational Symmetry, in Terms of  $J_0$  Bessel Functions". J. Appl. Phys. (To be published, Jan., 1979).

Chapter (7) has been submitted for publication as : "Charge distributions on foils of electrostatic one-foil lenses with rotational symmetry, as related to some electron optical properties".

Chapter (8) has been submitted for publication as : "The Inverse Interior Dirichlet Problem".

Appendix (1) was published as : "Series Expansions and Tables of Integrals of Products of some Bessel Functions". University of Zululand Publications, Series III, no. 20 (1977).

Appendix (2) was accepted for publication as : "Fourier-Bessel Series Solution of an Exterior Dirichlet Boundary Value Problem with Rotational Symmetry" (J. Appl. Phys., to be published).

Chs. (1) and (9) were added to place the various investigations into perspective, and Appendix (4) contains some preliminary results on the use of the solution given in Ch. (8). The contents of this thesis is the original work of the author, with the exception of Appendix (3), in which some properties of Bessel functions are given for quick reference.

I wish to extend my thanks to the heads and staff of the computer centres and libraries of the Universities of Natal (Durban) and of Zululand for their valued cooperation, and express my appreciation for the professional way in which Mrs. H.L. Bisschoff handled the typing and Mrs. R. van Schalkwyk prepared the figures for this manuscript.

I would like to acknowledge the financial support given by the Publication and Research Committee of the University of Zululand and the encouragement of Prof. F.K. Peters, the previous head of the Department of Physics of the University of Zululand, and Prof. B. Spoelstra, his successor. As locum tenens, Prof. J.A.V. Fairbrother relieved me of my lecturing responsibilities during the past semester and in this way made possible the preparation of this manuscript. Mr. C.H. Rohwer is thanked for always being willing to discuss problems of a mathematical nature. I gained much from his broad knowledge and experience of numerical analysis.

I also remember with gratitude the influence and examples set by my late father, mother and close family circle, the encouragement of those that educated me, and in particular the personal sacrifices made by my wife, son and daughter during the course of this study.

J.P. van der Merwe

Dept. of Physics

University of Zululand

Empangeni, Rep. of South Africa.

December, 1978.

## C O N T E N T S

Preface	1
Contents	5
Ch. (1) Outline of electron optical problems to be investigated, and choice of mathematical model.	11
1. Introduction	11
2. Description of electron optical systems to be investigated	13
3. Description of focal properties to be considered	14
4. Outline of methods currently used to optimize electron optical systems	17
5. Electron optical optimization: Moses and Szilagyí	43
6. Optimization by a gradient method	44
7. Summary of proposed study and outline of chapters	49
Ch. (2) Some electron optical properties of Fourier-Bessel basis fields	52
1. Introduction	52
2. Electron optical properties of the Fourier-Bessel fields	52
3. Precision of the results	61
4. Physical approximation	61
5. Some conclusions	63
Ch. (3) An analytical study of weak basis fields and of some syntheses of two components	66

1.	Introduction	66
2.	Trajectory approximation	66
3.	The radial velocity $v_r$	67
4.	The angular deflection $\theta_i$	69
5.	The radial displacement $\delta r$	69
6.	The focal distance $z_d$	70
7.	The principal plane	71
8.	The focal length $z_{fr}$	71
9.	Longitudinal spherical aberration	71
10.	Theoretical values compared with ray tracing results	72
11.	Condition for nought spherical aberration	74
12.	Quality of correction	75
13.	Existence of negative spherical aberration	76
14.	Physical implementation	78
15.	Limitation on the expansion radius $A$	79
16.	Conclusion	81
Ch. (4)	Syntheses representing strong two-foil lenses with reduced spherical aberration, as obtained by computer ray tracing	82
1.	Introduction	82
2.	Potential fields and some electron optical properties	84
3.	Reduction of spherical aberration by synthe- sis	88
4.	The optimization procedure	92

5.	Discussion of some syntheses	96
6.	Correction of the spherical aberration of a given lens	100
7.	Physical implementation	102
8.	Conclusion	106
Ch. (5)	Modelling of open lenses by means of Fourier-Bessel series	109
1.	Introduction	109
2.	Basic solutions	111
3.	Formulation of the problem	114
4.	Determination of $E_n$	114
5.	Physical approximation	121
6.	Precision	124
7.	Implications for electron optical design	126
8.	Conclusion	128
Ch. (6)	Fourier-Bessel series solution of potential fields with rotational symmetry, in terms of $I_0$ Bessel functions	129
1.	Introduction	129
2.	Formulation of the boundary value problem	131
3.	Applicability of the solution to open lenses	133
4.	Proof	134
5.	The ratio $L/L_e$	135
6.	Convergence of the series	140
7.	The use of Lanczos $\sigma$ -factors	142
8.	Application to immersion lenses	144



9.	Description of wide angle lenses	144
10.	Advantages of the method	145
11.	Remark on Fourier-Bessel integral representation	147
12.	Possibility of increasing precision	149
13.	Conclusion.	149
Ch. (7)	The electron optical properties of a class of one-foil lenses, as related to the charge distribution on the foil	150
1.	Introduction	150
2.	Conditions for convergence and zero spherical aberration	153
3.	The boundary value problem and solution	159
4.	Focal properties of the various configurations	161
5.	Relationships between $\sigma(r)$ , $\phi(0;z)$ and $\phi(A;z)$	172
6.	Conclusions	178
Ch. (8)	The inverse interior Dirichlet problem	181
1.	Introduction	182
2.	The Fourier-Bessel series method	185
3.	Properties of the Fourier-Bessel solutions	190
4.	Conclusions	109
Ch. (9)	Conclusions	214
1.	Introduction	214
2.	Optimization methods	215
3.	Properties of individual fields	216
4.	Syntheses of individual fields	217

5.	Strong two-foil lenses	218
6.	Fourier-Bessel series representations of one-foil and open systems	218
7.	A study of one-foil lenses	221
8.	Configurations associated with axial potential distributions – the inverse interior Dirichlet problem	222
9.	Concluding remarks	224
Appendix (1) Series expansions and tables of integrals of products of some Bessel functions		226
1.	Introduction	227
2.	Series expansions for the Bessel product integrals	227
3.	Precision	232
Appendix (2) The method of auxiliary Fourier-Bessel series		255
1.	Introduction	255
2.	Fourier-Bessel solutions	258
3.	Elimination of images	268
4.	Convergence of the Fourier-Bessel series	271
5.	Capacitance	275
6.	Conclusion	277
Appendix (3) Some properties of Bessel functions		278
Appendix (4) Some electron optical properties of the "zero spherical aberration one-foil lens"		280
1.	Introduction	280
2.	Discussion of the results	280

Appendix (5) Notation	284
Appendix (6) Summary	286
Appendix (7) References	288

## CHAPTER 1

### OUTLINE OF ELECTRON OPTICAL PROBLEMS TO BE INVESTIGATED, AND CHOICE OF MATHEMATICAL MODEL

#### 1. INTRODUCTION

Electron optics, as a branch of science, may be considered to have a history of almost a century, inaugurated in 1880 by Crookes and, independently, by Goldstein with their experiments with free electrons. The discoveries by Wiechert and Fleming that electrons can be focussed by a magnetic coil, followed two decades later, and the construction of the first electrostatic lens may be credited to Wehnelt who succeeded in 1905 in converting the divergent cathode lens into a convergent immersion objective by inserting the third lens component which now bears his name. [For references on the early history of the subject, see, e.g., Myers (1940) and Glaser (1956)]

These discoveries and experiments served to stimulate the more complete and more systematic investigation of the relationships between the electric or magnetic fields and the nature of the deflections caused by them; in the decade following 1925 these relationships were discovered experimentally and predicted theoretically by E. Brüche, M. Knoll, E. Ruska, C.J. Davisson, C.J. Calbick, H. Busch, W. Glaser, J. Picht, O. Scherzer and others.

The first comprehensive monographs were written by Glaser (1933) and Brüche and Scherzer (1934), and the first English language

textbooks followed some five years later. Several textbooks, monographs and reviews have appeared since, a selection of which is listed with the references.

The industrial possibilities of electron optics provided both the stimulus and the financial support for more detailed studies, which were subsequently carried out in America, the United Kingdom and France, as well. The U.S.S.R. and Japan were late to start, but have intensified their research efforts during the past decade and a half. Apart from experimenting with the actual lenses, various models [see Section (4)] have been used to simulate electron optical elements that could be used in, i.a., television cameras and tubes, and electron microscopes.

Due to the availability of the digital computer, a change in approach has occurred during the past 25 years, enabling the electron optical properties of complicated configurations to be calculated to a high level of precision.

The purpose of this study is to investigate and demonstrate the use of certain orthogonal functions in the description of the potential and intensity fields of electron optical systems, and in the calculation of certain focal properties. The possibility will be discussed of developing a systematic procedure by means of which optimization of a system can be carried out.

## 2. DESCRIPTION OF ELECTRON OPTICAL SYSTEMS TO BE CONSIDERED

Although some of the methods to be discussed in later chapters may, with little or no modification, be applicable to a broader class of electron optical systems, the configurations discussed in the rest of this dissertation are restricted to those which are purely electrostatic, have rotational symmetry, and are free from space charge. It is assumed that particles are not accelerated to such high velocities that relativistic effects need be taken into account, and that apertures are large enough that the wave nature of the charged particles need not be considered. The inner radii of electrodes will be taken large enough that the trajectories of particles are not measurably affected by fields that can be attributed to the electrode images of the particles [Hubert (1949)]. It is also assumed that the space charge of the beam which is focused, is so small that its effect on the trajectories of the individual particles may be neglected. By requiring that particles should not leave the lens on the entrance side, mirrors are also excluded.

Although the theory will apply to both positive and negative particles, it will be assumed throughout the text – for the sake of brevity – that the charged particles to be focused are electrons and not positive ions.

Not only open lenses, but also systems with one or more plane conducting foils will be considered. The foils are assumed

to be thin enough to be transparent to electrons of sufficiently high energy. [A summary of the properties of foils currently manufactured can be found in the papers cited in Section (1) of Ch. (7). The theory of one-foil configurations can, of course, also be applied to cathode lenses or immersion objectives.]

### 3. DESCRIPTION OF FOCAL PROPERTIES TO BE CONSIDERED

The determination of first order focal properties of electron optical systems can be done fairly easily by existing methods, although it may be remarked that the Fourier-Bessel methods to be described allow an increase in the attained precision through an increase in computer time only, whereas most of the other methods would require an increase in the computer memory size as well.

Much more of a problem area in electron optics is the calculation of higher order focal properties, in which cases it may prove to be more difficult to obtain the required precision.

The objective of this study is not so much to arrive at a particular electron optical configuration in which the combined detrimental effects due to various aberrations have been minimized in a balanced way, but rather to concentrate on the one geometrical aberration which limits the resolution of images of point objects on the optical axis, namely the spherical aberration. [Various measures quantifying this aberration are defined

and applied in Chs. (2), (3) and (4).] A considerable amount of research has been concentrated on the elimination of spherical aberration, and it is shown in the comprehensive review by Septier (1966) that magnetic lenses are by far superior to open electrostatic lenses as far as this aberration is concerned. It is generally accepted that, according to the proof given by Scherzer (1936), electrostatic lenses cannot show negative spherical aberration, unless one of the following actions is taken [see Septier (1966) for references] :

3.1 Elements may be introduced which deviate from rotational symmetry. This possibility has been explored by many workers, and a considerable number of papers on theoretical and experimental results have been published.

3.2 High frequency potentials on certain electrodes may be used. This approach by Kompfner (1941) seems to have been abandoned, due to practical difficulties.

3.3 Negative charge may be introduced into the region between the particle to be focused, and the optical axis [see also Ch. (7)]. This can be done in various ways :

a) Introduction of a high density electron beam or cloud in the lens region; this suggestion is not simple to implement in practice, and very little progress has been reported.



- b) An axial conducting electrode may be introduced into the lens region; it has been found experimentally that correction can be effected for rays within a narrow band of radial distances, and a refinement of the method is required, possibly using a combination of the solutions of Ch. (6) and Appendix (2).
- c) The charge may be induced on an electrode that forms part of an annular aperture; Schwarzer (1976) has performed experiments with small annular apertures, but apparently not with the present principle in mind.
- d) The charge may be induced on one or more gauzes or grids; it is, however, found that the openings in the gauzes act as miniature lenses with their own aberrations.
- e) The charge may be induced on one or more conducting foils which are thin enough as to be transparent to high energy electrons.
- f) The charges may be induced on the cathode or anode of a system.

Of the methods (3.3a)-(3.3f) the first four will be considered to be outside the scope of this study [although the solution of Appendix (2) is likely to be applicable to the boundary value

problems associated with method (3.3b)]. Method (3.3e) will be investigated in Chs. (2), (3), (4) and (7), and it will be found that the solution of Ch. (7) applies to case (3.3f) as well.

Before outlining [in Section (5)] the approach proposed for this study, a brief review will be given in the next section of the various methods that have until now been applied to study the electron optics of electrostatic lenses and, more specifically, to minimize the spherical aberration.

#### 4. OUTLINE OF METHODS CURRENTLY USED TO OPTIMIZE ELECTRON OPTICAL SYSTEMS

Methods used during the past fifty years to optimize electron optical systems may be divided into two broad groups namely

- a) empirical methods which, on a basis of trial and error, vary some lens parameters in the hope that the resulting trail may bring the designer close to an optimum design, and
- b) methods which, founded on some mathematical considerations, provide a trail leading to an optimum system (noting however that there would be no guarantee that a global and not a local extremum is reached).

Broadly speaking, the methods of Sections (4.1) and (4.2) may be grouped under category (a), and the methods of Section (5) under

category (b).

#### 4.1 Empirical methods based on proposed configurations

These studies are based on experiments with actual devices or analogical or mathematical models. A small number of parameters can usually be varied, subject to pre-defined constraints. Parameters include a) physical dimensions of electrodes and of gaps between electrodes and b) potentials at which the electrodes are kept.

Constraints include :

- a) the number of electrodes,
- b) the topological nature of electrodes (e.g. tubular rather than annular),
- c) the preferred shape within a chosen topological class (e.g. tubular electrode rather than a disc with an aperture),
- d) maximum absolute values of potentials on electrodes
- e) maximum absolute values of electric intensities in the lens region,
- f) maximum or minimum potentials at particular points within the lens, e.g. at axial saddle points,
- g) presence or absence of electric intensity at points or surfaces within the configuration, e.g. at the cathode or anode,

- h) electron optical constraints, e.g. one aberration should not exceed a specified value when another aberration is minimized.

In the following subsections brief surveys will be given of the types of electron optical problems solved by means of the various methods. The methods themselves have been described in various handbooks and reviews, and will not be discussed here.

#### 4.1.1 Experiments with physical lenses or systems

First and third order focal properties have been determined by performing experiments with actual devices of a broad variety. After the pioneering work of German groups in the nineteen thirties, a comprehensive set of graphs were published by Spangenberg (1943) which were used for more than two decades for the design of systems containing immersion and Einzel lenses. As recently as 1969 his data on immersion lenses were used by Heddle (1969) to design three-tube lenses with small chromatic aberration; the latter lenses were, in turn, tested experimentally.

Rang (1948) attempted to find projective Einzel lenses with reduced distortion, Liebman (1949) and Heise et al. (1949) investigated Einzel lenses, and Lippert et al. (1952 and 1953) measured first and third order focal properties of three-electrode lenses of which the elec=

trode shapes were varied. Hanszen (1958) compared the spherical aberration of symmetrical and asymmetrical Einzel lenses, finding that – as in glass optics – the asymmetry can be exploited to reduce the spherical aberration. Further investigations on three-electrode lenses consisting of tubes of unequal or equal diameters were carried out by Varakin et al. (1974), Bobykin et al. (1976) and Heddle et al. (1970); and Imhof et al. (1968) attempted to design a three-aperture lens which could form images of fixed position, using particles of variable energy.

In most of the studies quoted above, the shapes of, and potentials on electrodes were varied and, when a design with favourable properties was obtained, the result could not really have been anticipated. In contrast, Septier et al. (1959) investigated open lenses with electrodes which approximated hyperbolae of revolution, hoping that the fact that  $\partial\phi/\partial r \propto r$  for fields  $\phi(r,z)=k(r^2/2-z^2)$  might result in a reduction of the spherical aberration of open lenses as well. [See Zashkvara et al. (1977) for a theoretical treatment, and for further references]. This hope was not realized, because the openings in the electrodes cause a change in the flux pattern; no matter how small the holes are made, the lens changes from a foil lens to an open lens, causing the lens properties to change fundamentally, as can easily be shown by Gauss'

law. A more detailed discussion of this point will be given in Ch. (7).

Apart from the work on open lenses, experimental measurements were carried out on a field-emission illumination system by Veneklasen (1972) and on a combined objective and anode lens by Liebl (1972), the latter lens being used to focus both the primary and secondary beams in a microprobe. Möllenstedt et al. (1973) used annular rather than circular apertures to increase the contrast in emission microscopes, but apparently without realizing that a charge distribution induced on the central part of the aperture electrode can be used to reduce the spherical aberration of the lens [see Ch. (7)]. Annular apertures were also compared with circular apertures by Schwarzer (1975a and 1975b) as far as image contrast and the electron energy distribution in the emission-electron microscope were concerned.

The effects of grids inside electron lenses were investigated by Bernard (1953b) and by Mayo et al. (1972). The reduction of the spherical aberration of magnetic lenses by means of a one-foil lens was investigated by Hibino et al. (1976 and 1977), Ichihashi et al. (1971 and 1973) and Maruse et al. (1970a and 1970b); and Wittels (1975) measured focal properties of a two-foil lens.

Apart from the quasi-hyperbolic lens of Septier et al. (1959), it may be said of the above studies that in most cases severe constraints prevented optimum designs to be obtained; the constraints in the majority of cases being i) a restriction on the number of electrodes, and ii) the requirement that the electrodes should have simple shapes.

#### 4.1.2 The use of analogical techniques

Up to a decade ago it was not uncommon to use physical analogues to solve the boundary value problems associated with lens fields, in order to carry out ray tracings by, e.g., electromechanical devices or analogue computers. Francken (1967) wrote a review of the methods available, a book edited by Vitkovich (1966) was published on modelling, Verster (1963) gave a detailed description of an integrator he coupled to an electrolytic tank, Der Shvarts (1966) described applications of his "matrix integrator", Heinemann et al. (1968) described their simulation of a three-electrode cathode lens, Firestein et al. (1963) described ray tracing performed by digital computer using field data provided by a resistance network, and Ashley (1972) designed thick lenses by combining an analogue and a digital computer.

During the past decade, the advantages of carrying out the complete simulation by digital computer have become

obvious, resulting in the phasing out of the methods summarized in this subsection.

#### 4.1.3 The use of finite difference techniques

An alternative to physical analogues is the use of mathematical models, briefly outlined in the next four subsections. The use of finite differences has a history going back to pre-computer days – with, e.g., Motz et al. (1946) calculating the potential field in an electrostatic lens by manual relaxation, followed by numerical ray tracings. Due to the availability of the digital computer, finite difference techniques have dominated the field of electron optical design for the past two decades. The various finite difference solutions applicable to the interior Dirichlet boundary value problem have been analysed in great detail, and several reviews have appeared, i.a. Young et al. (1963), Weber (1967), Binns et al. (1973) and Lenz (1973). The review by Weber also discusses ray tracing, using field data at mesh points, and Lenz advances a number of reasons why finite difference methods may be preferable to the finite element method of Section (4.1.4).

The following reports represent a selection of investigations that have been carried out since the last reviews cited :



Following the first order analysis of two-tube lenses by Natali et al. (1972a and 1972b), Dichio et al. (1974 and 1975), and Kuyatt et al. (1974) investigated their third order properties. El-Kareh et al. (1972) and Shimizu (1974) studied three-aperture lenses and Saito et al. (1977) calculated first and third order focal properties of three-tube Einzel lenses. Cleaver (1975) simulated field emission electron guns for electron microprobes; Riddle (1978) used finite differences to calculate the axial potential in Einzel lenses used in field emission electron guns; and Henkelman et al. (1974) studied mirrors formed by the cathode and two further lens elements, for use in an electron spectrometer.

A probable reason for the continuing popularity of this method is the ease of programming, if the boundaries have reasonably simple shapes. Two disadvantages are i) the need to increase the size of the computer memory if the precision is to be increased, resulting in an increase in the amount of computation per iteration, and also in the number of iterations required, and ii) the necessity to manipulate large amounts of information which may eventually not be required (for instance, even if only the axial potential is required, the relaxation process still involves all the grid values in zonal regions).

Small gaps between electrodes can be accommodated readily,

but problems may arise when the configuration consists of a few ring shaped electrodes separated by large gaps; in such a case problems associated with the exterior Dirichlet problem — as discussed in Appendix (2) — will have to be overcome. In these cases the charge calculation method of Section (4.1.5) is probably the most convenient to use.

#### 4.1.4 The use of finite elements

Although the use of finite elements has gained popularity in many diverse fields, and the method has been studied in great detail by numerical analysts, it is interesting to note that apparently only one group has made extensive use of finite elements in electron optical design. References on applications studied by Munro and by Bunting may be found in the review paper by Munro (1973). The remark on gaps [see Section (4.1.3)] applies to this method as well, and the amount of programming needed (if an existing package cannot be used) probably counterbalances the advantages of the method.

#### 4.1.5 The source calculation method

If an (unknown) function  $D(\underline{s})$  represents the volume charge density at points (defined by the position vector  $\underline{s}$ ) in and near an electron optical system, and a (known) function represents the potential distribution in the same region, then  $V(\underline{s})$  can be expressed in terms of  $D(\underline{s})$  by means of

Coulomb's law. On the other hand,  $D(\underline{s})$  can be related to  $V(\underline{s})$  in terms of a Fredholm integral equation of the first kind. The solution of such an integral equation can be obtained by a variety of methods, as discussed in the review by Miller (1974).

When used in practical electron optical design, the conducting electrodes defining the electron optical configuration are normally divided into a sufficiently large number ( $N$ ) of elements, and the surface charge density on the  $i$ -th element represented by a variable,  $\sigma_i$ . The potentials at a chosen number ( $n$ ) of points on the electrodes can be represented in terms of these variables. Since the potentials on the electrodes have been pre-defined, a set of linear algebraic equations results, and the  $\sigma_i$  can be found if  $n \geq N$ . Normally the solution is obtained by performing a matrix inversion, in which case the precision attainable is largely dependent upon the computer word length.

When the  $\sigma_i$  is known, the potential at any point in space can be calculated, using Coulomb's law. The potential is given in the form of a series, the terms of which have elliptic integrals as factors. It is also possible to express the electric intensity  $\underline{E}$  at any point in terms of a series (again involving elliptic integrals), so that  $\underline{E}$  need not be calculated from the potential, as required by the finite difference and finite element methods.

Some theoretical aspects of the charge calculation method have been discussed by Cruise (1963), Lewis (1966), Singer et al. (1970), Mautz et al. (1970), and Appelt (1973a and 1973b). Du Toit (1976) and Viljoen (1976) applied the method in the analysis of image intensifier tubes, the latter paper discussing the matter of precision in some detail. Read et al. (1970) studied the first and third order focal properties of two-cylinder lenses, and a book of tables of properties of a wide variety of lenses was compiled by Harting et al. (1976).

By summary, it appears as if this method is a versatile one, allowing electron optical calculations of fairly high precision to be carried out. That the potential need not be defined everywhere on a closed surface, is an important advantage.

#### 4.1.6 The use of orthogonal functions

As stated in Section (2), this study is concerned with electron optical systems without space charge. We may therefore assume that everywhere, except on the electrodes, the potential  $\phi(\underline{s})$  satisfies Laplace's equation.

$$\nabla^2 \phi = 0 \tag{1.1}$$

The function  $\phi$  can, among others, be chosen to be of the form  $\phi(r, \theta, z) = R(r) \Theta(\theta) Z(z)$  (1.2)

or of the form

$$\phi(\rho, \theta, \Psi) = R(\rho) \Theta(\theta) \Psi(\Psi) \quad (1.3)$$

in which  $(r; \theta; z)$  and  $(\rho; \theta; \Psi)$  are polar coordinates of cylindrical and spherical symmetry, respectively. Although it may happen in some special cases that part of an electron optical system may have spherical symmetry, it is found that for the majority of configurations, the form with cylindrical symmetry is the most profitable choice.

Using the standard method of separation of variables and requiring that  $\phi$  should not be a function of  $\theta$ , the following differential equation results :

$$\frac{1}{r} \frac{\partial}{\partial r} \left[ r \frac{\partial \phi}{\partial r} \right] + \frac{\partial^2 \phi}{\partial z^2} = 0 \quad (1.4)$$

Substitution from Eq. (1.2) into Eq. (1.4) results in :

$$\frac{\partial^2 Z}{\partial z^2} = BZ \quad (1.5)$$

and

$$\frac{\partial^2 R}{\partial r^2} + \frac{1}{r} \cdot \frac{\partial R}{\partial r} + BR = 0 \quad (1.6)$$

in which B is the separation constant.

Eq. (1.6) is satisfied by four Bessel functions of order zero, namely  $I_0$  and  $K_0$ , the modified Bessel function of the first and second kind, resp., and  $J_0$  and  $Y_0$ , the un-

modified Bessel function of the first and second kind, resp. [To represent higher order Bessel functions, the subscript "0" will be replaced by the order, n. For a short list of properties of Bessel functions, see Appendix (3).] In view of possible misunderstanding due to the relationship  $I_0(x) = J_0(ix)$ , the arguments of all Bessel functions appearing in this manuscript will be considered to be real.

For negative values of B, the functions  $I_0$  and  $K_0$  apply, in which case  $Z(z)$  is a trigonometrical sine or cosine function. For positive values of B, the functions  $J_0$  and  $Y_0$  apply, and  $Z(z)$  is a hyperbolic sine or cosine function. For  $B=0$ ,  $R \propto \log_e(r)$  and  $Z \propto z$  are also solutions, but the latter two solutions will not be given further consideration in this chapter.

The general solution for  $\phi$  therefore includes members of the following families of functions (referred to in this manuscript as Fourier-Bessel functions) :

$$K_0(\alpha r) \sin(\alpha z), K_0(\alpha r) \cos(\alpha z); \quad (1.7)$$

$$I_0(\beta r) \sin(\beta z), I_0(\beta r) \cos(\beta z); \quad (1.8)$$

$$J_0(\gamma r) \sinh(\gamma z), J_0(\gamma r) \cosh(\gamma z); \quad \text{and} \quad (1.9)$$

$$Y_0(\delta r) \sinh(\delta z), Y_0(\delta r) \cosh(\delta z). \quad (1.10)$$

The method of choosing the families to be included in a solution, and of assigning amplitudes to particular members of the families, will depend upon the general approach followed. In the majority of electron optical studies

reported, a configuration of electrodes is proposed, and then – using various analytical or numerical methods – suitable combinations of functions are obtained so as to find a function  $\phi$  which approximates the potentials on the electrodes to an acceptable degree of precision. These applications will be reviewed in Section (4.1.6.1).

The other approach is to follow some optimization algorithm which is expected to result in a Fourier-Bessel series representing the optimum field (i.e. optimized i.r.o. some predefined criteria). This approach will be discussed in Section (5).

#### 4.1.6.1 Some properties of Fourier-Bessel potential fields

Before discussing in Section (4.1.6.2) the use of Fourier-Bessel functions in electron-optical design, the Fourier-Bessel series representation of the potential field in the vicinity of a given physical configuration will be considered briefly.

By way of introduction, it may be pointed out that the members of the families of functions of Eqs. (1.7)-(1.10) are solutions of certain basic boundary value problems. In the examples given below, the functions listed in Eqs. (1.7) and (1.8) with a cosine factor will not be considered because they can be changed to the form with

the sine factor, through a z-transformation representing a translation. As far as Eqs. (1.9) and (1.10) are concerned, it may be noted that  $\cosh(z) + \sinh(z) = \exp(z)$ , and that  $\cosh(z) - \sinh(z) = \exp(-z)$ ; for ease of visualisation, only

$$J_0(\gamma r) \exp(-\gamma z) \text{ and } Y_0(\delta r) \exp(-\delta z) \quad (1.11)$$

will be considered, noting that members with exponentials with positive argument can be obtained by reversing the sense of the z-axis. The chosen functions will now be considered briefly.

i) The function  $\phi(r; z) = K_0(\alpha r) \sin(\alpha z)$ : (1.12)

This function represents the solution of the following boundary value problem :

$$\nabla^2 \phi(r > A; z) = 0 \quad \text{for } 0 < z < L \quad (1.13)$$

$$\phi(r=A; z) = K_0(n\pi A/L) \sin(n\pi z/L) \text{ for } 0 \leq z \leq L \quad (1.14)$$

$$\phi(r; 0) = \phi(r; L) = 0 \quad \forall r > A \quad (1.15)$$

in which  $n\pi A/L = \alpha$  ; A and L are non-zero lengths and n is a positive integer. [The case A=0 is not allowed, because  $K_0(r \rightarrow 0) \rightarrow \infty$  .]

Superpositions of these functions are employed in the solution of the exterior Dirichlet boundary value problem of Appendix (2), and is of use in configurations of two cylindrical electrodes [see also Yeh et al. (1969)].

ii) The function  $\phi(r; z) = I_0(\beta r) \sin(\beta z)$ : (1.16)



This function represents the solution of the following boundary value problem :

$$\nabla^2 \phi(r < A; z) = 0 \quad \text{for } 0 < z < L \quad (1.17)$$

$$\phi(0; z) = \sin(n\pi z/L) \quad \text{for } 0 \leq z \leq L \quad (1.18)$$

$$\phi(r; 0) = \phi(r; L) = 0 \quad \forall r \quad (1.19)$$

in which A and L are non-zero lengths and n is a positive integer.

Superpositions of these functions are used in the solution of the inverse interior Dirichlet problem of Ch. (8), which is applied in Ch. (9).

iii) The function of Eq. (1.16) also represents the solution of the following boundary value problem :

$$\nabla^2 \phi(r < A; z) = 0 \quad \text{for } 0 < z < L \quad (1.20)$$

$$\phi(A; z) = I_0(n\pi A/L) \sin(n\pi z/L) \quad \text{for } 0 \leq z \leq L \quad (1.21)$$

$$\phi(r; 0) = \phi(r; L) = 0 \quad \forall r < A \quad (1.22)$$

Superpositions of these functions are used in the solution of the interior Dirichlet problem, as applied in Chs. (2) - (7), and in several examples to be discussed in this section.

iv) The function  $\phi(r; z) = J_0(\gamma r) \exp(-\gamma z) :$  (1.23)

This function is the solution of the following boundary value problem (an interior problem with quasi-Dirichlet conditions) :

$$\nabla^2 \phi(r; z > 0) = 0 \quad \forall r \quad (1.24)$$

$$\phi(r; 0) = J_0(rZ_{0n}/A) \quad \forall r \leq A \quad (1.25)$$

$$\phi(A; z \geq 0) = 0 \quad (1.26)$$

in which  $A$  is a length, and  $Z_{0n}$  is the  $n$ -th zero of  $J_0$ .

Superpositions of these functions are employed in Ch. (5) and in several examples to be quoted in this section.

v) The function of Eq. (1.23) is also the solution of the following exterior-type Dirichlet problem :

$$\nabla^2 \phi(r > A; z > 0) = 0 \quad (1.27)$$

$$\phi(r; 0) = J_0(rZ_{0n}/A) \quad \forall r \geq A \quad (1.28)$$

$$\phi(A; z \geq 0) = 0 \quad (1.29)$$

This type of boundary value problem has apparently not yet found application in electron optical problems, and will not be given further consideration.

vi) The function  $\phi(r; z) = Y_0(\delta r) \exp(-\delta z)$  : (1.30)

The function  $J_0$  in case (v) may be replaced by  $Y_0$ , but apparently nothing is gained in this way, since  $Y_0$  is clumsier to handle both numerically and analytically.

The function cannot be replaced by  $Y_0$  in case (iv), due to the singularity of  $Y_0$  at  $z=0$ . No further consideration will be given to the  $Y_0$  Bessel functions in the rest of this study.

#### 4.1.6.2 The use of Fourier-Bessel fields in electron optics

The representation of simple electron optical configurations by means of Fourier-Bessel integrals have been known for a long time, but due to the complexities of evaluating these integrals [see Ch. (6) and Appendix (2)], the latter were initially utilized only to obtain analytical approximations for the potential inside an immersion lens consisting of two infinitely long juxtaposed coaxial cylinders of equal diameter and with no gap between them. Approximations were obtained for paraxial regions by Gray (1939) and Bertram (1940), and for zonal regions by Bertram (1942), using Fourier-Bessel functions of  $I_0$ -type as described in case (ii) of Section (4.1.6.1).

Bernard (1951a) considered a grid lens consisting of a grid at a potential  $\phi_1$ , placed in the gap of negligible size between two juxtaposed coaxial cylinders of equal diameter, which are held at a potential  $\phi_2 \neq \phi_1$ . Starting from the Fourier-Bessel integral formulated in terms of  $I_0$  Bessel functions, he found an analytical approximation for the axial potential, which he used to calculate the first order focal properties of the grid lens [Bernard (1951b)].

Cook and Heddle (1976) used  $J_0$  Bessel functions [case (iv) of Section (4.1.6.1)] to describe the same immersion lens as Gray, but allowing a finite gap size between the two

tubes. Assuming a linear potential variation in the gap, he calculated the first order focal properties of the lens.

To represent a three-tube Einzel lens with negligible gap sizes, Werner (1971) divided the space inside the lens into three regions, to which three different series expansions in terms of  $I_0$  functions applied [case (iv) of Section (4.1.6.1)]; first and third order focal properties were found.

Wittels et al. (1976) used subregions to describe the potential in a two-foil Einzel lens with a circular aperture in the central electrode. Orlov (1967/8) also accommodated an aperture in a closed immersion lens by dividing the lens interior into four subregions;  $I_0$  and  $K_0$  Bessel functions were used. The potential distribution in a three-tube Einzel lens with gaps between the tubes (and assuming a linear potential variation in the gaps) was described by Anicin et al. (1976), and Read (1969a) used  $J_0$  Bessel functions to find an analytical expression for the potential in a two-aperture immersion lens; the approximation was used in subsequent studies of symmetrical and asymmetrical Einzel aperture lenses [Read (1969b and 1970)]. Finally the Fourier-Bessel series representations of less common configurations with rotational symmetry may be mentioned, e.g. transaxial systems [Mel'nikov (1971)], capacitor-like systems [Heerens

et al. (1975) and Heerens (1976)], a tube inside another coaxial tube [Lebedev et al. (1960)], and juxtaposed coaxial cylinder with unequal diameters [Yeh (1975 and 1976)].

Summarizing, it can be stated that the above configurations do not allow much freedom in the choice of electrodes. In most cases configurations were chosen as to facilitate the derivation of the Fourier-Bessel representation and/or allow ease of manufacture; consequently only discs or tubes were apparently utilized. The latter restrictions will be lifted for two-foil lenses in Chs. (2)-(4), for open lenses in Chs. (5) and (6), for one-foil lenses in Ch. (7) and for open, one-foil and two-foil lenses in Ch. (8), in order to investigate, i.a., whether the restrictions mentioned did not seriously hamper the optimization of systems.

#### 4.1.7 Analytic functions

The functions of Section (4.1.6.1) could have been discussed under this heading, but due to the different techniques used, the functions which are members of orthogonal sets have been discussed separately. As far as the "non-orthogonal" analytic functions are concerned, it is very seldom possible to "derive" the form that a function should take to represent a given configuration or a theoretically optimized system : normally various functions of convenient

forms are investigated, and a particular one selected which  
i) shows the most favourable electron-optical properties,  
or ii) gives the best approximation to the potential  
field due to a given set of electrodes.

Although most of the investigations reported are of an  
empirical nature, dividing lines cannot always be drawn  
with certainty, and Section (4.2) is devoted to the elec-  
tron optical use of analytic functions, whatever the nature  
of the approach.

#### 4.2 Lenses represented by analytic axial potential functions

In view of the expense of machining electrodes of various types  
for use in the experimental studies of Sections (4.1.1) and (4.1.2)  
the use of a simple mathematical model has its obvious attractions.  
In pre-computer days it would have been particularly advantageous  
to find a potential field which is expressed in closed form in  
such a way that not only the trajectory, but also the cardinal  
points can be derived in closed form. Unfortunately only a few  
such fields have been discovered, e.g. the parallel electric  
intensity field used by Gianola (1950) to reduce the spherical  
aberration of existing lenses. [Examples are also quoted by  
Glaser (1956) and Harman (1953)]. Consequently more complicated  
functions were often used, applying various methods to calculate  
the electron optical properties associated with such functions.

In the majority of cases, an axial potential function  $f(z)$  was chosen in such a way that  $\partial f/\partial z \rightarrow 0$  for  $|z| \rightarrow \infty$ , so that open lenses could be modelled. A popular method of analysis has been the use of expressions for the various focal properties, given in terms of  $f(z)$  and its derivatives. These expressions were derived by Glaser (1933) and Scherzer (1936) and they apply to paraxial rays. The vast majority of reports, in fact, deal with the paraxial focal properties of lenses. Among the more comprehensive treatments are Glaser (1933), Regenstreif (1951), Ramberg (1942) and Wendt (1951). The latter report includes a fundamental discussion on the types of analytical functions that allow physical implementation by means of a relatively small number of electrodes (in contrast to some of the fields of following chapters which can only be obtained by a large number of ring electrodes).

Various reasons were advanced for choosing particular axial potential distributions. For instance, Grivet et al. (1952) used a function which was shown to approximate the axial behaviour of the Fourier-Bessel series which Gray (1940) had obtained for two-tube lenses. The resulting saving in volume of computing was an important consideration, in view of the non-availability of computers.

Analytical models for paraxial regions were utilized by Dommasch (1965/66) for a disc with an aperture, by Typke (1966/67) in his

study of two-tube lenses with large voltage ratios, by Croitoru (1965/66) in treating weak lenses, by Adams et al. (1972a) for Einzel and non-Einzel three-element lenses, and by El-Kareh et al. (1971) for three-tube symmetrical Einzels. In some cases functions were attractive to investigate due to their mathematical forms but were not simple to approximate physically, e.g. the zero gap aperture lens of Read (1971) and the hyperbolic lens discussed by, i.a., Zashkvara et al. (1977); the latter could, in principle, be used as a foil lens, or portions of the closed lens could be used for special purposes, as explained in his report.

Further studies include the three-tube lenses of Ciric et al. (1976) and those by Kanaya et al (1972 and 1978) of immersion lenses and three-element lenses. Finally may be mentioned the two-volume study by El-Kareh et al. (1970a and 1970b) in which extensive tables are provided on a variety of lenses. The lack of precision of entries in some of the tables has, however, provoked unfavourable comment from reviewers who felt that alternative methods of higher precision should have been employed instead.

Grid lenses of various types were studied by Bernard (1951b , 1952 , 1953a and 1953b), and one-foil lenses by Hibino et al. (1976) and Ichihashi et al. (1973).

In all the above investigations, axial potential functions were



utilized, and paraxial focal properties obtained. In contrast, Kuroda et al. (1974) made use of an analytical potential at a fixed radial distance, and Johnson (1975) approximated the potential field in the region between two coaxial cones in a configuration designed to reduce the spread of the outer parts of a beam of charged particles.

In the above reports the emphasis was placed on finding an analytical approximation to a physical configuration of some kind, and not on whether such a configuration has any particular merit as far as the reduction of aberrations were concerned. As optimization methods, the above attempts are probably on a par with the experimental methods of Sections(4.1.1) and (4.1.2).

In a different category are the analytical functions arrived at on theoretical grounds. For instance, Scherzer (1936a) and (1936b) advanced some arguments based on the electron optical properties of paraxial regions to show why a particular bell-shaped potential distribution would result in a minimum third order spherical aberration. Similar distributions were investigated by Yamamoto (1974) who studied weak lenses by means of the Glaser bell shaped function, Yamazaki (1977) in his investigation of the influence of the magnification of an Einzel lens on its higher order focal properties, and by Yamazaki (1973) who compared the electron optical properties associated with his Gaussian potential distribution, with those of the Glaser, Regenstreif and the Bernard-Grivet models. A summary of further functions used in

electron optical design has been given by Skoltermo (1976a) and 1976b), together with inverse boundary value problem solutions [see also Ch. (8)].

In spite of claims [Gabor (1942) and Crewe (1977), and the discussion by Septier (1966) of fields suggested by Glaser and Scherzer] that certain distributions represent "ideal" lenses – for instance having a minimum of spherical aberration – it is normally found that modifications of these functions can lead to superior designs. The disadvantage of some of the abovementioned functions is that they allow very few degrees of freedom – in some cases the half-width is the only adjustable parameter. This also applies to the model used by Tonomura (1973) to design a field emission electron gun. The function is a polynomial of seventh degree which, however, has only a single adjustable parameter, due to the particular choice of polynomial.

A possible course of action to gain more degrees of freedom is that of superposing or juxtaposing suitable functions, and it was indeed found by Plass (1942) that an asymmetrical field obtained from a bell shaped distribution gave a reduced spherical aberration. Kanaya et al. (1966) combined Glaser's bell-shaped distributions to approximate thicker lenses, and investigated first and third order focal properties.

Finally the composite lenses studied by Glikman et al. may be

mentioned. Calculations were performed on juxtaposed tubular lenses of equal diameters. Glikman et al. (1974a) reported results on lenses with constant potential differences between the tubes, Glikman et al. (1974b) deal with juxtaposed Einzel lenses with either constant potential differences or constant ratios of electrode potentials, and Glikman et al. (1976) calculated the cardinal elements of juxtaposed immersion lenses with constant ratios between potentials on neighbouring electrodes. In all these cases it was found that an increase in the number of electrodes led to a decrease in the spherical aberration. [ It may be remarked here that the solution given in Ch. (6) allows this configuration to be represented by a Fourier-Bessel series, allowing both paraxial and zonal focal properties to be calculated to a high degree of precision, especially if the number of electrodes takes on a large value; in such a case the solution of Glikman et al. suffers from an increased error accumulation ].

Summarizing the analytical models discussed above, it may be stated that some models allowed precise calculations of first and third order focal properties to be made of particular classes of lenses, but that most of the procedures followed could not be expected to lead to absolute minima for the aberrations under consideration. This view is supported by the following two considerations: i) assuming that some "optimum" function  $\phi(0,z)=f(z)$  exists, and must be approximated on a certain axial interval, it is clear that in most cases cited in this subsection, no effort was made to ensure that the functions chosen constituted

a complete set on that interval; and ii) the procedures followed were usually not based on a mathematically founded optimization theory.

In Section (6) the possibility will be discussed of satisfying these two criteria in electron optical design.

#### 5. ELECTRON-OPTICAL OPTIMIZATION : MOSES AND SZILAGYI

In previous sections it became obvious that most of the approaches were of the trial and error type, offering no guarantee that an optimum system will result from the chosen procedure. In contrast, two approaches which are based on mathematically founded optimization procedures, and are in a category of their own, have been formulated and applied in recent years :

i) Moses (1973) has developed an optimization procedure which is based on variation theory and makes use of the paraxial ray equation. Restrictions on, e.g. the maximum allowed electric intensity can be accommodated by the theory, and one aberration can be reduced while demanding that other aberrations should not exceed certain limits. Moses has applied the theory to magnetic electron optical systems, but it does not seem to have become a popular method, probably due to its mathematical complexity, which fact Moses concedes. One must also note that the optimization is achieved for paraxial properties only.

ii) Szilagyí (1977) has developed a method based on a dynamic

programming search to reduce the spherical aberration of magnetic and electrostatic immersion lenses [Szilagyí (1978)]. The aberration to be minimized is expressed in terms of a piece-wise linear axial potential function, by means of the paraxial ray equation. The method appears to be simple enough to become more widely used in the future, but — as Moses' method — is presently formulated to optimize the system for paraxial properties only.

In Section (6) the possibility will be investigated of formulating a steepest descent method which can handle both paraxial and zonal electron optical properties.

## 6. OPTIMIZATION BY A GRADIENT METHOD

Various solutions to boundary value problems of Section (4.1.6.1) may be used in procedures to optimize different categories of lenses. Instead of giving here a general formulation of the method, a few specific examples will be discussed by way of illustration.

### 6.1 Example : two-foil lens

As a simple example, it may be required to find a function  $\phi(r;z)$  such that the lens corresponding to the function will focus a uniform, parallel beam of electrons entering the lens at  $z=0$ , to a disc of confusion of minimum diameter at  $z=z_f$ . The lens should have a radius  $A$ , a length  $L$ , and is closed off at  $z=0$  and

$z=L$  by plane conducting foils which are earthed (making the lens an Einzel lens). No axial electrode is allowed, and the field  $\phi(r<A, z)$  inside the lens will be created by a set of coaxial ring electrodes at  $r=A$ , for  $0 < z < L$ .

The problem can be tackled in two ways :

i) The potential at  $r=A$  can be written as

$$f(z) = \sum_{n=1}^N B_n \sin(n\pi z/L)$$

so that inside the lens,

$$\phi(r; z) = \sum_{n=1}^{\infty} B_n \sin(n\pi z/L) I_0(n\pi r/L) / I_0(n\pi A/L)$$

It is required to find the vector  $[B] = [B_1; B_2, \dots]$  so that the radius  $R_d$  of the disc of confusion reaches a minimum value.

A simple gradient method can now be followed by calculating  $R_d$  — through ray tracing — for  $\phi$  given by  $[B]_a = [1; 0; 0; \dots]$ , by  $[B]_b = [1; 0,001; 0; 0; \dots]$ , by  $[B]_c = [1; 0; 0,001; 0; 0; \dots]$ , etc. This allows an approximate calculation of  $\partial R_d / \partial B_2$ ,  $\partial R_d / \partial B_3$ , etc. The gradient  $\nabla R_d$  can be calculated from these derivatives, and a translation in function space can be undertaken in the direction of  $-\nabla R_d$ . The procedure is repeated until a sufficiently low value of  $R_d$  is reached. If the focal length is found to be shorter or longer than the stipulated value, the (uniform) velocity of the charged particles entering the lens is adjusted.

The advantage of the procedure is that it can be expected to lead to a function  $f(z)$  which approximates the true optimum function  $F(z)$ , since the trigonometric functions constitute a complete set on the interval  $(0,L)$ . The larger the value of  $N$ , the more closely  $f(z)$  can approximate  $F(z)$ .

A disadvantage of the procedure is that a large value of  $N$  will slow down the calculation of  $\nabla R_d$ , in view of the ray tracings. In Ch. (4) it is shown how time may be saved by using a better starting point than  $[B] = [1; 0; 0; \dots]$ .

ii) The problem may be formulated in terms of an axial function

$$g(z) = \sum_{n=1}^N C_n \sin(n\pi z/L)$$

so that, inside the lens,

$$\phi(r;z) = \sum_{n=1}^N C_n \sin(n\pi z/L) I_0(n\pi r/L)$$

As in i), a starting point  $[C]$  is chosen, and a path along the gradient followed until the optimum point is reached. The expression given above for  $\phi(r;z)$  again allows the potentials on a set of coaxial ring electrodes to be found. Without going into details, it may be remarked here that the approaches of i) and ii) may differ in efficiency, depending upon the  $A/L$  ratio.

## 6.2 Example : A one-foil lens

A lens which is open on the right hand side and has its left

hand side closed off by a conducting plane foil at  $z=0$ , is required to focus a uniform, parallel electron beam of radius  $A$  to a disc of confusion of minimum radius. The required focal length is also stipulated.

Again two approaches may be followed :

i) A function  $H(z)=\phi(A;z)$  is defined as follows :

$$H(z)=h(z)=\sum_{n=1}^N B_n \sin (n\pi z/L) \quad \text{for } 0 \leq z \leq L$$

and  $H(z)=0$  for  $L \leq z \leq L'$ ,

in which  $A$  is the given radius of the beam, and  $L$  and  $L'$  are lengths such that  $L \gg A$ ,  $L' \gg A$  and  $L' \gg L$ . Then the solution of Ch. (6) can be used to calculate  $\phi(r;z)$  inside the lens for any  $[B]$ . The same optimization procedure as described above can be used to find the optimum  $[B]$ .

ii) An axial function  $G(z)=\phi(0;z)$  may be defined :

$$G(z)=g(z)=\sum_{n=1}^N D_n \sin (n\pi z/L) \quad \text{for } 0 \leq z \leq L$$

and  $G(z)=0$  for  $L \leq z \leq L'$

and the procedure of i) followed, using the solution of Ch. (8) to the inverse interior Dirichlet problem.

### 6.3 Example : an open Einzel lens

The open lens version of the previous problem can again be tackled in two ways :

i) A function  $H(z)=\phi(A;z)$  may be defined :

$$H(z)=0 \quad \text{for } 0 \leq z \leq L$$



$$H(z)=h(z)=\sum_{n=1}^N B_n \sin [n\pi(z-L)/(L'-L)] \quad \text{for } L \leq z \leq L'$$

$$H(z)=0 \quad \text{for } L' \leq z \leq L''$$

Suitable restrictions will have to be imposed on  $L, L'$  and  $L''$ , e.g. that  $(L'-L) \gg A$ . A study of these restrictions have not yet been undertaken, and it is not known whether the set of approximating functions constitute a complete set in this case.

ii) Without going into details, it appears as if the restrictions of  $L, L'$  and  $L''$  may be less severe if, instead of defining  $\phi(A; z)$ , an axial potential function  $\phi(0; z)=G(z)$  is defined :

$$G(z)=0 \quad \text{for } 0 \leq z \leq L$$

$$G(z)=g(z)=\sum_{n=1}^N D_n \sin [n\pi(z-L)/(L'-L)] \quad \text{for } L \leq z \leq L'$$

$$G(z)=0 \quad \text{for } L' \leq z \leq L''$$

As in Section (6.2), case (ii), the solution to the inverse interior Dirichlet problem of Ch. (8) is utilized.

#### 6.4 Some general remarks on the proposed procedure

- i) In the example of Section (6.1) it is possible to find a symmetrical Einzel foil lens by equating all the B-coefficients of even index to zero, and not changing them in the course of the optimization procedure. The same approach, coupled with the correct choice of  $L'$  and  $L''$  will lead to a symmetrical open Einzel lens in the example of Section (6.3)
- ii) As mentioned in Section (6.1), the optimization procedure may be speeded up considerably by carefully choosing the

starting vector [B]. A suitable starting point may also be obtained from axial functions resulting from paraxial optimization procedures [e.g. the bell-shaped axial functions of Section (4.2)]. Favourable starting points may also be obtained from weak lens approximations – using results as presented in Chs. (4), (7) and (8).

## 7. SUMMARY OF PROPOSED STUDY AND OUTLINE OF CHAPTERS

The exploration of various techniques of utilizing Fourier-Bessel functions in electron optical design will constitute the main theme of this dissertation, and the techniques will be aimed at reducing the spherical aberration of space charge free electrostatic lenses with rotational symmetry. The  $I_0$  Bessel functions will be found to be of most use in simulating open, one-foil as well as two-foil lenses, and will receive most of the attention. [The  $K_0$  functions can be used in lenses with axial electrodes, using the solution of Appendix (2), and  $J_0$  functions are particularly useful in the analysis of mirrors, using solutions like those of Ch. (5). These applications are excluded from the present study.]

In Chapter (2) some electron optical properties of individual  $I_0$  Fourier-Bessel fields are studied with two objectives in mind : i) to find out whether these fields have any unique properties that may be found useful, and ii) to aid in understanding the behaviour of lenses synthesized from these fields.

In Chapter (3) a study is made of weak symmetrical fields, and analytical expressions obtained for various focal properties. An attempt is then made to synthesize two fields to reduce the spherical aberration.

In Chapter (4) syntheses are sought that would reduce the spherical aberration of strong symmetrical fields. The syntheses are attempted i.a. by using information about some properties of individual fields, as to provide suitable starting points for the gradient optimization procedure described in Section (6) of Chapter (1).

Whereas Chs. (2) - (4) deal with two-foil lenses, a Fourier-Bessel representation of a class of open lenses is given in Chapter (5). The lens region is divided into three parts, each represented by its own series, and both  $I_0$  and  $J_0$  functions are utilized. Integrals of products of Bessel functions are required for one of the derivations, and — since they are not available in literature — are tabulated in Appendix (1). Series expansions for the integrals are also given in this appendix.

Although the solution of Chapter (5) is useful for mirrors, convergence of some series are slow at certain points if lenses are described, and an alternative solution is given in Chapter (6), in which only  $I_0$  Bessel functions appear. The solution applies equally well to open, one-foil and two-foil lenses.

The computation of potentials may be speeded up considerably through the use of associated Fourier-Bessel series which can be formulated by taking into account aspects of the image charge model. Since the problem of convergence is more serious in exterior Dirichlet problems, the method of associated series is described in Appendix (2) for the exterior problem. This solution is also directly applicable to the study of axial electrode lenses, which are, however, excluded from this study.

Chapter (7) illustrates some applications of the solution of Ch. (6) by i) predicting the behaviour of one-foil lenses through a study of the charge distributions induced on the foil, ii) using the solution in ray tracing studies of some configurations which – in their weak forms – show negative spherical aberration, and iii) finding corrective elements which show zero convergence paraxially, but focus zonal rays with large negative spherical aberration.

In Chapter (8) the inverse interior Dirichlet boundary value problem is discussed, and approximate solutions presented. Electron optical properties of some of the solutions of Ch. (8) are briefly discussed in Chapter (9).

The contents of the first two appendices have already been discussed. In Appendix (3) some properties of Bessel functions often referred to in the text, are given for quick reference.

## CHAPTER 2

### SOME ELECTRON OPTICAL PROPERTIES OF FOURIER-BESSEL BASIS FIELDS

#### 1. INTRODUCTION

In Ch. (1) the following boundary value problem was considered :

$$\phi(r;0)=\phi(r;L)=0 \quad \forall r \leq A \quad (2.1a)$$

$$\phi(A;z)=f(z) \quad \text{for } 0 \leq z \leq L \quad (2.1b)$$

in which  $A$  and  $L$  are given lengths, and  $f(z)$  is a given function.

The solution, which describes a broad class of two-foil lenses (with plane foils at  $z=0$  and  $z=L$ ) is

$$\phi(r;z) = \sum_{n=1}^{\infty} B_n \sin(n\pi z/L) I_0(n\pi r/L) / I_0(n\pi A/L) \quad (2.2)$$

in which

$$B_n = (2/L) \int_0^L f(z) \sin(n\pi z/L) dz \quad (2.3)$$

In Ch. (4) an attempt is made to find functions  $f(z)$  for which at least two of the coefficients  $B_n$  are non-zero. To obtain such syntheses, it is necessary to have some information on the electron-optical properties of fields corresponding to functions  $f(z)$  for which only one coefficient  $B_n$  is non-zero. A report of a computer study of such fields is given in this chapter, whereas an analytical study of weak fields of the same type is found in Ch. (3).

#### 2. ELECTRON OPTICAL PROPERTIES OF THE FOURIER-BESSEL FIELDS

##### 2.1 Introduction

The electron optical properties of some of the electro-

static fields corresponding to  $n=1, 2, 3, \dots$  in Eq. (2.2) are described in this section. Due to the difficulty of finding analytical expressions for the integrals of Fourier-Bessel functions, the results of a numerical study are presented here.

To facilitate the description, the terms of the series in Eq. (2.2) are now referred to as Fourier-Bessel "components" or "component fields", and a system of indexing is introduced as follows :

$$C(\pm n) = \pm \frac{I_0(n \pi r/L)}{I_0(n \pi A/L)} \sin(n \pi z/L)$$

In this publication only objects at  $z \rightarrow -\infty$  are considered. As shown in Fig. (2.1), rays parallel to the  $z$ -axis and at different radii enter the field from the left. The field is zero for  $z < 0$  and  $z > L$ . For all the results shown, the value of the radius  $A$  has been taken as 0,2m and  $L$  was taken equal to 1m. The trajectories of electrons of different kinetic energies were calculated, and the ratio

$S = (\text{saddle point potential of field} / (\text{kinetic energy of electron in the field free region}))$

was found to be a convenient parameter. In the case of single component fields it is found that for a chosen value of  $S$ , the value of the radius  $A$  has no influence upon the electron-optical properties described here. When superposing two or more Fourier-Bessel fields, however, the radius  $A$  plays a most important part [see Chs. (3) and (4)].

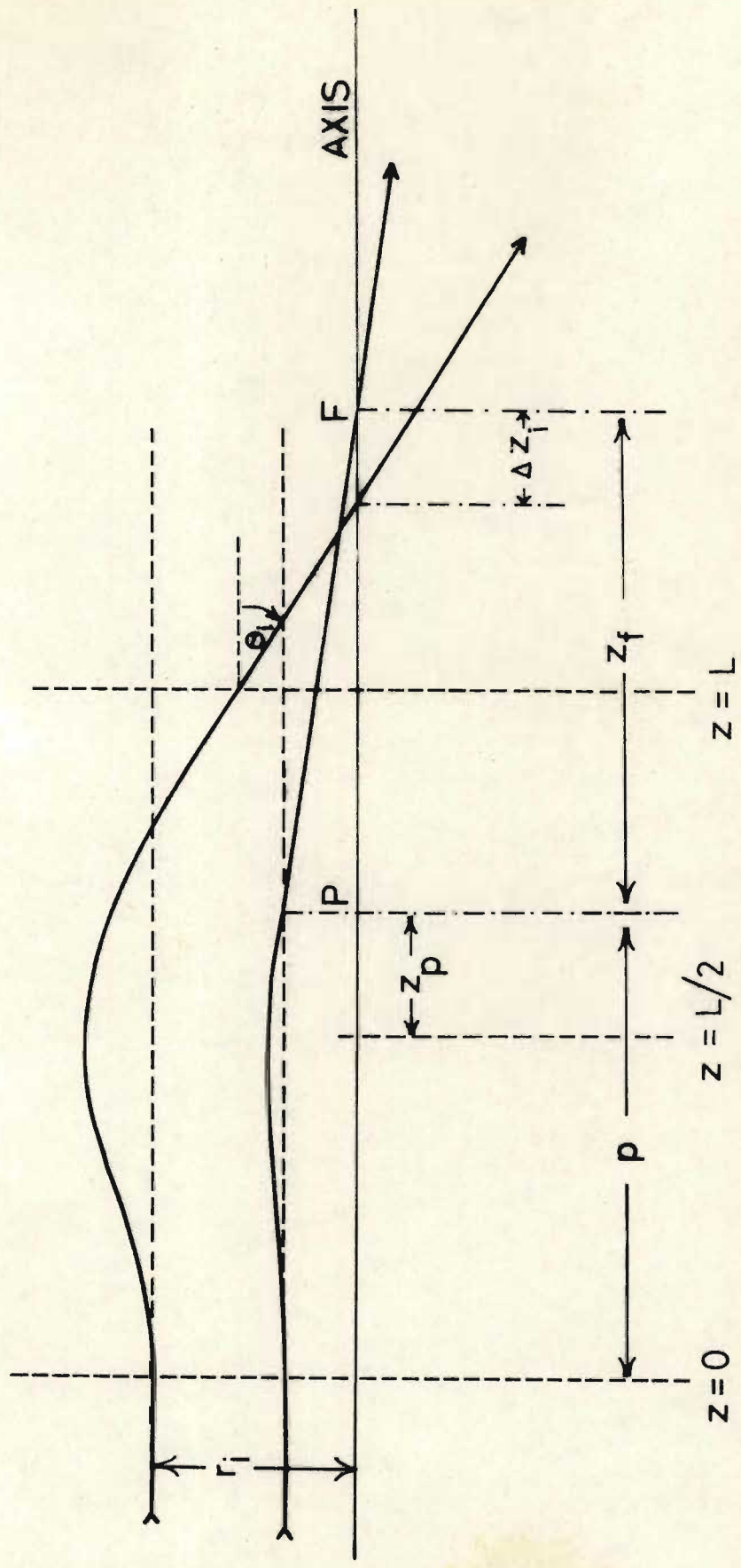


Fig. 2.1 Paraxial and zonal rays through electrostatic field.

Note on normalization: Normalization with respect to maximum electric intensity is required when comparing various lenses or component fields. In the case of C(1) and C(2), for instance, C(2) would contain electric intensity values at  $r = A$  which are twice as large as those found at comparable points in C(1), if they have the same length  $L$ . All single components can therefore be normalized with respect to maximum electric intensity by multiplying the physical dimensions of C(n) by a factor  $n$ .

The electron optical properties covered in this report are the focal distance, the position of the principal plane, the focal length and the spherical aberration. The chromatic aberration is mentioned briefly in Section (2.2).

## 2.2 The focal distance.

The Gaussian focal distance  $z_d$  (i.e. the distance between the Gaussian focal point and the point  $z = 0$ ) is plotted for various normalized component fields vs.  $1/S$  [Fig. (2.2)]. As in following graphs, only exterior focal points are represented (i.e. objective and no projective properties are shown). Component fields or ranges of  $S$  resulting in divergent lens action are also excluded from this chapter, but some of these cases are discussed in Ch. (3).

For small values of  $S$ , it seems as if  $z_d$  is proportional to  $1/S$ , for C(-1), C(-3) and C(-5).



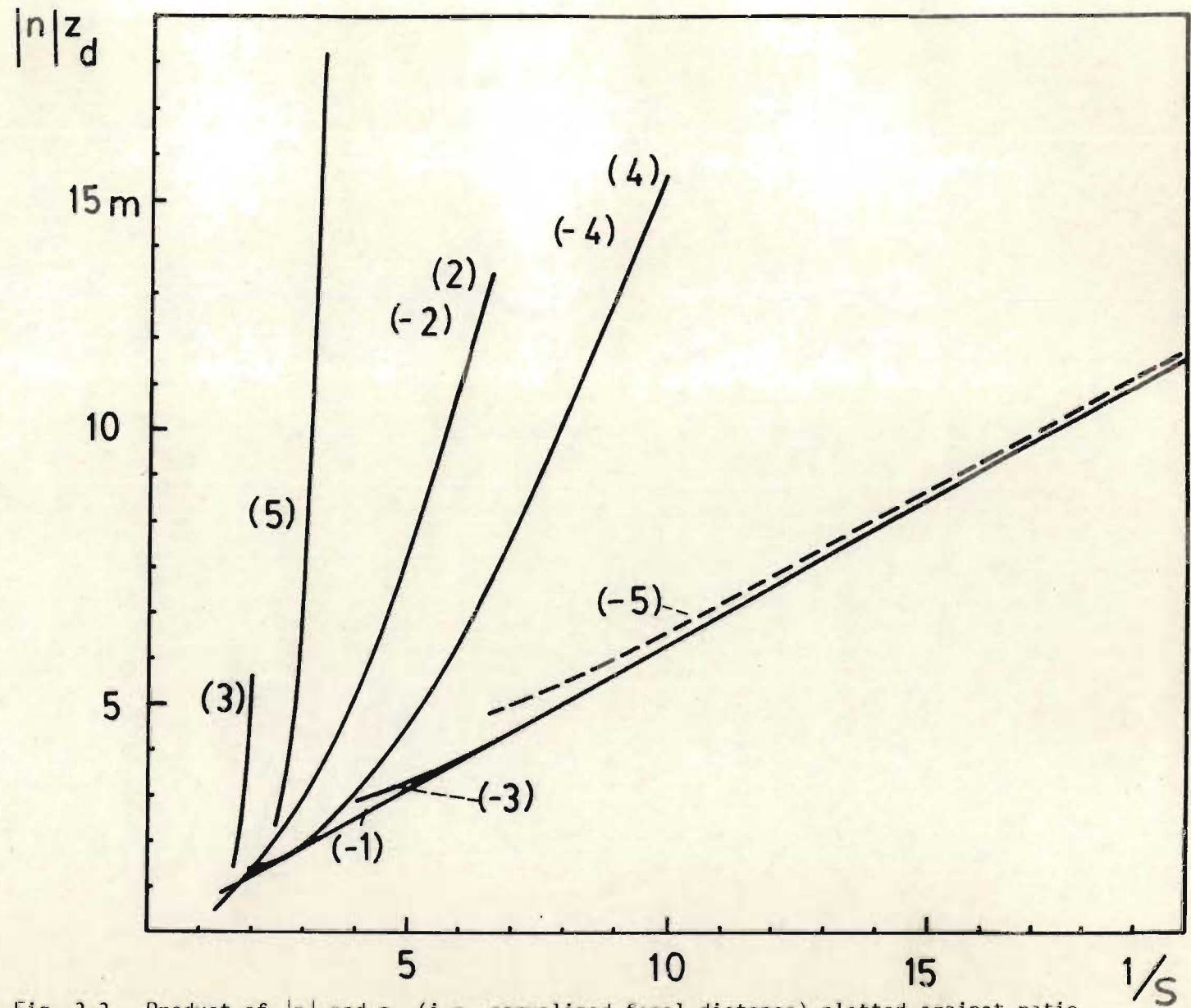


Fig. 2.2 Product of  $|n|$  and  $z_d$  (i.e. normalized focal distance) plotted against ratio  $(1/S)$  for various basis fields,  $C(n)$ . The values of  $n$  appear in brackets.

When  $z_d$  is plotted vs.  $1/S^2$ , straight lines are obtained for  $C(+2)$ ,  $C(+4)$ ,  $C(-2)$  and  $C(-4)$  in their weak ranges [Fig.(2.3)]. No simple relationship has been found for  $C(+3)$  and  $C(+5)$  in their convergent ranges.

Note on the chromatic aberration :

The chromatic aberration,

$$C_C = V \frac{\partial z_f}{\partial V}$$

may be found from Fig. (2.2) by noting that the slope of any of the curves may be equated to  $(1/V) \partial z_f / \partial V$  (where  $V$  is the potential energy of the electron in the field free region).

Low values of  $C_C$  are reached at low values of  $z_f$ , and the components  $C(-1)$  and  $C(4)$  appear to be superior to other components.

### 2.3 The principal plane.

The principal surface is defined [Fig. (2.1)] as the locus of the points of intersection of the linear extrapolations of the rays entering and leaving the field. As a first approximation the surface may be considered to be plane (the Gaussian principal plane) and the distance  $z_p$  between this surface and the geometrical centre of the field is plotted vs.  $S$  [Fig. (2.4)].

The curves may be divided into four groups, according to whether they are symmetrical or asymmetrical and initially accelerating or decelerating.

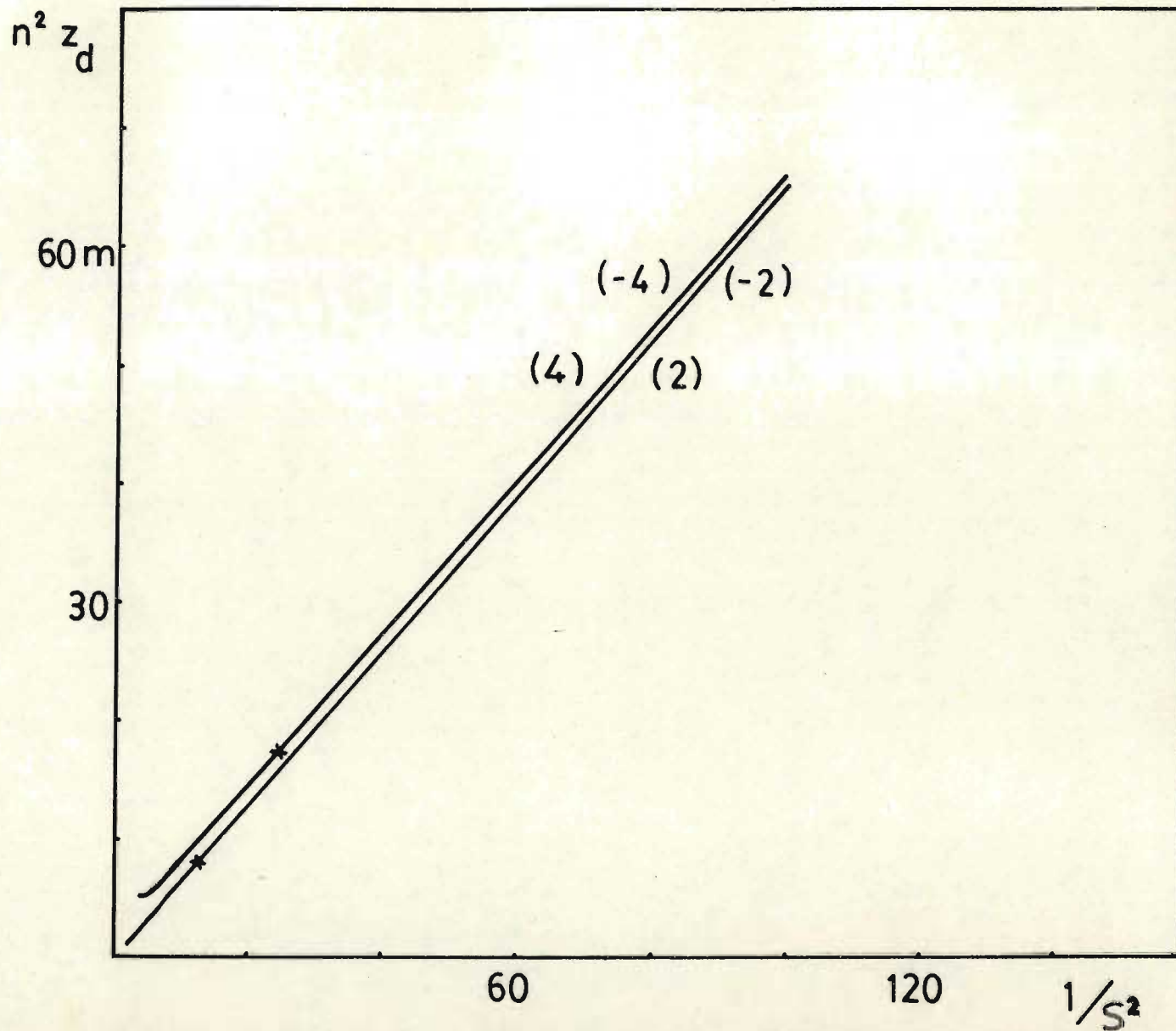


Fig. 2.3  $n^2 z_d$  plotted against ratio  $(1/S^2)$  for various basis fields  $C(n)$ . The graphs for the fields  $C(-2)$  and  $C(-4)$  do not reach lower focal distance values than indicated by the + symbols.

The large positive values of  $z_p$  for the fields  $C(+2)$  and  $C(+4)$  bring about short focal lengths for these fields; see also [Fig. (2.5)].

#### 2.4 The spherical aberration

The spherical aberration of electron lenses may be specified i.a. by expressing the longitudinal aberration  $\Delta J$  or transverse aberration  $\Delta r$  in terms of series expansions in which even powers of the angular aperture  $\theta_i$  or the linear aperture  $r_a$  appear.  $r_a$  may be measured in any of a number of possible aperture planes [see also Ch. (4)].

Although the values of  $\Delta J$  or  $\Delta r$  are known to several significant figures [see Section (3)], the less precise representation by means of the primary aberration coefficient

$$C_s = \frac{\Delta J}{\theta_i^2}$$

is used in this report to facilitate comparison of present results with published data.

If the dimensionless quantity  $C_s/z_f$  is used to indicate the quality of a field as far as spherical aberration is concerned, it may be seen from Fig. (2.5) that components  $C(n)$  of small  $n$  are superior.

The spherical aberration of some fields with divergent action is discussed in Ch. (3).

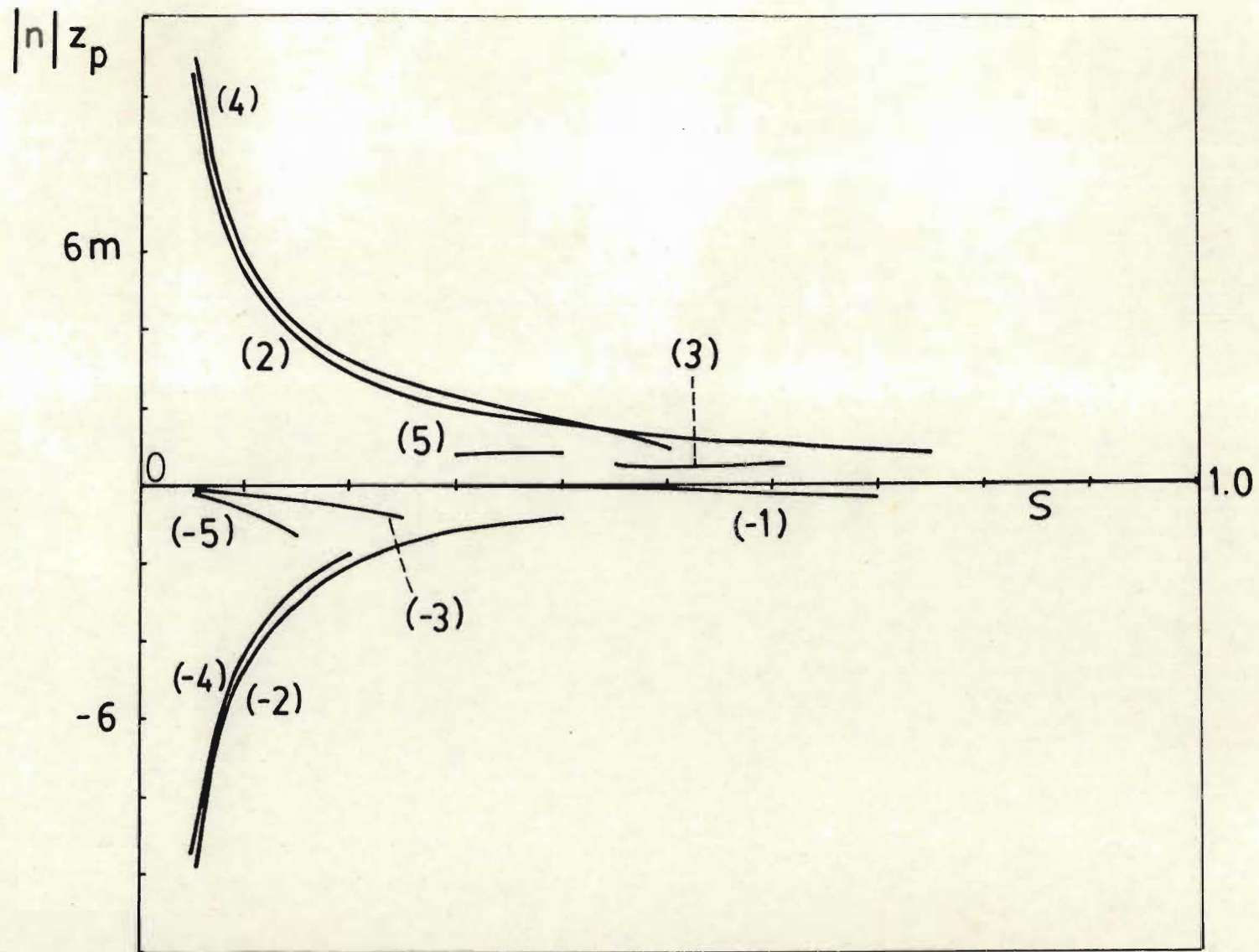


Fig. 2.4 The product of  $|n|$  and  $z_p$  (distance between principal plane and geometrical centre of field) is plotted against  $S$ .

### 3. PRECISION OF THE RESULTS.

A simple predictor-corrector method of ray tracing was used throughout this study. In calculating the force on the electron, modified Bessel functions of the first kind and of orders nought and one had to be evaluated. Since the rational approximation of tenth degree quoted by Abramowitz et. al. (1968) allowed a precision of 1 part in  $10^7$  only, the more time consuming series expansion of Eq. (2.7) had to be utilized for  $I_0$ , and a related one for  $I_1$ .

Although the arithmetic was carried out to 16 significant figures, the Bessel functions were normally evaluated to 12 significant figures only. The factor limiting the final precision reached, was the number of steps in the trajectory calculation, which varied from  $N=80$  to  $N=1280$ . The precision of  $z_f$  varied between 3 and 5 significant figures, depending upon the value of  $N$  and the strength of the lens. The precision of  $C_s$  varied between 1 and 3 significant figures.

### 4. PHYSICAL APPROXIMATION

Although the physical approximation of the Fourier-Bessel fields is discussed in more detail in Ch. (4), an example is given in Fig. (2.6) for a  $C(+1)$  field.

Equipotential lines are drawn for  $\phi(r,z)$ , as given by Eq. (2.2) for  $r < A$ , taking  $A_1=1$ , and  $A_n=0$ ,  $\forall n > 1$ .

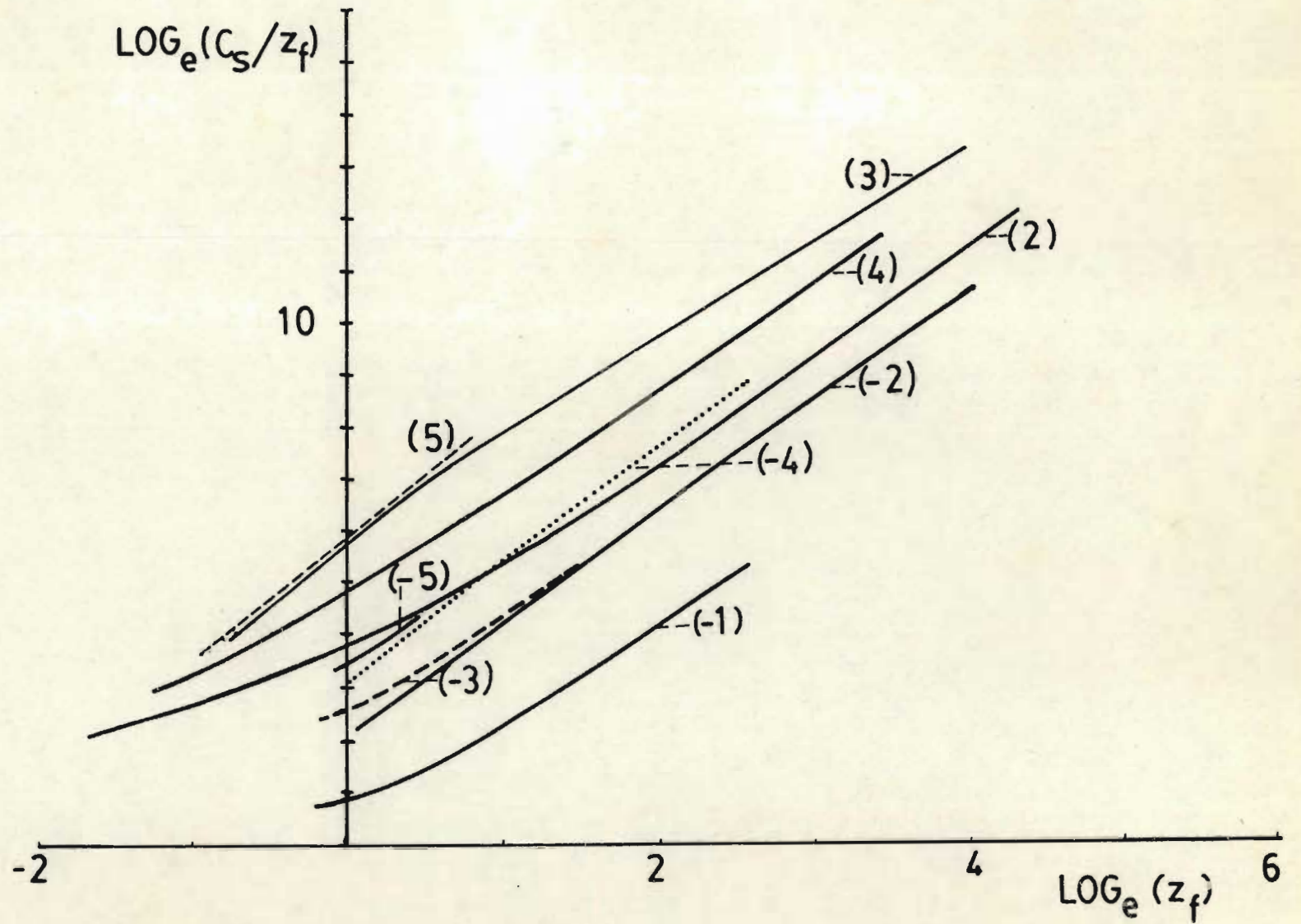


Fig. 2.5  $\text{Log}_e (C_s/z_f)$  plotted against  $\text{Log}_e (z_f)$ .

For the region  $r > A$ ,  $0 < z < L$ , we draw equipotential lines for [see Ch. (1)]:

$$\phi(r,z) = \frac{K_0(\pi r/L) \sin(\pi z/L)}{K_0(\pi A/L)}$$

A suitable equipotential line is chosen, and a physical electrode of this shape and with the corresponding potential placed in position.

The size of the gaps between this electrode and the planes  $z = 0$  and  $z = L$  depends i.a. upon the  $A/L$  ratio, and it may be required to position a number of ring electrodes to establish the required potentials in the gaps. The potentials of the ring electrodes are supplied from a resistance chain. If proper care is taken the physical configuration should be a fair approximation of the mathematical field of which the electron optical properties are known from the computer study.

## 5. SOME CONCLUSIONS

5.1 As far as the focal length is concerned, it seems as if the fields  $C(n)$  with low values of  $n$  are preferable if strong converging lenses are required. Particularly short focal lengths are reached with  $C(+2)$  due to the right shift of the principal plane.

5.2 Low values of the spherical aberration are reached with  $C(-1)$  which is matched only by  $C(+2)$  at short focal lengths.



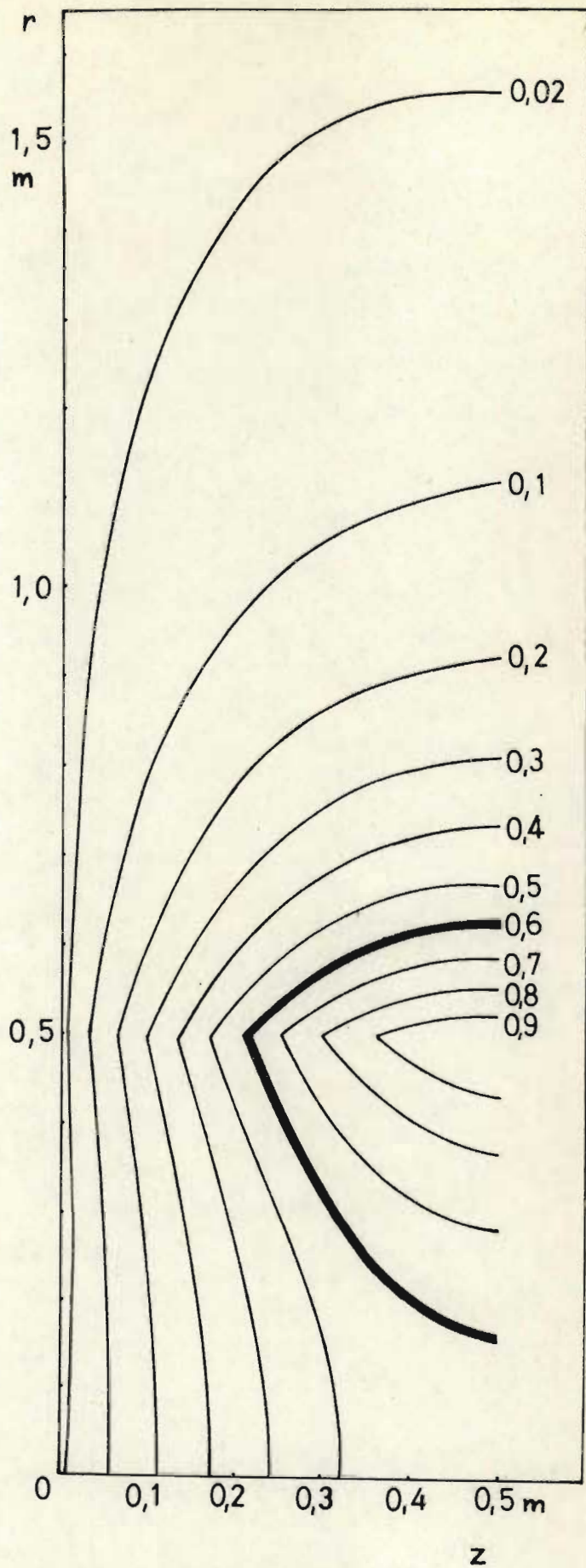


Fig. 2.6 Equipotential lines for the field  $C(+1)$  with  $A = 0,5$  and  $L = 1,0$ .  
Only the left upper quadrant is given.

From Fig. (2.5) it can be seen that fields of the same convergence have spherical aberrations which depend upon the values of  $n$ . The possibility therefore exists of superposing or juxtaposing two or more fields of different  $n$  in an attempt to reduce or eliminate the spherical aberration of the combined field. Such syntheses are discussed in the next two chapters.

5.3 Fields  $C(+3)$  and  $C(+5)$  are divergent for fast electrons (small  $S$ ), but are convergent for slow electrons (large  $S$ ), due to a reduced speed in the negative potential regions where the radial acceleration is negative. Only  $C(+1)$  is divergent for electrons of all velocities. A discussion of the possibility of divergent electron optical lenses is given in Ch. (3). See also Section (2.2) of Ch. (7) in this regard.

5.4 In the case of single component fields the chromatic aberration reaches a minimum for large values of  $S$ , where the spherical aberration is also minimized. This does not seem to be true for strong superposed fields, as shown in Ch. (4).

AN ANALYTICAL STUDY OF WEAK BASIS FIELDS AND OF SOME SYNTHESSES OF TWO COMPONENTS

1. INTRODUCTION

In Ch. (2) some electron optical properties of various Fourier-Bessel component fields

$$C(\pm n) = \pm \frac{I_0(n\pi r/L)}{I_0(n\pi A/L)} \sin(n\pi z/L)$$

were described.

In this chapter an approximate analytical study is made of weak fields, so as to systematize the results of the numerical studies of Chs. (2) and (4) and aid in predicting the properties of synthesized fields. Only rays entering the field in a direction parallel to the axis are considered here.

2. TRAJECTORY APPROXIMATION

When electrons pass through rotationally symmetrical electric intensity fields, it is found that both  $v_z$ , the longitudinal velocity and  $r$ , the radial coordinate, change.

To simplify the analytical integration it is assumed in this study that neither  $r$  nor  $v_z$  change appreciably. This implies either that the particles have high initial  $z$  velocities, or that the electric intensities are small, i.e. the ratio  $S$  of Section (2.1) of Ch. (2) is limited to small values only.

It may be shown that if this assumption is made for  $C(\pm n)$  with  $n$  an even number, the field will cause no convergence or divergence. For these asymmetrical fields the lens action results from the variations in  $v_z$  and  $r$ , and a different procedure must be followed [Ch. (4)].

The same remarks apply to both symmetrical and asymmetrical "open" lenses (i.e. lenses not closed off by thin conducting foils or gauzes). This can be seen by considering the electric intensity flux through an infinitely long coaxial cylinder. [It is shown in Ch. (5) that in Einzel type open lenses the flux caused by  $I_0$  (modified Bessel function) type potential fields is equal and opposite to the flux caused by the associated  $J_0$  (ordinary Bessel function) type fields.]

The results of Sections (4) - (9) apply to symmetrical fields only, in view of the above remarks.

### 3. THE RADIAL VELOCITY $v_r$ .

We investigate the trajectory of an electron of charge to mass ratio  $q_m$  which enters the field  $C(n)$  from the left, and parallel to the axis.

The radial velocity  $v_r(t)$  may be found by integration :

$$v_r(t) = \int_0^t a_r dt = \int_0^z \frac{a_r}{v_z} dz$$

The radial acceleration  $a_r$  is given by the radial derivative of  $C(n)$  :

$$a_r = \left| q_m \right| \frac{n\pi}{L} \frac{I_1(n\pi r/L)}{I_0(n\pi A/L)} \sin(n\pi A/L) \quad (3.1)$$

where  $I_1$  is the modified Bessel function of the first kind and of order one.

We now assume that  $r$  does not change appreciably (so that the Bessel functions need not be integrated here), and that  $v_z$  may be considered constant (removing  $v_z$  from the integration).

Integrating,

$$v_r(z) = \frac{\left| q_m \right|}{v_z} \frac{I_1(n\pi r/L)}{I_0(n\pi A/L)} \left[ 1 - \cos(n\pi z/L) \right] \quad (3.2)$$

At the exit plane,  $z = L$ , the radial velocity is

$$v_{re} = \frac{2 \left| q_m \right|}{v_z} \frac{I_1(n\pi r/L)}{I_0(n\pi A/L)} \quad \text{if } n = 1, 3, 5, \dots \quad (3.3)$$

$$\text{or } v_{re} = 0 \quad \text{if } n = 2, 4, 6, \dots$$

The constant  $q_m$  may be eliminated by substituting

$(2 \left| q_m \right| / v_z^2) I_0(0) / I_0(n\pi A/L)$  by  $S$  :

$$v_{re} = S v_z I_1(n\pi r/L) \quad \text{for } n = 1, 3, 5, \dots \quad (3.4)$$

4. THE ANGULAR DEFLECTION,  $\theta_i$ .

The angular deflection  $\theta_i$  at the exit plane is given by

$$\theta_i = \text{arc tan}(v_{re}/v_z) \doteq 2 |q_m| \frac{I_1(n\pi r/L)}{I_0(n\pi A/L)} \text{ for } n = 1, 3, 5, \dots \quad (3.5)$$

$$\doteq S I_1(n\pi r/L)$$

5. THE RADIAL DISPLACEMENT  $\delta r$

The radial displacement may be found by integration :

$$\delta r = \int_0^T v_r(t) dt$$

$$\doteq |q_m| \frac{1}{v_z} \int_0^z \frac{I_1(n\pi r/L)}{I_0(n\pi A/L)} \left[ 1 - \cos(n\pi z/L) \right] dz$$

if  $v_z$  may be assumed to be constant.

As a first approximation of ratio  $\delta r/r$  may be assumed to be very small, so that the Bessel function  $I_1(n\pi r/L)$  need not be integrated.

Integrating :

$$\delta r = \frac{|q_m| I_1(n\pi r/L)}{v_z I_0(n\pi A/L)} \left[ z - \frac{L\pi}{n} \sin(n\pi z/L) \right] \quad (3.6)$$

At the exit plane :

$$\delta r_e = |q_m| \frac{L}{v_z} \frac{I_1(n\pi r/L)}{I_0(n\pi A/L)} \quad (3.7)$$

$$\text{or} = \frac{LS}{2} J_1(n\pi r/L) \quad (3.8)$$

$$\text{or} = \frac{Lv_{re}}{2v_z} \quad (3.9)$$

6. THE FOCAL DISTANCE,  $z_d$ .

The focal distance  $z_{dr}$  (i.e. the distance between  $z = 0$  and the point where the axis is cut by the ray entering the field at a radial distance  $r$ ) may be calculated from

$$\frac{z_{dr} - L}{r + \delta r_e} = \cot(-\theta) = \frac{v_z}{-v_{re}}$$

as follows from Fig. (2.1)

Substituting for  $\delta r_e$  from Eq. (3.7) and for  $v_{re}$  from Eq. (3.3) we find

$$z_{dr} = \frac{-r}{S J_1(n\pi r/L)} + \frac{L}{2} \quad (3.10)$$

The Gaussian focal distance  $z_{dg}$  is found by calculating

$$\begin{aligned} z_{dg} &= \lim_{r \rightarrow 0} z_{dr} \\ &= \lim_{r \rightarrow 0} \left[ \frac{-r}{S \frac{n\pi r}{2} \left[ 1 + \frac{(n\pi r)^2}{8} + \dots \right]} + \frac{L}{2} \right] \\ &\doteq L \left[ \frac{2}{n\pi S} + \frac{1}{2} \right] \end{aligned} \quad (3.11)$$

in which  $I_1$  has been replaced by its series expansion. The above expressions are valid for all  $C(n)$  for which  $n$  is negative and odd.

#### 7. THE PRINCIPAL PLANE

From Fig. (3.1) it follows that

$$\frac{(L/2) - z_{pg}}{\delta r} = \frac{v_z}{v_{re}}$$

where  $z_{pg}$  is the distance between the Gaussian principal plane and the centre of the field.

$$\text{Substituting from Eq. (3.9) we find } z_{pg} = 0 \quad (3.12)$$

#### 8. THE FOCAL LENGTH, $z_{fr}$ .

The focal length of a ray entering the field at a radial distance  $r$  is found from Eqs. (3.10) and (3.12)

$$z_{fr} = \frac{-r}{S I_1(n\pi r/L)} \quad (3.13)$$

and the Gaussian focal length is found from Eqs. (3.11) and (3.12) :

$$z_{fg} = \frac{2L}{n\pi S} \quad (3.14)$$

#### 9. LONGITUDINAL SPHERICAL ABERRATION

The longitudinal spherical aberration  $\Delta J$  is found from Eqs. (3.10) and (3.11) :

$$\Delta J = z_{dr} - z_{dg} \doteq \frac{n\pi r^2}{4S L} \quad (3.15)$$

using the series expansion for  $I_1$ , and neglecting terms containing



fourth and higher powers of  $r$ .

Taking into account the conventional definition of the sign of  $\Delta J$ , as expressed by Eq. (3.15), we note that the fields  $C(n)$  with  $n$  negative and odd will have positive spherical aberration, i.e. zonal rays will cut the axis closer to the centre of the field, than paraxial rays.

The longitudinal spherical aberration constant  $C_s$  as referred to an object at  $z \rightarrow \infty$  is given by

$$\begin{aligned} C_s &= \frac{\Delta J}{\theta^2} = \frac{\pi r^2}{4S^3 L I_1^2(\pi r/L)} \\ &= \frac{L}{\pi S^3} \end{aligned} \quad (3.16)$$

in which Eq. (3.5) has been used, and in a series expansion for  $I_1$  all terms containing powers of  $r$  higher than one have been neglected.

The relative longitudinal spherical aberration constant is given by :

$$C_{sf} = \frac{C_s}{zfg} = \frac{1}{2S^2} \quad (3.17)$$

#### 10. THEORETICAL VALUES COMPARED WITH RAY TRACING RESULTS

The theoretical predictions of the above sections are compared in Table (3.1) with the results of the computer ray tracings of Ch. (2),

Table (3.1) : Comparison of theoretical ( $X_{th}$ ) and computed values ( $X_{num}$ ) of  $v_{re}$ ,  $r_e$ ,  $z_d$ , and  $\Delta J$  for rays of different radii  $r$ . The ratio  $(X_{th}-X_{num})/X_{th}$  is given.  $S = 0,02$ .

$X \backslash r$	0,001m	0,004m	0,016m	0,064m
$v_{re}$	-4,0E-3	-4,0E-3	-4,0E-3	-4,0E-3
$r_e$	N.A.	-1,2E-2	-1,2E-2	-1,2E-2
$z_{dr}$	4,1E-3	4,1E-3	4,1E-3	4,1E-3
$\Delta J$	N.A.	0,38	0,024	1,0E-3

Table (3.2): The ratios  $R_3$  and  $R_4$  for various values of  $n$ .

Radius  $r = 0,1 L$ .

	$n$ ↓	$R_2$	$R_3$	$R_4$	$R_2+R_3+R_4$
Cor- red- ted  by means of  B.C.(n)	3	0	$-4,56 \times 10^{-4}$	$-9,38 \times 10^{-6}$	$-4,65 \times 10^{-4}$
	5	0	$-1,26 \times 10^{-3}$	$-6,77 \times 10^{-5}$	$-1,33 \times 10^{-3}$
	7	0	$-2,48 \times 10^{-3}$	$-2,55 \times 10^{-4}$	$-2,74 \times 10^{-3}$
Uncor- rected	-	$1,23 \times 10^{-2}$	$4,11 \times 10^{-3}$	$7,60 \times 10^{-5}$	$1,65 \times 10^{-2}$

by quoting relative differences between the theoretical and numerical values, for various rays entering a weak field C(-1) characterized by  $S = 0,02$ .

#### 11. CONDITION FOR NOUGHT SPHERICAL ABERRATION

From Eq. (3.11) and Fig. (3.1) it follows that if all the rays cross the axis at the same point,

$$\frac{r}{z_{fg}} = \sin(-\theta) = \frac{-v_{re}}{v_z} \quad (3.18)$$

so that we require that

$$v_{re} \propto r \quad (3.19)$$

for a field that shows zero spherical aberration. The condition of Eq. (3.18) is valid for weak fields only, in view of the approximate nature of Eq. (3.11).

Replacing the Bessel function  $I_1$  in Eq. (3.4) by its series expansion, we have for any field C(n) :

$$v_{re} = 2|q_m| \frac{n\pi r}{2L} \left\{ 1 + \frac{(n^2\pi^2 r^2)}{8L^2} + \frac{(n^4\pi^4 r^4)}{192L^4} + \dots \right\} \quad (3.20)$$

$I_0(n\pi A/L)$

from which it can be seen that Eq. (3.19) will be satisfied only if all terms but the first in the face brackets of Eq. (3.20) can be eliminated. We also note that i) the sign of  $v_{re}$  depends upon the sign of  $n$ , and ii) the convergence of the series in Eq. (3.20) depends upon  $n^2$ . If we aim to eliminate third order spherical aberration completely, we could superpose a field C(-1) and a

field  $B$  times  $C(n)$ , with  $n$  positive and odd, and  $B$  a constant chosen so as to equate the magnitudes of the terms containing  $r^2$  in the given series.

Writing  $x = \pi r/L$  and  $y = \pi A/L$ ,

$$v_{re} = \frac{2|q_m|}{v_z} \left[ \frac{-I_1(x)}{I_0(y)} + \frac{B I_1(nx)}{I_0(ny)} \right]$$

$$= \frac{-2|q_m|}{I_0(y)} \left[ I_1(x) - D I_1(nx) \right]$$

with  $D = \frac{B I_0(y)}{I_0(ny)}$

Replacing the Bessel functions  $I_1$  by their series expansions, and simplifying :

$$v_{re} = \frac{-x}{v_z I_0(y)} \left[ (1-Dn) \frac{x^2}{8} (1-Dn^3) \frac{x^4}{192} (1-Dn^5) \frac{x^6}{9216} (1-Dn^7) \right. \\ \left. + \dots \right] \quad (3.21)$$

To eliminate the  $x^2$  term, we choose

$$1 - Dn^3 = 0$$

i.e.  $B = \frac{I_0(n \pi A/L)}{n^3 I_0(\pi A/L)} \quad (3.22)$

## 12. QUALITY OF CORRECTION

To evaluate the degree to which the spherical aberration has been reduced, it may be helpful to investigate the contributions of the

terms in the series of Eqs. (3.20) and (3.21). Let  $R_i$  be the ratio of the  $i$ -th term and the first term in either of the expansions, and let us investigate a ray of radius  $r = 0,1L$ . With  $D = 1/n^3$  it is shown in Table (3.2) that correction by means of  $C(3)$  is superior to  $C(5)$  and  $C(7)$ . For a more complete elimination of the spherical aberration, it would be profitable to eliminate not only the third order aberration, but higher orders as well; see Chs. (4), (7) and (9).

#### 12.1 Ray tracing results.

The spherical aberration coefficient  $C_s$  has been calculated from the focal points of rays entering the field  $C(-1) + B.C(3)$  parallel to the axis. Table (3.3) shows  $C_s$  values for various radii and values of  $B$ .  $S = 0,02$  for all the rays. It is seen that the uncorrected field (i.e.  $B=0$ ) shows a considerably larger aberration than the corrected fields. From Eq. (3.22) we predict that the third order spherical aberration should vanish with  $B=0,212$  (for the expansion radius  $A=0,2L$ ), but the results in the table indicate a slightly larger value, probably  $B=0,222$ .

### 13. EXISTENCE OF NEGATIVE SPHERICAL ABERRATION

In Section (12) it was seen that the corrected field had values  $R_3$  and  $R_4$  which were negative. Investigation of Eq. (3.21) shows that if  $D$  is gradually reduced,  $R_2, R_3, R_4$ , etc., would in turn all become positive. On the other hand, if  $D$  is chosen to be larger than  $1/n^3$ , all the terms after the first in the expansion would be

Table (3.3): The spherical aberration coefficient  $C_s$  as calculated from rays of different initial radii  $r$ , passing through fields  $C(-1) + B.C(3)$ , for various values of the amplitude factor  $B$ . The value  $B=0$  refers to the uncorrected field  $C(-1)$ .  $S = 0,02$  and  $A/L = 0,2$ .

$r \backslash B$	0	0,212	0,217	0,222
0,01	$1,2 \times 10^3$	74	36	0,66
0,02	$1,2 \times 10^3$	72	37	-1,0
0,03	$1,2 \times 10^3$	70	34	-3,8
0,04	$1,2 \times 10^3$	66	31	-7,8
0,05	$1,2 \times 10^3$	61	26	-12,9
0,06	$1,2 \times 10^3$	55	20	-19,1

negative for all  $r < A$ . This implies that such a field would show negative spherical aberration for all rays of  $r < A$ . Table (3.3) also shows some negative values of  $C_S$ .

The existence of negative spherical aberration and the possibility of reducing the spherical aberration of a positive lens by means of a juxtaposed negative lens have been reported before [see Ch. (7) for a discussion of current literature].

In the solutions described in Sections (11) and (12), the correction is not brought about by juxtaposing two fields, but by superposing fields with divergent and convergent actions.

The presence of the conducting foils introduces a discontinuity into the field, and therefore the above results do not constitute a violation of Scherzer's Theorem [Scherzer (1936)] (which asserts the impossibility of negative spherical aberration in rotationally symmetrical fields).

#### 14. PHYSICAL IMPLEMENTATION

A more complete discussion of the ways in which the field syntheses may be brought about by physical electrodes is given in Ch. (4) but by summary it may be stated that some fields may be obtained by positioning relatively few (one or three) conducting electrodes between the two outer earthed electrodes (type I), whereas in other cases it is required to position a much larger number of ring electrodes in the space between the central electrode and the outer

earthed electrodes (type II).

Fig. (3.1) shows equipotential lines for the field  $C(-1) + 0,212 C(3)$ , and it can be seen that the type II solution applies here. Ring electrodes are shown by circles, and the suggested central electrode by a heavy solid line.

15. LIMITATION ON THE EXPANSION RADIUS A.

For a field of type II the potentials of the electrodes would be obtained from a potential divider resistor chain, and it may be advantageous to limit the electrode potential to one polarity only, so that all the potentials can be obtained from one power supply. This will be the case as long as the constant B does not exceed a certain maximum value  $B_m$ , and it can be shown that

$$B_m = \frac{1}{n} \quad (3.23)$$

so that Eq. (22) becomes 
$$\frac{I_0(n\pi A_m/L)}{I_0(\pi A_m/L)} = n^2 \quad (3.24)$$

in which  $A_m$  is the maximum expansion radius for physical configurations of single polarity. Solving Eq. (3.24) it is found that  $A_m/L = 0,4517; 0,3302$  or  $0,2654$  for  $n = 3; 5$  or  $7$  respectively. On the basis of this information and the contents of Table (3.2) it seems as if the choice of  $n = 3$  would be the most advantageous for weak fields.



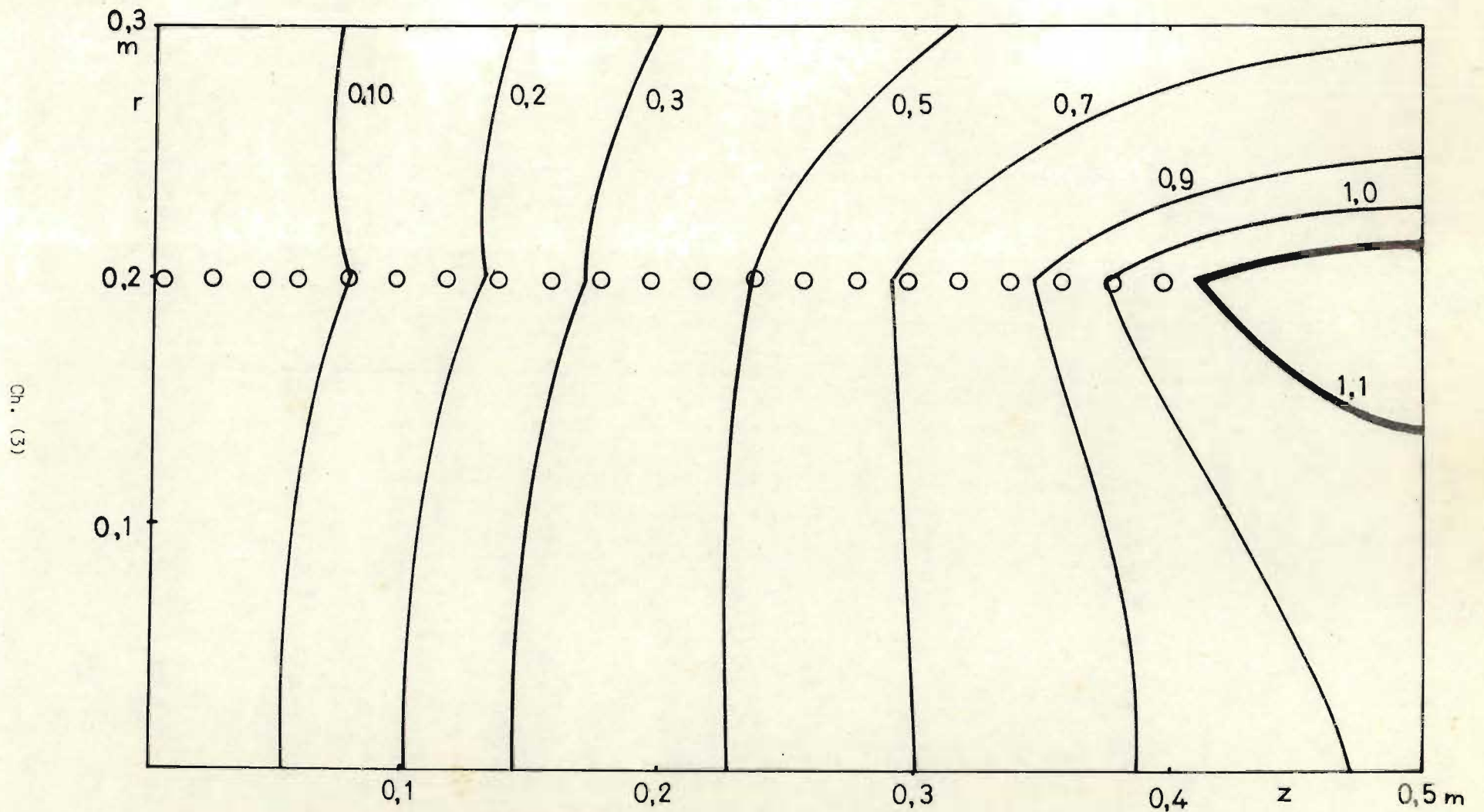


Fig. 3.1 Equipotential lines for the field  $C(-1) + 0,212 C(3)$  with  $A = 0,2m$  and  $L = 1,0m$ .

Only the left upper quadrant is given.

16. CONCLUSION

Both analytical predictions and ray tracing results point at i) the possibility of reducing the spherical aberration by superposing certain weak Fourier-Bessel fields, and ii) the occurrence of negative spherical aberration values for some weak fields.

Because of the simplifying assumptions of Section (2), the theory of this chapter cannot be expected to apply to strong fields, and the electron optical properties of the latter are found by computer ray tracing, as is discussed in Ch. (4).

SYNTHESES REPRESENTING STRONG TWO-FOIL LENSES WITH REDUCED SPHERICAL ABERRATION, AS OBTAINED BY COMPUTER RAY TRACING

1. INTRODUCTION

In Ch. (2) it was seen that the basis fields  $C(\pm n)$  individually showed large spherical aberration,  $C_S$ , and this was explained in Ch. (3) for weak fields, by investigating the series expansions for  $C(\pm n)$ . In Ch. (3) it was also shown how a reduction in  $C_S$  could result from combining two basis fields. Only weak fields were dealt with, and it was not possible to obtain small values for  $C_S$  for paraxial and zonal rays simultaneously if the syntheses were restricted to two fields only.

In this chapter an attempt will be made to obtain a reduction in  $C_S$  for strong fields, and up to four fields will be allowed in order to accommodate both paraxial and zonal rays. As in the previous two chapters, the functions  $\phi_n(r; z)$  are chosen with only the following restrictions in mind :

- i) the designed lens will be a foil lens and only parallel plane foils are allowed (in view of the fact that plane foils are much easier to produce than those of specified curvature);
  
- ii) the lens will be symmetrical w.r.t. the plane  $z = L/2$ , where  $L$  is the distance between the two foils (for simplicity we take  $L = 1\text{m}$  in this study);

iii) the final field must be such that it can be approximated by physical electrodes; therefore we exclude distributions containing terms  $K_0(r)$ , the modified Bessel functions of the second kind and of order zero. [See also Section (4.1.6.1.i) of Ch. (1) and Section (5) of Ch. (9)].

In later chapters, conditions i) and ii) will be dropped, allowing open and/or asymmetrical lenses to be investigated.

The functions  $\phi(r; z)$  chosen in this study are the only basic solutions of Laplace's equation and the boundary conditions listed in Section (2), and therefore the author believes that the required potential field  $\Psi_r(r; z)$  (in our case the space charge free symmetrical foil lens of minimum spherical aberration which can be approximated by real electrodes) can be expressed as a superposition

$$\Psi_r(r; z) = \sum_{n=1}^{\infty} B_n \phi_n(r; z) \quad (4.1)$$

in the sense of a two-dimensional Fourier-Bessel expansion; and that a suitable systematic procedure will allow the determination of the constants  $B_n$  in the above series.

While recognizing that the syntheses obtained in this chapter are not optimized, but only represent improvements on the field used as a starting point, the author is, at the same time, of the opinion that in some previous investigations the optimum distributions could not be found, because of restrictions on the solution subsets; the restrictions are introduced by the a priori choices of elec=

trode forms (in some experimental studies) or classes of preferred functions (in some theoretical studies).

It must be reiterated here that the syntheses of this chapter are obtained with only one objective in mind, namely the reduction of spherical aberration in strong two-foil lenses. This objective has been chosen to illustrate the use of Fourier-Bessel methods, and it may happen that the syntheses arrived at in the process of reducing  $C_s$ , may have other lens aberrations with increased values.

## 2. POTENTIAL FIELDS AND SOME ELECTRON OPTICAL PROPERTIES

In Chs. (2) and (3) some electron optical properties were given of symmetrical component fields

$$\phi_{\pm n}(r; z) = C(\pm n) \equiv \pm \frac{I_0(n\pi r/L)}{I_0(n\pi A/L)} \sin(n\pi z/L) \quad (4.2)$$

where  $A$  is the expansion radius,  $I_0$  is the modified Bessel function of the first kind and of order zero, and  $n$  is an odd integer.

In Ch. (2) it was shown that the component fields of different  $n$ -values but of equal power show different spherical aberration values, so that the possibility seems to exist that components of different  $n$  values and carefully chosen amplitudes may be used to reduce the spherical aberration of the synthesis.

In Ch. (3) it was shown that an electron which passes through a weak field  $C(n)$  with a  $z$ -velocity,  $v_z$ , will have a radial velocity  $v_{re}$  and radial displacement  $\delta_{re}$  at the exit given by :

$$v_{re} \doteq S v_z I_1(n\pi r/L) \quad (4.3)$$

$$\text{and } \delta_{re} \doteq \frac{L v_{re}}{2 v_z} \quad (4.4)$$

where  $n$  is an odd integer,  $I_1$  is the modified Bessel function of the first kind and of order one; and  $S$  is the ratio of the saddle point potential to the kinetic energy of the particle in the field-free region  $z < 0$  or  $z > L$ :

Therefore the weak lens condition for zero spherical aberration

$$v_{re} \propto r \quad (4.5)$$

is not satisfied, as is shown by the series expansion of  $I_1$ :

$$I_1(n\pi r/L) = \frac{n\pi r}{2L} \left[ 1 + \frac{n^2 \pi^2 r^2}{8L^2} + \frac{n^4 \pi^4 r^4}{192L^4} + \dots \right] \quad (4.6)$$

Eqs. (4.3) and (4.4) were obtained analytically by assuming that neither  $v_z$  nor  $r$  changes appreciably as the electron passes through the field, i.e. the field is relatively weak. See Section (11) of Ch. (3).

For stronger fields the above assumptions are no longer valid, and a rigorous analytical treatment does not seem feasible. However, if we assume that  $r$  does not change appreciably, but that  $v_z$  varies, it is possible to find an expression for  $v_{re}$  by analytical integration, namely

$$v_{re} = - \frac{qn}{|qn|} S v_0 I_1(n\pi r/L) \left[ 1 + \frac{qn}{|q|} \cdot \frac{\pi H(r)}{8} + \frac{H^2(r)}{4} \right] \quad (4.7)$$

for fields  $C(\pm n)$ ; here  $v_0$  is the value of  $v_z$  outside the lens, and

$$H(r) = \frac{2|q| I_0(n\pi r/L)}{mv_0^2 I_0(n\pi A/L)} = S I_0(n\pi r/L)$$

This expression for  $v_{re}$  can not be expected to be sufficiently precise to attempt syntheses for strong lenses, but can serve as a useful guide.

To establish whether the assumption that  $r$  may be considered constant for purposes of Eq. (4.7) is a realistic one, rays were traced by computer through a C(3) field, and  $v_{re}$  calculated for the following cases :

- a) both  $r$  and  $v_z$  are allowed to vary;
- b) changes in  $v_z$  are suppressed during computation;
- c) changes in  $r$  are suppressed during computation.

In Fig. (4.1) the ratios

$$R_1 = \frac{(v_{re})_b - (v_{re})_a}{(v_{re})_a} \quad (4.8)$$

$$\text{and } R_2 = \frac{(v_{re})_c - (v_{re})_a}{(v_{re})_a} \quad (4.9)$$

are plotted against  $r_i$ , the radius of the ray as it enters the field. It can be seen that for the  $S = 0,01$  case the rays b) and c) correspond very closely to a), the correct ray; the Gaussian focal length in this case is 20 L. For the field  $S = 0,05$ , which gives a Gaussian focal length of 4 L, the correspondence between

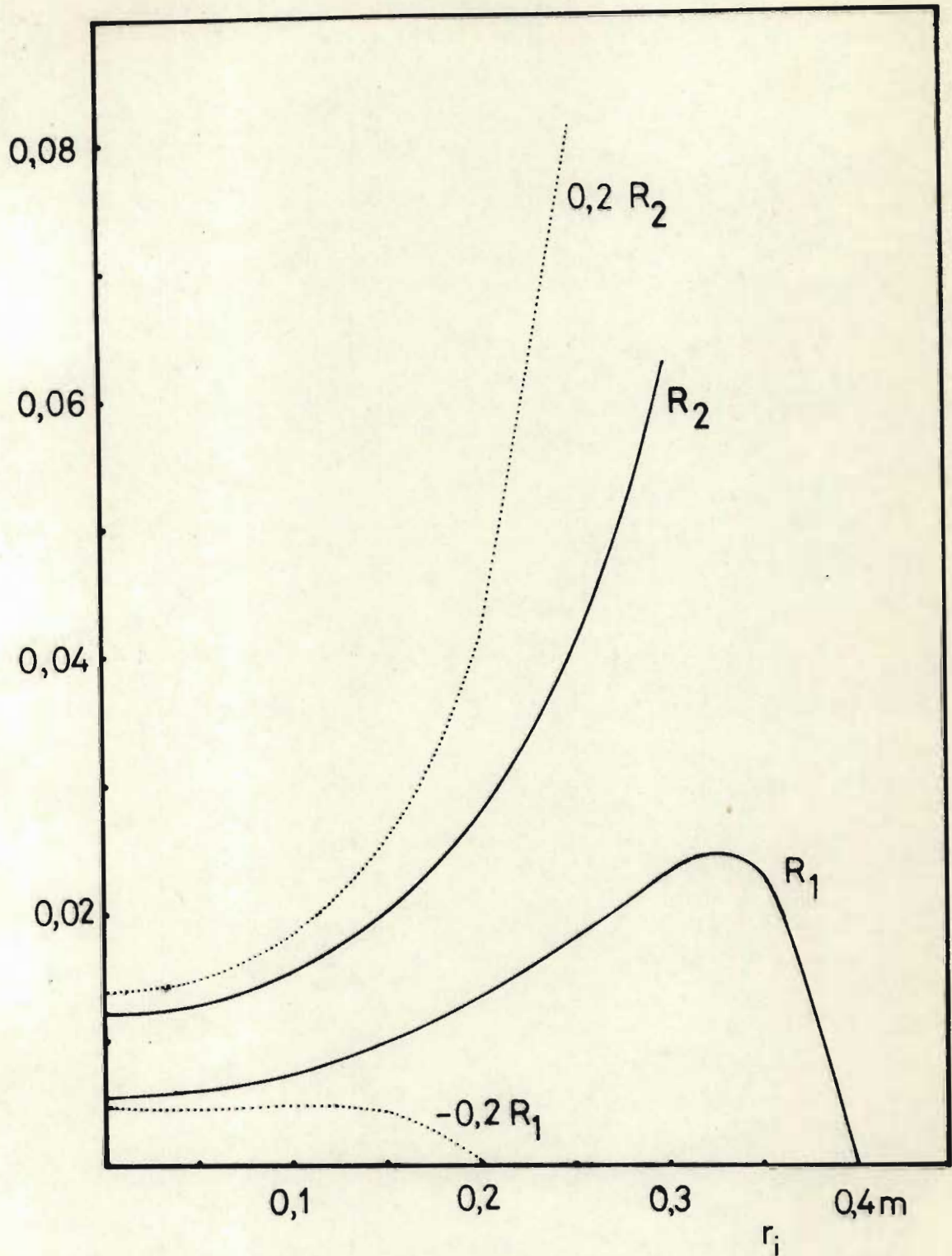


Fig. 4.1 The ratios  $R_1$  and  $R_2$  of Eqs. (4.8) and (4.9) plotted for the field  $C(+3)$  against the ray radius  $r_i$  at  $z = 0$ .

Solid lines :  $S = 0,01$

Dotted lines :  $S = 0,05$



b) and a) is still fair, whereas there is a rather large difference between c) and a). It may be noted that the assumption that  $r$  and/or  $v_z$  stays constant will be useful for weak fields  $C(\pm n)$  with even  $n$  but not with odd  $n$ ; nor for fields resembling open lenses.

In view of the above consideration one may describe the exit radial velocity by means of the following relationship

$$v_{re} = I_1(n\pi r/L) \sum_{i=0}^N A_i \left[ I_0(n\pi r/L) \right]^i \quad (4.10)$$

in which the constant  $A_i$  may be found by means of a least squares procedure. For our present purpose Eq. (4.7) suffices and the constants  $A_0$  and  $A_1$  may be obtained from Eq. (4.7). The quality of the fits are shown in Fig. (4.2) for  $N = 0, 1$  and  $2$ .

A similar description can be given of  $\delta_{re}$ , the radial displacement at the exit :

$$\delta_{re} = I_1(n\pi r/L) \sum_{i=0}^N D_i \left[ I_0(n\pi r/L) \right]^i \quad (4.11)$$

### 3. REDUCTION OF SPHERICAL ABERRATION BY SYNTHESIS

Our aim is to determine the constant in Eq. (4.1) so as to minimize the spherical aberration. It is known that the spherical aberration is not a lens constant, and this study is limited to

- i) objects at  $z \rightarrow -\infty$  and
- ii) strong fields.

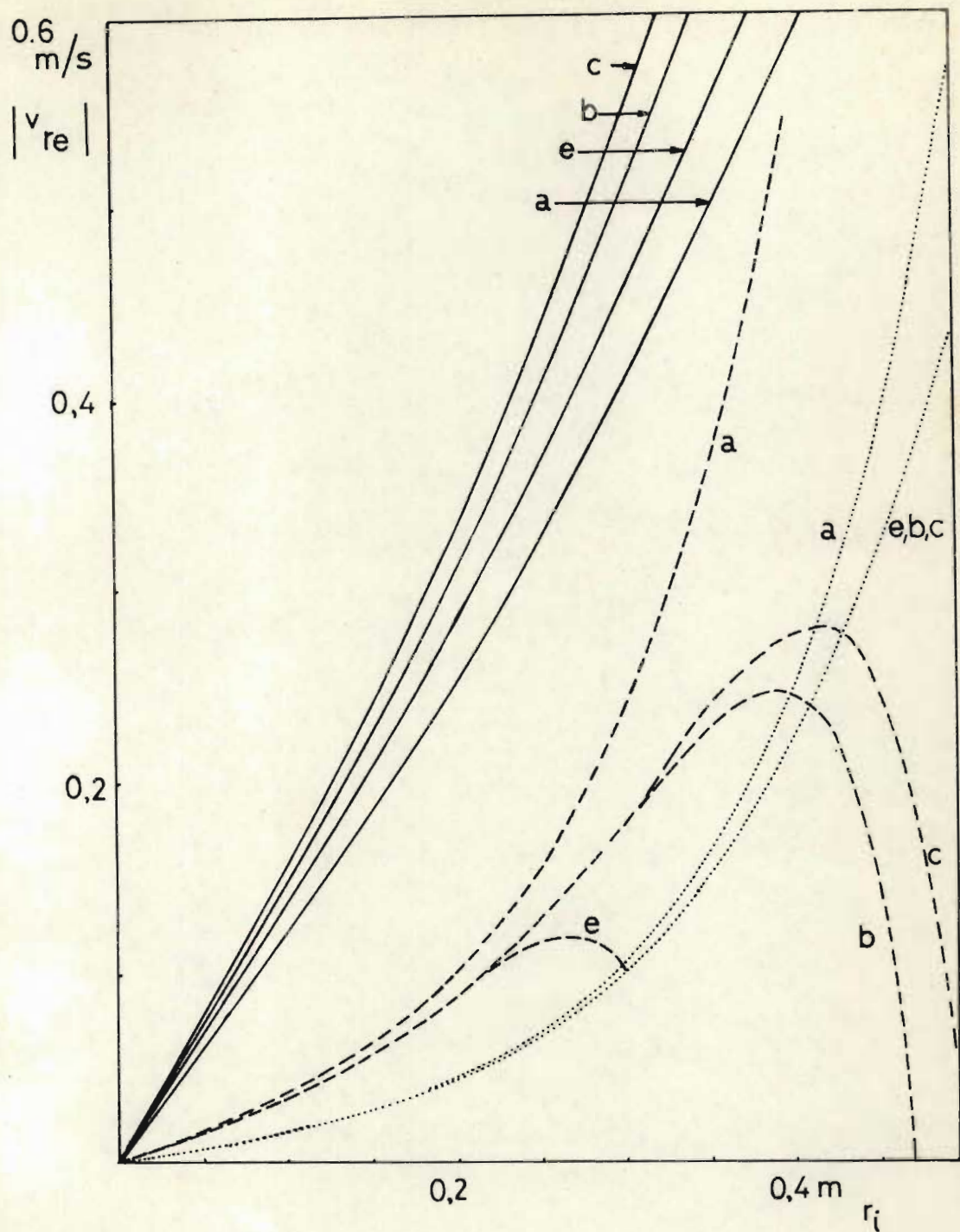


Fig. 4.2 The exit radial velocity  $v_{re}$  plotted against the ray radius  $r_i$  at  $z = 0$ .

$v_{re}$  is found : by ray tracing (lines e) and by using Eqs.(4.7) and (4.10) with  $N = 0$  (lines a),  $N = 1$  (lines b) and  $N = 2$  (lines c).

Dotted lines : field C(+3) and  $S = 0,01$

Solid lines : field C(+3) and  $S = 0,05$

Dashed lines : field C(-1) and  $S = 0,5$

First a measure must be defined to characterize the presence (or absence) of spherical aberration. In principle the constants  $A_i$  and  $D_i$  can be tabulated, since the longitudinal or transverse spherical aberrations ( $\Delta J_L$  or  $\Delta J_T$ ) can be found from these constants. Alternatively the polynomial expansion for  $\Delta J_L$  or  $\Delta J_T$  can be given, and the primary aberration constant  $C_5$  specified [Section (9) of Ch. (2)]. The latter approach is useful for the paraxial case, or when the third order aberration predominates. In the present study, however, the spherical aberration of low orders is reduced to such an extent that several terms in the (possibly alternating) series will have to be considered. This makes the comparison of various syntheses difficult, and therefore the disc of confusion itself is used as measure of the quality of the synthesis.

Subsequent to ray tracing through a synthesized field, the radius of the disc of confusion may be calculated for various planes  $z = z_i$ , so as to locate the cross-over plane. The radius of the disc of confusion in this plane is called  $R_{1,0}(r_b)$ , the subscript indicating that 100% of the incoming rays pass through this disc, assuming that a parallel electron beam of uniform density and radius  $r_b$  enters the field at  $z = 0$ .

A plane may also be found in which the radius  $R_{0,66}(r_b)$  is minimized (i.e. the radius of the disc through which 66% of the incoming beam passes). It is obvious that both  $R_{1,0}(r_b)$  and  $R_{0,66}(r_b)$  would depend upon  $r_b$ ; therefore the radii may be calculated and plotted for various values of  $r_b$ .

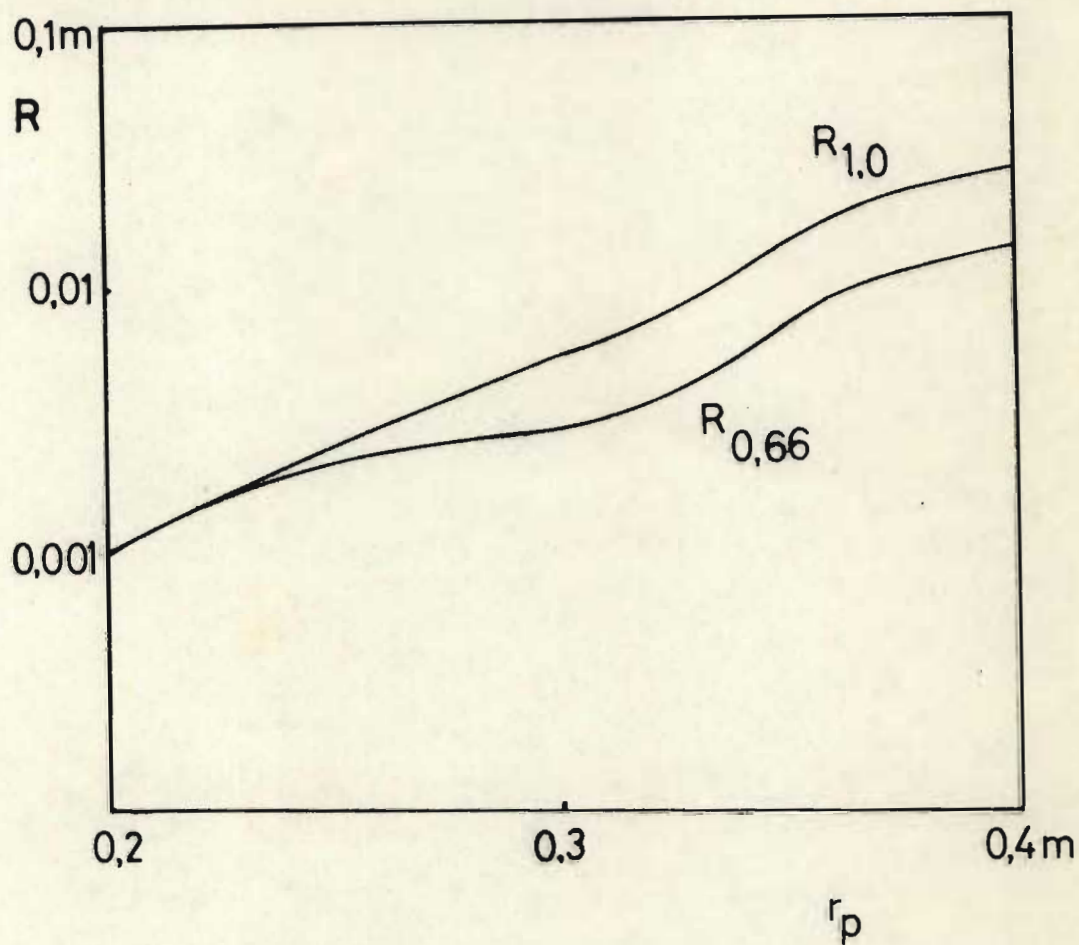


Fig. 4.3 The radii of the circles of confusion  $R_{1,0}$  and  $R_{0,66}$  for the field  $S_5$  of Table (4.1) plotted versus the radius  $r_p$  of the beam at  $z = 0$ .

To show the extent to which the spherical aberration has been reduced, the radii  $R_{1,0}$  and  $R_{0,66}$  are also [see Fig. (4.3)] found for the uncorrected field C(-1).  $v_0$ , the z-velocity at  $z = 0$ , is adjusted to obtain a focal length equal to that of the syntheses.

The ratios  $T_{1,0}(r_b)$  and  $T_{0,66}(r_b)$  are then calculated for the various  $r_b$ , with

$$T_p(r_b) = \frac{R_p(r_b) \text{ of the uncorrected field C(-1)}}{R_p(r_b) \text{ of synthesis}} \quad (4.12)$$

The values of  $R_{1,0}(r_b)$  and  $T_{0,66}(r_b)$  are plotted against  $r_b$  for various syntheses in Figs (4.4) and (4.5), and may be taken as a measure of the extent to which the spherical aberration of the C(-1) field has been reduced.

#### 4. THE OPTIMIZING PROCEDURE

Before the optimizing procedure can be carried out, an objective has to be defined, which involves choosing a beam radius  $r_b$  (depending upon the required aperture) and deciding whether  $T_{1,0}$  or  $T_{0,66}$  must be optimized. The expansion radius  $A$  of Eq. (2.2) must also be chosen, as well as an approximate focal length. From figures in Ch. (2) the amplitude of C(-1) can then be found, or the initial beam velocity  $v_z$  adjusted to obtain the focal length. (In this paper the constants  $B_n$  are of the order of 1V. For practical lenses, the constants would be multiplied by some suitably large factor).

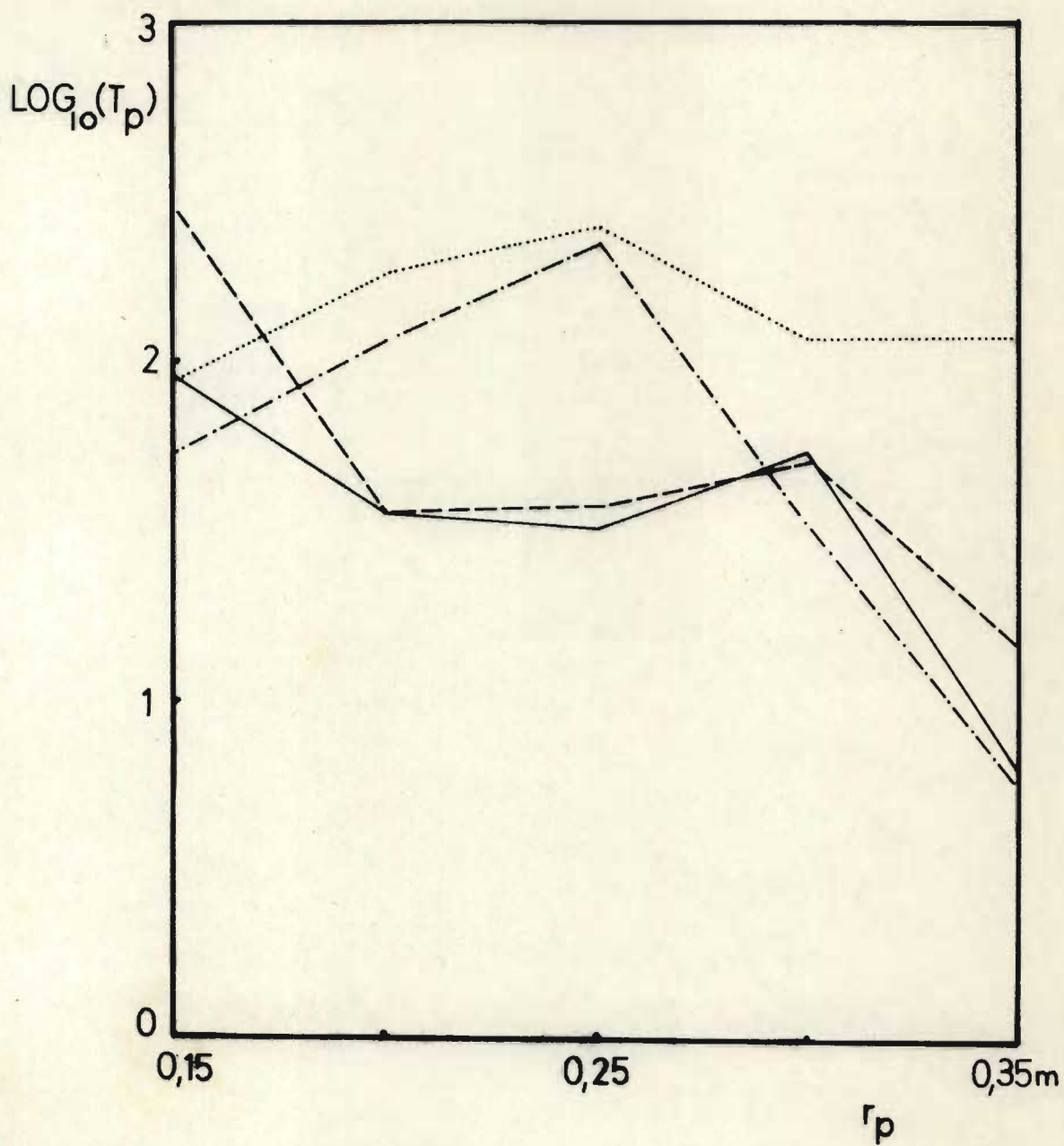


Fig. 4.4 The ratios  $T_{1,0}$  and  $T_{0,66}$  of Eq. (4.12) plotted against  $r_p$  for the syntheses  $S_1$  and  $S_4$

- $T_{1,0}$  for  $S_1$
- - - - -  $T_{0,66}$  for  $S_1$
- · - · -  $T_{1,0}$  for  $S_4$
- $T_{0,66}$  for  $S_4$

Two procedures to accomplish the synthesis are now described.

#### 4.1 Steepest descent method :

Component fields  $k_n(C(n))$ , with  $n = 3, 5, 7$ , etc., and  $k_n$  small fractions, are added to  $C(-1)$  one at a time and ray tracing carried out by computer. The changes  $\Delta T_p$  for each of the perturbations can then be found, allowing  $\partial T_p / \partial k_n$  to be calculated for  $n = 3, 5, 7, \dots$ . These derivatives allow the calculation of the gradient used in the steepest descent method. Due to the high precision required in the calculation of the  $R_p(r_b)$  values, the calculation of the gradients may make excessive demands on computer time, so that this method may not be very fast, especially if some of the constants  $B_n$  of Eq. (4.1) are fairly large.

#### 4.2 The "zone" method :

This is a trial and error method which can be used to obtain approximate syntheses fairly quickly, and which is based upon some understanding of Eqs. (4.6) and (4.10).

It can be seen from Eq. (4.10) that  $v_{re}$  is proportional to a function which is almost a Bessel  $J_1$  function of  $r$ , so that the field  $C(-1)$  will show positive spherical aberration (i.e. zonal rays have shorter focal lengths than paraxial rays). We therefore want to introduce perturbations that will increase the focal lengths of the zonal rays, without affecting the focal lengths of the paraxial rays excessively. Consideration of the terms in Eq. (4.6) shows that this can be accomplished by using a field  $B_3C(+3)$  for the

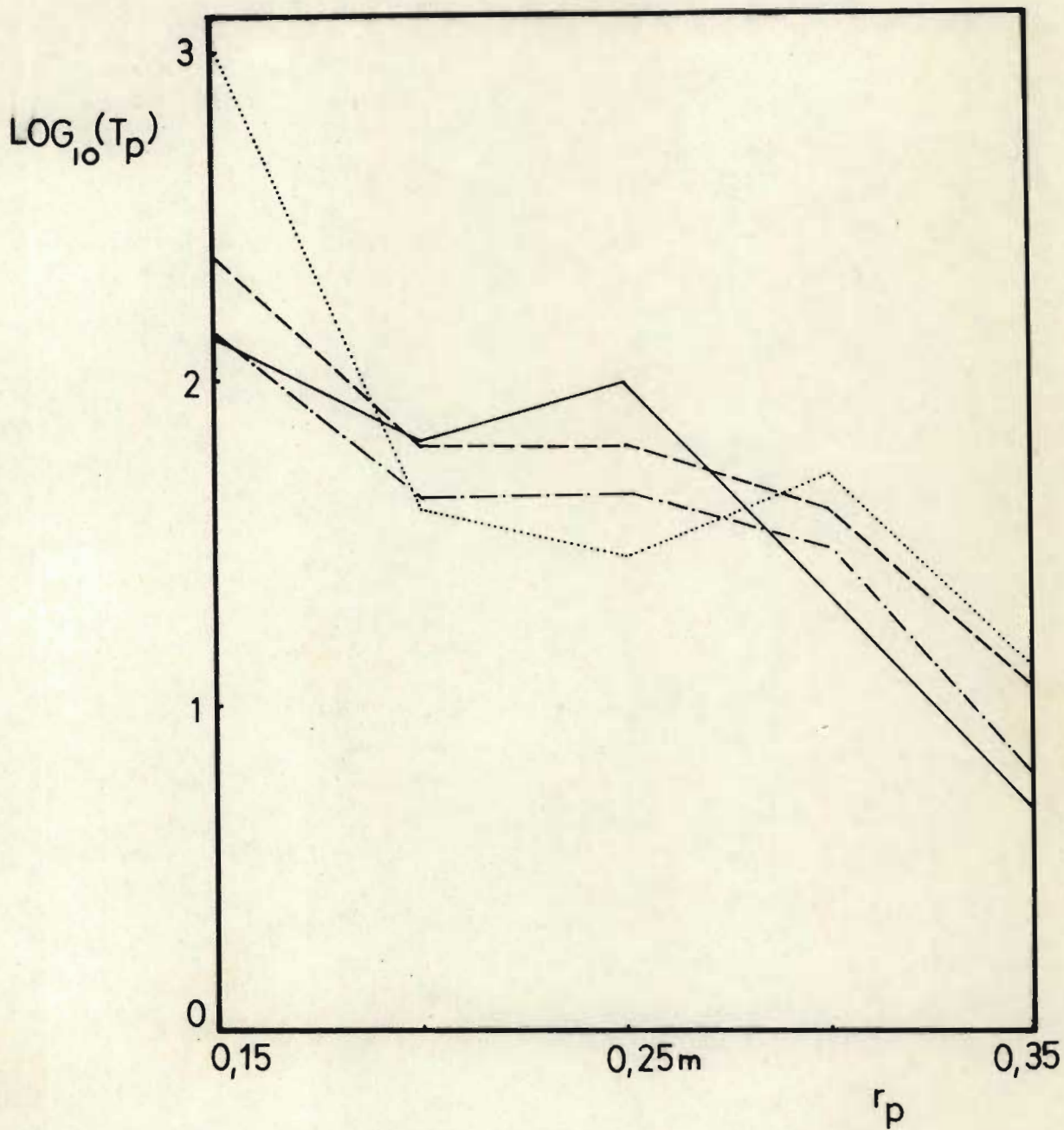


Fig. 4.5 The ratios  $T_{1,0}$  and  $T_{0,66}$  of Eq. (4.12) plotted against  $r_p$  for the syntheses  $S_2$  and  $S_3$

- $T_{1,0}$  for  $S_2$
- - - - -  $T_{0,66}$  for  $S_2$
- · - · -  $T_{1,0}$  for  $S_3$
- $T_{0,66}$  for  $S_3$



correction of rays just outside the paraxial region; usually  $0 < B_3 < 1$ . For the zonal regions the fields C(5) or C(7) would be more effective than C(3) in increasing the focal lengths, because of the factor  $n^4$  in the terms  $n^4 \pi^4 r^4 / 192 L^4$  in Eq. (4.6).

One can therefore divide the region  $0 < r < r_b$  into (fairly arbitrary) "zones of influence" in which e.g. the fields C(3), C(5), C(7) and C(9) are used for focal length reduction of rays in the zones  $0 < r < 0,25 r_b$ ;  $0,25 r_b < r < 0,5 r_b$ ;  $0,5 r_b < r < 0,75 r_b$  and  $0,75 r_b < r < r_b$ , respectively.

Constants  $B_3$ ,  $B_5$ ,  $B_7$  and  $B_9$  are therefore chosen, and varied according to the outcome of ray tracings by computer. The syntheses  $S_a$ ,  $S_b$ ,  $S_c$  and  $S_d$  discussed in the next paragraph were obtained after only a few adjustments each, requiring considerably less computer time than the steepest descent method would have required.

## 5. DISCUSSION OF SOME SYNTHESSES

Some electron optical properties of four synthesized fields are discussed in this section. The syntheses discussed are given for illustrative purposes only, and were arrived at within a few trials with the "zone" optimization method. They can provide starting points for a steepest descent method. Some information about the syntheses are given in Table (4.1), in which  $S_5$  is the (uncorrected) field  $0,295 C(-1)$ .

Table (4.1) : Some characteristics of the syntheses : the coefficients  $B_n$  of Eq. (1), the initial ray velocity  $v_0$ , the Gaussian focal point  $z_{fg}$  and the principal plane position,  $z_p$ .

Syn-thesis	$B_1$	$B_3$	$B_5$	$B_7$	$B_9$	$v_0$ (m/s)	$z_{fg}$ (m)	$z_p$ (m)
$S_1$	0,295	-0,24	0,00	-0,03	-0,04	1,3380	4,242	-0,0345
$S_2$	0,295	-0,24	0,00	-0,03	-0,30	1,3380	4,242	-0,0346
$S_3$	0,295	-0,24	0,00	-0,02	-0,40	1,3380	4,242	-0,0345
$S_4$	0,295	-0,24	0,02	-0,08	-0,40	1,3380	4,237	-0,0346
$S_5$	0,295	0,00	0,00	0,00	0,00	1,4545	4,263	-0,0362

### 5.1 Reduced disc of confusion

The values of  $R_{1,0}$  and  $R_{0,66}$  for  $S_5$  are given in Fig. (4.3), and the ratios  $T_{1,0}$  and  $T_{0,66}$  are shown in Figs. (4.4) and (4.5), for syntheses  $S_1$  and  $S_4$ , and  $S_2$  and  $S_3$  respectively. It can be seen that very significant changes in the spherical aberration can be brought about by rather small changes in the coefficients  $B_n$ . This is illustrated graphically in Fig. (4.6) by plotting the function  $\Psi(A,z)$ , i.e. the potential at the expansion radius  $A$ , for each of the syntheses.

Due to the close correspondence between the functions in the paraxial region, the single heavy solid line represents the function  $\Psi(0,x)$  for each of the syntheses  $S_1$ ,  $S_2$ ,  $S_3$  and  $S_4$ .

Figs. (4.7) and (4.8) show the upper left quadrants of the fields  $\Psi(r,z)$  for  $S_1$  and  $S_2$ , respectively. A discussion of the physical approximation of these fields is given in Section (7).

### 5.2 Role of object position

Since the spherical aberration of a lens depends, i.a., upon the object distance  $z_0$ , one may expect a synthesis found by minimizing the spherical aberration for  $z_0 \rightarrow -\infty$ , to be non-optimal for other object positions. Calculations have been made for  $T_{1,0}$  for the synthesis  $S_4$ , with  $z_0 = 10L$  and  $5L$ , and the results are given in Fig. (4.9). It appears that the correction is effective in the paraxial region for a wide variety of object positions, but that

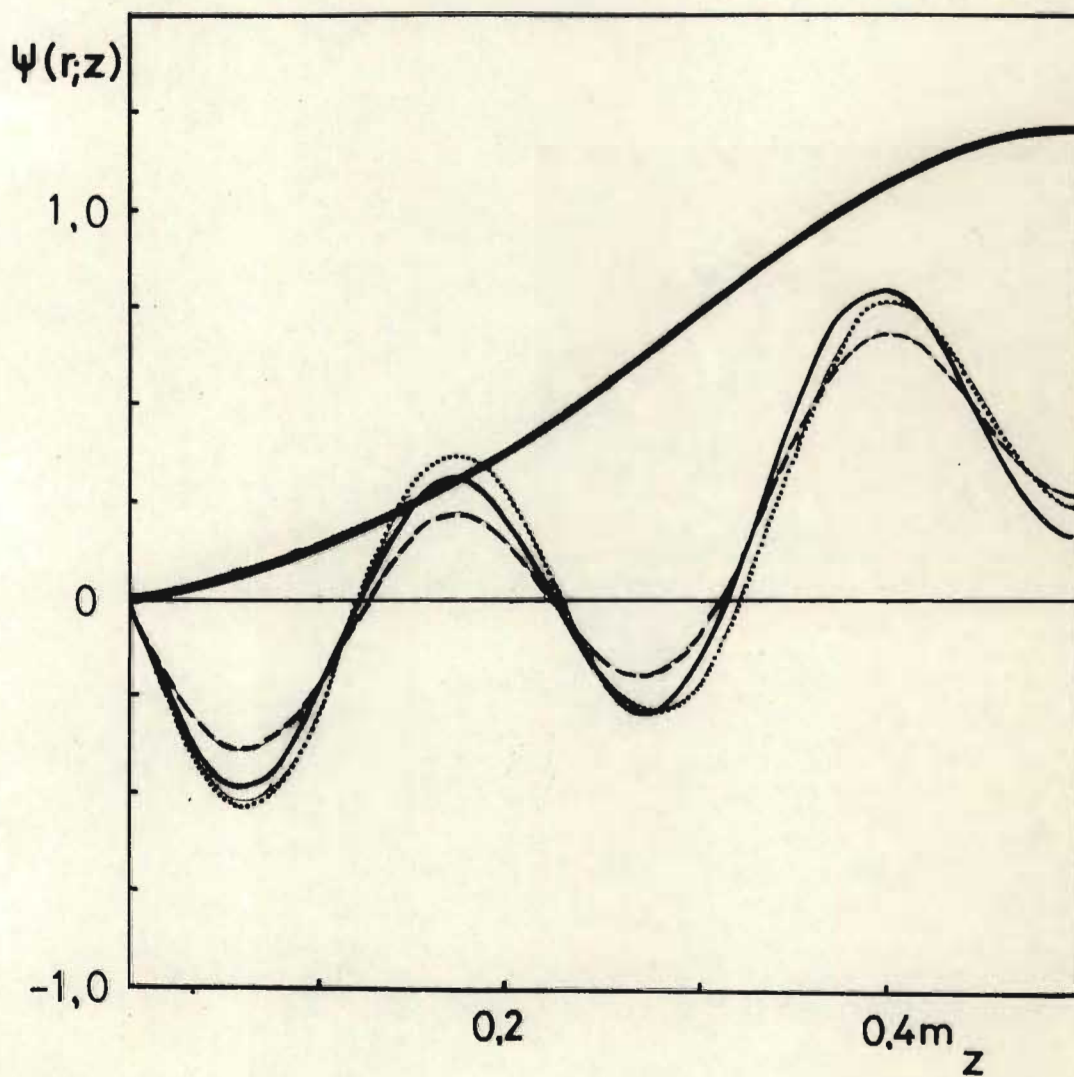


Fig. 4.6 The potential function  $\psi(r, z)$  for various syntheses, plotted vs.  $z$ .

- (light)  $\psi(A, z)$  for  $S_1$  and  $S_3$
- - -  $\psi(A, z)$  for  $S_2$
- ⋯  $\psi(A, z)$  for  $S_4$
- (heavy)  $\psi(0, z)$  for  $S_1, S_2, S_3$  and  $S_4$

this does not apply to zonal rays.

### 5.3 Negative spherical aberration

Fig. (4.10) gives the longitudinal spherical aberration

$$\Delta J = z_f(r) - z_f(0)$$

for various syntheses and for the uncorrected field, as a function of the radius  $r$  of the ray at  $z = 0$ .

It can be seen that some curves show negative spherical aberration. The possibility of obtaining negative aberration was predicted for weak fields, but in the present study it was found to be relatively easy to obtain negative spherical aberration for rays of  $r < A$ , in the case of strong fields as well, [see also Section (6)].

## 6. CORRECTION OF SPHERICAL ABERRATION OF A GIVEN LENS

The spherical aberration of all open lenses (i.e. lenses not containing thin conducting foils) seems to be positive. Because of the ease of obtaining negative spherical aberration in the foil lenses described above, it seems to be possible to use suitably designed foil lenses to correct the spherical aberration of existing lenses, if the  $v_{re}$  vs.  $r$  and  $\delta r_e$  vs.  $r$  characteristics of the given lens is known. The optimization procedure of Section (4) can still be used, the only difference being that the rays entering the field being synthesized will now have a certain known radial velocity distribution in need of adjustment.

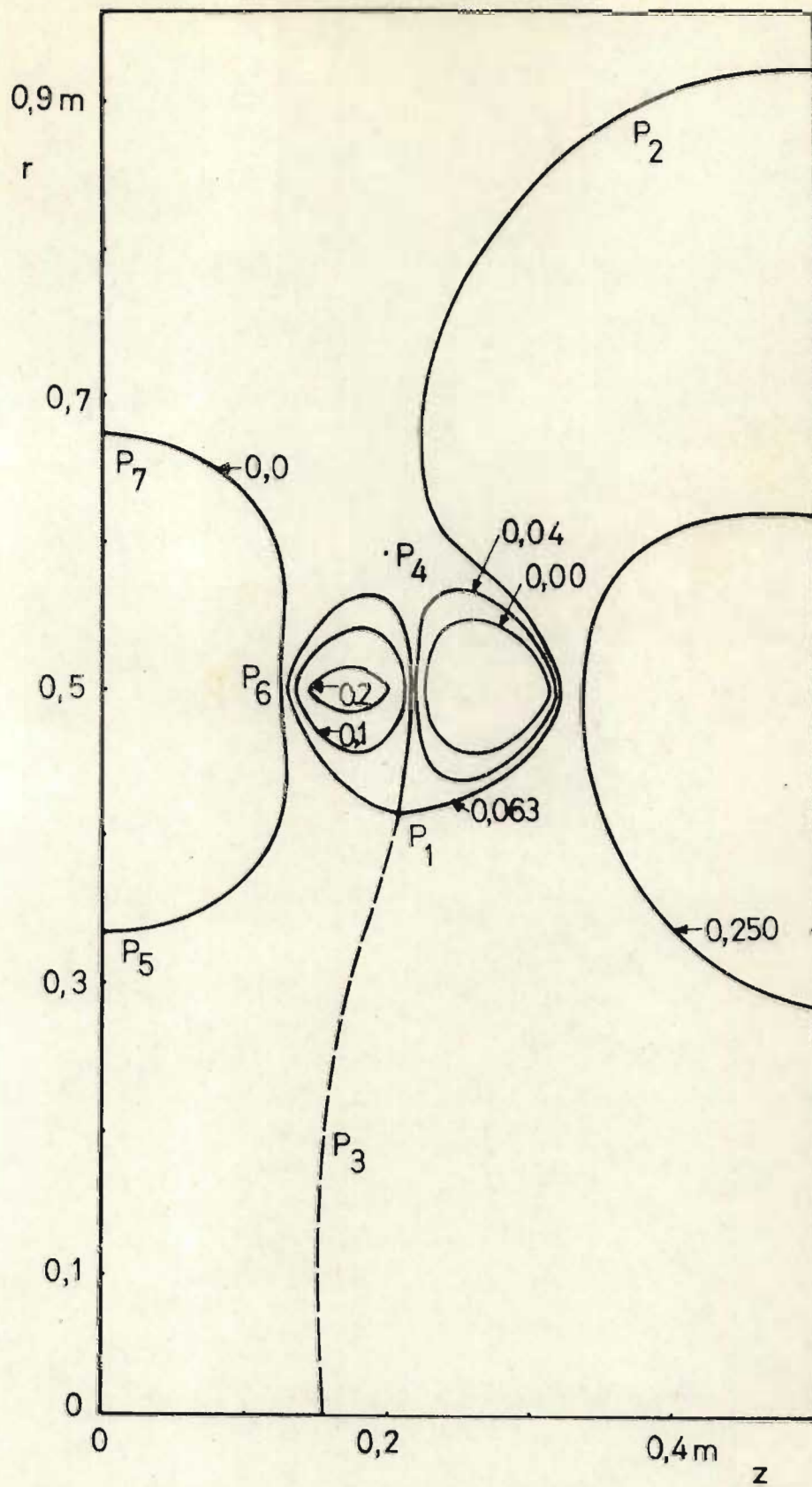


Fig. 4.7 Upper left quadrant of the field  $\psi(r; z)$  for synthesis  $S_1$ , showing cross-sectional equipotential lines.

It also seems possible to obtain a synthesized field which will show zero (Gaussian) convergence, but only the required negative spherical aberration. If placed behind a given lens, such a lens would correct the spherical aberration of the given lens, without affecting its (Gaussian) focal length. Syntheses of this type are also discussed in Ch. (7).

## 7. PHYSICAL IMPLEMENTATION

The ways in which the mathematical fields discussed above can be obtained by means of physical electrodes, were discussed in Chs. (2) and (3) as far as relatively simple fields are concerned. The fields of the syntheses  $S_1 - S_4$  can again be obtained by means of a large number of metal ring electrodes of radius  $r_e$ , with  $A \gg r_e \gg r_a$ , the aperture radius. Alternatively a field like that of  $S_1$  [Fig. (4.7)] can also be obtained by relatively few electrodes, in the following way :

- i) an electrode at 0V is positioned as shown by  $P_5, P_6, P_7$ ; it may touch or be integrated with the plane electrode at  $z = 0$ ;
- ii) an electrode is placed at the 0,250 equipotential surface; if a smaller aperture at  $z = L/2$  can be tolerated, a lower equipotential surface may be chosen;

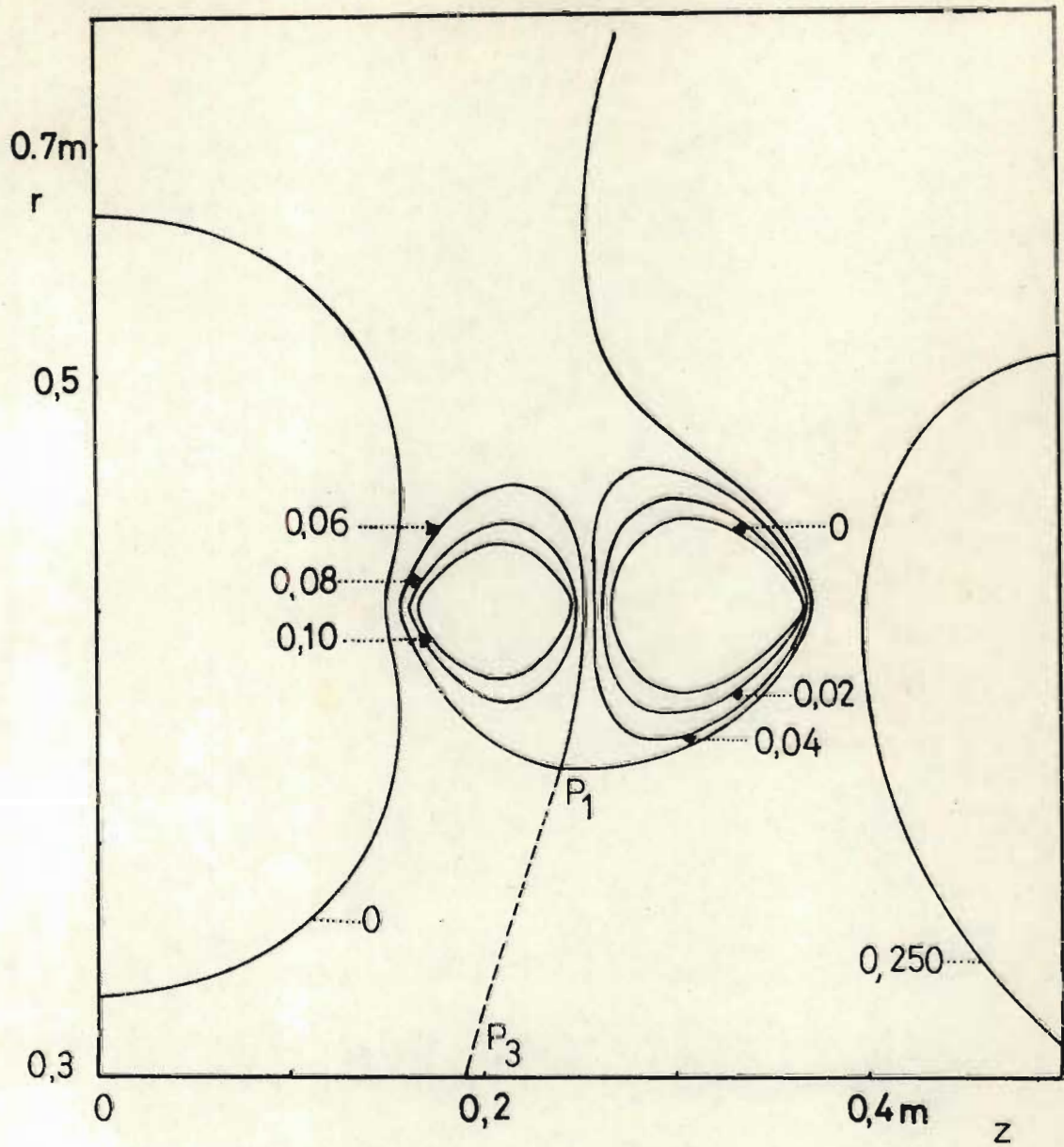


Fig. 4.8 Part of the upper left quadrant of the field  $\psi(r;z)$  for the synthesis  $S_2$ , showing cross-sectional equipotential lines.



iii) as far as the region between the above electrodes is concerned, there are the alternatives of positioning two electrodes (e.g. 0,00 and 0,08) or choosing the unique surface (0,063) passing through the off-axis saddle point  $P_1$  (strictly speaking, this is a saddle line). Although the part of the electrode between  $P_1$  and  $r = A$  is the more important part of the electrode in defining the potentials in the region  $r < A$ , it would be advisable to suspend the electrode by means of the curved part passing through  $P_2$ . A slit or holes are made in this electrode to allow the suspension of the central (i.e. 0,250) electrode to pass through.

It may be noted that a further off-axis saddle point is located at  $P_4$ , but it does not seem to be useful for purposes of electrode design.

It should also be noted that in the design of the electrodes it is important to minimize the gap sizes between the electrodes, at  $r = A$ . For sufficiently small gaps the potentials in the lens region should be a fair physical approximation of the synthesis.

To illustrate how the electrode shapes for the various syntheses differ, part of the left upper quadrant of the  $S_2$  synthesis is

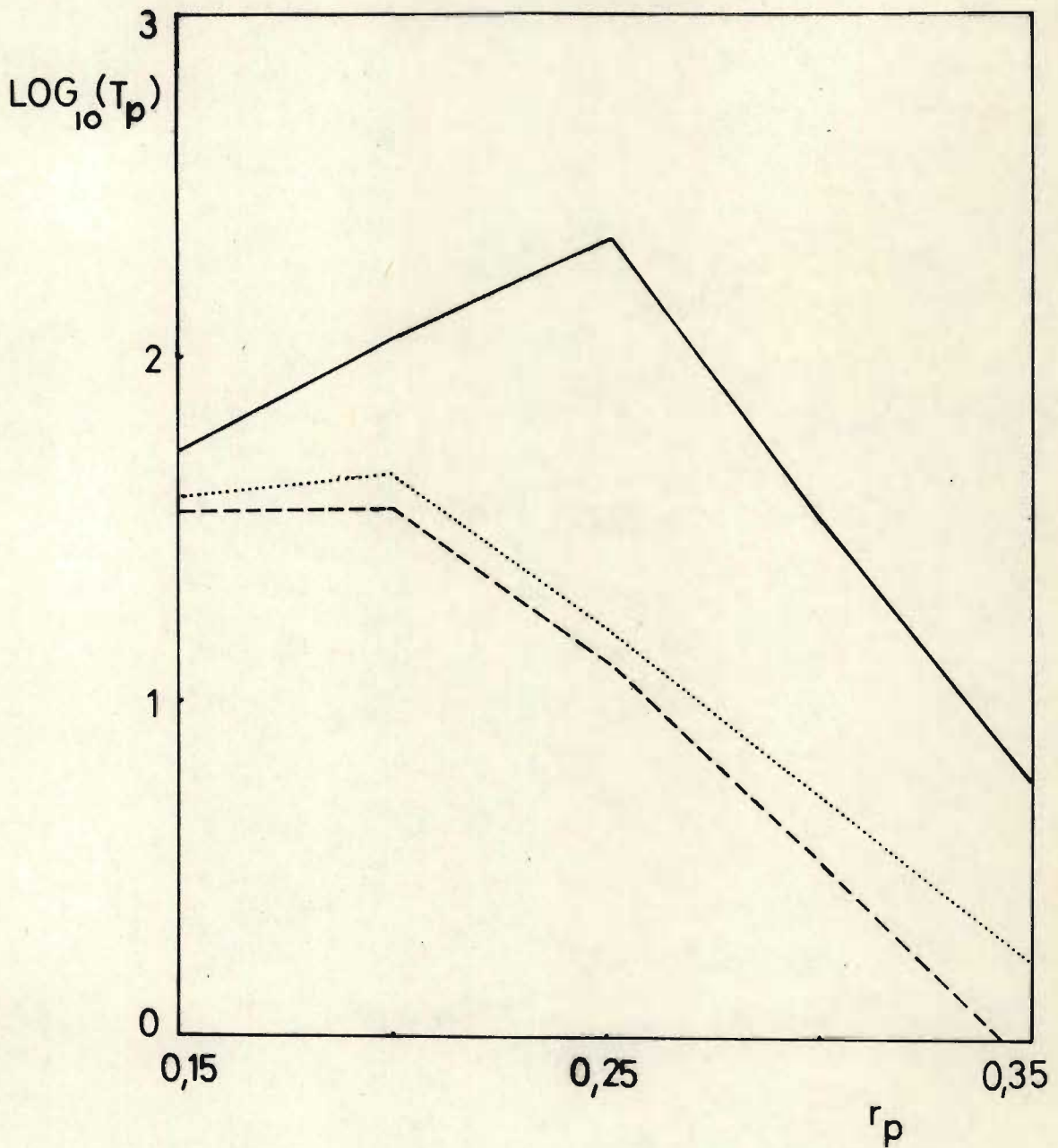


Fig. 4.9  $\text{Log}_{10}(T_{1.0})$  plotted against  $r_p$  for synthesis  $S_4$ , showing the effect of the object position  $z_0$ .

—————  $z_0 \rightarrow -\infty$   
 .....  $z_0 = -10L$   
 - - - - -  $z_0 = -5L$

shown in Fig. (4.8).

The dashed line  $P_1P_3$  [in Figs. (4.7) and (4.8)] is given only to show the equipotential surface and does not form part of a physical electrode.

An important consideration in the design of lenses is that of reducing the maximum electric intensities between the electrodes, wherever possible. If the equipotential curves of Figs. (4.7) and (4.8) are studied, or the potential functions of Fig. (4.6), it can be seen that the potential gradients appearing in the syntheses are far in excess of the values found in the  $S_5$  (i.e. uncorrected  $C(-1)$ ) field. It seems as if the correction of spherical aberration is accomplished at the expense of freedom in choosing high electrode potentials or small lens dimensions.

## 8. CONCLUSION

A method has been described which allows the design of electrostatic foil lenses of rotational symmetry in a systematic way in terms of superposed basic Fourier-Bessel potential fields. As an example it was shown how the spherical aberration of foil lenses can be reduced significantly by

- i) allowing electrodes of curved cross sections and/or
- ii) allowing more than one central electrode and/or

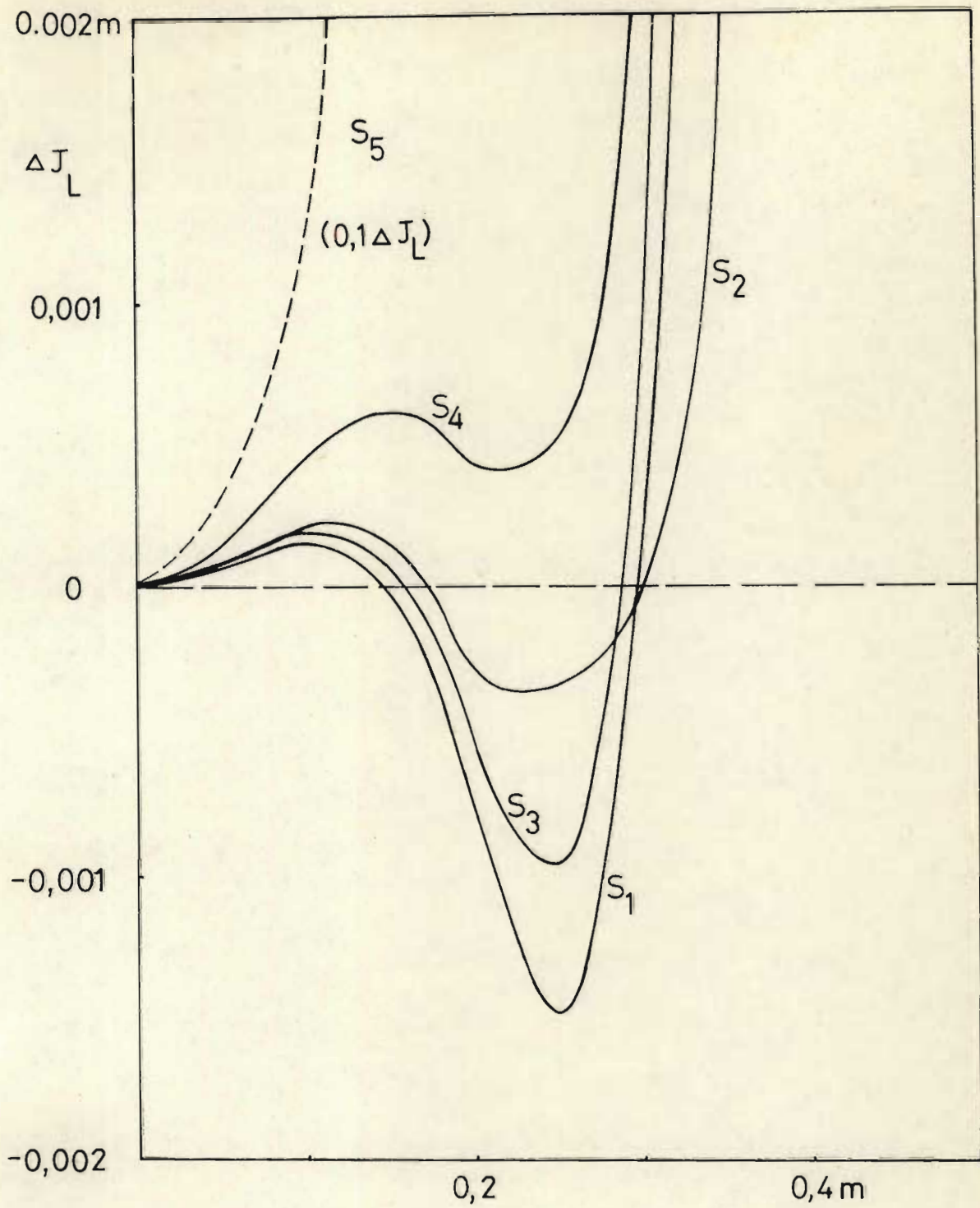


Fig. 4.10 The longitudinal spherical aberration  $\Delta J$  plotted against the radius of the ray at  $z = 0$ .

Solid lines : syntheses  $S_1 - S_4$ .

Dotted line represents  $0,1\Delta J$  for  $S_5$ , the uncorrected C(-1) field.

- iii) allowing both positive and negative potential regions within the lens.

The syntheses of Section (5) could be obtained by means of the optimization methods described, because a relatively small number of coefficients  $B_n$  had to be accommodated (a larger number of coefficients would have resulted in superior syntheses by means of the gradient method, but would at the same time have required more computer time).

When dealing with open lenses, it will be shown in Chs. (5), (6) and (8) that these lenses cannot be represented by a series truncated after a small number of terms. It therefore appears as if a different approach will have to be followed when optimizing open lenses.

MODELLING OF OPEN LENSES BY MEANS OF FOURIER-BESSEL SERIES

The preceding three chapters dealt with some electron optical properties of two-foil lenses. To study one-foil lenses or foilless systems, a new type of representation in terms of Fourier-Bessel functions will have to be found, and this chapter discusses one such a solution, in which both  $I_0$  and  $J_0$  Bessel functions appear. In Ch. (6) a solution is discussed which can be considered to be a variant of the present solution, and which has a number of advantages as far as the modelling of lenses is concerned. For the modelling of mirrors, the solution given in this chapter is probably superior to that of Ch. (6). Yet another approach is that of Ch. (8), in which a solution of the inverse interior Dirichlet problem is given.

In this chapter a solution  $\phi(r; z)$  is given of a rotationally symmetric boundary value problem :  $\phi(A; z) = 0$  for  $z \leq 0$  and  $z \geq L$ ; and  $\phi(A; z) = F(z)$  for  $0 < z < L$ .  $A$  and  $L$  are given constants and  $F(z)$  is a given function which is symmetrical with respect to the plane  $z = L/2$ . The solution is in the form of an infinite Fourier-Bessel series, the coefficients of which can be found without inverting matrices. It is shown that the given field can be approximated physically by means of two long equipotential cylinders and one or more central electrodes of curved cross section. Since the electric intensity is also known at all points, the solution allows a precise determination of the electron optical properties of a wide variety of electrostatic Einzel lenses with curved electrodes.

1. INTRODUCTION

Fourier-Bessel series solutions of the electrostatic fields in

the vicinity of certain simple configurations with rotational symmetry have been known for some time. Examples are pairs of equidiameter coaxial cylinders of finite or infinite length and negligible separation [Weber (1950)], a pair of thin apertures of equal diameter [Read (1969a)], three thin apertures [Read (1969b and 1970)], a pair of equidiameter coaxial cylinders with finite separation [Read et. al. (1970)] and three equidiameter coaxial cylinders with negligible separation [Werner (1971)].

If used in electron optical design, the above configurations do not leave much freedom to change the form of the image forming field. By allowing the central element of a lens to be curved, more freedom is gained, but it appears that most investigations of this nature have been limited to the two-foil lenses described in Chs. (2) to (4) as well as by Wittels et al. (1976), in which case the presence of the thin conducting foils constitutes a limitation to practical applications.

In this chapter a solution is given for an open configuration (i.e. absence of thin foils) which allows curved central elements to be introduced. Another feature of this solution is that it is analytical in the sense that no matrix inversion need be carried out (required in many of the cited papers because collocation requirements result in a set of simultaneous linear equations). This results in minimal computer requirements, allowing electric potential or intensity calculations to be carried out even on desk top computers.

## 2. BASIC SOLUTIONS :

In the absence of space charge, Laplace's equation for rotational symmetry is :

$$\frac{1}{r} \cdot \frac{\partial}{\partial r} \left( r \frac{\partial \phi}{\partial r} \right) + \frac{\partial^2 \phi}{\partial z^2} = 0 \quad (5.1)$$

We are interested in solutions of the form  $\phi(r; z) = R(r)Z(z)$ , satisfying certain boundary conditions :

### Solution "B"

$$\text{Let } \phi = 0 \text{ at } z = 0 \text{ and } z = L \quad (5.2a)$$

$$\text{and } \phi = F(z) \text{ at } r = A, 0 \leq z \leq L \quad (5.2b)$$

$F(z)$  is a continuous function.

Then

$$\phi(r; z) = \sum_{n=1}^{\infty} \frac{B_n I_0(n\pi r/L)}{I_0(n\pi A/L)} \sin(n\pi z/L) \quad \forall r < A \quad (5.3)$$

where  $I_0$  is the modified Bessel function of the first kind and of order zero. The coefficients are obtained by Fourier analysis at  $r=A$  :

$$B_n = \frac{2}{L} \int_0^L F(z) \sin(n\pi z/L) dz \quad (5.4)$$

### Solution "E" :

$$\text{Let } \phi = 0 \text{ at } r = A$$

$$\text{and } \phi = f(r) \text{ at } z = 0 \quad (5.5)$$

then

$$\phi(r; z) = \sum_{n=1}^{\infty} E_n \exp(-\lambda_{0n} z) J_0(\lambda_{0n} r) \quad \forall r < A \quad (5.6)$$

where the constants  $\lambda_{0n} = Z_{0n}/A$ ,  $Z_{0n}$  are the solutions of  $J_0(z) = 0$ .



The coefficients may be found by Fourier analysis at  $z = 0$  :

$$E_n = \frac{2 \int_0^A r f(r) J_0(\lambda_{0n} r) dr}{A^2 [J_1(\lambda_{0n} A)]^2} \quad (5.7)$$

$J_0$  and  $J_1$  are the ordinary Bessel functions of the first kind and of orders nought and one, respectively.

Solutions by superposition :

We now consider [see Fig. (5.1)] three coaxial regions in space, and propose the following solutions (superpositions of solutions of types "B" and "E") which are chosen so as to make the potential function  $\phi(r; z)$  continuous at the boundaries between the regions :

Region I. For  $-\infty < z < 0$  :

$$\phi_I = \sum_{n=1}^{\infty} E_n J_0(\lambda_{0n} r) \left[ \exp(\lambda_{0n} z) + \exp[+\lambda_{0n}(z-L)] \right] \quad (5.8)$$

Region II. For  $0 < z < L$  :

$$\begin{aligned} \phi_{II} = & \sum_{n=1}^{\infty} B_n \frac{I_0(n\pi r/L) \sin(n\pi z/L)}{I_0(n\pi A/L)} \\ & + \sum_{n=1}^{\infty} E_n J_0(\lambda_{0n} r) \left[ \exp(-\lambda_{0n} z) + \exp[-\lambda_{0n}(L-z)] \right] \quad (5.9) \end{aligned}$$

Region III. For  $L < z < \infty$  :

$$\phi_{III} = \sum_{n=1}^{\infty} E_n J_0(\lambda_{0n} r) \left[ \exp(-\lambda_{0n} z) + \exp[-\lambda_{0n}(z-L)] \right] \quad (5.10)$$

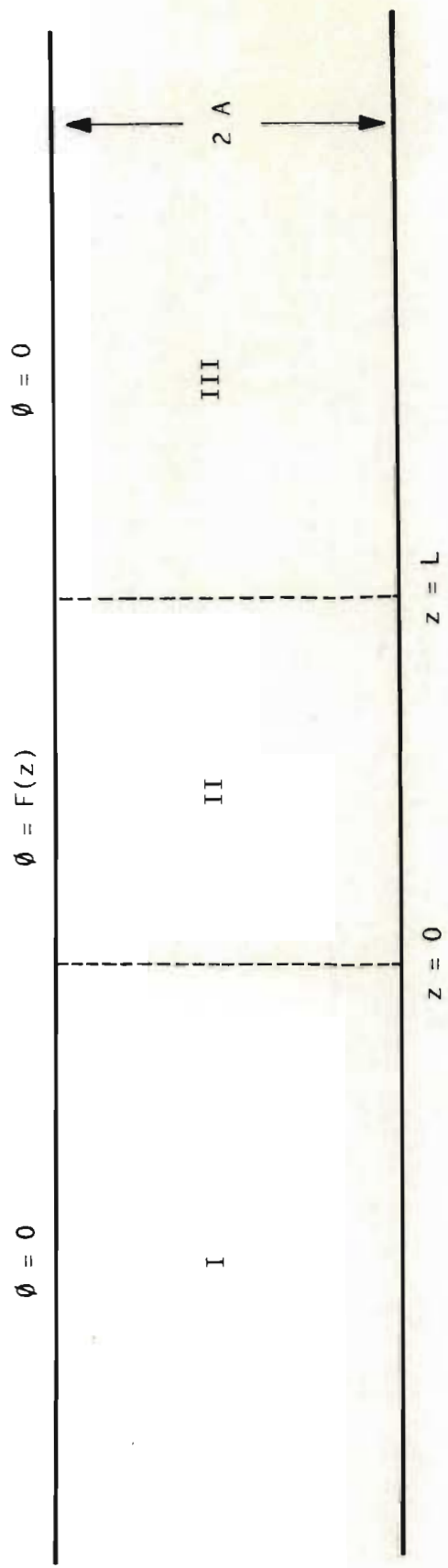


Fig. 5.1 Regions for basic solutions.

It can be seen that  $\phi_I = \phi_{II}$  at  $z = 0$   
 and that  $\phi_{II} = \phi_{III}$  at  $z = L$  (5.8)

We must note here that the same coefficients  $E_n$  appear in Eqs. (5.8) and (5.10). This implies that the function  $F(z)$  of Eq. (5.2b) must be symmetrical w.r.t.  $z = L/2$ , so that  $B_2 = B_4 = \dots = 0$ .

3. FORMULATION OF THE PROBLEM :

Suppose that the following potential fields are applied by means of external electrodes [see also Section (5)]:

$$\begin{aligned} \phi_I(A;z) &= 0 & \text{for } z \leq 0 \\ \phi_{II}(A;z) &= F(z) & \text{for } 0 < z < L \\ \phi_{III}(A;z) &= 0 & \text{for } z \geq L \end{aligned} \quad (5.11)$$

For any given continuous function,  $F(z)$ , Eq. (4) may be used to obtain the coefficients  $B_n$ . The type "B" part of the solution is, therefore, known. Since the function  $f(r)$  in Eq. (5.7) is, however, not known, the Fourier analysis of Eq. (5.7) can not be carried out, and we have to develop an alternative method to calculate the coefficients  $E_n$ . The potential  $\phi(r;z)$  would then be known in all three regions.

4. Determination of  $E_n$ :

Two relationships may be used to determine the coefficients  $E_n$ . An integral relationship, derived by applying Gauss' Theorem, is given in Section (4.1). A differential relationship is derived in Section (4.2) by requiring that  $\partial \phi / \partial z$  be continuous at  $z = 0$

and  $z = L$ .

Although both relationships allow  $E_n$  to be calculated by means of Fourier analysis, the second one requires less computation.

#### 4.1 Integral relationship used in determination of $E_n$ .

An identity involving the coefficients  $E_n$  may be derived by applying Gauss's Theorem to an infinite cylinder (coaxial with the defined fields) of radius  $r < A$ . Because the cylinder contains no charge, the total outward flux should be zero, for all  $r < A$ . The flux entering the cylinder is caused by the type "B" solution, and the flux leaving the cylinder is caused by the type "E" solutions.

Therefore :

$$\sum_{n=1}^{\infty} B_n \int_0^L \frac{2\pi^2 r n}{L} \frac{I_1(n\pi r/L) \sin(n\pi z/L)}{I_0(n\pi A/L)} dz$$

$$= -4 \sum_{n=1}^{\infty} E_n \int_0^L 2\pi r \lambda_{0n} J_1(\lambda_{0n} r) e^{-\lambda_{0n} z} dz$$

$\forall r \leq A,$

$$\text{i.e.} \quad \sum_{n=1}^{\infty} E_n J_1(\lambda_{0n} r) = \frac{1}{2} \sum_{n=1,3,5}^{\infty} B_n \frac{I_1(n\pi r/L)}{I_0(n\pi A/L)} \quad (5.12)$$

Simpler final expressions will result if we change to a new varia=

ble,  $\rho = r/A$ . Therefore :

$$\sum_{n=1}^{\infty} E_n J_1(Z_{0n}\rho) = \frac{1}{2} \sum_{n=1,3,5}^{\infty} B_n \frac{I_1(n\pi A\rho/L)}{I_0(n\pi A/L)} \quad \forall \rho \leq 1 \quad (5.12a)$$

$$= g(\rho), \text{ say,}$$

There are various ways in which the  $E_n$  may be found.

#### 4.1.1 Determination of $E_n$ by matrix inversion.

One may write down series expansions for the left and right hand sides of Eq. (5.12) and require that the coefficients of  $r$ ,  $r^3$ ,  $r^5$ , etc., match. The result is an infinite set of equations in an infinite number of unknowns :

$$\sum_{n=1}^{\infty} E_n Z_{0n}^m = \frac{(-1)^{(m+1)/2} (\pi A/L)^{2m}}{2I_0(\pi A/L)} \quad (5.13a)$$

for  $m = 1, 3, 5 \dots$

Alternatively  $m$  values may be chosen for  $r$ , and substituted in Eq. (5.12). The point testing will result in  $m$  equations in an infinite number of unknowns. One may set  $E_p = 0 \quad \forall p > m/k$  where  $m$  is some chosen value which depends upon the precision required, and  $k$  is a constant which determines to which extent the resulting set of simultaneous linear equations will be overdetermined;  $k > 2$  is normally sufficient [Read (1969a) and Wittels et. al. (1976)].

The following set of equations is then solved in a least squares sense :

$$\sum_{n=1}^{p < m} E_n J_1(Z_{0n} \rho_j) = \frac{1}{2} \sum_{n=1}^{p < m} B_n \frac{I_1(n\pi A \rho_j / L)}{I_0(n\pi A / L)} \quad (5.13b)$$

where  $j = 1, 2, \dots, m$ .

#### 4.1.2 Direct determination of $E_m$

A difficulty encountered in the solution of Eq. (5.12) is that the functions  $J_1(Z_{0n} \rho)$  are not an orthogonal set of functions, due to the fact that the constants  $Z_{0n}$  are not the zeros of  $J_1$ , but of  $J_0$ . Therefore a Fourier analytical determination of the  $E_n$  [multiplying by  $\rho J_1(Z_{0n} \rho)$  and integrating between 0 and 1] is not possible.

We therefore first establish a set of orthonormal functions  $V_n$  in the following way :

$$\text{Let : } V_n(\rho) = \sum_{j=1}^{n-1} G_{nj} V_j(\rho) + G_{nn} J_1(Z_{0n} \rho) \quad (5.14)$$

in which the constants  $G_{ij}$  have to be chosen so as to

- (i) orthogonalize the set of functions  $V_j$  on the interval  $(0;1)$ , and
- (ii) normalize the functions on the interval  $(0;1)$  : i.e.

$$\int_0^1 V_i(\rho) V_j(\rho) d\rho = \delta_{ij}$$

The constant  $G_{ij}$  can be found by computer by means of a Gram-Schmidt orthonormalization procedure. In this procedure the values of the integral

$$Q_{ij} = \int_0^1 J_1(Z_{0i}\rho) J_1(Z_{0j}\rho) d\rho \quad \forall i, j. \quad (5.15)$$

are required, and a series expansion is given in Appendix (1), in which tables of numerically integrated values are also found. Examples of the coefficients  $G_{ij}$  are given in Table (5.1).

The orthonormal set of functions  $V_n$  now allows a Fourier series expansion for  $g(\rho)$ , namely :

$$g(\rho) = \sum_{n=1}^{\infty} H_n V_n(\rho) \quad (5.16)$$

in which the coefficients  $H_n$  may be found from

$$H_n = \int_0^1 g(\rho) V_n(\rho) d\rho \quad (5.17)$$

The procedure may, however, be streamlined by expressing the functions  $V_n(\rho)$  in terms of Bessel functions only :

$$V_n = \sum_{i=1}^n F_{ni} J_1(Z_{0i}\rho) \quad (5.18)$$

with  $F_{ii} = G_{ii} \quad \forall i$

and  $F_{ij} = \sum_{k=1}^{i-j} G_{ik} F_{kj} \quad \forall i \neq j$

[Values of some  $F_{ij}$  are listed in Table (5.2)]

The calculation of the coefficients  $H_n$  is now simplified :

Table (5.1) Coefficients  $G_{ij}$

$i \backslash j$	1	2	3	4	5
1	2,214274000	0	0	0	0
2	0,315389502	-2,838258426	0	0	0
3	0,108749122	-0,429911485	-3,399280258	0	0
4	0,083597809	-0,202562699	-0,477326603	-3,889315045	0
5	0,047408055	-0,151191597	-0,251407231	-0,503071876	-4,327159257

Table (5.2) Coefficients  $F_{ij}$

$i \backslash j$	1	2	3	4	5
1	2,214274000	0	0	0	0
2	0,698358774	-2,838258426	0	0	0
3	-0,059432104	1,220199894	-3,399280258	0	0
4	0,072015541	-0,00750858	1,622566897	-3,889315045	0
5	-0,021898888	0,126131105	0,038334866	1,956605014	-4,327159257

Table (5.3) Values of  $i$  as defined in Section (6)

$r \backslash z$	0,6	0,8	1,0	1,2	1,4	1,6	1,8	2,0
0,0	5	9	60	9	6	4	4	3
0,4	5	7	22	7	5	4	4	3
0,8	5	7	20	7	5	4	4	3



$$H_n = \sum_{i=1}^n F_{ni} W_i \quad (5.19)$$

in which

$$W_i = \int_0^1 g(\rho) J_1(Z_{0i}\rho) d\rho \quad (5.20)$$

The evaluation of the integral in Eq. (5.20) may be carried out numerically but series expansions for  $W_i$  for some simple functions  $g(\rho)$  are given in Appendix (1).

The coefficients  $E_n$  may now be calculated from Eqs. (5.12a), (5.16) and (5.18) :

$$E_n = \sum_{i=n}^{\infty} H_i F_{in} \quad (5.21)$$

#### 4.2 Differential relationship used in determination of $E_n$ .

As an alternative to Eq. (5.12) we may require that  $\partial \phi / \partial z$  be continuous at  $z = L$  (or at  $z = 0$ ). (This condition may be derived by applying Gauss' Theorem to a coaxial ring-like surface placed at  $z = L$ ). After simplifying,

$$\sum_{n=1}^{\infty} \frac{B_n n \pi I_0(n\pi r/L)}{L I_0(n\pi A/L)} = \sum_{n=1}^{\infty} 2\lambda_{0n} E_n J_0(\lambda_{0n} r) \quad (5.22)$$

$\forall r < A$

##### 4.2.1 Determination of $E_n$

Although a point testing technique [similar to Section (4.1)] may

be applied, finding  $E_n$  by matrix inversion, one may profitably make use of the orthogonality of the set of functions  $J_0(\lambda_{0n}r)$ , and solve for  $E_n$  by a conventional Fourier analysis. The result is :

$$E_n = \sum_{j=1,3,5,\dots}^{\infty} \frac{B_j j\pi}{A^2 L I_0(j\pi A/L) \lambda_{0n} [J_1(\lambda_{0n}A)]^2} \int_0^A r I_0(j\pi r/L) J_0(\lambda_{0n}r) dr \quad (5.23)$$

The integrations of Eq. (5.23) may be done numerically, but a series expansion is given in Appendix (1).

#### 5. PHYSICAL APPROXIMATION

It has been assumed up to now that a potential field  $\phi(A;z) \forall z$  is applied by means of external electrodes. The values  $\phi(A;z) = 0$  for  $z < 0$  and for  $z > L$  are applied by means of two coaxial cylindrical earthed electrodes. The application of the potential function  $\phi(A;z) = F(z)$ ,  $0 < z < L$  [see Eqs. (5.2b) and (5.9)], is more complicated, and three methods are suggested :

- (i) A set of coaxial conducting rings of radii  $A$  may be positioned between  $z = 0$  and  $z = L$ , with the required potentials supplied from potential dividers; an experimental study of the electron optical properties of the fields created by various potential functions  $F(z)$  can be carried out in this way to compare with the computer predictions.
- (ii) A cylindrical electrode with a resistive layer on the inside surface may replace the rings of (i); the thickness of the film is a function of  $z$ , so as to result in a

potential distribution  $F(z)$  if the film is earthed at  $z = 0$  and  $z = L$ , and a fixed potential is applied to the layer at  $z = L/2$ .

(iii) A more practical approach involves the field  $\phi(r; z)$  in the region  $r < A$ ,  $0 < z < L$ , rather than the field  $F(z)$  itself. For any given symmetrical [see Section (2)] function  $F(z) = \phi(A; z)$ , we make use of Eqs. (5.9) and (5.21) to find  $\phi(r; z)$  for  $r < A$ , which allows us to draw equipotential surfaces in Region II of Section (2). A suitable equipotential surface is chosen and a physical electrode positioned as to coincide with this surface [shown in Fig. (5.2) as the heavy line]. Close attention must be paid to the gaps between the electrodes, so as to ensure that the potential function  $\phi_g$  found in the gaps matches the required function  $F(z)$ ; otherwise the solutions of Eqs. (5.8), (5.9) and (5.10) will not be applicable. This may be accomplished by also considering the potential  $\phi_{IV}$  in region IV (i.e.  $0 < z < L$ ,  $r > A$ ).  $\phi_{IV}$  will satisfy Laplace's equation and the boundary conditions

$$\phi(r; 0) = \phi(r; L) = 0 \quad \forall r > A \quad (5.24a)$$

$$\phi(A; z) = F(z) \quad 0 < z < L \quad (5.24b)$$

if we take

$$\phi_{IV}(r; z) = \sum_{n=1}^{\infty} \frac{B_n K_0(n\pi r/L) \sin(n\pi z/L)}{K_0(n\pi A/L)} \quad (5.25)$$

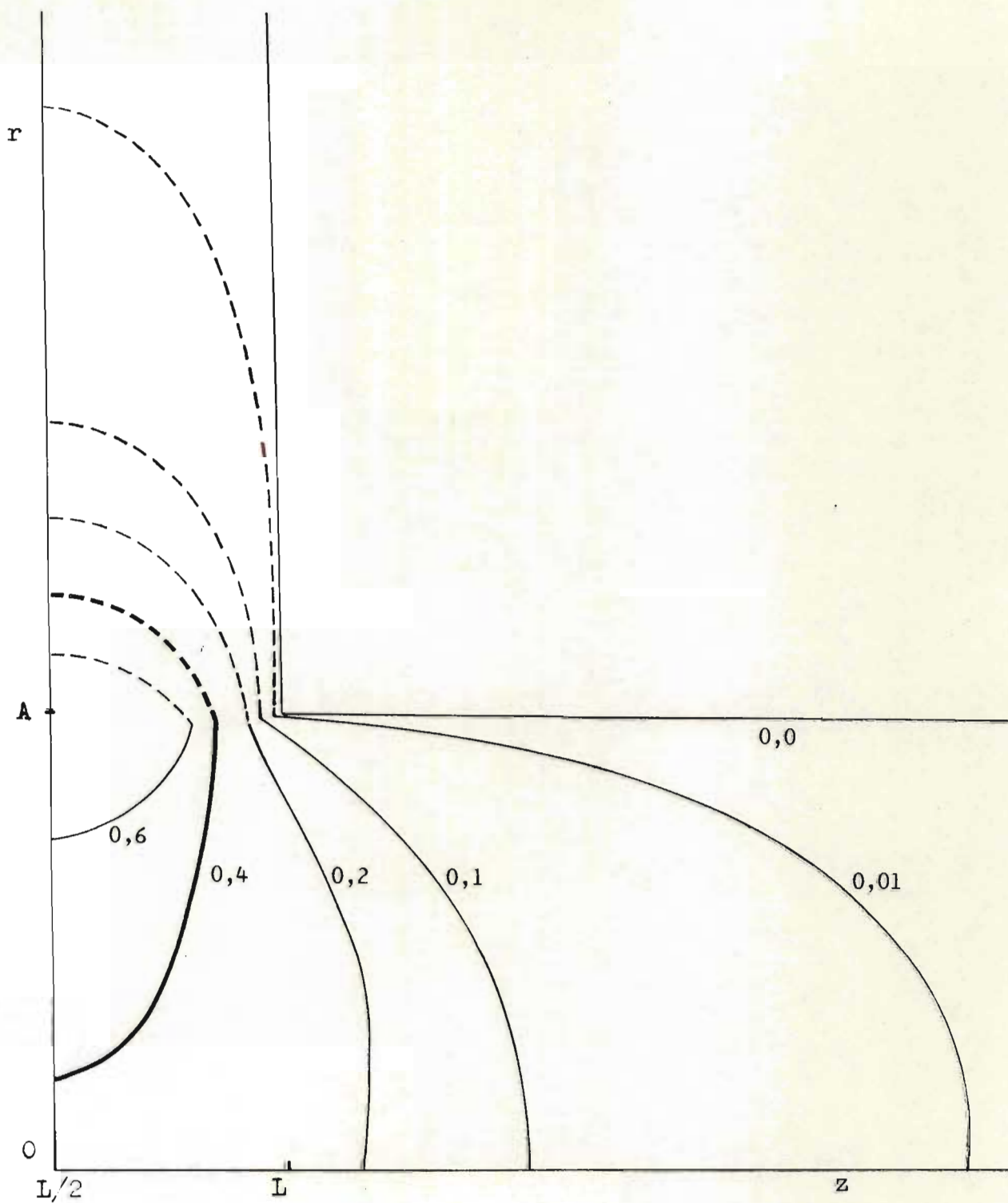


Fig. 5.2 Equipotential lines for  $f(z) = \sin(\pi z/L)$  and  $L = A = 1,0$ .  
 Only the region  $z > L/2$  is shown.

where  $K_0$  is the modified Bessel function of the second kind and of order zero.

The dotted lines in Fig. (5.2) show equipotential lines of a cross section of  $\Phi_{IV}$ , and the heavy dotted line shows how the physical electrode should be continued into region IV. One or more shielding electrodes may also be positioned to coincide with any of the equipotential surfaces represented by dotted lines terminating at points in the gaps. This will ensure that  $\phi_g$  matches  $F(z)$ , as long as the support of this electrode does not cause excessive deviations from  $\phi_{IV}$  as given by Eq. (5.25). In the event of a mismatch, a reduction in the size of the gaps (i.e. through a judicious choice of the ratio  $A/L$ ) will ensure that the potentials in the paraxial regions are not affected excessively.

The two parallel plane equipotential surfaces of Eq. (5.24a) may be replaced by a single curved electrode which follows any of the dotted equipotential lines representing a sufficiently low potential. Holes (or a slit) in this electrode allow the supports of the central electrode to pass through.

If the above precautions are taken, the physical configuration should be a fair approximation to the mathematical model of Eqs. (5.8), (5.9), (5.10) and (5.11).

## 6. PRECISION

The potential  $\phi(r;z)$  is given by two series, involving the Bessel

functions  $I_0$  and  $J_0$  [Eqs. (5.8-5.10)]. The function  $F(z)$  would normally [see Section (7)] be a superposition of a few chosen trigonometrical functions, so that the  $I_0$  series would be a finite one. We therefore consider the convergence of the  $J_0$  series only.

The convergence of the  $J_0$  series depends upon i) the values of the coefficients  $E_n$  and ii) the position of the point  $(r;z)$ .

Due to the exponential functions the series converges very fast for all  $|z| \gg L$ ; on the other hand, convergence is slowest for the points  $(0;0)$  and  $(0;L)$ . This is demonstrated in Table (5.2) for a configuration with  $A = 1$ ,  $L = 1$  and  $F(z) = \sin(\pi z/L)$ . Let  $T_i$  represent the  $i$ -th term of the series, and

$$R_i = \frac{T_i}{\sum_{j=1}^i T_j}$$

The numbers in the table are the values of  $i$  for which  $R_i < 10^{-3}$ .

It is found that this series alternates for points  $(r \ll A; z)$  but does not alternate for points  $(r \doteq A; z)$ . The method applied to accelerate convergence would therefore normally depend upon the position of the point.

For an alternating series an Euler transformation may be used to advantage, and a relative precision of  $10^{-6}$  may be reached with 18 terms at the points  $(0;0)$  or  $(0;L)$ .

For some combinations of fields  $F(z)$  and values of  $A$  it may be found that convergence of the series at  $(r; z = 0)$  or  $(r; z = L)$  is too slow to be acceptable [e.g. requiring values of  $E_n$  which may not be available from values of integrals tabulated in Appendix (1)]. For such points one may either perform a bivariate interpolation of suitably high degree, or carry out a finite difference relaxation procedure in a selected part of the field, or make use of a Taylor expansion

$$\begin{aligned} \phi(r; z) &= \sum_{j=0}^{\infty} \frac{(z-z_0)^j}{j!} \frac{\partial^j \phi(r; z_0)}{\partial z^j} \\ &= \sum_{j=0}^{\infty} \frac{(z-z_0)^j}{j!} \sum_{n=1}^{\infty} E_n J_0(Z_{0n} r/A) (Z_{0n}/A)^j \\ &\quad \times \left[ \exp(-Z_{0n} z_0/A) + \exp[-Z_{0n}(z_0-L)/A] \right] \end{aligned}$$

where, e.g.  $z_0 = 1,15L$  and  $z \doteq L$

The precision of  $\phi(r; z)$  would also depend upon the precision of the coefficients  $E_i$ , and therefore care should be taken to evaluate the integrals of Eq. (5.23) sufficiently precisely.

## 7. IMPLICATIONS FOR ELECTRON OPTICAL DESIGN

The main advantage of the Fourier-Bessel series approach in solving this field problem is that the electron optical properties of electrostatic fields corresponding to certain basic mathematical fields may be studied individually or as perturbations, and syntheses obtained in a systematic way [as in Ch. (4)] so as to optimize

certain electron optical properties. One may, for example, include the fields  $\phi_n(r; z)$  resulting from the applied potential functions  $F(z) = \pm \sin(\pi z/L)$ ,  $\pm \sin(3\pi z/L)$ , etc., in the synthesis in an attempt to obtain an Einzel lens with certain specified electron optical properties.

Further advantages are that the boundary value problem can be solved to the required precision with a minimal amount of computation compared to, e.g., the iterative methods; and no interpolation is required when calculating trajectories, because the field is known at all points. (When used for ray tracing, however, one would normally calculate  $\phi$  and some derivatives at regular grid points, and store these matrices on disc for various functions  $F(z)$ . Synthesized fields are then obtained by matrix addition).

It may also be noted that series expansions exist for the derivatives  $\partial^n \phi / \partial z^n$  and  $\partial^n \phi / \partial r^n$  of all orders, allowing the use of high order trajectory calculations. [Dirmikis et. al (1975)]

### 7.1 The introduction of apertures

If thin grounded coaxial discs with apertures of equal radii  $r_a < A$  are introduced at  $z = 0$  and  $z = L$ , Eqs. (5.12) and (5.22) apply only to  $r < r_a$ . For  $r > r_a$ ,  $\phi(r; 0) = \phi(r; L) = 0$ . The author has not succeeded in obtaining a direct solution for this configuration, although a least squares solution seems feasible, by means of a point testing procedure which involves Eq. (5.8), (5.9) or (5.10) for  $r > r_a$ , and Eq. (5.12) or (5.22) for  $r < r_a$ . This problem



requires some further investigation as does a related problem in which the central cylinder has a larger radius than the outer cylinders [Yeh (1975 and 1976)].

## 7.2 Asymmetrical Fields

Fields similar to those found in immersion lenses and image intensifiers may be treated by a modification of the method described here, and will be discussed in a future paper.

## 8. CONCLUSION

A Fourier-Bessel series solution can be found for certain Einzel configurations. The method is a direct one, and no limitation has been found on the precision that can be reached. The method can be applied to advantage in electron optical design.

In the next chapter another solution to the same boundary value problem will be presented; the solution may be considered to be a variant of the present one, and offers some advantages when lenses rather than mirrors are modelled.

## CHAPTER 6

### FOURIER-BESSEL SERIES SOLUTION OF POTENTIAL FIELDS WITH ROTATIONAL SYMMETRY, IN TERMS OF $I_0$ BESSEL FUNCTIONS

The Fourier-Bessel series representation of open electrostatic configurations discussed in the previous chapter is more suited to the modelling of electrostatic mirrors than of lenses. One reason is that the lens region is divided into three parts, each having its own solution. The second is that for the central region, both  $I_0$  and  $J_0$  functions appear in the series, and a third reason is that the convergence of the series is rather slow in some regions.

In this chapter a solution for the modelling of closed, semi-open and open configurations is discussed, in which these disadvantages have been eliminated. A Fourier-Bessel series representation in terms of  $I_0$  Bessel functions is given for the potential distribution in certain open Einzel or immersion type electrostatic configurations with rotational symmetry described by  $\phi(A;z) = F(z)$ ,  $0 < z < L$ ; and  $\phi(A;z) = 0 \forall z < 0$  and  $\forall z > L$ .  $F(z)$  is a given function and  $A$  and  $L$  are constants. The method is a direct one — no iterations or matrix inversions are required — and a superior rate of convergence in the paraxial region is achieved through the elimination of  $J_0$  Bessel functions. The precision reached is apparently limited by the computer word length only, programming is of a simple nature, and computer memory requirements are modest enough to allow implementation on small desk top computers.

#### 1 INTRODUCTION

The analytical determination of the coefficients of Fourier-Bessel

series representations of the electrostatic potential or intensity fields in the vicinity of certain simple configurations of electrodes with rotational symmetry has been reported in several papers [Gray (1939), Weber (1950), Chorlton (1968) and Werner (1971)]. It has, however, been found that the analytical determination of the Fourier coefficients tends to be cumbersome, unless the electrodes have simple shapes and/or are small in number and/or have negligibly small gaps between the electrodes. Relaxation of these restrictions have been brought about by calculating the coefficients by computer, and solutions have been published for some closed and open configurations [Read (1969a , 1969b , 1970), Read et al. (1970), Wittels et al. (1976), Yeh (1975 , 1976 and 1977), Andreev et al. (1976), Mel'nikov (1971), Anicin et al. (1976) and Cook et al. (1976)]. A solution resulting in one or more inner electrodes of curved cross section, was discussed in Ch. (5).

In the latter case the solution contains both the unmodified ( $J_0$ ) and modified ( $I_0$ ) Bessel functions of the first kind and of order zero. [ Since  $I_0(x)=J_0(ix)$ , possible misunderstanding is eliminated by restricting the arguments of Bessel functions to real values only.]

Although the expression of the fields in terms of  $J_0$  functions may be of use in understanding the properties of the fields in the outer regions, it would offer several advantages if a series representation can be found from which the  $J_0$  fields have been eliminated, since this may result in the simplification of various calculations

connected with electron optics.

## 2 FORMULATION OF THE BOUNDARY VALUE PROBLEM

Let  $\phi(r; z)$  be the potential at a point  $(r; z)$  w.r.t. a cylindrical polar coordinate system, and consider the following boundary value problem :

$$\phi(A; z) = F(z) \text{ for } 0 < z < L \quad (6.1)$$

$$\phi(r; 0) = \phi(r; L) = 0 \text{ for } 0 \leq r \leq A \quad (6.2)$$

Since the solution of the boundary value problem is needed for electron optical purposes, we restrict  $F(z)$  to functions that can be approximated by, or be associated with, configurations of physical electrodes. It can therefore be expected that  $F(z)$  satisfies the Fourier analytical Dirichlet conditions, so that it can be represented by either a Fourier integral (for  $L \rightarrow \infty$ ) or a Fourier series (for finite  $L$ ). For most functions  $F(z)$  the evaluation of the Fourier integral will be carried out by computer, involving a numerical integration which closely resembles the computer evaluation of a Fourier series [see also Section (11)]. For the present discussion we therefore limit  $L$  to finite values, in which case

$$F(z) \sim \sum_{m=1}^{\infty} B_m \sin(m\pi z/L) \quad (6.3)$$

with

$$B_m = \frac{2}{L} \int_0^L F(z) \sin(m\pi z/L) dz \quad (6.4)$$

The potential  $\phi(r; z)$  is then given by

$$\phi(r; z) \sim \sum_{m=1}^{\infty} B_m \frac{I_0(m\pi r/L) \sin(m\pi z/L)}{I_0(m\pi A/L)} \quad (6.5)$$

which is a convergent series if the series of Eq. (6.3) is convergent, since  $I_0(m\pi r/L) < I_0(m\pi A/L) \quad \forall r < A$ .

It will be shown in the next section that the solution given by Eq. (6.5) can also be used to approximate the solution of the following boundary value problem:

$$\phi(A; z) = F(z) \quad \text{for } 0 < z < L \quad (6.6)$$

$$\phi(A; z) = 0 \quad \text{for } z < 0 \quad \text{and } z > L \quad (6.7)$$

This boundary value problem describes "open" electrostatic lenses, in contrast to the "closed" lenses of Eqs. (6.1) and (6.2). In this paper the terms "open" and "closed" lenses refer to the absence or presence of conducting electrodes at  $z=0$  and  $z=L$ ; whereas charged particles have to penetrate thin conducting foils when entering and leaving closed lenses, open lenses have extended regions on both sides where  $\nabla\phi$  is negligible as far as the electron optical properties of the lens are concerned. The conditions under which the solution of Eq. (6.5) applies to open lenses will be discussed in the next paragraph.

Finally it may be noted that, since the open lenses of Eqs. (6.6) and (7) may be closed off by conducting electrodes at  $z \rightarrow -\infty$  and  $z \rightarrow +\infty$ , the region  $r < A$  is still fully enclosed by a boundary with

specified potential values, so that the problem is still a conventional interior Dirichlet problem.

### 3 APPLICABILITY OF SOLUTION TO OPEN LENSES.

Consider a field  $\phi(r; z)$ , represented by Eq. (6.5) and which has the following property :

$$|\nabla \phi(r; z)| < \epsilon \quad (6.8)$$

for all  $r$  and for  $0 < z < (L - L_e)/2$  as well as for  $(L + L_e)/2 < z < L$  where  $\epsilon$  and  $L_e$  are constants, the values of which are determined by the nature of the boundary value problem and the precision to which  $\phi(r; z)$  must be found (see following sections). For the present let us assume  $\epsilon \doteq 10^{-7} \max |\phi(r \leq A; z)|$  and  $L_e \doteq 4A$ .

The the following can be postulated : If  $L$  is sufficiently larger than  $L_e$ , then

- a) the conducting electrodes at  $z=0$  and  $z=L$  together with the charges induced on their surfaces may be removed without causing a significant change in the potentials in the region  $(L - L_e)/2 < z < (L + L_e)/2$ ,  
or
- b) if the problem is reformulated in terms of images, rather than induced surface charges, the charge distributions giving rise to the potential fields given by Eq. (6.5) for the regions  $z < 0$  and  $z > L$  will have no significant influence on the potentials in the region  $(L - L_e)/2 < z < (L + L_e)/2$ , and may be neglected. The boundary conditions

of Eq. (6.7) will therefore apply :

$$\phi(A; z) = F(z) = 0 \quad \forall z < 0 \quad \text{and} \quad z > L$$

#### 4. PROOFS

Proofs of varying mathematical rigour may be given for the postulates [e.g. showing that Eq. (6.5) represents an approximation to the Fourier integral solution to the boundary value problem defined by Eqs. (6.6) and (6.7)], but for the sake of brevity the following arguments from electrostatics theory are given :

- i) Conducting electrodes are superfluous if no free or induced charges are found on them; since  $|\nabla\phi| < \epsilon$  at  $z=0$  and  $z=L$ , these electrodes may be removed. This is equivalent to stating that the image charge distributions may be neglected as far as potential calculations in the region  $0 < z < L$ ,  $r < A$  are concerned.
- ii) The potentials at the ends of a conducting tube of radius  $A$  and length  $L_+$  have negligible influence on the potentials at the centre of the tube if the ratio  $L_+/A$  is sufficiently large. This can be shown by investigating the analytical solution [Chorlton (1968)] to the boundary value problem  $\phi(r; 0) = C = \phi(r; L_+) \quad \forall r < A$  and  $\phi(A; z) = 0, \quad 0 < z < L_+$ :

$$\phi(r; L_+/2) = \sum_{n=1}^{\infty} 2E_n J_0(\lambda_n r) \quad (6.9)$$

$$\text{in which } E_n = \frac{2C \sinh(\lambda_n L_+/2A)}{A \lambda_n \sinh(\lambda_n L_+/A) \cdot J_1(\lambda_n)}$$

and  $\lambda_n$  is the nth zero of  $J_0(z)$  [Abramowitz et al. (1970)]. Table (6.1) gives  $\phi(0;L_+/2)$  as a function of  $L_+$ , for  $A=C=1,0$ . For  $L_+/A \gg 1$ , the following approximation is useful :

$$\phi(r;L_+/2) = \frac{2 C \exp(-\lambda_1 L_+/2A) J_0(\lambda_1 r)}{A \lambda_1 J_1(\lambda_1)}$$

Although the use of Eq. (6.5) as a solution to Eqs. (6.6) and (6.7) may seem plausible in view of the given postulates, it must still be shown that sufficient precision can be obtained without undue computational effort.

##### 5. THE RATIO $L/L_e$

Eq. (6.8) defines  $L_e$  to be a measure of the physical extent of the region (the so-called lens region) where the magnitude of the gradient of the potential is not negligible (i.e.  $> \epsilon$ ). Since the value assigned to  $\epsilon$  depends upon the precision required for the electron optical calculation, the value of  $L_e$  is affected by this choice as well.

To complicate matters, the relationship between  $L_e$  and  $\epsilon$  is no simple one; in Ch. (5) it was shown that for a given function  $F(z)$  a representation can be found for  $\epsilon$  as a series of exponential functions and only for large values of  $z$  can  $\epsilon$  be approximated by a single exponential function.

For illustrative purposes,  $L_e$  is calculated for three functions



Table (6.1) : The potential  $\phi(0;L_+/2)$ , at the centre of a cylinder of radius  $A=1\text{m}$  and length  $L_+$ , as given by Eq. (6.9).

$L_+(\text{m})$	$\phi(0;L_+/2)$ (V)
1	0,767825
2	0,278674
5	$0,784435 \times 10^{-2}$
10	$0,192165 \times 10^{-4}$
20	$0,115255 \times 10^{-9}$
40	$0,414607 \times 10^{-20}$
80	$0,268261 \times 10^{-41}$

Table (6.2) :  $L_e$  of Section (5) as influenced by the choice of  $\epsilon$  (in V/m) for three function types. The functions i), ii) and iii) are defined by Eqs. (6.10), (6.11) and (6.12) respectively.  $A=1,0$  m. The value of  $L_e/2$  is listed in metres.

Function \ $\epsilon/2$	$10^{-3}$	$10^{-4}$	$10^{-5}$	$10^{-6}$	$10^{-7}$	$10^{-8}$
i)	3,7	4,7	5,7	6,7	7,7	8,7
ii)	3,6	4,5	5,5	6,4	7,4	8,4
iii)	3,9	4,9	5,9	6,9	7,8	8,8

$F(z)$ , chosen to represent function types of varying smoothness :

Type (i) is a rectangular function, i.e. a function with a singularity in the gradient :

$$\begin{aligned} F(z) &= 0 \quad \forall z < (L/2 - L_f) \text{ and } \forall z > (L/2 + L_f) \\ F(z) &= C_1, \quad (L/2 - L_f) < z < (L/2 + L_f) \end{aligned} \quad (6.10)$$

in which  $C_1$  and  $L_f$  are constants. We take here  $C_1=1V$  and  $L_f=1,0m \ll L/2$ . Type (ii) is a B-spline, i.e. a continuous function with a continuous gradient :

$$\begin{aligned} F(z) &= 0, \quad \forall z < (L/2 - 3\lambda/2) \\ F(z) &= C_2(z - L/2 + 3\lambda/2)^2, \quad (L/2 - 3\lambda/2) < z < (L/2 - \lambda/2) \\ F(z) &= C_2\{C_3 - 2(z - L/2 + \lambda/2)(z - L/2 - \lambda/2)\}, \quad (L/2 - \lambda/2) < z < (L/2 + \lambda/2) \\ F(z) &= C_2(z - L/2 - 3\lambda/2)^2, \quad (L/2 + \lambda/2) < z < (L/2 + 3\lambda/2) \\ F(z) &= 0 \quad \forall z > (L/2 + 3\lambda/2) \end{aligned} \quad (6.11)$$

in which  $C_2=(2/3)V/m^2$ ,  $C_3=1m^2$  and  $\lambda=1m$

Type (iii) is an exponential function, i.e. an analytic function :

$$F(z) = C_4 \exp(-Dz^2) \quad \forall z \quad (6.12)$$

in which  $C_4=1V$ .

The value of  $L_e$  for various choices of  $\epsilon$  is given in Table (6.2).

If we take the constant  $D$  in Eq. (6.12) equal to  $1,0/m^2$ , the three types of field will have approximately the same value  $L_e$  on the basis of  $\epsilon \approx 10^{-6}V$ . In all three cases  $A$  was taken as  $1m$ .

To determine the influence of the choice of  $L$  upon the precision

of  $\phi(r;z)$  as calculated by means of Eq. (6.5),  $L$  was equated to 5, 10, 20 and 40 m and  $\phi(r;z)$  calculated in each case for a number of different points  $(r;z)$ . Let these values be called  $\phi_5(r;z)$ ,  $\phi_{10}(r;z)$ , etc.

The differences

$$\delta_L \equiv |\phi_L(r;z) - \phi_{40}(r;z)|$$

have been calculated and are given in Table (6.3). Care has been taken to calculate the Fourier coefficients of Eq. (6.5), to approximately 9 significant figures, and in the summation of each series a sufficient number of terms were included to ensure that the truncation error was less than  $10^{-9}$ . It therefore seems reasonable to assume that the differences  $\delta_L$  may be ascribed to the violation of the criteria of the postulates of Section (3). Investigating the differences of  $\delta_{10}$  and  $\delta_{20}$  it seems a fair assumption that the difference between  $\phi_{40}(r;z)$  and the correct solution  $\phi_\infty(r;z)$  should be smaller than  $10^{-9}$ .

As shown in the next section, the convergence of the series of Eq. (6.5) is strongly dependent upon the choice of the ratio  $L_a=L/A$ , and the value of  $L$  chosen in practice will again depend upon the value of the precision  $\epsilon'$  of the potential  $\phi$  as required by the electron optical problem. For  $\epsilon' = 10^{-8}V$ ,  $L$  can be taken equal to 20 m.

Fig. (6.1) shows equipotentials for the type (iii) function. (This

Table (6.3) : The values (in V/m) of  $\delta_L$  of Section (5) as a function L, for the three function types of Eqs. (6.10), (6.11) and (6.12) resp. For each function  $\delta_L$  is listed for points a, b and c with coordinates (0;L/2), (0;L/2+2) and (0;L/2+4) resp. A= 1 m

Function	Point	L		
		5 m	10 m	20 m
i)	a	$1 \times 10^{-4}$	$<10^{-9}$	$<10^{-9}$
	b	$6 \times 10^{-3}$	$4 \times 10^{-8}$	$<10^{-9}$
	c	N.A.	$5 \times 10^{-6}$	$<10^{-9}$
ii)	a	$5 \times 10^{-5}$	$1 \times 10^{-9}$	$<10^{-9}$
	b	$2 \times 10^{-2}$	$2 \times 10^{-8}$	$<10^{-9}$
	c	N.A.	$3 \times 10^{-6}$	$<10^{-9}$
iii)	a	$2 \times 10^{-4}$	$1 \times 10^{-9}$	$<10^{-9}$
	b	$1 \times 10^{-2}$	$7 \times 10^{-8}$	$<10^{-9}$
	c	N.A.	$1 \times 10^{-5}$	$<10^{-9}$

type of function could not be handled by the Fourier-Bessel method of Ch. (5) unless a large  $L_a$  ratio is chosen; in that event the contributions from the  $J_0$  Bessel functions will be negligible, and the method of Ch. (5) becomes identical to the method described in this chapter. The potentials  $\phi(r>A; z)$  have been found by means of the solution given in Appendix (2), where both interior and exterior equipotential lines are also shown for the case where  $F(z)$  is a step function.

## 6. CONVERGENCE OF THE SERIES

As stated in Section (2), the series of Eq. (6.5) will be convergent if the series of Eq. (6.3) is convergent. To be useful in practice, the series must have a high rate of convergence, which is generally not obtained with high  $L_a$  ratios. It is therefore important to choose  $L_a$  a ratio which complies with the requirements of Sections (5) and (6), but is low enough to give an acceptable rate of convergence.

The convergence of the series of Eq. (6.5) can be seen to depend upon two factors : the convergence of the series for  $F(z)$  and the ratio  $I_0(n\pi r/L)/I_0(n\pi A/L)$ .

The convergence of the series for  $F(z)$  is a function of  $z$ , and also depends upon the nature of  $F(z)$ . It is therefore not feasible to express the convergence as a function of  $z$  and  $r$ ; for a rough estimate one may, however, calculate a value of  $n_c$  such that the func=

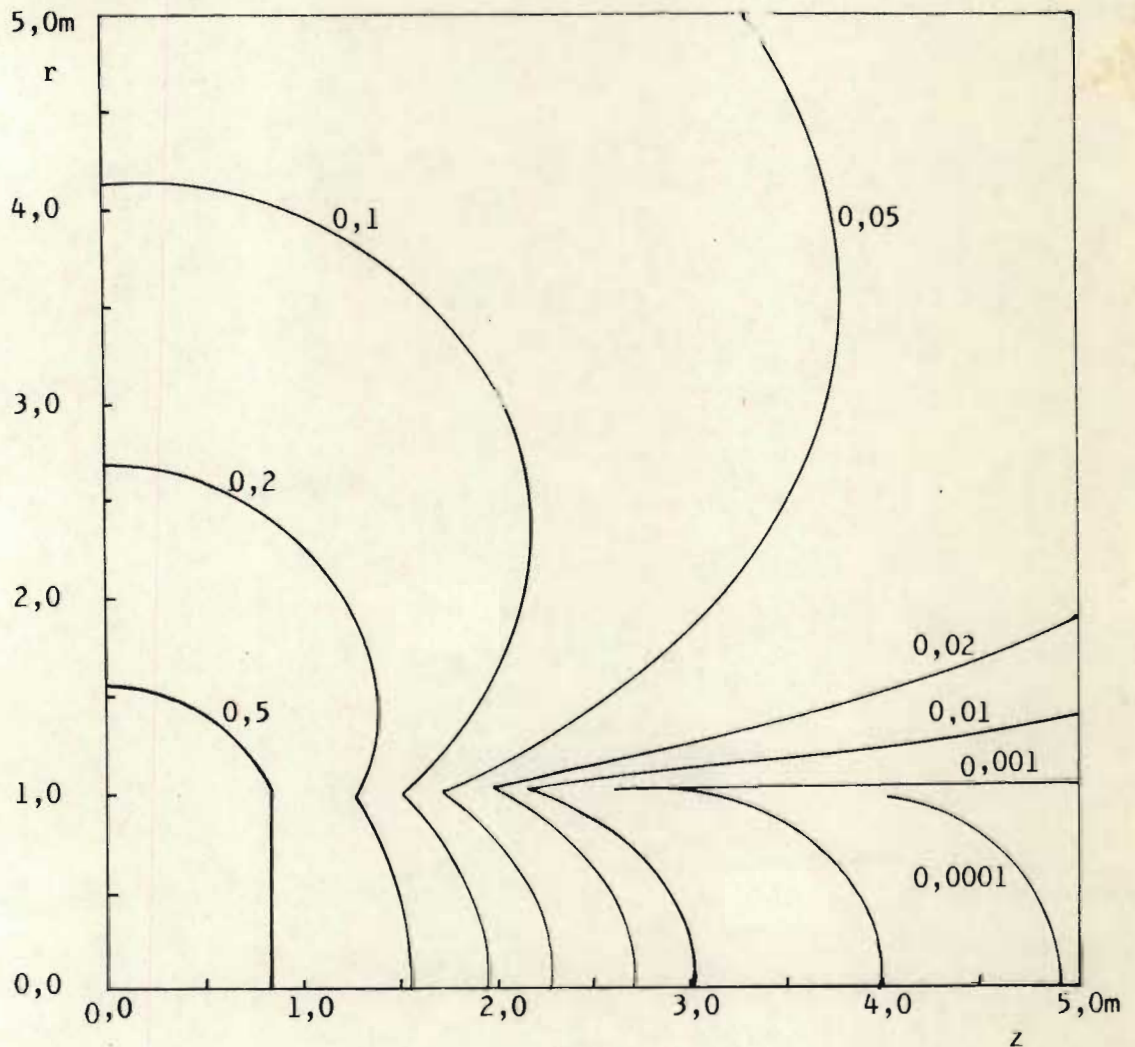


Fig. (6.1) Equipotential lines for boundary value problem of Eq.(6.12), for part of upper right quadrant.

$D=1,0$ ;  $A=1,0$ ;  $L_a=320$ .

Interior and exterior equipotentials are shown.

$L_a$  was given this large value to allow the precise determination of exterior potential values.

tion  $B_n I_0(n\pi r/L)/I_0(n\pi A/L) < \epsilon' \forall n > n_c$ . The value of  $n_c$  will be determined by the nature of  $F(z)$  and will be a function of  $r$ ; values of  $n_c$  are listed in Table (6.4) for the three functions of Section (5), and for various values of  $\epsilon'$ .

It can be concluded that for functions resembling (i), (ii) and (iii), high precision electron optical calculations (e.g. absolute error of potentials  $< 10^{-7}V$ ) may be carried out with series truncated after a few tens of terms. The number of terms may be reduced by means of accelerating methods, one of which is mentioned in the next section.

## 7. THE USE OF LANCZOS $\sigma$ -FACTORS

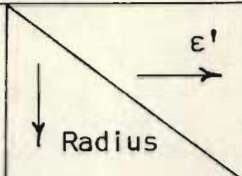
If  $F(z)$  includes any discontinuities (e.g. step functions) a Fourier analytical representation of  $\phi(r;z)$  will be affected by the Gibbs phenomenon in the vicinity of the discontinuity [Carlslaw (1930)]. Since true step function discontinuities are not found in physical configurations – finite gaps are required between electrodes at different potentials – it is profitable to make use of Lanczos  $\sigma$ -factors [Lanczos (1957)] and represent  $\phi(r;z)$  by a finite series :

$$\phi(r;z) \sim \sum_{m=1}^{N-1} B_m \left\{ \frac{\sin(\pi m/N)}{(\pi m/N)} \right\} \sin(m\pi z/L) \frac{I_0(m\pi r/L)}{I_0(m\pi A/L)}$$

in which the Lanczos  $\sigma$ -factors are shown in braces.

The terms in the braces can be seen to cause an acceleration of convergence (for  $N=101$  the last term of the finite series will

Table (6.4) :  $n_c$  of Section (5) given for two values of the radius  $r$ , for the three function types of Eqs. (6.10), (6.11) and (6.12). No accelerating methods have been applied here.  $A=1,0$  m and  $L=20$  m.

Function			$10^{-4}$	$10^{-6}$	$10^{-8}$	$10^{-10}$
			i)	$r=0$	24	38
	$r=A/2$	35	59	80	100	
ii)	$r=0$	20	59	72	79	
	$r=A/2$	33	63	77	100	
iii)	$r=0$	15	19	23	26	
	$r=A/2$	16	20	24	28	



be 100 times smaller than the corresponding term of the original series) and because the calculation of the Lanczos  $\sigma$ -factors are based upon a spatial averaging process, the Gibbs overshoot at the discontinuity and associated ripple elsewhere will be smoothed out.

## 8. APPLICATION TO IMMERSION LENSES

Consider the following function  $F(z)$  :

$$F(z) = 0, \quad 0 < z < (L/3 - d)$$

$$F(z) = g(z), \quad (L/3 - d) < z < (L/3 + d)$$

$$F(z) = C_i, \quad (L/3 + d) < z < L/2$$

Let  $F(z)$  be symmetrical w.r.t.  $z = L/2$ , let  $d$  be a constant  $\ll L$ , and let  $g(z)$  be a given continuous function with the properties :

$$g(z) = 0 \text{ for } z = L/3 - d$$

$$\text{and } g(z) = C_i \text{ for } z = L/3 + d$$

It can be seen that the regions near  $L/3$  and  $2L/3$  represent immersion lenses for which Eq. (6.5) will represent the potentials  $\phi(r; z)$  to any degree of precision by taking the  $L/A$  ratio sufficiently large. By means of different functions  $g(z)$  a wide variety of immersion lenses can be described. Since the remarks of the previous sections on the applicability of Eq. (6.5) to Einzel lenses apply here as well, no detailed discussion on the immersion lens representations is given here.

## 9. DESCRIPTION OF WIDE ANGLE LENSES

It may seem from the given examples as if the  $L_a$  ratio must be significantly larger than 1,0 for all given functions  $F(z)$ , so

that wide angle lenses are excluded. This is not the case, and lenses with  $\nabla \phi \neq 0$  at  $z=0$  and  $z=L$  have been found for  $L_a < 1$ , if  $F(z)$  is allowed to oscillate between large positive and negative values, not unlike some zonal fields found as approximate solutions to the inverse interior Dirichlet problem for certain non-analytic potential distributions [see Ch. (8)].

#### 10. ADVANTAGES OF THE METHOD

The Fourier-Bessel solution given by Eq. (6.5) has a number of advantages when compared to alternative methods of solving the Dirichlet boundary value problem :

- a) The method is a direct one, employing no iterative procedures.
- b) No matrices need be inverted, resulting in high precision (apparently limited only by the computer word length) and extremely modest computer memory requirements — a desk top computer with a few kilobytes can be used.
- c) The programming is simple, requiring a few tens of statements in BASIC or FORTRAN.
- d) In addition to  $\phi(r;z)$ , any derivatives of  $\phi$  are obtained in series form by differentiating Eq. (6.5), allowing very high precision calculation of the derivatives used, e.g., in trajectory calculations [Dirmikis et al. (1975)].

- e) The potential and its derivatives are calculated for any point  $(r; z)$  without needing interpolation (as in the finite difference method, where values are normally known on a regular grid only).
- f) Compared to the Fourier-Bessel solution of Ch. (5), the present formulation is superior for paraxial calculations, because of fast convergence near the axis, for all values of  $z$ . (In contrast, the former expansion has two zones on the axis where convergence is slow, necessitating the use of accelerating methods).
- g) The solution is in a form which is suitable for use in electron optical optimization programs as has been described in Ch. (4) for closed configurations.
- h) The solution is of use [Ch. (8)] in formulating a solution to the inverse internal Dirichlet problem (i.e. the axial potential distribution is given, and off-axis potentials have to be found). The present approach allows approximate solutions of high precision to be found for given analytic as well as non-analytic axial potential distributions, in contrast to the analytic continuation method [Skolleremo (1976a and 1976b)] which is restricted to analytic functions only.

One disadvantage of present solution that must, however, be mentioned, is that  $F(z)$  must be known  $\forall z$ . This is a disadvantage

shared by the finite difference and finite element approaches, but not by the integral equation method. Fourier methods to handle gaps between electrodes require further investigation.

#### 11. REMARK ON FOURIER-BESSEL INTEGRAL REPRESENTATION

As stated in Section (2), we can represent  $F(z)$  of Eq. (6.1) by a Fourier integral, if  $F(z)$  is not periodic. In this case the solution to the boundary value problem of Eqs. (6.6) and (6.7) can be written as a Fourier-Bessel integral

$$\phi(r; z) = \int_0^{\infty} B(\omega) \frac{I_0(\omega r) \sin(\omega z)}{I_0(\omega A)} d\omega \quad (6.13)$$

$$\text{where } B(\omega) = \frac{\pi}{2} \int_0^{\infty} F(z) \sin(\omega z) dz \quad (6.14)$$

When used in practice, the integration of Eq. (6.13) has to be carried out by computer. If, for example, the trapezium rule or Simpson's rule is applied, a finite Fourier-Bessel series is in effect utilized to approximate the integral. This means that a periodic function is used to approximate the non-periodic function  $\phi(r; z)$ . This periodic function can approximate  $\phi(A; z) = F(z)$  to the required precision within the required region of interest (i.e.  $0 < z < L$ ), because the integral of Eq. (6.13) is a Fourier integral for  $r=A$ , and no longer a Fourier-Bessel integral. Einarsson (1968, 1971 and 1972) has shown by computer studies that the integration of a Fourier integral by cubic splines (as suggested by Quade

and Collatz) is superior to the Filon, trapezium and Simpson methods, and allows high precision to be reached [see also Einarsson (1976) for the use of Richardson extrapolation for increased precision]. The quality of fit of  $\phi(A;z)$  for the region  $0 < z < L$  is not adversely affected by the periodicity of the Fourier series.

For  $r \neq A$  the situation is completely different. Some thought will show that if  $\phi(A;z)$  is periodic (w.r.t.  $z$ ), then  $\phi(r < A; z)$  for  $0 < z < L$  corresponds to the boundary value problem of Eqs. (6.1) and (6.2), and not of Eqs. (6.6) and (6.7). Care should therefore be taken to determine the period of the finite Fourier-Bessel series resulting from the discretization of the function  $B(\omega)$  of Eq. (6.13), a process normally inherent in the numerical computation of the Fourier-Bessel integral. If the period is too small to meet the requirements of Section (3), totally wrong values of  $\phi(r < A; z)$  may be obtained.

The Fourier-Bessel series approach outlined in this chapter has not been optimized as far as computational efficiency is concerned. The present formulation shows similarity to the trapezium rule integration of the Fourier-Bessel integral of Eq. (6.13) which is not an efficient method if calculation of integrand values is time consuming. Fewer evaluations of Bessel functions can result from using Simpson's rule, or deriving the Fourier-Bessel equivalent of Filon's formula for the Fourier integral (likely to be complicated) or using cubic splines in a way similar to Einarsson. These possibilities have not been explored, the purpose of the present paper

being to offer a solution which is simple and is easily programmed.

## 12. POSSIBILITY OF INCREASING PRECISION

For the interior Dirichlet problem the precision of the solution given above should be sufficient for most electron optical purposes. For the exterior Dirichlet problem the convergence of the Fourier-Bessel series may, however, be so slow for the larger  $r/L$  ratios, that methods must be applied to eliminate the effect of the grounded plane electrodes, by taking into account the effects of either the induced charge distributions on these electrodes, or of the equivalent charge images [Appendix (2)]. These corrections are equally applicable to the interior Dirichlet problem.

## 13. CONCLUSION

A Fourier-Bessel series representation is given for the potential distribution in certain open Einzel or immersion type electrostatic configurations with rotational symmetry. The method is a direct one and eliminates the use of  $J_0$  Bessel functions, resulting in superior convergence in the paraxial region. The precision reached is apparently limited by the computer word length only, programming is of a simple nature, and computer memory requirements are modest enough to use small desk top computers.

As an example of the use of the solution discussed in this chapter, some electron optical properties of one-foil lenses are discussed in Ch. (7).

## C H A P T E R 7

### THE ELECTRON OPTICAL PROPERTIES OF A CLASS OF ONE-FOIL LENSES, AS RELATED TO THE CHARGE DISTRIBUTION ON THE FOIL

The Fourier-Bessel series solution given in Ch. (6) allows open, one-foil and two-foil lenses to be modelled. The solution is used in this chapter, not to optimize lenses as far as a particular electron-optical property is concerned, but rather to predict electron optical patterns of behaviour of a class of one-foil lenses, by varying a small number of parameters. It can be expected that, by investigating the roles played by the parameters, sufficient insight will be gained to decide on a course to be followed, should optimization be required.

In this study weak one-foil lenses are investigated by emphasizing relationships between some focal properties and the charge distributions induced on the foil. The earthed foil is placed at  $z=0$ , the region  $z \leq 0$  is at zero potential, and the following potential distribution is applied at  $z > 0$  :

$$\phi(A;z)=0, 0 \leq z \leq z_0 ; \phi(A;z)=V_m \sin [n\pi (z-z_0)/L_9],$$

$$z_0 \leq z \leq z_0+L_9 ; \phi(A;z)=0 \forall z > z_0+L_9. \quad V_m \text{ is either } +1V \text{ or } -1V,$$

and  $z_0$  and  $L_9$  are varied one at a time. The cases  $n=1$  and  $n=2$  are considered. It is shown that the resulting foil lenses show broader patterns of behaviour than might be construed from current literature.

#### 1. INTRODUCTION

It is a well established property of open electrostatic electron optical lenses that they show positive spherical aberration, i.e.

that for instance for an object at  $z \rightarrow -\infty$ , the rays passing through the lens at larger radial distances cross the optical axis  $Oz$  at points closer to the lens than paraxial rays do. This is also the case with objects placed at any finite distance.

Open systems have the further property that they are convergent in their first operating range. (Rays crossing the axis inside the lens are refocussed and may cross the axis any number of times, but these operating ranges of higher order are excluded from this discussion.)

In a comprehensive review article Septier (1966) showed that most of the efforts to correct electrostatic systems with rotational symmetry were based on the introduction of an electrostatic charge into the lens region traversed by the rays : either a charge distribution on an axial electrode, or space charge in the form of an electron cloud or beam, or charge distributions on conducting foils which are thin enough to be highly transparent to electrons [Wittels (1975)].

Due to the presence of the conducting foils, the so-called foil lenses have properties that differ fundamentally from open (i.e. foilless) configurations ; it is, for example, possible to design divergent lenses and also lenses with negative spherical aberration. It is also possible to replace the foil by a gauze or a grid, but the openings in the gauze act individually as miniature open lenses, requiring a more complex analysis [Verster (1963)]



than foil lenses. And although some of the results reported in this paper will apply to gauze lenses as well, the text will mainly refer to foil lenses.

Of the papers on foil or gauze lenses, some deal with curved foils [Hoch et al. (1976)] or gauzes [Verster(1963)]; these are difficult to manufacture and are excluded from this discussion. Others deal with (converging) magnetic lenses which are combined with (diverging) foil lenses so as to obtain an overall reduction in spherical aberration [Maruse et al. (1970), Maruse, Hiratake and Ichihashi (1970), Maruse, Ichihashi and Hiratake (1970), Ichihashi and Maruse (1971) and (1973), Hibino and Maruse (1976) and Hibino et al. (1977)]. Only the electrostatic part of such combinations will be covered by examples in Section (4).

Of the purely electrostatic lenses the special case [Gianola (1950) and Mayor et al. (1972)] of a uniform intensity field between two parallel foils or gauzes is excluded from this discussion, because its lens action is brought about by changes in the velocity  $v_z$  parallel to the optical axis only; parallel beams are not converged or diverged, and to be effective to reduce the positive spherical aberration of converging beams, it must be used in its strong form. Electrostatic lenses with two foils as discussed in Chs. (2)-(4) and by Wittels (1975) and Munro et al. (1977) are also excluded, because of the additional scattering of the particles by the second foils.

Lenses with single foils or grids have been described for simple [Verster (1963), Young (1975), and Bernard (1951a , 1951b and 1952)] and more elaborate [Hoch et. al. (1976), Scherzer (1949), and Typke (1972a and 1972b)] configurations, and in the majority of cases the electron optical properties have been related to the physical dimensions of and potentials on the electrodes. This makes the qualitative understanding of the behaviour of the lenses a difficult task, because lenses that have very similar shapes often show patterns of behaviour that are fundamentally different. Typke (1968 , 1972a and 1972b) approached the correction of lenses with spherical aberration by using the paraxial lens equation to predict under which conditions space and surface charge distributions can be expected to reduce aberrations of various types and orders.

The approach of this chapter is to consider some simple boundary potential distributions and find the corresponding charge distributions on the foil. It is then shown how the charge distributions affect the focal properties of the lenses. In this way the behaviour of a wide variety of foil lenses can be explained qualitatively and quantitatively for paraxial as well as zonal rays.

## 2. CONDITIONS FOR CONVERGENCE AND ZERO SPHERICAL ABERRATION

In open lenses both the radial distance  $r$  and the  $z$  velocity of the charged particle vary as it passes through the lens. [We use

cylindrical polar coordinates  $(r; z)$ , with the optical axis coinciding with the  $Oz$  axis]. Both these effects, which may be labelled the  $O_r$  and  $O_z$  effects, contribute to i) making the lens convergent and ii) causing overall positive spherical aberration. If  $r$  and  $v_z$  had remained constant, the net impulse on the particle would have been zero, as may be deduced from Gauss' law.

In foil lenses a third effect (which may be labelled the F effect) has an influence on the impulse received by the particle, due to the fact that the total charge within a cylinder  $r=r_0$  will in general not be zero, resulting by Gauss' law in a net non-zero impulse on a particle passing through the lens at an (almost) constant radial distance  $r_0$  and an (almost) constant  $v_z$ .

It can be seen that, for fast particles, the deflection due to the F effect will be much stronger than that due to the  $O_r$  and  $O_z$  effects so that the focal properties of weak foil lenses may be ascribed mainly to the F effect. For stronger lenses the  $O_r$  and  $O_z$  effects increase in importance and this may, e.g. cause a lens which shows negative spherical aberration at long focal lengths, to show positive spherical aberration at short focal lengths, as shown in Ch. (4) and as reported by Hoch et al. (1976). It can also cause a lens which is divergent for fast particles to be convergent for slow particles, as shown in Ch. (2). The main purpose of this chapter is to discuss the focal properties due to the F-effect, for various simple configurations, explaining their

behaviour as weak lenses. The behaviour of the same configurations used as strong lenses can be understood qualitatively by mentally superposing the  $O_r$  and  $O_z$  effects.

## 2.1 Condition for a lens to be convergent

Consider an electron which enters a foil lens from a field free region  $z < 0$ . The earthed foil is found at  $z=0$ , and various other electrodes with rotational symmetry cause a non-zero potential field  $\phi(r; z)$  at  $z > 0$ , extending up to  $z=L_g$ , the lens length. (Strictly speaking,  $L_g \rightarrow \infty$  in one-foil lenses, but for practical purposes  $L_g$  may be taken as such a distance that  $\partial\phi/\partial r$  and  $\partial\phi/\partial z$  have been reduced to  $10^{-6}$  of their maximum values). At  $z=0$ , the particle is characterized by  $r=r_0$ ,  $v_z \neq 0$ ,  $v_r=0$ .

The total radial impulse experienced by an electron is proportional to

$$\tau(r_0) = \int_0^{\infty} \frac{\partial\phi}{\partial r}(r_0; z) dz \quad (7.1)$$

Using Gauss' law,

$$\begin{aligned} q(r_0) &= 2\pi \int_0^{r_0} r \sigma(r) dr \\ &= -2\pi\epsilon_0 r_0 \int_0^{\infty} \frac{\partial\phi}{\partial r}(r_0; z) dz = -2\pi\epsilon_0 r_0 \tau(r_0) \quad (7.2) \end{aligned}$$

in which  $\sigma(r)$  is the surface charge density on the foil and  $q(r_0)$  is the charge on the foil between the axis and  $r=r_0$ .

Normally  $\sigma(r)$  is calculated from  $\partial\phi(r;0)/\partial z$ , so that

$$\tau(r_0) = -\frac{q(r_0)}{2\pi\epsilon_0 r_0} = -\frac{1}{\epsilon_0 r_0} \int_0^{r_0} r \frac{\partial\phi(r;0)}{\partial z} dr \quad (7.3)$$

It can be seen that weak electron lenses with  $\tau$  positive or negative will result in divergent or convergent lenses, respectively.

It will also be seen in Section (4) that  $q(r)$  need not have the same sign  $\forall r$ . It is therefore more correct to say that  $q(r_0) < 0$  or  $> 0$  will cause an electron entering the lens at radial distance  $r_0$ , to diverge or converge, respectively.

## 2.2 Conditions for zero, positive and negative spherical aberration

If the trajectories of particles through weak lenses are investigated, it can be shown by simple geometry that the constant  $\beta$  in the approximate relationship  $\tau \propto r^\beta$  will determine whether the longitudinal spherical aberration

$$S_4(r_0) \equiv f_z(0) - f_z(r_0) \quad (7.4)$$

of a parallel ray passing through  $(r_0;0)$  will be zero or non-zero;  $z=f_z(r_0)$  is the focal point of this ray. [The proportionality given above represents a concise alternative to the more conventional series formulation  $\tau = C_1 r + C_2 r^3 (1 + C_3 r^2 + C_4 r^4 + \dots)$  The conditions  $\beta < 1$ ,  $\beta = 1$  or  $\beta > 1$  are used as substitutes for mathematically more rigorous but clumsier statements as, e.g.,  $C_2 < 0$ ,  $C_2=0$  or

$C_2 > 0$  for  $C_1 > 0$ ,  $C_3 > 0$ ,  $C_4 > 0$ , etc; similar statements then have to be given to cover the many other possibilities.]

#### The case $\beta = 1,0$

Weak lenses with  $\beta=1,0$  show zero spherical aberration. This condition can be satisfied approximately by a variety of one-foil and two-foil lenses. It may be of interest to compare lenses with plane foils and  $\beta = 1,0$  (labelled Zero Spherical Aberration Plane Foil Lenses, ZSAPFL) with the unique class of lenses in which the impulse received in the vicinity of  $(r;z)$  is proportional to  $r$ ,  $\forall z$ ; this condition is met by [see, e.g., Zashkvara et. al. (1977)] the potential distribution  $\phi(r;z) = r^2 - 4z^2$  (labelled the Ideal Double Foil Lens, IDFL). i) The ZSAPFL and IDFL, although equivalent in their weak forms, can be expected to behave differently in their strong forms; computer ray tracing results will be reported elsewhere; (ii) the equipotentials of the ZSAPFL are all curved, except for  $|z| \rightarrow \infty$  or  $r \rightarrow \infty$ , making such a design more difficult to implement; (iii)  $|\nabla \phi(r;z)|$  increases with  $r$  and  $|z|$  in the IDFL, whereas in the ZSAPFL  $|\nabla \phi(r;z)|$  decreases within  $z = L_g$  to a sufficiently low value that the foil at  $z = L_g$  becomes superfluous and may be discarded.

In view of the above differences, the ZSAPFL has distinct advantages, if only the spherical aberration has to be eliminated.

#### The condition $\tau \propto r^\beta$ , $\beta \neq 1,0$

Here  $\beta > 1$  and  $\beta < 1$  result in  $S_1 > 0$  and  $S_1 < 0$  resp., for convergent

lenses, and  $S_1 < 0$  and  $S_1 > 0$  for divergent lenses. Septier (1966) has stated that "it is thus possible to cancel, or even reverse the sign of  $C_3$ " (third order spherical aberration) "by altering the potential on the grid. This is possible only when the lens is divergent, however; a grid lens free of aberration cannot be used on its own, but only as a correcting element". Although this is correct for the special class of foil lenses studied by Bernard (1951a, 1951b and 1952), and may appear to apply to the more complex configurations [Bernard (1953a and 1953b)] approximated by his analytical model, it will be seen in Section (4) that it is possible to design foil lenses which show positive and negative spherical aberration irrespective of whether the lens is convergent or divergent. (Convergent foil lenses with negative spherical aberration have been reported in Ch. (4), and also by Hoch et. al. (1976), but without pointing out that Septier's statement was contradicted. A theoretical treatment given by Scherzer (1949) also predicted that a convergent lens can be designed with  $S_1 = 0$ , and not ruling out the possibility that  $S_1 < 0$  could be obtained by varying some parameters).

It may be remarked that if  $\tau(r) \propto r^\beta$  is differentiated w.r.t.  $r$ , it is seen for convergent lenses, for instance, that the conditions  $\beta < 1,0$ ;  $\beta = 1,0$  and  $\beta > 1,0$  correspond to negative, zero and positive spherical aberration, respectively.  $\sigma(r)$ , rather than  $\tau(r)$  can therefore be represented graphically, so that for convergent lenses  $\sigma(r)$  vs.  $r$  graphs which decrease in absolute value,

remain constant or increase in absolute value, indicate negative, zero and positive spherical aberration, respectively. A similar statement can be formulated for divergent lenses.

### 3. THE BOUNDARY VALUE PROBLEM AND SOLUTION

Variations of the following configuration are considered : the plane  $z = 0$  represents a plane earthed conducting foil which is thin enough to be sufficiently transparent to electrons. A set of ring electrodes, all of radius  $r = A$ , provide the following potential distribution :

$$\phi(A; z) = 0 \quad 0 \leq z \leq z_0 \quad (7.5a)$$

$$\phi(A; z) = V_m \sin [n \pi (z - z_0)/L_g] , \quad z_0 \leq z \leq z_0 + L_g \quad (7.5b)$$

$$\phi(A; z) = 0, \quad z \geq z_0 + L_g \quad (7.5c)$$

For all the cases reported here,  $A = 1m$  and  $V_m = + 1V$ . The cases  $V_m = -1V$  are not represented graphically, but feature in some of the discussions. For a chosen value of  $n$  ( $n$  is either 1 or 2), either  $L_g$  is varied, keeping  $z_0 = 0$ ; or  $z_0$  is varied, keeping  $L_g = 1,0m$ . These variations seem to allow a qualitative explanation of the behaviour of most of the simple configurations that are of practical interest.

A solution for  $\phi(r; z) \forall r \leq A$  and  $z \geq 0$  was given in Ch. (6) in the form of a Fourier-Bessel series [see also Appendix (2)]:

$$\phi(r; z) = \sum_{n=1}^{\infty} B_n \sin (n \pi z/L) \frac{I_0(n \pi r/L)}{I_0(n \pi A/L)} \quad (7.6)$$



in which

$$B_n = \frac{2}{L} \int_0^L \phi(A; z) \sin(n \pi z/L) dz, \quad (7.7)$$

$I_0$  is the modified Bessel function of the first kind and of order zero, and  $L$  is a length which is chosen sufficiently larger than  $A$  that  $(L - L_0)/A \gg C$ , a constant which is normally taken larger than 5, depending upon the precision required. Making use of the discussion of the solution in Ch. (6),  $L$  was chosen to be 10m, allowing the series in Eq. (7.6) to be truncated after about 40 terms for  $r = 0$ , or about 80 terms for  $r = 0,8A$ .

The Fourier analysis of Eq. (7.7) is simple to carry out, using Eq. (2.532) of [Gradshteyn et al. (1965)]. The electric intensity  $\partial\phi/\partial z$  is found by differentiating the series of Eq. (7.6). Although it has been found to be more instructive to give a graphical representation of  $\sigma(r)$  rather than of  $\tau(r)$ , the latter can easily be found from Eq. (7.6) by making use of Eq. (6.561.7) of Gradshteyn et al. (1965) or of Section (2.3.2) of Appendix (2).

It may be pointed out that if the region  $z < 0$  is field free, a resultant force acts on the foil along the  $z$ -axis, resulting in severe mechanical stresses and possible deformation. The  $z$ -components of these stresses may be eliminated by introducing into the region  $z < 0$  a potential distribution  $\phi_1(A; z < 0) = \phi(A; |z|)$ ; the analysis given above applies equally well to  $z < 0$ , provided the sign of  $V_m$  is reversed.

#### 4. FOCAL PROPERTIES OF THE VARIOUS CONFIGURATIONS

The focal properties of the various configurations are summarized in Tables (7.1) and (7.2). The seventh column gives graph numbers in the figures listed in column 6. Separate graphs are not given for the  $V_m = -1V$  lenses, but the graphs are similar to those with  $V_m = +1V$  provided that the entities on the vertical axes have their signs reversed. The reversal of sign is indicated by appending (-) to the graph number. Under the heading "C/D" the entries "C" or "D" indicate that the electron lens is convergent or divergent, respectively. In the column headed "S<sub>1</sub>", a -1, 0 or +1 indicates that the spherical aberration is negative, (paraxially) very small, or positive, respectively. No indication is given of the magnitude of the aberration; an estimate may be obtained by studying the rate of change of the  $\sigma(r)$  vs.  $r$  graphs. The entry ( $\pm 1$ ) in brackets in the last column indicates that the value of  $S_1$  in the transition region cannot easily be determined from the  $\sigma(r)$  graphs only; the value of  $S_1$  in this region may be found by studying the corresponding  $\tau(r)$  graphs as well. Finally, the presence of more than one entry in the last two columns indicates that paraxial rays are described by the first entry and zonal rays by the second entry.

Remarking on some of the entries, it may be pointed out that the simplest type of foil lens is represented by nos. 11-20. In these lenses the radial force has one sign throughout the trajectory, so that the lenses 11-15 are uniformly convergent and 16-20 are uniformly divergent, irrespective of the focal length of the lens. The

Table (7.1) : Classification of one-foil lenses, with  $n=1$  in Eq. (7.5b)

No.	$n$	$V_m$	$z_0$	$L_g$	Fig. no.	Graph no.	C/D	$S_1$
1	1	1	0,0	1,0	1 ; 2	a	D	-1
2	1	1	0,5	1,0	1 ; 2	b	D	0; +1
3	1	1	1,0	1,0	1 ; 2	c	D	+1
4	1	1	1,5	1,0	1 ; 2	d	D	+1
5	1	1	2,0	1,0	1 ; 2	e	D	+1
6	1	-1	0,0	1,0	1 ; 2	a(-)	C	+1
7	1	-1	0,5	1,0	1 ; 2	b(-)	C	0; -1
8	1	-1	1,0	1,0	1 ; 2	c(-)	C	-1
9	1	-1	1,5	1,0	1 ; 2	d(-)	C	-1
10	1	-1	2,0	1,0	1 , 2	e(-)	C	-1
11	1	1	0,0	0,5	5 ; 6	a	D	+1
12	1	1	0,0	1,0	5 ; 6	b	D	+1
13	1	1	0,0	1,5	5 ; 6	c	D	+1
14	1	1	0,0	2,0	5 ; 6	d	D	+1
15	1	1	0,0	2,5	5 ; 6	e	D	+1
16	1	-1	0,0	0,5	5 ; 6	a(-)	C	-1
17	1	-1	0,0	1,0	5 ; 6	b(-)	C	-1
18	1	-1	0,0	1,5	5 ; 6	c(-)	C	-1
19	1	-1	0,0	2,0	5 ; 6	d(-)	C	-1
20	1	-1	0,0	2,5	5 ; 6	e(-)	C	-1

Table (7.2) : Classification of one-foil lenses, with  $n=2$  in Eq. (7.5b)

No.	n	$V_m$	$z_0$	$L_g$	Fig. no.	Graph no.	C/D	$S_1$
21	2	+1	0,0	1,0	3 ; 4	a	C;D	-1; ( $\pm 1$ ); -1
22	2	+1	0,5	1,0	3 ; 4	b	D	-1; +1
23	2	+1	1,0	1,0	3 ; 4	c	D	+1
24	2	+1	1,5	1,0	3 ; 4	d	D	+1
25	2	-1	0,0	1,0	3 ; 4	a(-)	D;C	+1; ( $\pm 1$ ); -1
26	2	-1	0,5	1,0	3 ; 4	b(-)	C	+1; -1
27	2	-1	1,0	1,0	3 ; 4	c(-)	C	-1
28	2	-1	1,5	1,0	3 ; 4	d(-)	C	-1
29	2	+1	0,0	0,5	7 ; 8	a	C;D	+1; ( $\pm 1$ ); -1
30	2	+1	0,0	1,0	7 ; 8	b	C;D	-1; ( $\pm 1$ ); -1
31	2	+1	0,0	1,5	7 ; 8	c	D	-1
32	2	+1	0,0	2,0	7 ; 8	d	D	-1
33	2	+1	0,0	2,5	7 ; 8	e	D	-1
34	2	-1	0,0	0,5	7 ; 8	a(-)	D;C	-1; ( $\pm 1$ ); +1
35	2	-1	0,0	1,0	7 ; 8	b(-)	D;C	+1; ( $\pm 1$ ); -1
36	2	-1	0,0	1,5	7 ; 8	c(-)	C	+1
37	2	-1	0,0	2,0	7 ; 8	d(-)	C	+1
38	2	-1	0,0	2,5	7 ; 8	e(-)	C	+1

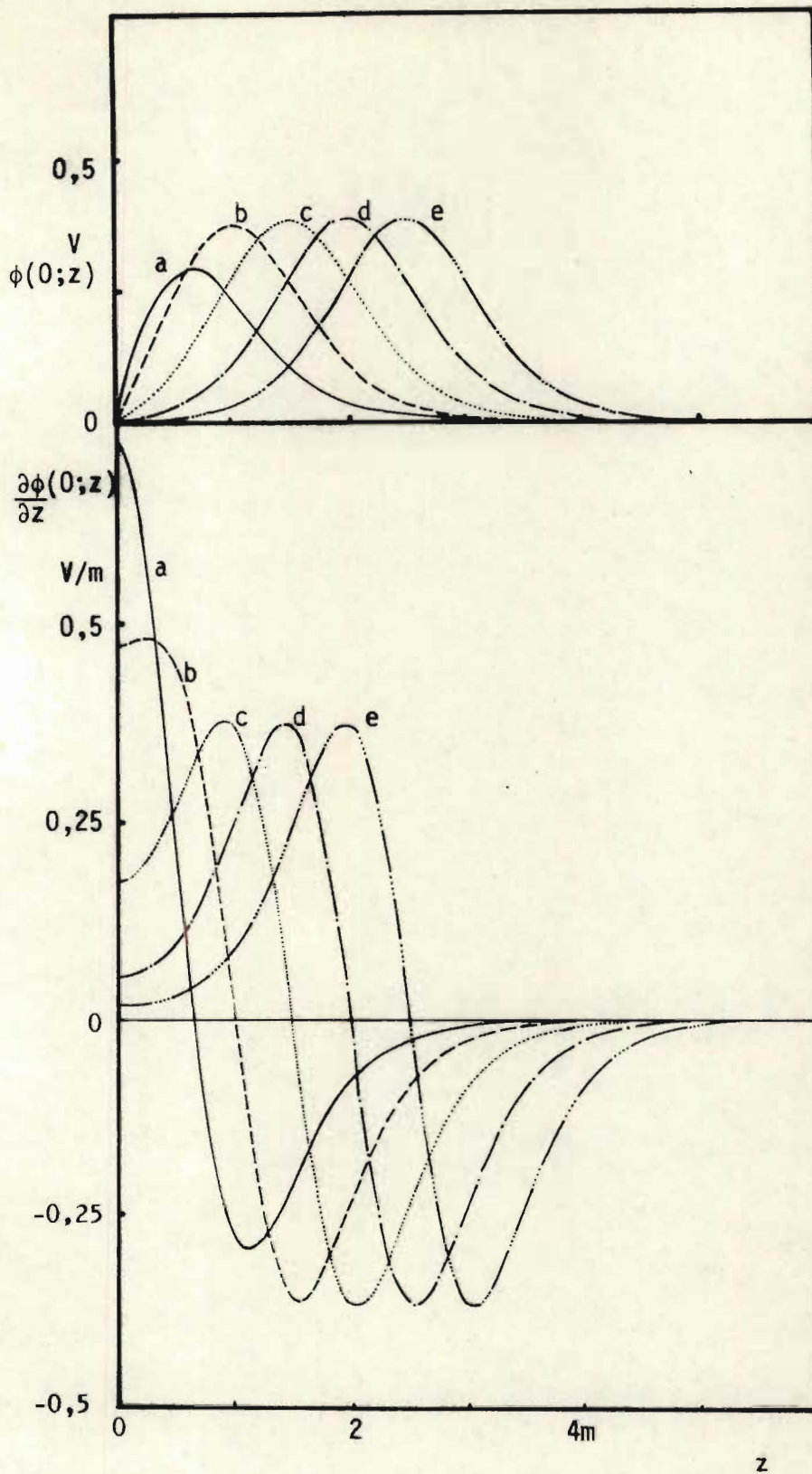


Fig.(7.1)  $\phi(0; z)$  vs.  $z$  (top) and  $(\partial/\partial z)\phi(0; z)$  vs.  $z$  (bottom) for lenses 1 to 5. Lens parameters are given in Table (7.1)

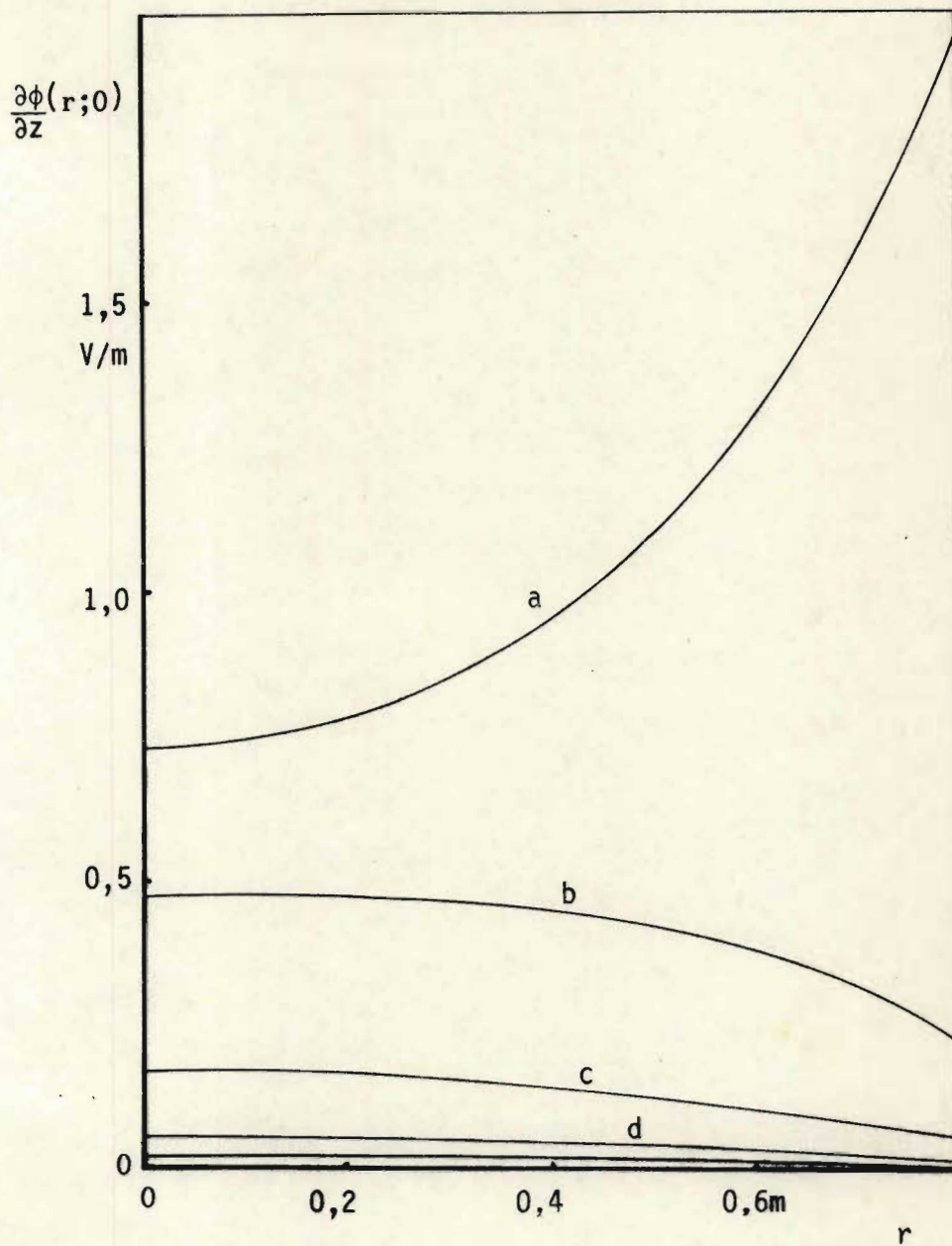


Fig.(7.2)  $(\partial/\partial z)\phi(r;0)$  vs.  $r$ , for lenses 1 to 5. Lens parameters are given in Table (7.1)

values of  $S_1$  and  $S_1/f$  are, however, dependent upon  $f$  [see, e.g., Ch. (2) for the analogous two-foil lens behaviour], although the sign of  $S_1$  remains unchanged. Lenses consisting of two coaxial tubes separated by a small gap, with one tube closed off by a foil on the gap side [Verster (1963) and Young (1975)] show this type of behaviour, as does a lens consisting of two coaxial tubes of radius  $A$ , separated by a gap in which a foil of radius  $R \gg A$  is placed [Bernard (1951a, 1951b and 1952), Klemperer et al. (1971), and Grivet (1965)].

If in the latter lens  $R < A$ , so that the foil has to be supported by a thicker electrode [Hoch et al. (1976), Scherzer (1949), and Typke (1972b)], the field can change fundamentally, in that i)  $\beta$  of Section (2.2) may be reduced to values lower than 1,0, so that ii) regions are introduced where  $\partial\phi/\partial r$  changes its sign along the trajectory, so that iii) the convergent  $O_r$  and  $O_z$  effects may in some cases exceed the F-effect, causing the lens to be divergent for fast particles, but convergent for slow particles. Point (i) is illustrated by nos. 2-5 and 7-10.

Although entries 7-10 represent convergent lenses with negative spherical aberration, the value of  $|S_1|$  is comparatively small, so that the change-over from a negative to a positive value of  $S_1$  may occur at a relatively large value of  $f$ . To obtain convergent lenses of short focal length but with  $S_1 \leq 0$ , one can investigate configurations which correspond qualitatively to lens 21 (=30), for

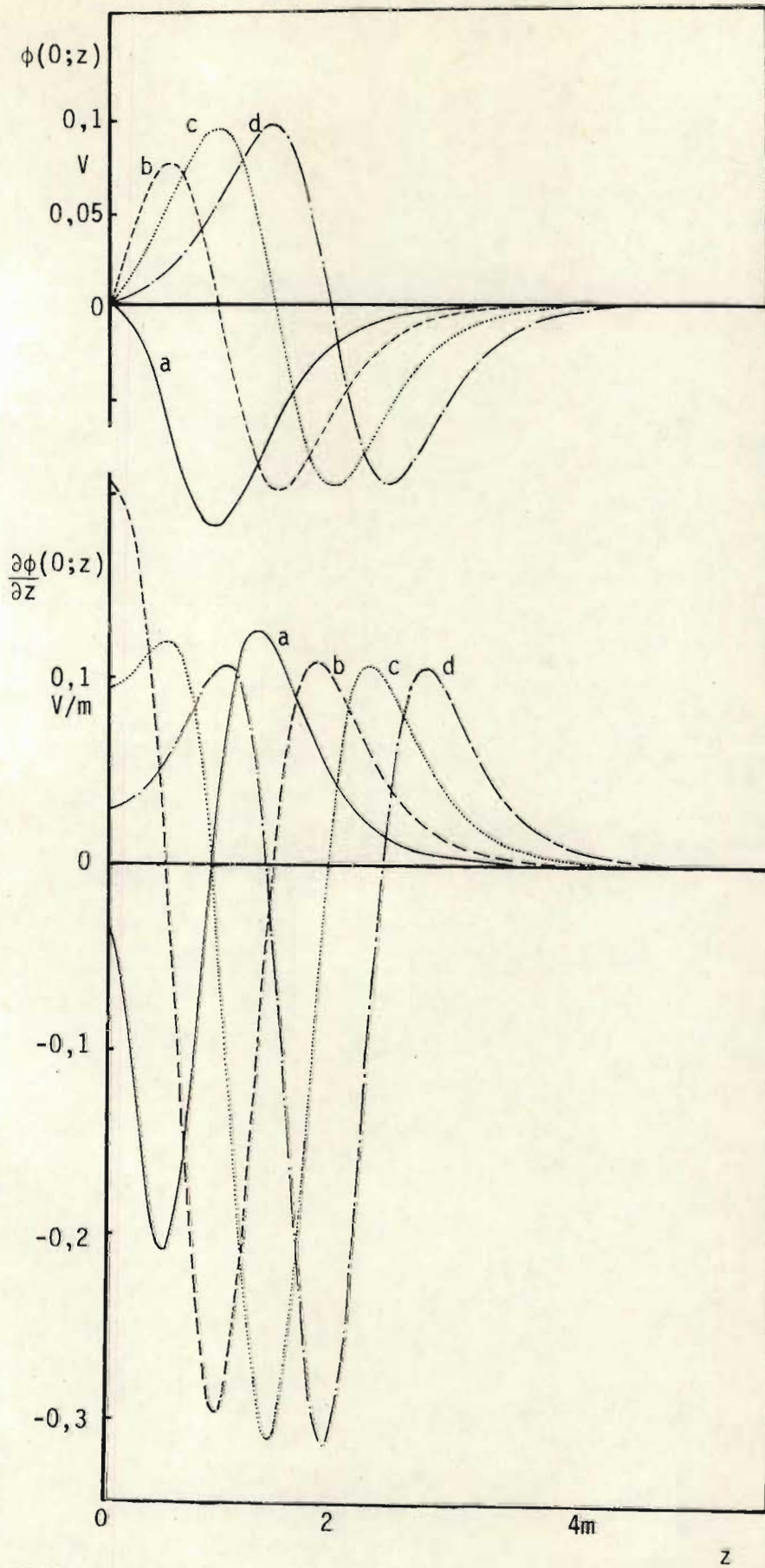


Fig.(7.3)  $\phi(0; z)$  vs.  $z$  (top) and  $(\partial/\partial z)\phi(0; z)$  vs.  $z$  (bottom) for lenses 11 to 15. Lens parameters are given in Table (7.1)



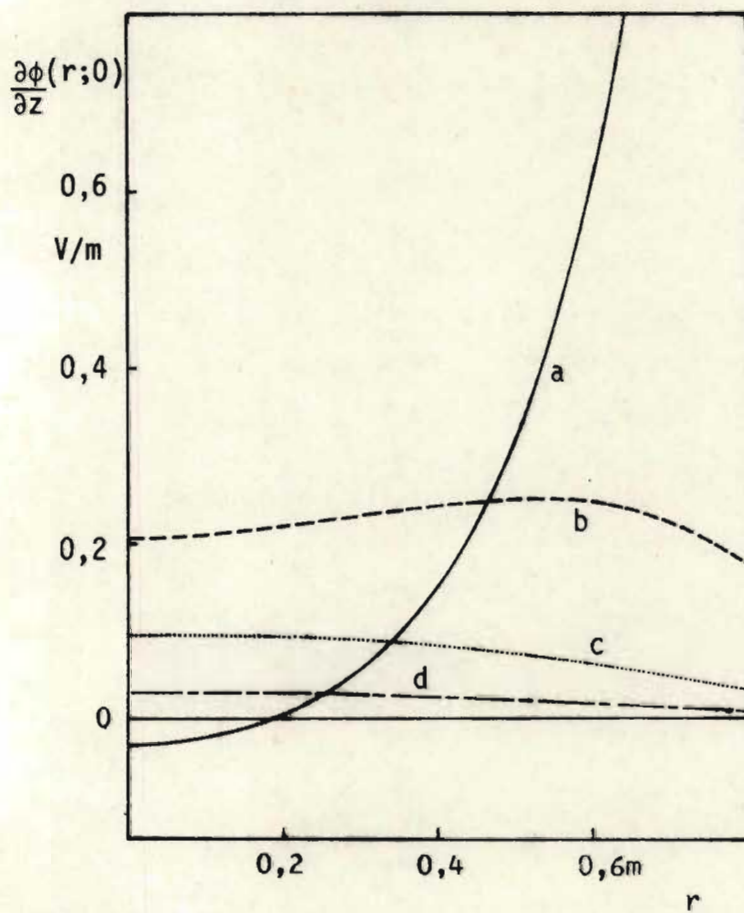


Fig.(7.4)  $(\partial/\partial z)\phi(r;0)$  vs.  $r$ , for lenses 11 to 15.  
 Lens parameters are given in Table (7.1)

which  $(\partial/\partial r)[(\partial/\partial z) \phi(r;0)]$  has a relatively large value in the paraxial region. This is accomplished by introducing a region of opposite polarity along  $r = A$ , which may be obtained in practice by an electrode [see, e.g., Typke (1972a and 1972b)] which plays a part not unlike a conventional Wehnelt electrode. Fig. (9) compares the negative spherical aberration of lens 21 with lens 3 for a range of focal lengths.

Several entries between nos. 21 and 38 have such a large spherical aberration that the focal length has a sign in the zonal region which differs from its sign in the paraxial region. The nature of a potential field of this type is shown in Fig (10); in this case,  $n = 4$ , and the entry is not represented in the tables.

Regarding entries 22 and 23, it may be seen that for some value of  $L_g$  between 1,0 and 1,5,  $\partial\phi(0;0)/\partial z$  will be zero, but  $\partial\phi(r>0;0)/\partial z > 0$  (the value of  $L_g$  turns out to be 1,065 for  $n = 2$ , or  $L_g = 1,612$  for  $n = 4$ ). This configuration will show zero convergence paraxially, but will be divergent for zonal regions; this lens is therefore a zero convergence lens showing negative spherical aberration. (If the sign of  $V_m$  is changed, positive spherical aberration will result). It may be introduced as a correcting element in order to remove positive spherical aberration from a system, without affecting its focal length. The possibility of obtaining such an element was mentioned in Ch. (4) and  $\phi(r;z)$  and  $(\partial/\partial z) \phi(r;z)$  graphs are given in Figs. (7.10) and (7.11).

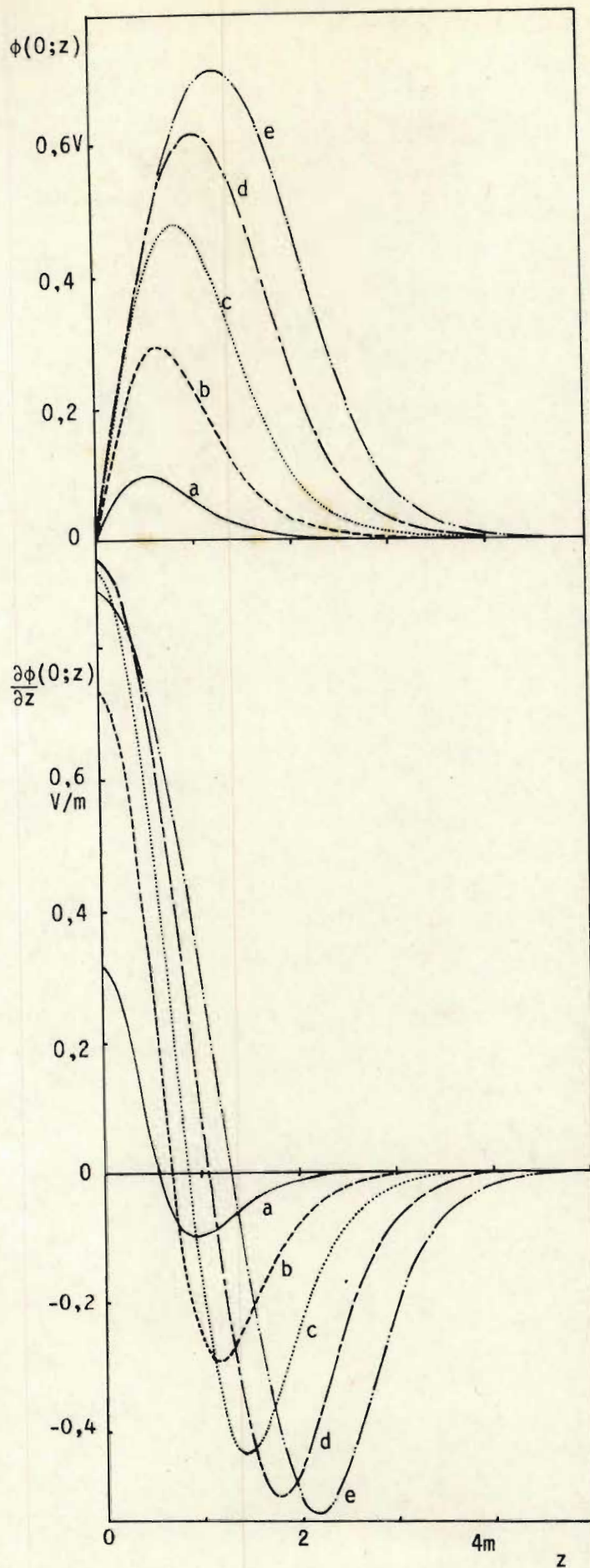


Fig.(7.5)  $\phi(0;z)$  vs.  $z$  (top) and  $(\partial/\partial z)\phi(0;z)$  vs.  $z$  (bottom) for lenses 21 to 24. Lens parameters are given in Table (7.2)

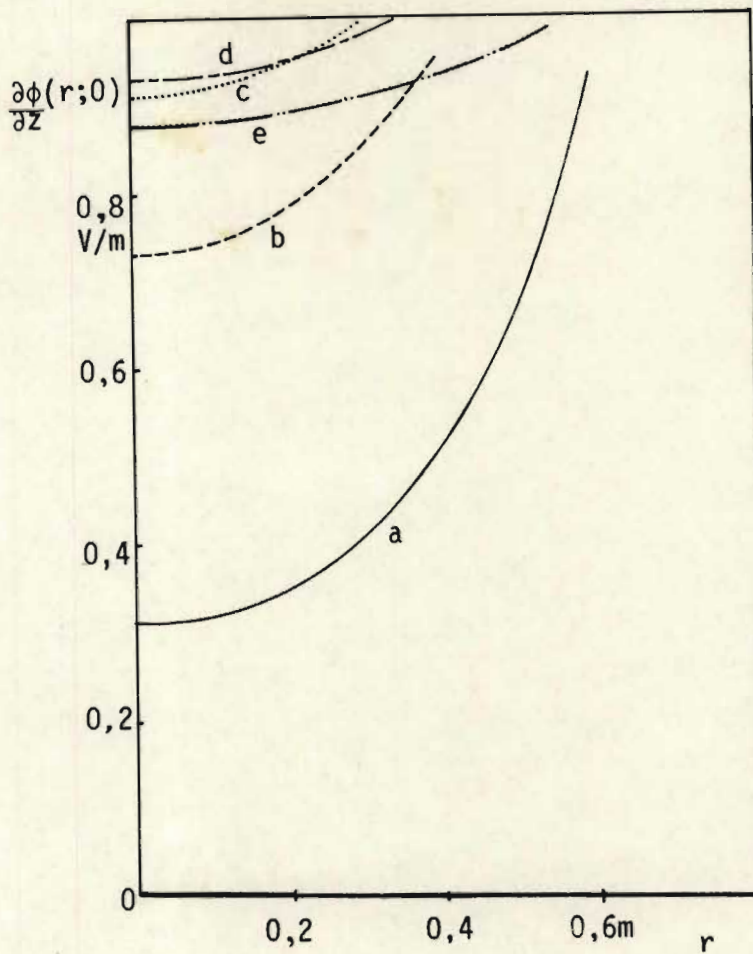


Fig.(7.6)  $(\partial/\partial z)\phi(r;0)$  vs.  $r$ , for lenses 21 to 24. Lens parameters are given in Table (7.2)

5. RELATIONSHIPS BETWEEN  $\sigma(r)$ ,  $\phi(0;z)$  AND  $\phi(A;z)$

In view of the wide variety of functions  $\tau(r)$  obtained by the rather simple boundary potential distributions  $\phi(A;z)$  considered in the previous sections, the possibility will now be investigated of determining a function  $\phi(A;z)$  that will result in a pre-specified (impulse) function  $\tau(r)$  which is considered suitable to correct the spherical aberration of a given lens. One may, for example, wish to correct a lens that shows third order spherical aberration  $C_3$ , by juxtaposing a correcting lens with  $\tau(r) \propto r^3$ . From Eq. (7.3) we deduce that  $q(r) \propto r^3$ ,  $\sigma(r) \propto r^2$  and therefore  $(\partial/\partial z)\phi(r;0) \propto r^2$ ; take

$$\frac{\partial\phi(r;0)}{\partial z} = kr^2 \quad (7.8)$$

It is known that an analytic function  $\phi(r;z)$  satisfies Laplace's equation, and is uniquely determined by the behaviour of the function along the axis, as shown by the expansion

$$\phi(r;z) = \sum_{n=0}^{\infty} \frac{(-1)^n}{(n!2^n)^2} \cdot \frac{\partial^{2n} \phi(0;z)}{\partial z^{2n}} r^{2n} \quad (7.9)$$

which can be derived, i.a., by analytic continuation. More specifically,  $\phi(r;z_0)$  is uniquely determined by  $\phi$  and its even  $z$  derivatives at a point  $z_0$ ; the same applies to  $\phi(0;z)$ ,  $\forall z$ .

Differentiation of Eq. (7.9) shows that the boundary value problem of Eq. (7.8) will be solved if a function  $\phi(0;z)$  is found satisfying

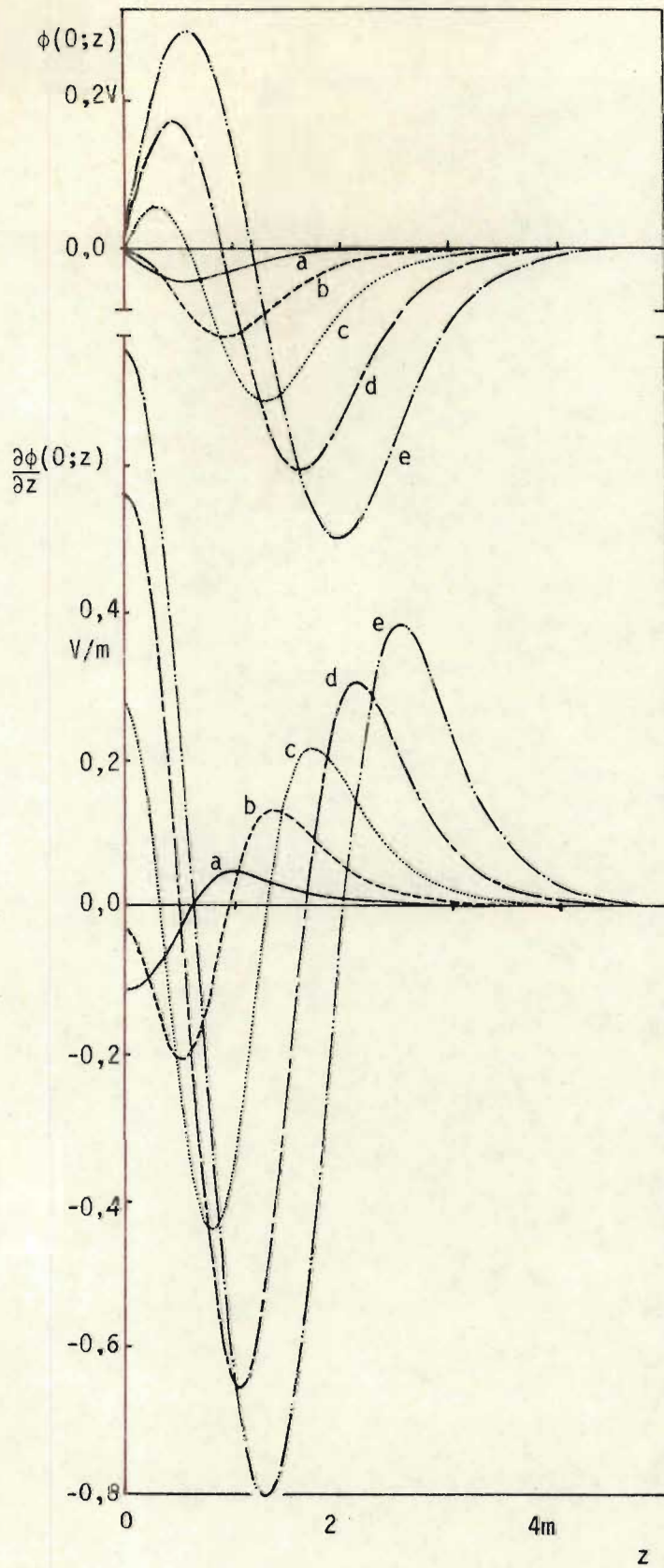


Fig.(7.7)  $\phi(0;z)$  vs.  $z$  (top) and  $(\partial/\partial z)\phi(0;z)$  vs.  $z$  (bottom) for lenses 29 to 33. Lens parameters are given in Table (7.2)

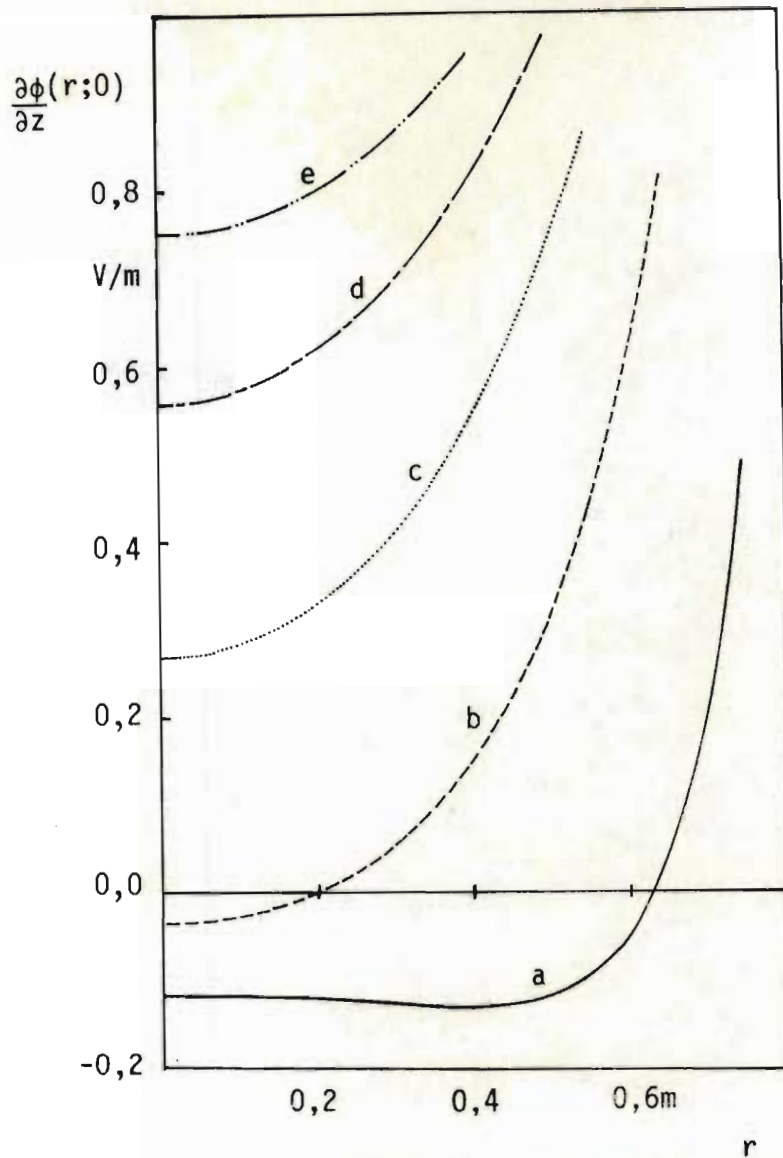


Fig.(7.8)  $(\partial/\partial z)\phi(r;0)$  vs.  $r$ , for lenses 29 to 33. Lens parameters are given in Table (7.2)

$$kr^2 = \frac{\partial \phi}{\partial z}(r; z) = \sum_{n=0}^{\infty} \frac{(-1)^n}{(n!2^n)^2} \cdot \frac{\partial^{2n+1} \phi(0;0)}{\partial z^{2n+1}} r^{2n} \quad (7.10)$$

It may seem as if the solution of this equation is a straightforward matter, because, for instance, the function  $\phi(0; z) = (-k/3)z^3$  satisfies Eq. (7.10). However,  $\phi(0; z \rightarrow \infty) \rightarrow \infty$ , and the condition  $(\partial/\partial z)\phi(0; z)=0$  is satisfied for  $z = 0$  only; consequently the function  $\phi(r; z)$  cannot represent a one-foil lens. It is therefore required that an analytic function  $\phi(0; z)$  be found which behaves (approximately) like  $(-k/3)z^3$  near  $z = 0$ , but is such that  $(\partial/\partial z)\phi(0; z)$  reaches sufficiently low values within the specified lens length  $L_0$ . This is no simple task, especially because piece-wise continuous functions are excluded if Eq. (7.9) must be applied to obtain  $\phi(r \neq 0; z)$ ; see, e.g., Skölleremo (1976a and 1976b). Attempts to circumvent the obstacle of having to use a single analytic function are described in Ch. (8). Not a single function, but a series is utilized; it has the following properties: i) the basis functions are trigonometrical, and therefore analytic; ii) the coefficients are chosen in such a way that Eq. (7.8) is approximately satisfied for small values of  $z$ ; and iii) the coefficients are chosen so as to let  $(\partial/\partial z)\phi(0; z)$  reach negligibly small values near  $z=L_0$ .

Having found the series representing  $\phi(0; z)$ , Eq. (7.9) can be used to find  $\phi(r \neq 0; z)$ , although it must be realized that an increased approximation error is propagated to the zonal regions, so that



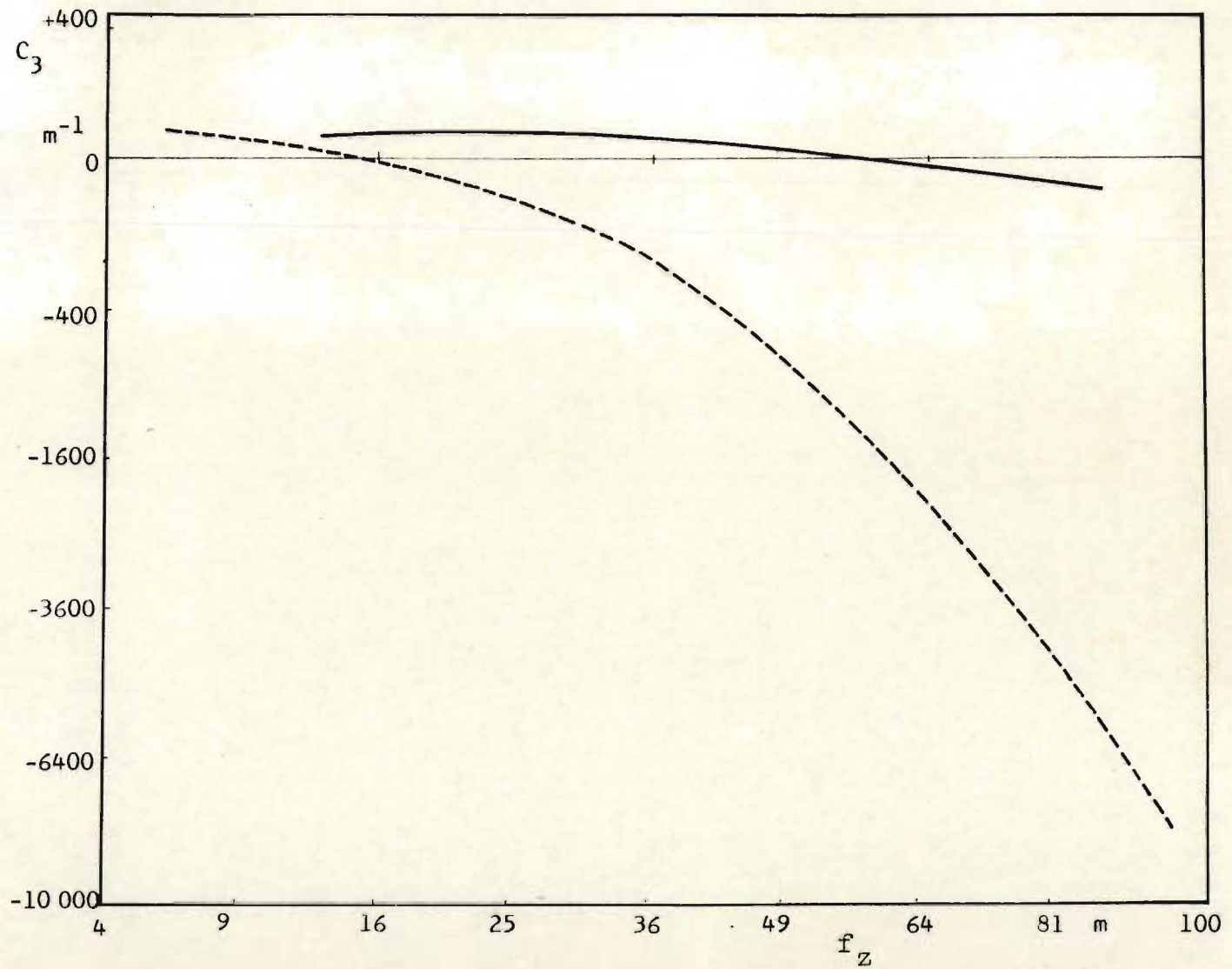


Fig.(7.9) The spherical aberration coefficient  $c = [f_z(0.0001R) - f_z(0.1R)] / (0.1R)^2$  plotted against the paraxial focal length  $f_z(0.0001R)$ . — : lens 3, - - - : lens 21.

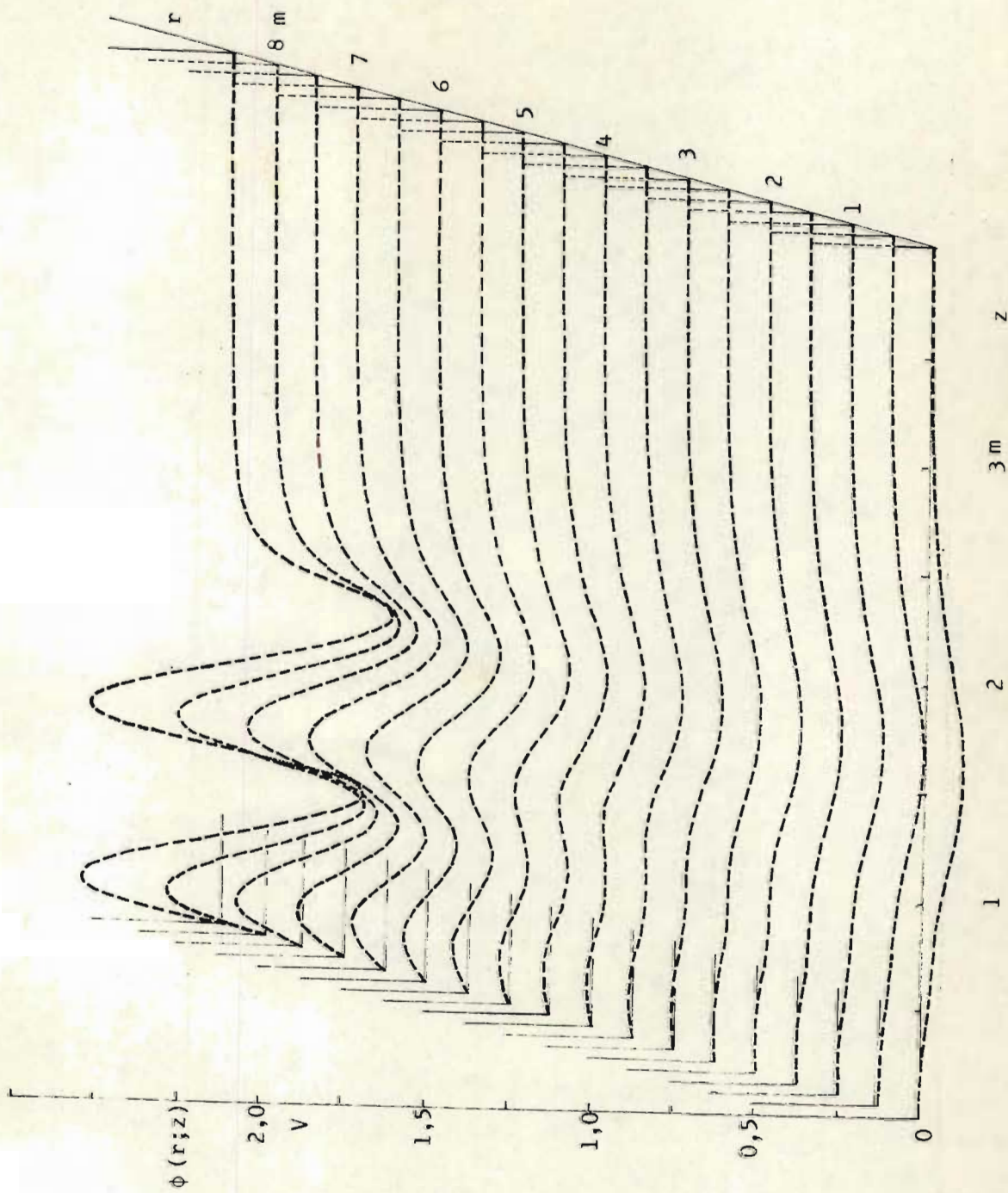


Fig. (7.10)  $\phi(r_0; z)$  vs.  $z$  for various values of  $r_0$ , for a lens with  $n=4$ ,  $V_m=1V$ ,  $R=1m$ ,  $L_g=1,612m$  and  $z_0=0$ .

$(\partial/\partial z)\phi(r;0)$  may differ from the expected value for large values of  $r$ ; this affects  $\tau(r)$  as well. A more detailed discussion is given in Ch. (8).

For two-foil lenses an alternative to the above approach may be formulated, based on Eq. (7.6). Differentiation of this equation gives

$$kr^2 = \frac{\partial\phi(0;z)}{\partial z} = \sum_{n=1}^{\infty} C_n I_0(n\pi r/L) \quad (7.11)$$

in which  $C_n = B_n n\pi / [L I_0(n\pi A/L)]$ . If the constants  $C_n$  can be found, satisfying Eq. (7.11) approximately, the problem is solved. This may be attempted by i) considering the series as a finite one and by point testing obtain an overdetermined system of linear equations from which  $C_n$  may be found by matrix inversion; or ii) by orthogonalizing the functions  $I_0(n\pi r/L)$  so that Eq. (7.11) can be used to find  $C_n$  by Fourier analysis [the description of such a procedure is given in Ch. (5)]. Due to the nature of the  $I_0$  Bessel functions, it will be found in cases i) as well as ii) that the matrices are not well conditioned, and precise solutions of Eq. (7.8) should not be expected.

## 6. CONCLUSIONS

By relating the impulse experienced by a charged particle passing through a one-foil lens, to the charge distribution on the foil, and then investigating the charge distributions due to variations of piece-wise sinusoidal potential distributions  $\phi(A;z)$ , it has been

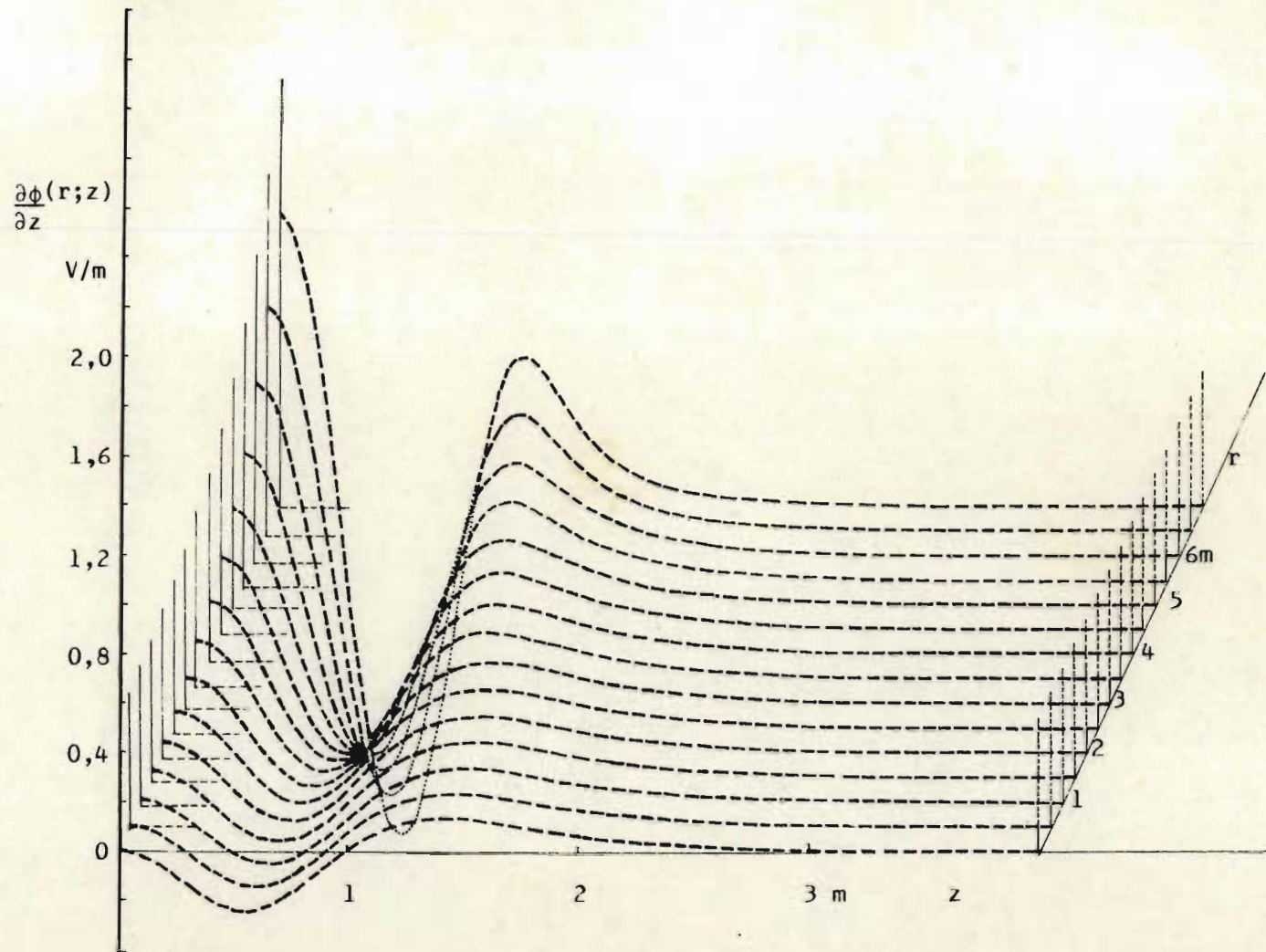


Fig.(7.11)  $(\partial/\partial z)[\phi(r_0, z)]$  for various values of  $r_0$ , for a lens with  $n=2$ ,  $V_m=1V$ ,  $R=1m$ ,  $L_g=1,065m$  and  $z_0=0$ .

shown that foil lenses can have i.a. the following patterns of behaviour for particles entering the lens at a radial distance  $r < A$ , and at a velocity  $v_z$  :

- i) convergent  $\forall r$  and  $\forall v_z$
- ii) convergent  $\forall r < r_0$  and  $\forall v_z$ ; divergent  
 $\forall r > r_0$  and  $\forall v_z > (v_z)_0$ ; but convergent  
 $\forall v_z < (v_z)_0$
- iii) divergent  $\forall r$  and  $\forall v_z$
- iv) convergent  $\forall r > r_0$  and  $\forall v_z \gg (v_z)_0$ ; divergent  
 $\forall r < r_0$  and  $\forall v_z \gg (v_z)_0$ ; but convergent  
 $\forall r$  and  $\forall v_z \ll (v_z)_0$
- v) convergent and  $S_1 > 0 \forall v_z$
- vi) convergent and  $S_1 < 0 \forall v_z > (v_z)_0$
- vii) divergent and  $S_1 < 0 \forall v_z$
- viii) divergent and  $S_1 > 0 \forall v_z > (v_z)_0$

in which  $r_0$  and  $(v_z)_0$  are constants dependent upon the nature of the configuration, and  $S_1$  is given by Eq. (7.4).

The list is not comprehensive, but serves to show that foil (or grid) lenses are not limited to types i), iii), v) and vii) as might be deduced from current literature.

It is also shown that lenses with negative (or positive) spherical aberration but with negligible convergence can be obtained by a careful choice of boundary potential function; such a correcting lens can be introduced into a lens system without affecting its focal length.

## CHAPTER 8

### THE INVERSE INTERIOR DIRICHLET PROBLEM

In the preceding chapters the electron optical properties were investigated of potential fields brought about by a set of equidiameter coaxial ring electrodes held at potentials given by a function  $f(z)$ . Properties of some two-foil lenses and one-foil lenses were investigated, and the Fourier-Bessel series solution of Ch. (6) would allow a similar study to be undertaken of open lenses.

It may, however, be argued that a much more direct approach will result if a function on the axis itself is investigated. The possibility of performing an optimization in this way was already suggested in Section (6) of Ch. (1). To allow this approach to be implemented, requires that a solution to the inverse interior Dirichlet problem be utilized. In this chapter the possibility is investigated of finding an approximate solution to this problem in terms of Fourier-Bessel functions.

It will be shown that an infinite number of rotationally symmetrical functions  $\Psi(r;z)$  can be found which approximate a given function  $f(z)$  on the optical axis  $Oz$  ( $r$  and  $z$  being cylindrical polar coordinates). The  $\Psi(r;z)$  are given in the form of a finite Fourier-Bessel series and it is shown how a solution that can be used in electron optical design can be selected by carefully assigning values to the following parameters : the number of terms in the series, the period of the series and the amount of smoothing introduced. In this way a compromise is established between the quality of the axial approximation, the magnitude of potential gradients to be contended with in zonal regions, and the sizes of apertures allowed. Two-foil, one-foil, and open lenses can be modelled, and given axial potential functions can be accommodated which are either i) analytic, ii) continuous, but with piece-wise continuous  $z$ -derivatives, or iii) in the form of a set of experimentally determined values.

It will be shown that the method requires no matrix inversion, the computer programming is of a simple nature, and memory requirements are modest enough to allow implementation of the program on small desk-top computers.

## 1. INTRODUCTION

The inverse interior Dirichlet problem considered in this chapter is the following :

$$\nabla^2 \phi(r;z) = 0 \quad \forall r < R \text{ and } \forall z \quad (8.1)$$

$$\phi(0;z) = f(z) \quad \forall z \quad (8.2)$$

It is required to find  $\phi(r;z) \forall z$  and  $\forall r < R$ , a given finite radius.  $r$  and  $z$  are cylindrical polar coordinates, and  $f(z)$  is a given finite

function which is defined for all  $z$ , has at most a finite number of discontinuities, and satisfies

$$\lim_{|z| \rightarrow \infty} f(z) = 0 \quad (8.3)$$

The solution of this problem is of interest in electron optical design because of the possibility of determining (or postulating) axial potential fields which are expected to have certain desired paraxial electron optical properties [Skölleremo (1976a and 1976b)]. To implement such a design, the potential field in zonal regions must then be calculated to make it possible to determine the shapes and potentials of conducting electrodes which will give rise to the chosen axial potential distribution.

Two possible methods of finding the solution were given by Scherzer in some of his first papers on theoretical electron optics, namely the integral expression [Scherzer (1936a)]

$$\phi(r; z) = \frac{2}{\pi} \int_0^{\pi/2} \operatorname{Re}[\phi(z + i r \sin \alpha)] d\alpha \quad (8.4)$$

and the series expansion [Scherzer (1933)]

$$\phi(r; z) = \sum_{n=0}^{\infty} \frac{(-1)^n}{(n! 2^n)^2} \cdot \frac{\partial^{2n} f(z)}{\partial z^{2n}} \cdot r^{2n} \quad (8.5)$$

The possibility of using a finite difference method was mentioned by Cosslett (1946) who quoted some unpublished results by Motz. The nature of the method is not known.



Solving the inverse problem by first calculating the charge distribution (for instance on the surface  $r=R$ ) which will give rise to  $\phi(0;z)$ , and then using Coulomb's law to find  $\phi(r > 0;z)$  was suggested recently by Hawkes (1973) and Du Toit (1976), but a practical implementation of the method could not be traced.

Some properties of the first two methods will be discussed briefly.

### 1.1 The integral method

Although this method requires that the function  $f(z)$  is given as a simple analytical expression, it is found that for most functions  $f(z)$  the integral of Eq. (8.4) cannot be obtained in closed form [Glaser (1956)]. The integral may be represented by a series, as shown by Scherzer (1936a) for his potential field of minimum spherical aberration, and as also suggested by Berz (1950), but the most profitable use of this method was made by Sköllermo (1976a and 1976b) who determined the real part of the integrand analytically, and then performed the quadrature by computer. In these comprehensive papers, a number of electric and magnetic fields of interest to electron optics were discussed. It is, however, important to note that only analytic functions  $f(z)$  can be accommodated by this method.

### 1.2 The series expansion method

Although Eq. (8.5) has been quoted [Scherzer (1933), Cosslett (1946), Glaser (1956), Maloff et al. (1938), Plass (1942) and Harman (1953)] for a few decades as the standard method of finding  $\phi(r;z)$  for the

paraxial regions, it is hampered by the same limitation as the integral method, namely that  $f(z)$  should be an analytic function.

If  $f(z)$  is a function which has a discontinuity in a  $z$ -derivative of any order at  $z=z_1$ , for instance,  $\phi(r > 0; z_1)$  will be found to be discontinuous at  $z=z_1$ . The method is therefore unsuitable for functions  $f(z)$  with piecewise continuous  $z$ -derivatives, the reason being that the right hand side of Eq. (8.5) is determined by the axial potential distribution in the close vicinity of the point  $(0; z)$  only. This is no problem if  $f(z)$  is an analytic function, because  $f(z)$  is known  $\forall z$  (and for the whole complex domain) if  $f(z)$  is specified for a line element of infinitesimal length [Berz (1950)].

If  $f(z)$  is given in the form of a discrete set of experimentally determined values, severe problems will be encountered [Olsen et al. (1966)] in calculating the higher derivatives, requiring smoothing by, e.g., performing a least squares fit to the given data.

## 2. THE FOURIER-BESSEL SERIES METHOD

Depending on the reason why the solution to the boundary value problem of Eqs. (8.1) and (8.2) is required, it may be found that the solution of the following boundary value problem is also acceptable as a substitute :

$$\nabla^2 \Psi = 0 \quad \forall z \quad \text{and} \quad \forall r < R \quad (8.6)$$

$$\Psi(0; z) = f(z) + \epsilon(z) \quad \forall |z| < Z \quad (8.7)$$

where  $\epsilon(z) = \Psi(0;z) - \phi(0;z)$  is the error of approximation of which the absolute value is restricted to values smaller than  $\epsilon_1$ ,  $\forall |z| < Z$ . The constant  $Z$  is a given length which is related to (and for purposes of this chapter will be considered to be equal to) the lens length, i.e. the paraxial region where the electric intensity is large enough to be of importance in electron optical computations.

At this point it may be remarked that, although a choice of a sufficiently small  $\epsilon_1$  may ensure that  $\Psi(0;z)$  is an acceptable approximation to  $\phi(0;z)$ , it may happen that  $\Psi(r > 0;z)$  turns out to be a poor approximation to  $\phi(r > 0;z)$ , depending on the nature of the given function  $\phi(0;z)$ , and the resulting  $\epsilon(z)$ . A few further general remarks on the properties of  $\Psi(r > 0;z)$  may be given here :

- i) There are infinitely many functions  $\epsilon(z)$  that satisfy Eq. (8.7). Consequently there are infinitely many functions  $\Psi(r > 0,z)$  that satisfy Eqs.(8.6) and (8.7). Especially for larger values of  $r$ , the various solutions may differ appreciably from each other.
  
- ii) It was pointed out by Berz (1950) that further conditions may be laid down, restricting the behaviour of  $\Psi(r > 0;z)$ . One may, for instance, require that plane OV equipotentials are located at  $z=0$  and  $z=L$ , so as to enable a two-foil lens having parallel, plane foils to be modelled.

- iii) In the absence of a restriction of the type just mentioned, it will be found that the behaviour of  $\epsilon(|z| > Z)$  will still influence  $\Psi(r > 0; |z| < Z)$ , especially for large values of  $r$ . [If  $\epsilon(r)$  is considered to be an analytic function, this statement may be rephrased by remarking that  $\Psi(r; z)$  will be determined not only by  $\epsilon(z_0)$ , but by all the  $z$ -derivatives of  $\epsilon$  at any chosen point  $z=z_0$ ].
- iv) In view of the above considerations, it would be profitable, having found a solution  $\Psi(r; z)$  satisfying Eqs. (8.6) and (8.7), to establish whether its properties are compatible with the requirements of the physical problem which necessitated the choice of  $f(z)$  of Eq. (8.2) in the first place. This will be illustrated by Sections (3) and (4).

### 2.1 The choice of approximating function, $\Psi(r; z)$

The approximating function,  $\Psi(r; z)$  discussed in this chapter is in the form of a series

$$\Psi(r; z) = \sum_{n=1}^N A_n W_n(r; z) \quad (8.8)$$

in which the functions  $W_n(r; z)$  are separable :

$$W_n(r; z) = g_n(z)h_n(r) \quad (8.9)$$

The sets of functions  $g_n(z)$  are chosen from a relatively small list of sets for which the integral [see Eq. (8.4)]

$$W(r; z) = \frac{2}{\pi} \int_0^{\pi/2} \operatorname{Re}[g(z + i r \sin \alpha)] d\alpha \quad (8.10)$$

can readily be found in closed form. Some are discussed briefly :

2.1.1 The function  $W(r; z)$  resulting from integrating  $g_n(z) = C_{n1} + C_{n2}z + C_{n3}[z \arctan(z) + 1]$  is given by El-Kareh et al. (1970), but it does not seem simple to accomplish a fit of a given axial potential by Eq. (8.8), using functions of this type. See El Kareh et al. (1970) for references on attempts to use superpositions of these functions.

2.1.2 For the functions  $g_n(z) = z^n$ , the functions  $W_n(r; z)$  can easily be found analytically, giving  $1, z, z^2 - r^2/4$ , etc., for  $n=0, 1, 2$ , etc. When transformed to spherical polar coordinates  $(\rho, \phi, \theta)$ , the functions are  $\rho^n P_n(\cos \theta)$ ,  $P_n$  being  $n$ -th order Legendre functions.

Approximating a function  $f(z)$  by a series based on the polynomials  $z^n$  presents no problem, especially if they are used in orthonormalized form, but the trigonometrical functions of Section (2.1.5) are probably more convenient because of some practical reasons; see, i.a., Sections [2.2(ii)] and [2.2(iii)] of Ch. (7).

2.1.3 The integrals of the functions  $g_n(z) = z^{-n}$  can similarly be shown to be  $\rho^{-n} P_n(\cos \theta)$ , and they have the advantage that

$z^{-n} \rightarrow 0$  for large  $z$ , but the approximation of a given function  $f(z)$  by means of a series based on  $z^{-n}$  is not as simple as, e.g. the Fourier technique of Section (2.1.5).

2.1.4 The functions  $g_n(z) = \exp(-nz)$  can be integrated [using Eq. (9.1.18) of Abramowitz et al. (1970)] to give solutions  $\exp(-nz)J_0(nr)$ , in which  $J_0$  is the unmodified Bessel function of the first kind and of order zero. The functions  $\exp(-nz)$  can in principle be used, especially if orthogonalized [a computer procedure is given in Ch. (5)], but they are not very suitable for orthogonalization, and it is unlikely that high precision approximations of "non-exponential" functions  $f(z)$  will be accomplished. [The functions  $\exp(-nz)Y_0(nr)$ , which are also solutions of Laplace's equation, are also rejected because the Bessel functions  $Y_0(r \rightarrow 0) \rightarrow -\infty$ .]

2.1.5 The functions  $g_n(z) = \sin(nz)$  and  $\cos(nz)$  can be integrated [using Eq. (9.6.16) of Abramowitz et al. (1970)] to give  $\sin(nz)I_0(nr)$  and  $\cos(nz)I_0(nr)$ , in which  $I_0$  is the modified Bessel function of the first kind and of order zero. (The functions  $\sin(nz)K_0(nr)$  and  $\cos(nz)K_0(nr)$  which are solutions of Laplace's equation, are rejected because the Bessel functions  $K_0(r \rightarrow 0) \rightarrow \infty$ . The functions  $\cos(nz)I_0(nr)$  are also discarded because they can be converted to the form  $\sin(nz)I_0(nr)$  through a phase change.

Of all the functions mentioned above, the set  $g_n(z) = \sin(nz)$

are probably the most convenient for approximating  $f(z)$ , due to the simplicity of the Fourier-analytical procedures, and the balance of the paper is devoted to the resulting solutions.

### 3. PROPERTIES OF THE FOURIER-BESSEL SOLUTIONS

It can be shown [Lanczos (1957)] that not only  $\sin(nz)I_0(nr)$ , but also

$$\Psi(r; z) = \int_0^{\infty} A(\omega) \sin(\omega z) I_0(\omega r) d\omega \quad (8.11)$$

is a solution of Laplace's equation. Taking  $r=0$ , the function  $A(\omega)$  can be found from the Fourier transform

$$A(\omega) = \frac{\pi}{2} \int_0^{\infty} \Psi(0; z) \sin(\omega z) dz \quad (8.12)$$

which is applicable to a function  $\Psi(0; z)$  which is not periodic.

Due to the computational difficulties [see Appendix (2)] of dealing with the Fourier-Bessel integral of Eq. (8.11), we rather investigate a solution of the form

$$\Psi(r; z) \sim \sum_{n=1}^N A_n \sin(n\pi z/L) I_0(n\pi r/L) \quad (8.13)$$

in which the coefficients

$$A_n = \frac{2}{L} \int_0^L f(z) \sin(n\pi z/L) dz \quad (8.14)$$

are found by Fourier analysis. [See Bertram (1940 and 1942) for an

alternative way of avoiding the computational difficulties mentioned above].

It can be seen that the function  $\Psi(0; z)$  will be periodic, with a period  $2L$ ; if  $f(z)$  is periodic with period  $2L_1$ , the choice  $L=L_1$  will obviously be made. If  $f(z)$  is not periodic, care must be taken in assigning a value to  $L$ , because this choice may affect the nature of the solution  $\Psi(r > 0, z)$  in the region of interest  $|z| < Z$ , as mentioned in Section (2); see also Section (3.2).

### 3.1 Convergence of the series

The factor  $I_0(n\pi r/L)$  in the series of Eq. (8.13) has a near-exponential behaviour for large arguments, forcing us to restrict  $N$  to finite values, except in cases where the functions  $f(z)$  in Eq. (8.14) result in Fourier coefficients  $A_n$  such that the product  $A_n I_0(n\pi r/L)$  goes to zero rapidly enough, for large  $n$ . And if the latter condition is not satisfied, it will be found that the function  $\Psi(r; z)$  oscillates violently if large values are assigned to  $N$  and  $r$ . Therefore there appears to be a limitation to the precision to which a given axial function  $f(z)$  may be approximated by a function  $\Psi(0; z)$  resulting from a set of physical electrodes : i) a large value of  $N$  ensures that the truncation error of the Fourier series representing  $f(z)$  is acceptably small; this requirement is in conflict with the requirement that ii) large values of  $N$  must be avoided so as to limit  $|\Psi(r > 0; z)|$  or  $|\nabla\Psi(r > 0; z)|$  to values that are small enough that they can be used in practical designs without running the risk of field emission between the electrodes. iii) One way of effecting



the compromise between i) and ii) is to restrict  $r$  to relatively small values, or more precisely, to small  $r/L$  ratios. iv) Another alternative is to restrict  $f(z)$  to relatively smooth functions; this will ensure that  $A_n$  goes to zero more rapidly.

It therefore appears that in the practical use of the solution of Eq. (8.13) a trade-off must be contended with between the following factors : i) a good axial approximation, ii) small gradients of  $\Psi$  in the zonal regions, iii) the use of large  $r/L$  ratios allowing strong lenses with large apertures to be modelled, and iv) the freedom to approximate functions  $f(z)$  which are not very smooth. For a fifth factor, see Section (3.2.4).

One way of accommodating non-smooth axial functions (e.g. piece-wise linear functions) is the use of Lanczos  $\sigma$  - factors which are arrived at by performing a spatial averaging process [Lanczos (1957)]. The process may be repeated any number of times to obtain further smoothing – and faster convergence – so that the series of Eq. (8.13) is replaced by the following one :

$$\Psi(r; z) \sim \sum_{n=1}^N A_n \left\{ \frac{\sin[\pi n/(N+1)]}{n\pi/(N+1)} \right\}^P \sin(n\pi z/L) I_0(n\pi r/L) \quad (8.15)$$

in which  $A_n$  is still given by Eq. (8.14), and  $P$  is a constant equal to the number of times the smoothing process has been performed. (The Lanczos  $\sigma$ -factor is the expression shown in braces). In Section (3.2.3) it will be seen that large values of  $P$  allow larger apertures to be accommodated, but also cause a deterioration in the

quality of the approximation of the axial potential function.

### 3.2 Discussion of some examples

The examples presented in the figures have been chosen to illustrate the points discussed in Section (3.1). The parameters referred to in this section are those that appear in Eq. (8.15).

#### 3.2.1 Systems with analytic axial potential distributions

As shown in Fig. (8.1) the present method represents an alternative to the methods traditionally used to solve the inverse interior Dirichlet problem for analytic functions. Here  $f(z) = C_1 \exp(-C_2 z^2)$  with  $C_1 = 1V$  and  $C_2 = (1m)^{-2}$ ;  $P=0$ ,  $L=20$  and  $N=60$ .

For functions not as smooth as the above one, the equipotential diagram does not appear to be the best graphical way to illustrate the behaviour of  $\Psi(r;z)$ ; graphs showing  $\Psi(r;z)$  as a function of two variables are given for the remaining functions.

#### 3.2.2 Systems with continuous axial potential distributions, but discontinuous z-derivatives; role of r

Fig. (8.2) shows that the Fourier-Bessel approach can provide a solution  $\Psi(r;z)$  corresponding to an axial distribution  $\Psi(0;z)$  which approximates a function  $f(z)$  which has discon=

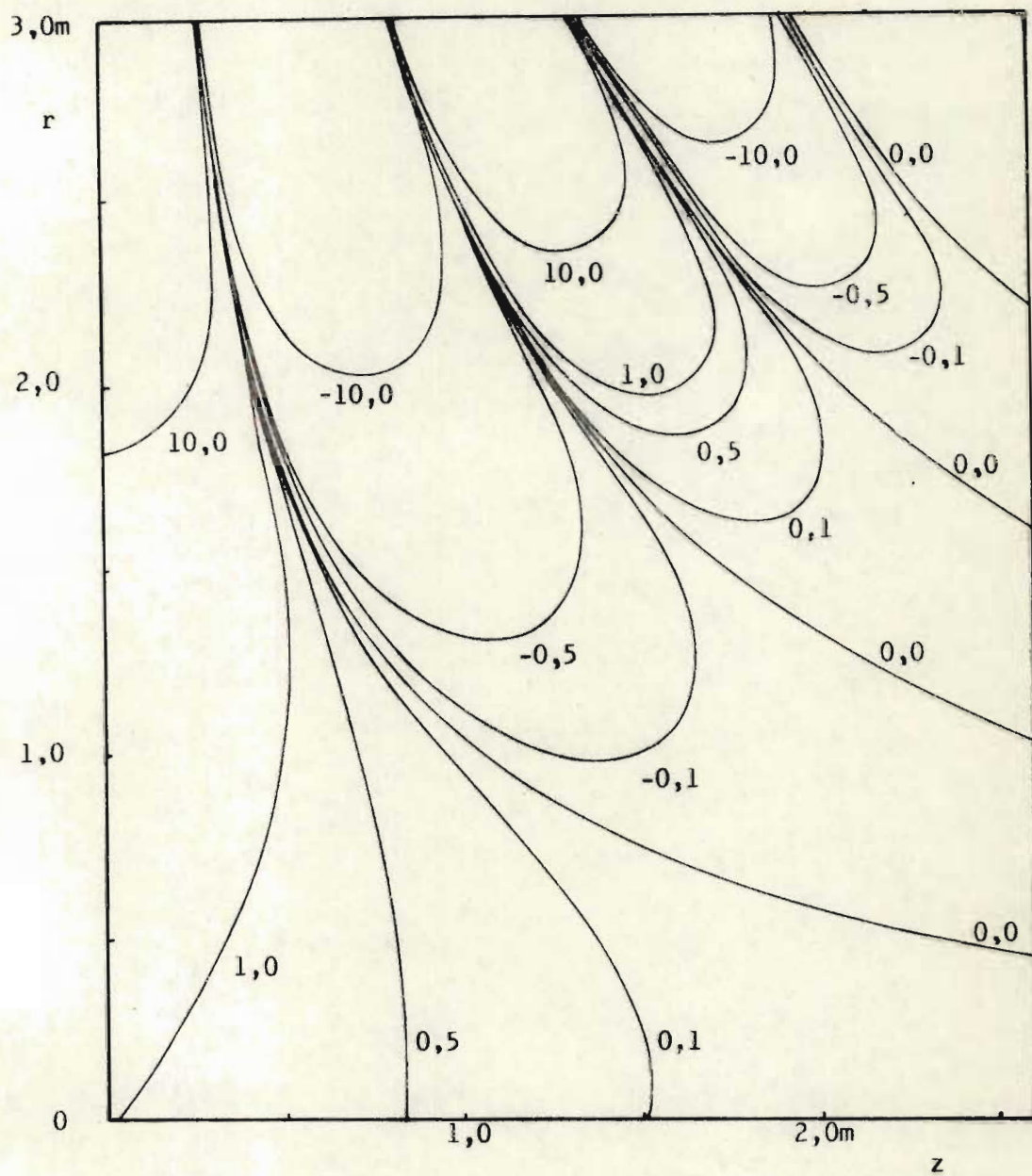


Fig. (8.1) Cross section of equipotential surfaces of  $\psi(r; z)$  corresponding to the axial function  $f(z)$  defined in Section (3.2.1). Potentials are given in volts.

tinuous derivatives :

$$f(z) = 0 \quad \text{for } 0 < z < C_2 \quad (8.16a)$$

$$f(z) = C_1 \sin[\pi(z - C_2)/C_3] \quad \text{for } C_2 < z < C_3 \quad (8.16b)$$

$$f(z) = 0 \quad \text{for } C_3 < z < L \quad (8.16c)$$

in which  $C_1=1V$ ,  $C_2=2m$ ,  $C_3=4m$ ,  $L=6m$ ,  $P=3$  and  $N=140$ .

It can be seen that  $\Psi(r; z)$  shows an oscillating behaviour in zonal regions, for z-values at which  $\partial^n f / \partial z^n$  is discontinuous for any  $n > 0$ .

### 3.2.3 Systems with continuous axial potential distributions but discontinuous z-derivatives; role of P

If it is required to accommodate particle beams of larger radius, the function  $\Psi(r, z)$  must show an acceptably smooth behaviour in zonal regions where suitably chosen conducting electrodes must be positioned. This may be accomplished by assigning a high value to P (or more precisely, by increasing the P/N ratio); this is illustrated in Fig. (8.3) for the function defined by Eqs. (8.16a) - (8.16c), with  $N=140$  and  $P=5, 10$  or  $15$ . On the other hand the quality of the axial approximation deteriorates with larger P, in the regions in which  $f(z)$  changes rapidly.

### 3.2.4 Systems with continuous axial potential distributions but discontinuous z-derivatives; role of L.

In the design of two-foil lenses, the period L of the

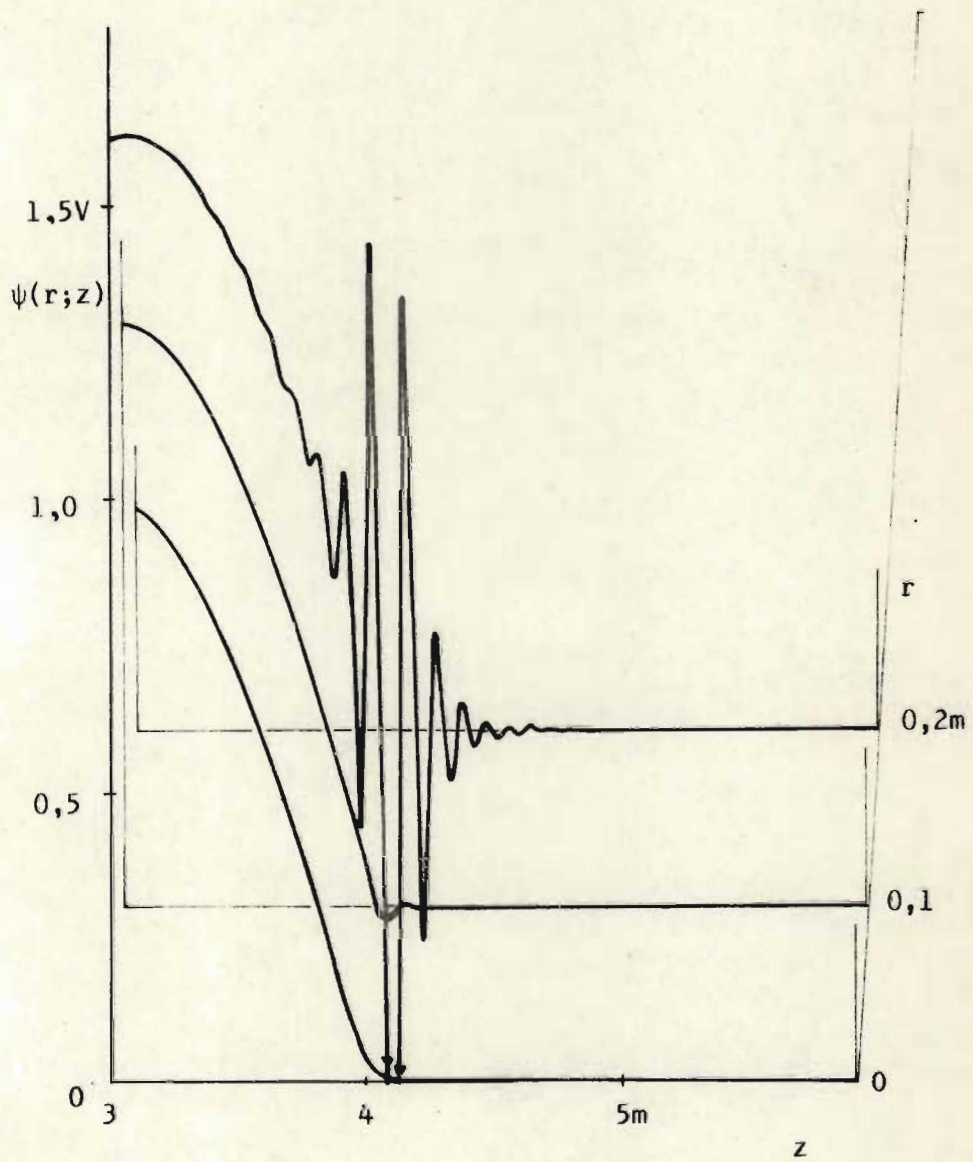


Fig. (8.2)  $\psi(r; z)$  corresponding to the axial function  $f(z)$  defined in Section (3.2.2)

Fourier-Bessel expansion of Eq. (8.13) can be assigned any of the values of the examples illustrated by Figs. (8.1-8.9) depending upon the value of  $|\nabla\Psi(r;z)|$  required at  $z=0$  or  $z=L$ .

In Eq. (8.16) let  $C_3-C_2 \equiv L_1$ . Then with open (i.e. foilless) lenses, the following additional requirement applies :  $f(z)$  must be zero for sufficiently large regions  $0 < z < (L-L_1)/2$  and  $(L+L_1)/2 < z < L$  as to ensure that  $|(\partial/\partial z)\Psi(r;z)|$  shall be so small at  $z=0$  and  $z=L$  that the magnitudes of charge distributions induced on the circular regions  $r < R$  on the foils at  $z=0$  and  $z=L$  are reduced to values low enough that these parts of the foils may be discarded by introducing apertures in the foils. (By "small enough" is meant that the electron-optical properties are not changed significantly by the presence or absence of these distributions). In Ch. (6) and Appendix (2) discussions are found of the circumstances under which parts of electrodes can be discarded in solutions of the interior and exterior Dirichlet problems, respectively. For our present problem, some information of a similar nature is given in Fig. (8.10). For any given function  $f(z)$ , the induced charge distributions  $\sigma(r;0)$  or  $\sigma(r;L)$  at  $z=0$  or  $z=L$  may be obtained by differentiating Eq. (8.13). For instance,

$$\sigma(r;0) = -\epsilon_0 \sum_{n=1}^N (A_n n\pi/L) I_0(n\pi r/L) \quad (8.17)$$

in which  $\epsilon_0$  is the permittivity of free space. The values of  $L$ ,  $N$  and  $P$  can then be increased until it is found that

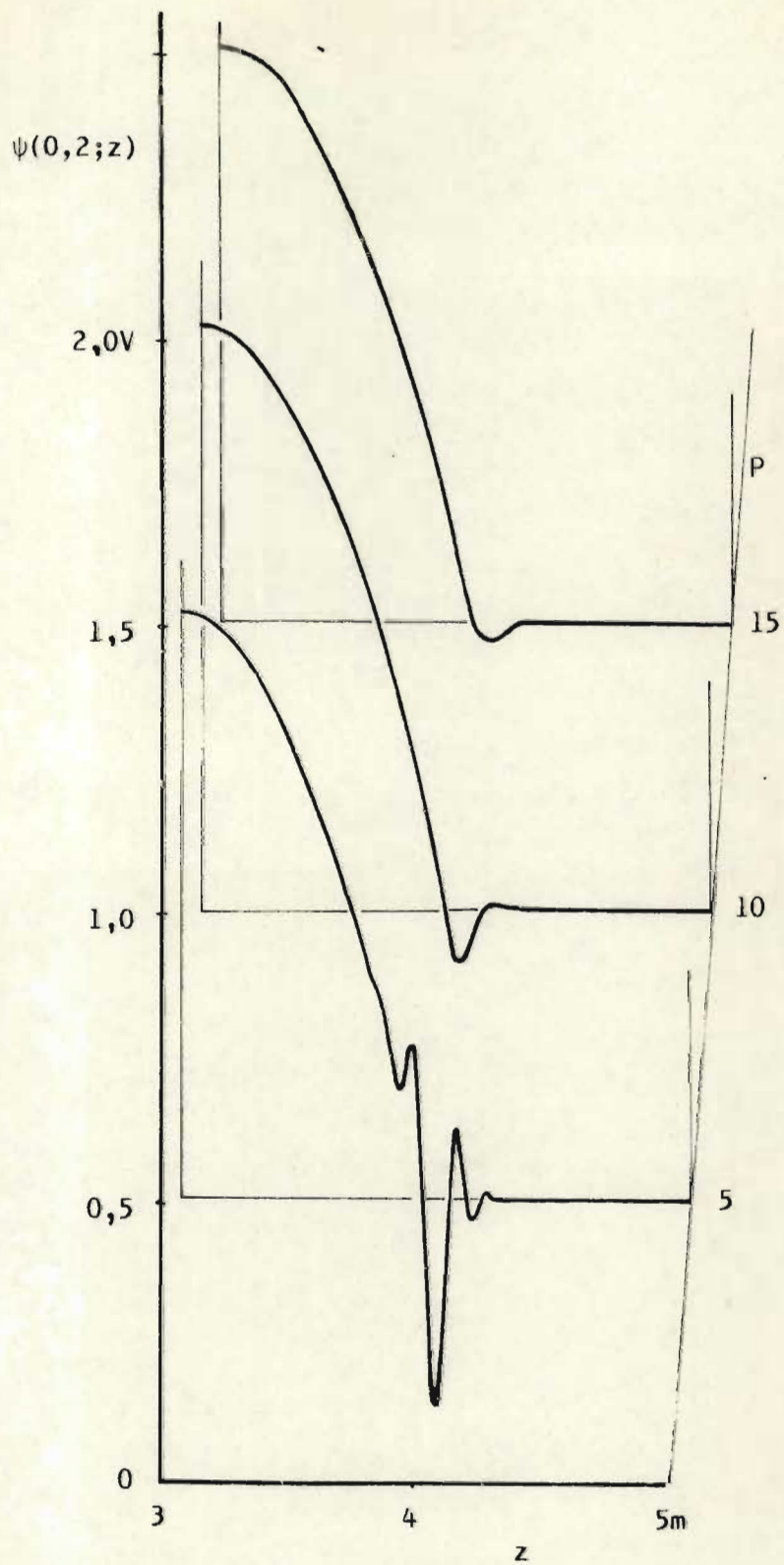


Fig. (8.3)  $\psi(0,2;z)$  corresponding to the axial function  $f(z)$  defined in Section (3.2.3), for various values of  $P$ .

$|\sigma(r;0)| < \epsilon_c \quad \forall r < R$ , a specified aperture;  $\epsilon_c$  is a small constant, the value of which can be estimated by analyzing the electron-optical properties of the configuration -- see also Ch. (7). For the computation of second order focal properties, a smaller value must be assigned to  $\epsilon_c$  than for first order properties; in the former case,  $\epsilon_c$  should probably not exceed  $10^{-6} \epsilon_0$  times the maximum potential gradient found in that region inside the lens which is traversed by the electrons.

One must note that if  $L$  is increased without increasing  $N$  at the same time, the quality of approximation of the non-zero part of  $f(z)$  will deteriorate. This is illustrated in Fig. (8.4) for the function defined in Eqs. (8.16a - 8.16c). Here  $N=20$ ,  $P=1$  and  $L=3, 9$  or  $27$  m. To the list of factors [Section (3.2)] among which a compromise must be found, must therefore be added a fifth one, namely the freedom to choose a sufficiently large value of  $L$  to allow open or semi-open systems to be modelled.

Reference to Fig. (8.10) will also show that an increase in  $N$  must be accompanied by an increase in  $P$ , if the charge distributions on the foils must be minimized. This will in turn affect the quality of approximation of  $f(z)$  in regions where  $f(z)$  changes rapidly, as discussed in Section (3.2.3)



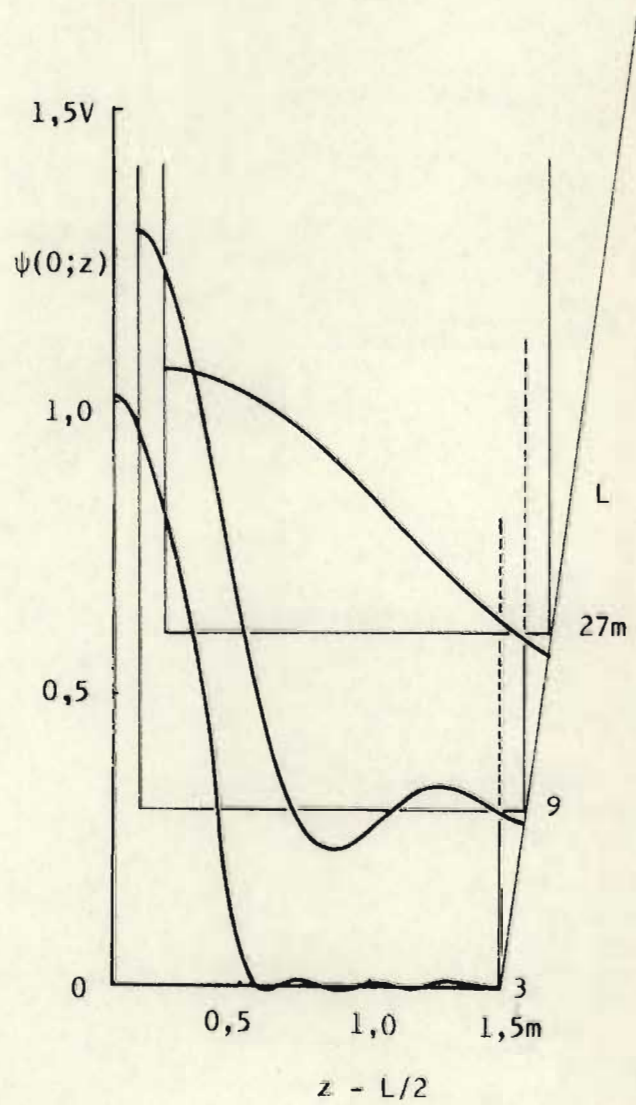


Fig. (8.4)  $\psi(0; z)$  corresponding to the axial function  $f(z)$  defined in Section (3.2.4) for various values of  $L$ .  
 $C_1=1V$ ;  $C_2=L/2-0,5m$  and  $C_3=L/2+0,5m$ .

### 3.2.5 One-foil lenses

For one-foil lenses the condition stipulated above for  $\sigma$  need be satisfied on one side only. In Ch. (7) it is shown how the charge distribution on the remaining foil may be used to obtain certain electron optical properties. In this way, for instance, a convergent lens region may be introduced into the region  $z > 0$ . Whereas the field of Fig. (8.6) has a uniformly convergent or uniformly divergent action, depending on the sign of  $C_1$ , it is shown in Ch. (7) that the fields of some one-foil lenses may be divergent for fast particles but convergent for slow ones. [See also Sections (3.2.6)-(3.2.8)].

Fig. (8.5) shows the behaviour of  $\Psi(r;z)$  near the foil, for a function  $f(z)$  defined by Eqs. (8.16a) - (8.16c) and with  $C_1=1V$ ,  $C_2=0,5$  m and  $C_3=1,5$  m.  $N=20$  ;  $P=2$  and  $L = 6$  m.

### 3.2.6 Piece-wise linear functions : the "zero spherical aberration two-foil lens".

Figs. (8.6 - 8.9) show that piece-wise linear distributions are handled with varying degrees of success, depending on the nature of the distribution. These systems may be labelled "Lenses with Separated Longitudinal and Radial Force Fields", or LSLRFF, and they differ from normal electron optical systems in that a trajectory may be divided into sections where, paraxially, either i) a z-force exists, resulting in a translation and an angular deflection which can be given in closed form if

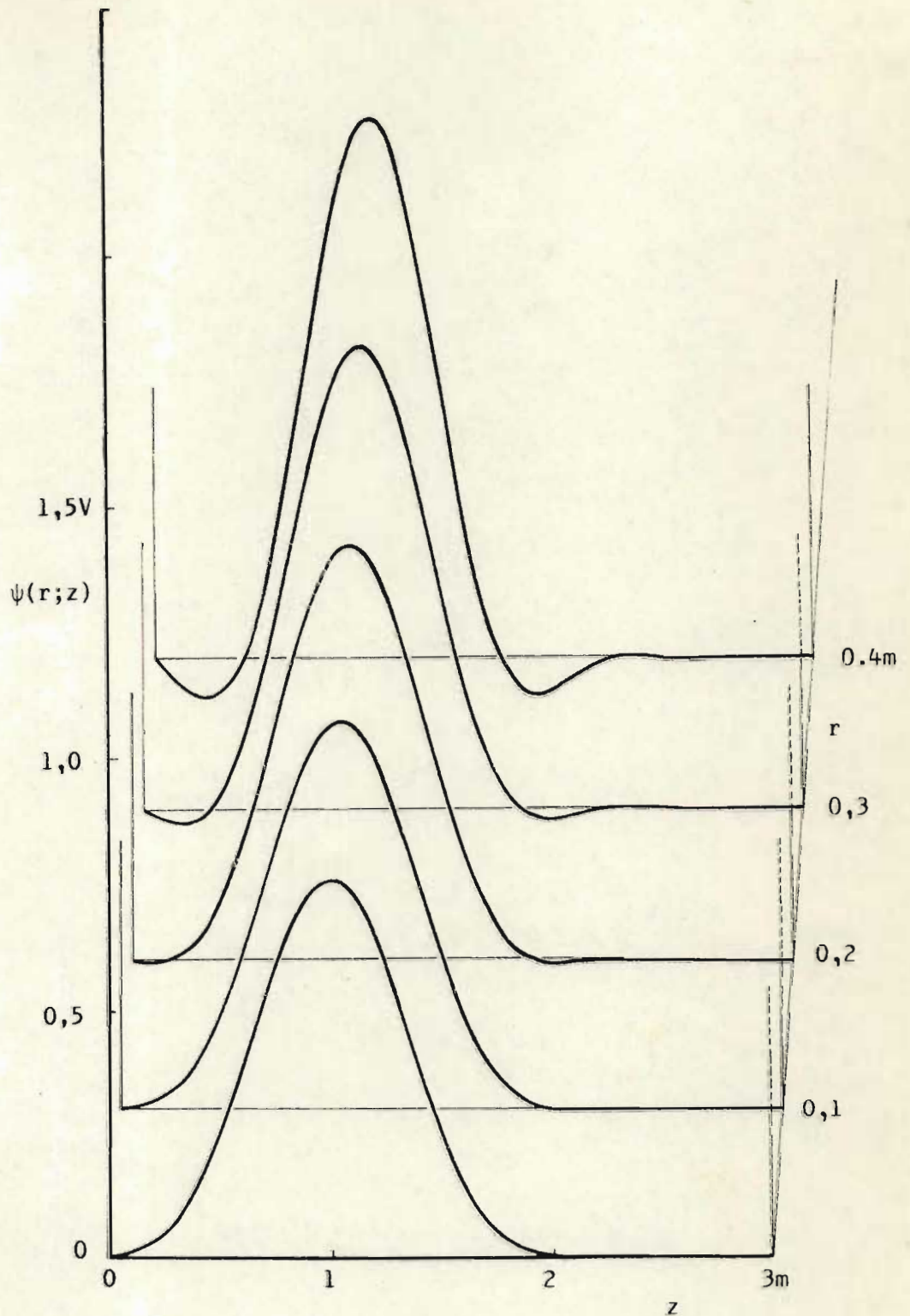


Fig. (8.5)  $\psi(r; z)$  corresponding to the axial function  $f(z)$  defined in Section (3.2.5).

the initial conditions are known; or ii) only a radial force exists; the latter force is found to be non-negligible only at or near values of  $z$  where  $(\partial/\partial z)\Psi(0;z)$  changes, and therefore has the effect of an impulse, which results in an angular deflection only. Due to the presence of the radial force fields, these lenses differ from those considered by Gianola (1950) and also differ from systems consisting of parallel conducting electrodes with coaxial apertures in that the latter have well separated paraxial force components only if the radii of the apertures are quite small compared to the distance between the electrodes. The LSLRFF of Fig. (8.6) appears to have well separated force components for much larger  $r/L$  ratios.

If a beam of fast particles passes through the two-foil lens of Fig. (8.6), the radial impulse received by a particle at  $(r; L/2)$  will be proportional to the charge inside a coaxial cylinder of radius  $r$  [see, e.g., Ch. (7)]. As can be seen from the slopes of the graphs at  $z=0$  in Figs. (8.6) and (8.7), an LSLRFF with  $\Psi(0;z) \propto z$  results in  $\sigma(r;0)$  being approximately constant. Using Eq. (8.17) it has been calculated that by a suitable choice of  $N$  and  $P$ , the absolute relative error  $|\left[\sigma(r;0) - \sigma(0;0)\right]/\sigma(0;0)|$  can be reduced to  $10^{-9}$  or less, for  $0 \leq r < 0,2L$ . The impulse received by fast particles will be proportional to  $r$ , so that the beam is focussed without spherical aberration into a single spot on the axis. This is only one demonstration of the close relationship between

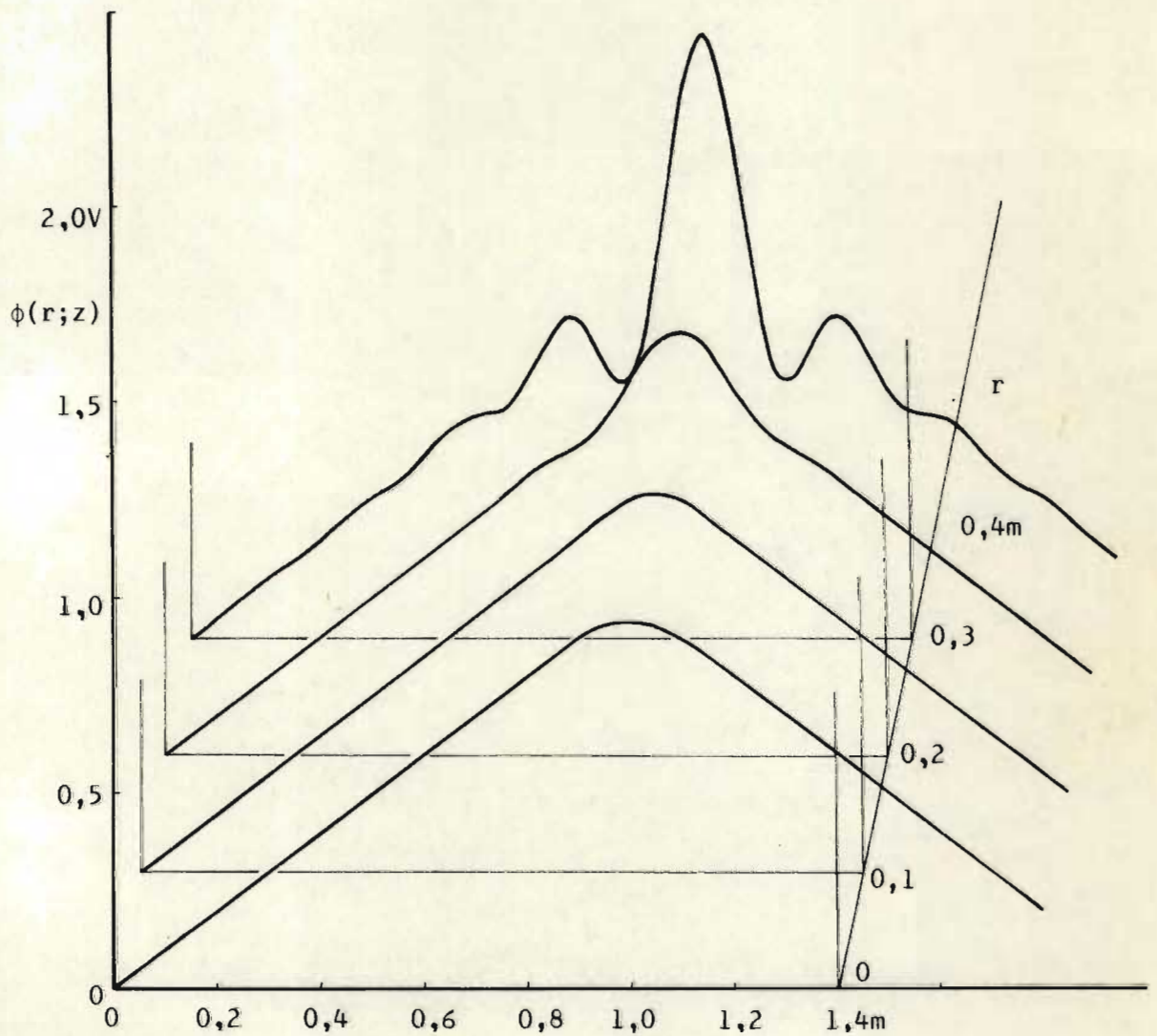


Fig. (8.6)  $\psi(r; z)$  corresponding to the axial function  $f(z)$  defined in Section (3.2.6).

$\sigma(r;0)$  and  $\Psi(0;z)$ , which has been discussed in more detail in Ch. (7). The related general problem of having to determine  $\Psi(0;z)$  which is found on the axis in the presence of a given charge distribution,  $\sigma(r;0)$ — the solution of which may be required in the design of correcting two-foil lenses - is not so simple to solve, and results found so far have not been precise enough to warrant discussion at this stage.

Fig. (8.6) shows  $\Psi(r;z)$  for the function

$$f(z) = C_1 z / (0,5L), \quad 0 \leq z \leq L/2$$

$$f(z) = C_1 (L-z) / (0,5L), \quad L/2 \leq z \leq L$$

with  $C_1=1V$ ,  $L=2$  m,  $N=20$  and  $P=2$

### 3.2.7 Piece-wise linear functions : "zero spherical aberration one-foil lens"

Fig. (8.7) shows  $\Psi(r;z)$  which approximates a one-foil lens with constant  $\sigma(r;0)$  on the foil at  $z=0$ .  $f(z)$  is defined by the line passing through the following points of the diagram :  $(0m; 0V)$ ,  $(2m; 1V)$ ,  $(4m; 1V)$  and  $(6m; 0V)$ .  $L=6$  m,  $N=80$  and  $P=8$

Since  $\sigma$  is constant, and  $\nabla\Psi(r < 0,3m; z)$  is negligible near  $z=L/2$ , the field shown for  $0 \leq z \leq L/2$  approximates a zero spherical aberration cathode lens (or, if the polarity is reversed, a zero spherical aberration anode lens). The lenses will show small spherical aberration for beams that

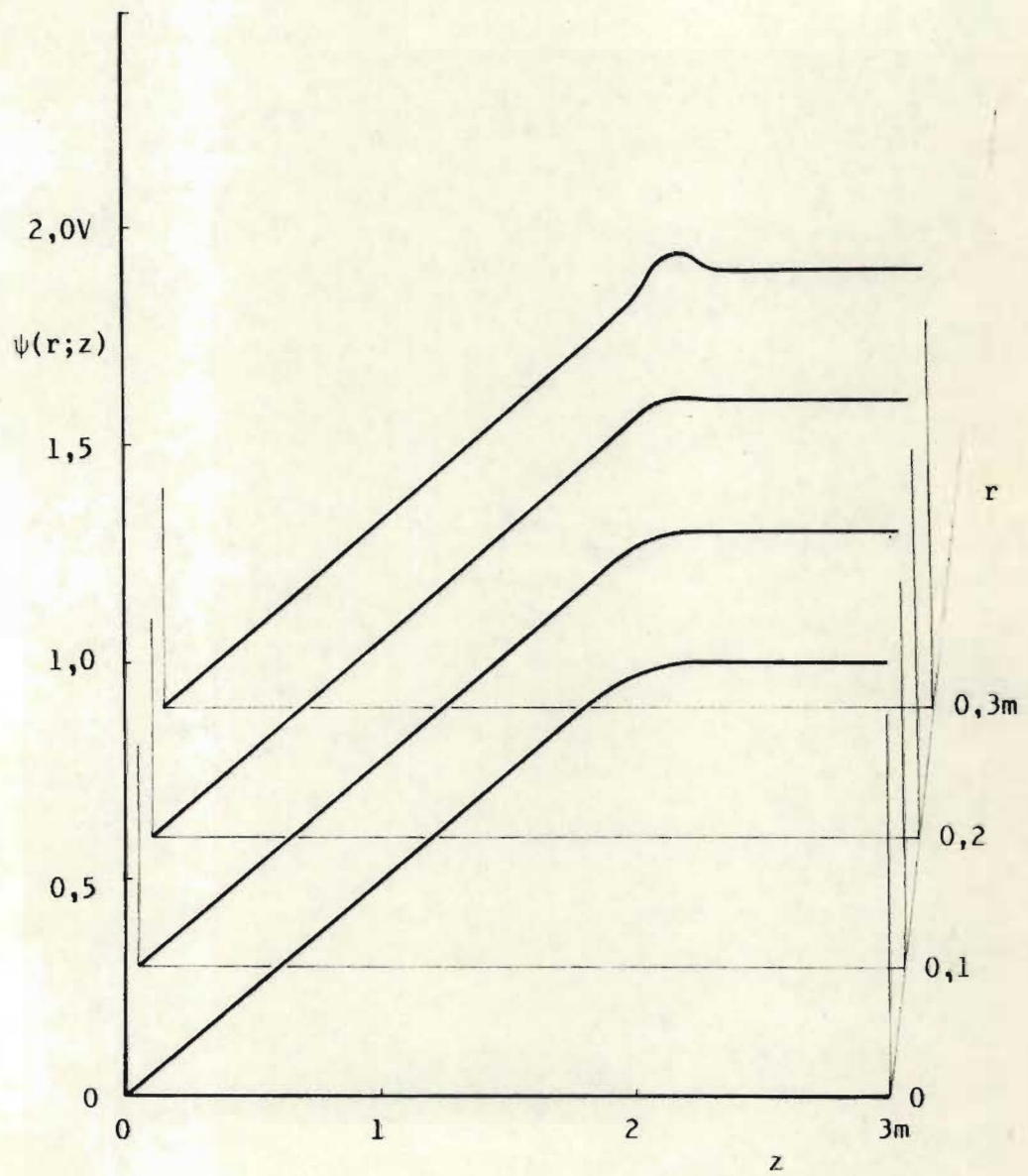


Fig. (8.7)  $\psi(r; z)$  corresponding to the axial function  $f(z)$  defined in Section (3.2.7).

are parallel at  $z=0$ . Due to the field-free region found for  $2m < z < 4m$ , the change in spherical aberration brought about when a converging or diverging beam passes through an electric field which is parallel to the axis [Gianola (1950)], is absent here, so that the spherical aberration observed should not be affected much by the (uniform) velocity at which the beam enters the lens. This implies that the spherical aberration is a weak function of the lens strength, and in this respect the field of Fig. (8.7) differ from the field of Fig. (8.6) [See App. (4)]

### 3.2.8 Piece-wise linear functions : Einzel lenses

As with Fig. (8.5) the introduction of axial regions where  $f(z)=0$ , allows Einzel lenses to be approximated. The difference between the electron optical properties of systems like this one, in which the radial and axial force components are well separated, with those [e.g. Fig. (8.2), or the B-splines of Eqs. (6.11)] in which it is not the case, will be reported elsewhere.

$f(z)$  of Fig. (8.9) is defined by the line passing through the following points on the diagram :  $(0m;0V)$ ,  $(1,5m;0V)$ ,  $(3m;1V)$ ,  $(4,5m;0V)$  and  $(6m;0V)$ .  $L=6m$ ,  $N=80$  and  $P=8$ .

### 3.2.9 Piece-wise linear functions : Immersion lenses

Fig. (8.9) shows one way of obtaining an LSLRFF of immersion type : the region  $0 < z < L/2$  represents an immersion lens if,



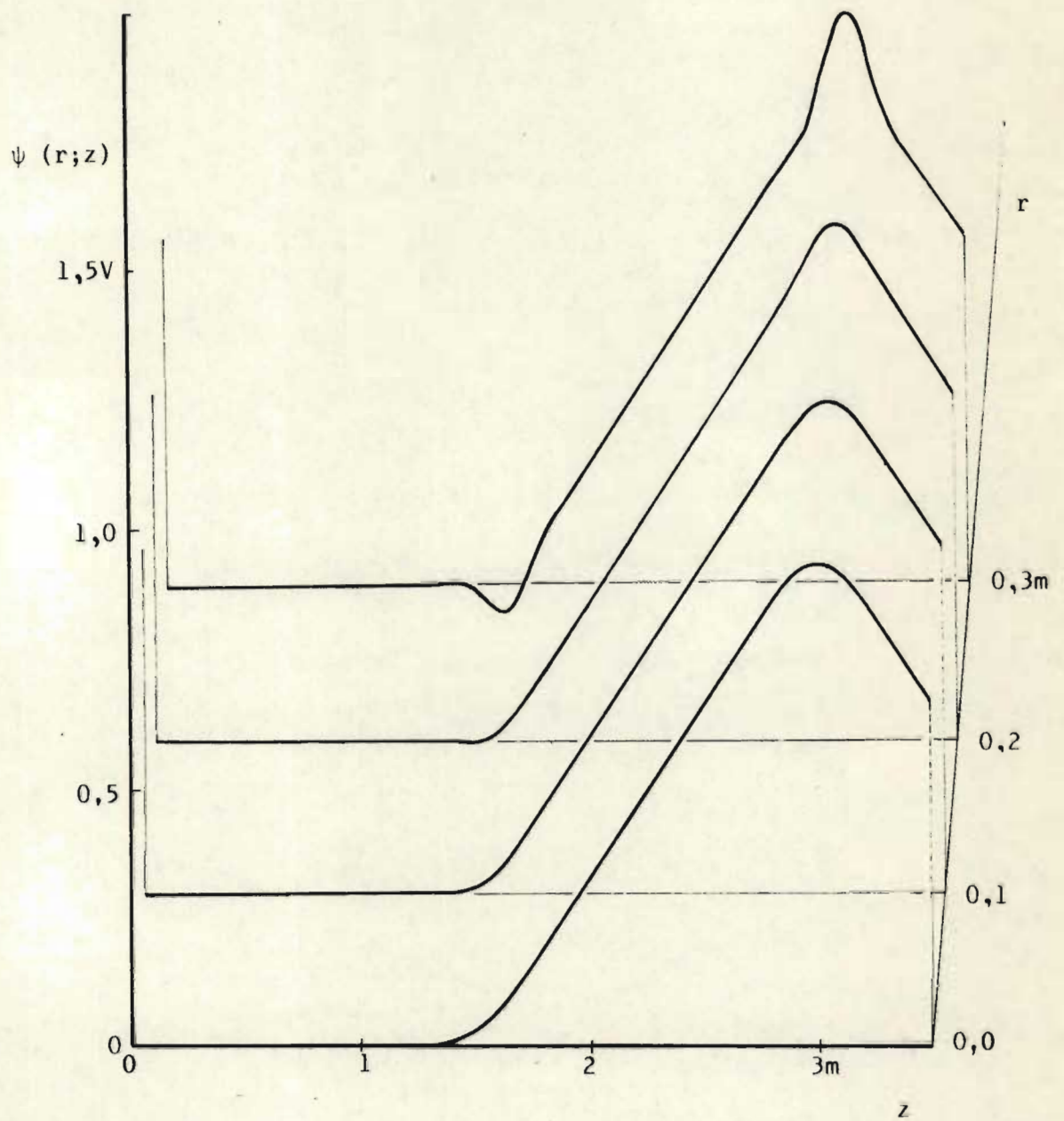


Fig. (8.8)  $\psi(r; z)$  corresponding to the axial function  $f(z)$  defined in Section (3.2.8)

e.g.,  $f(z)$  is defined by the line passing through the following points on the diagram :  $(0m;0V)$ ,  $(1m;0V)$ ,  $(2m;1V)$ ,  $(5m;1V)$  and  $(6m;0V)$ .  $L=12m$ ,  $N=80$ , and  $P=8$ .

#### 4. CONCLUSIONS

The Fourier-Bessel method presented in this paper can be used to obtain an approximate solution of the inverse interior Dirichlet problem defined in Section (1), for axial potential functions which are

- i) analytic, in which case it represents an alternative to the integral method of Section (1.1) and the series expansion method of Section (1.2).
- ii) continuous but have piece-wise continuous  $z$ -derivatives; for these functions the alternatives mentioned in i) can not be applied, and the suggested alternative of calculating an approximate charge distribution  $\sigma(r > 0; z)$  that gives rise to the given potential distribution, does not appear to have been implemented to date. The latter method would involve the inversion of large matrices if a precise solution is required, whereas the Fourier-Bessel method requires no matrix inversion.
- iii) given in the form of a set of experimentally determined axial potentials.

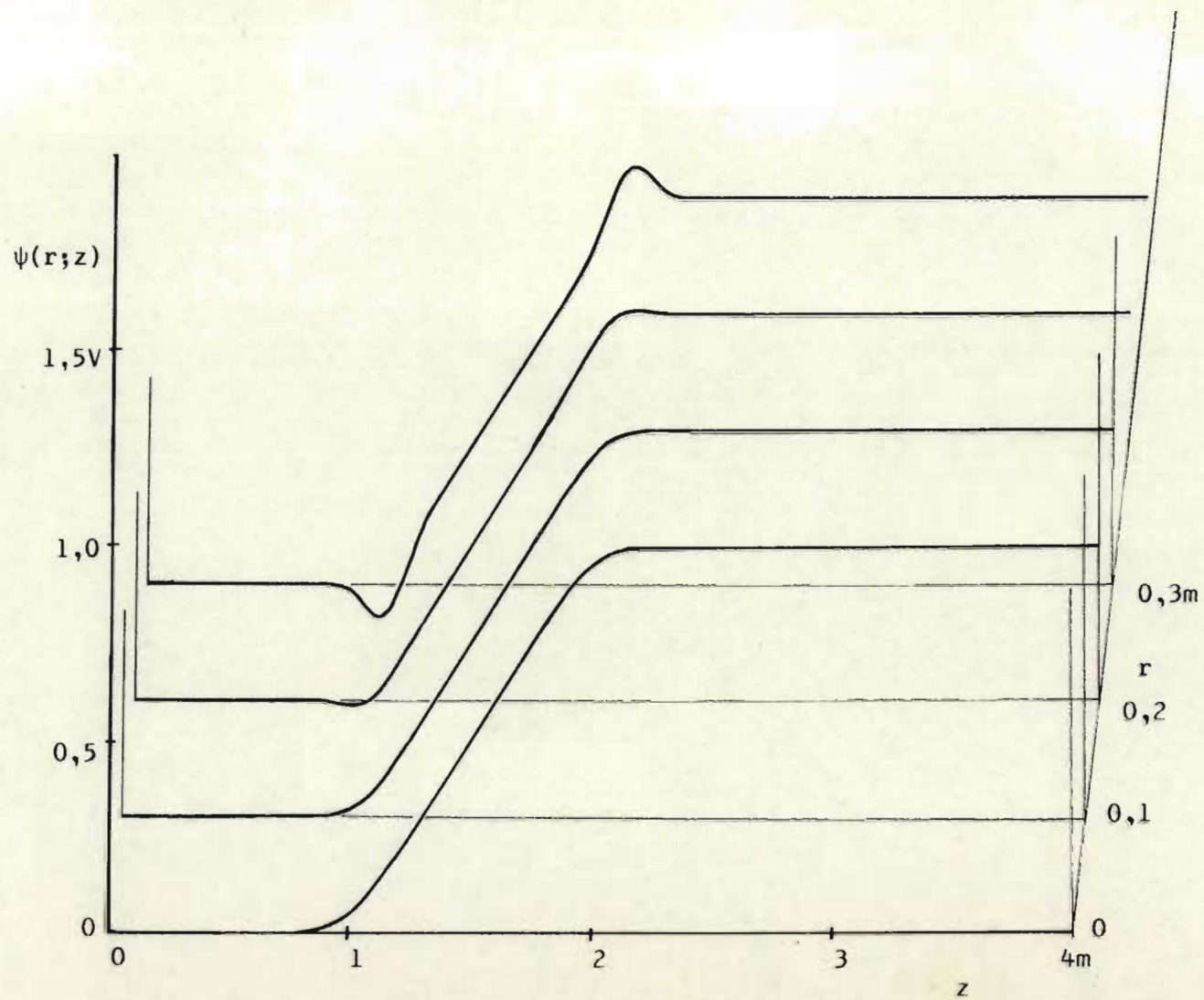


Fig. (9.9)  $\psi(r; z)$  corresponding to the axial function  $f(z)$  defined in Section (3.2.9).

- iv) piece-wise continuous; in this case, the convergence of the series  $\Psi(0;z)$  is so slow that the solution  $\Psi(r > 0;z)$  is of little practical use.

In using the Fourier-Bessel solution of Eq. (8.15), the roles played by some parameters must be taken into account :

- i) if  $N$ , the number of terms included in the series, is large, a good axial approximation will be obtained, but  $\Psi(r > 0;z)$  may oscillate violently w.r.t.  $z$ ;
- ii) a large value of  $P$  which is a measure of smoothing introduced, will result in a reduction of the oscillations mentioned in i); it may also improve the quality of approximation in axial regions where the function is fairly constant, but may result in a deterioration of the approximation where the axial function varies rapidly;
- iii) larger values of  $L$ , the half-period of the Fourier-Bessel series, may be required to allow open (i.e. foilless) lenses to be modelled, but will also result in a slower convergence of the series, again causing large gradients in zonal regions.

From the infinity of solutions  $\Psi(r;z)$  which approximate the given axial function  $f(z)$ , a solution that can be used in practical electron optical design can be selected by assigning particular

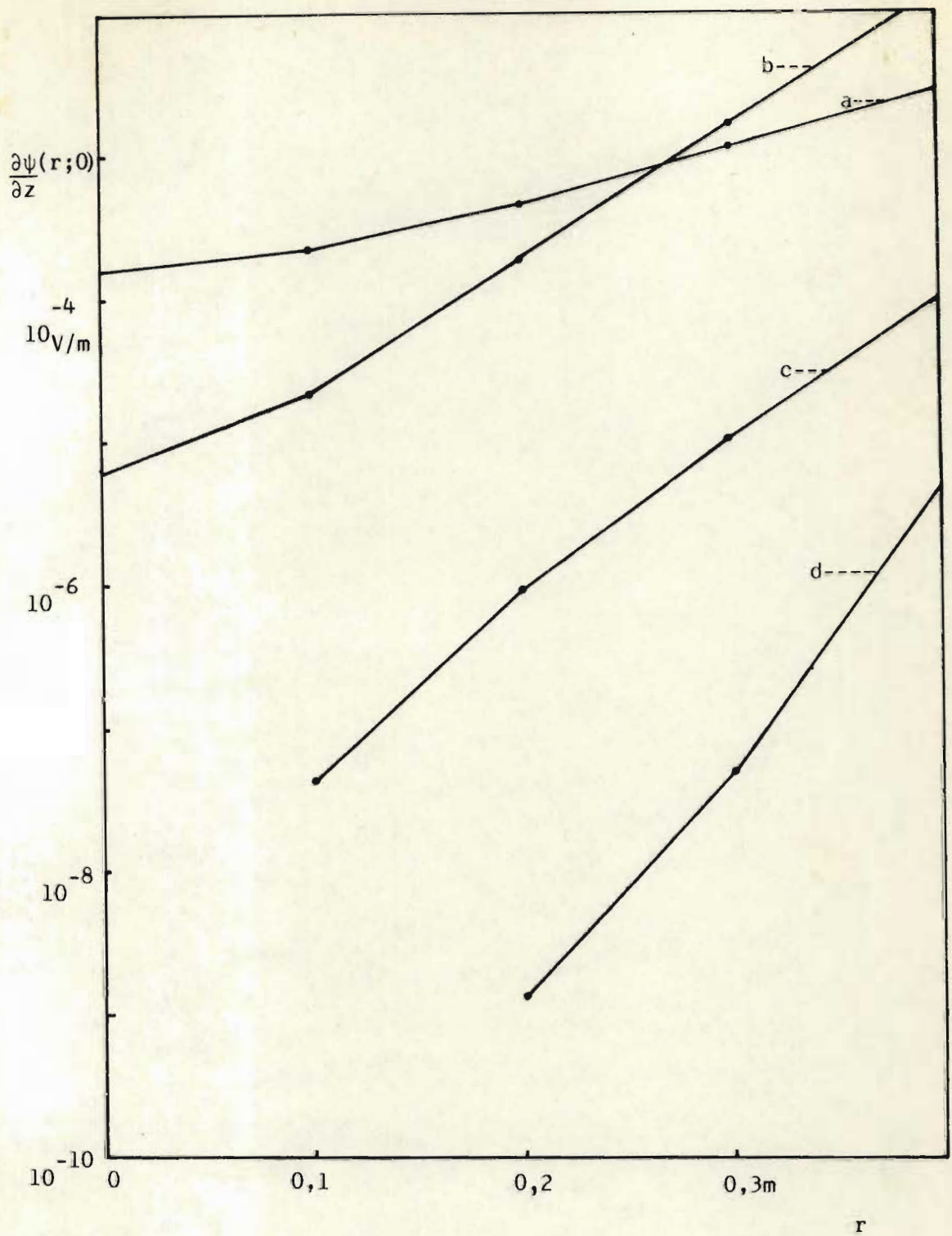


Fig. (8.10)  $(\partial/\partial z)\psi(r;0)$  corresponding to the function  $f(z)$  defined by Eqs.(8.16). For all curves,  $L=6$ .

Curve a :  $N=20, P=2$

Curve b :  $N=40, P=2$

Curve c :  $N=40, P=4$

Curve d :  $N=140, P=10$

values to  $N, P$  and  $L$ .

Due to the absence of matrix inversion, computer memory requirements are modest enough that desk-top computers can be used to obtain solutions, and the programming is found to be straightforward, involving a few tens of statements in FORTRAN or BASIC.

CONCLUSIONS

1. INTRODUCTION

In Ch. (1) it was stated that the objective of the study is the investigation of the possibility of using orthogonal functions in electrostatic electron optics, and that the efforts would be concentrated on the reduction of the spherical aberration of systems of rotational symmetry, rather than the minimization of the resultant effect of all the aberrations of a particular device.

Various approaches were followed : the properties of individual fields of the form  $I_0(\alpha r) \sin(\alpha z)$  were investigated analytically and by computer ray tracing, and syntheses attempted of two or four fields. Physical devices creating the above fields would be of the two-foil type.

To study one-foil or open lenses, Fourier-Bessel series had to be found to represent such configurations. Two possibilities were investigated, namely the determination of the focal properties of fields associated with functions  $f(z)$  describing the potential i) on a set of equidiameter coaxial ring electrodes, or ii) on the axis. The solution to case i) was applied in a study of the expected behaviour patterns of simple one-foil lenses, and the solution to case ii) was used to study some focal properties associated with piece-wise linear axial potential distributions. Both in cases i) and ii) the solution can be cast in a form which will

allow an optimization by steepest descent to be carried out.

In Sections (2) to (7) some results obtained by the various approaches just mentioned, are investigated in some more detail.

## 2. OPTIMIZATION METHODS

The vast majority of experimental and computational studies carried out to optimize electron optical elements i.r.o. various criteria, have been of a trial and error type; this also applies to most of the analytical studies in which the paraxial focal properties associated with analytical axial potential functions are calculated.

In Section (5) of Ch. (1) two important approaches are mentioned which fall in a different category, being based on mathematically founded optimization theory. In these approaches (by Moses and by Szilagyí) the paraxial ray equation plays an essential role, and at this stage it seems as if these methods are restricted to paraxial optimization.

In Section (6) of Ch. (1) it is suggested that the optimum field (i.e. the unknown field which is to be found) be represented by a finite Fourier-Bessel series with undetermined coefficients. The latter can then be found by carrying out a steepest descent procedure which involves computer ray tracing. If the Fourier-Bessel functions are elements of a set which is complete on a suitably chosen interval, the finite series should approximate the optimum solution. And by including zonal rays in the ray tracing, it is



ensured that the optimization applies to both paraxial and zonal regions.

Information obtained in the investigation of the solutions to the boundary value problems of Chs. (4)-(6) and (8) can be expected to be of use when the suggested optimization procedure is put into practice. A brief survey of results reported in Chs. (2) - (8) will now be given.

### 3. PROPERTIES OF INDIVIDUAL FIELDS

Since the  $K_0$  and  $Y_0$  Bessel functions are singular on the axis, and the fields  $J_0(\alpha r) \exp(-\alpha z)$  are not simple to produce by means of physical electrodes, the only fields studied individually were of the type  $I_0(\alpha r) \sin(\alpha z)$ . (Some focal properties of fields with  $J_0$ ,  $K_0$  and Legendre functions as factors have also been investigated, but in an effort to reduce the length of this dissertation, these results will be reported elsewhere).

The ray tracings showed that the fields  $I_0(\alpha r) \sin(\alpha z)$  differed from those of open lenses in a number of respects : they tend to be more highly converging, they can be divergent, and they can exhibit negative spherical aberration,  $C_s$ . (It was also seen that, apart from uniformly convergent or uniformly divergent fields, some fields may be found which are divergent for fast particles but convergent for slow particles; the sign of  $C_s$  of the latter group of fields may also be different for slow and for fast particles.)

It was also found that  $C_S$  was dependent on  $\alpha$ , which suggested that two fields of different  $\alpha$  values and polarities may be superposed to obtain a reduction in  $C_S$  for the resultant field. Attempts at obtaining such syntheses were described in Chs. (3) and (4).

#### 4. SYNTHESES OF TWO FIELDS

In Ch. (3) the behaviour of weak fields of the type  $I_0(\alpha r) \sin(\alpha z)$  was studied analytically, and it was possible to obtain closed form expressions for various focal properties of individual fields. These expressions were valid for zonal as well as paraxial regions, in contrast to the majority of analytical studies reported in literature, where the use of the paraxial ray equation restricted the analysis to paraxial focal properties.

As a control, ray tracings through weak fields were carried out by computer, and the results corresponded well with the theoretical predictions.

Using the results obtained for individual fields, syntheses of two fields were obtained analytically, which had greatly reduced values of  $C_S$  for paraxial rays.

It is possible to formulate a Fourier technique to synthesize a larger number of fields so as to extend the correction to rays at larger radial distances. One such procedure involves the inversion of a matrix which is not very well behaved, so that only

five or six fields can normally be accommodated, unless the computer has a word length in excess of the usual extended precision (approximately fifteen significant figures). Another procedure involves the orthogonalization of the  $I_1$  Bessel functions, but in doing this the same problem of computer word length puts a limit on the number of fields handled. A description of these procedures and some results will be published elsewhere.

#### 5. STRONG TWO-FOIL LENSES

The approximations used in Ch. (3) do not apply to strong lenses; consequently the focal properties of syntheses representing strong lenses in Ch. (4) were obtained by computer ray tracings.

Two methods were outlined of obtaining syntheses of reduced  $C_s$  values. The first method is based on an understanding of the properties of individual fields, and its use resulted in a reduction of the circle of confusion by factors as large as 1000 for non-paraxial cases. Only four fields were used in the syntheses which could be chosen as starting points for the steepest descent method also described in the chapter. Any number of fields can be accommodated by the latter method [see Section (6) of Ch. (1)], and results obtained with this method will be reported elsewhere.

#### 6. FOURIER-BESSEL SERIES REPRESENTATIONS OF ONE-FOIL AND OPEN SYSTEMS

In Chs. (5) and (6) Fourier-Bessel series solutions are given for

the modelling of one-foil and open systems. In Ch. (5) the lens region is divided into three parts, each of which is represented by a different series (involving  $J_0$  and  $I_0$  functions), whereas the single solution (involving  $I_0$  functions only) given in Ch. (6) describes the complete lens region.

The latter solution is more easily programmed, and the convergence of the series is acceptable at all points. The solutions of Chs. (5) and (6) can also be combined — using the solution of Ch. (5) to model the outer lens regions, for which the convergence of the  $J_0$ -series is superior.

If the solution of Ch. (6) is used on a routine basis to analyse electron optical systems, it would be important to improve the convergence of the series at the cost of some additional programming. This can be done by investigating the role played by the  $z$ -period ( $2L$ ) of the first term in the series. In Ch. (6) it was shown that a large value of  $L$  increased the accuracy of the solution, but at the same time slowed down the convergence of the series. In Appendix (2) it is shown how associated Fourier-Bessel series may be derived which, if added to the original solution, allow smaller values of  $L$  to be tolerated. The method is based on the electrostatic theory of images, and is described for an exterior Dirichlet boundary value problem (in view of the fact that the problem of convergence is much more serious in exterior than in interior problems). The computer time needed to evaluate the potential or electric intensity at a point may be reduced by one or more orders

of magnitude, depending on the precision required.

[It may also be mentioned that the solution of Appendix (2) can be utilized in analytical and ray tracing studies of configurations with axial electrodes. It can be shown — by taking into account the properties of the  $K_0$  Bessel functions — that such systems can show divergent or convergent behaviour, and that foilless convergent systems can show negative spherical aberration. Combining the solution of Ch. (6) and Appendix (2) may allow systems to be obtained with reduced  $C_s$  in a cylindrical region between two sets of coaxial ring electrodes; see also Sections (3.3b) and (3.3c) of Ch. (1). It is intended to make a study of the suggested method in the near future.]

In conclusion it may be mentioned that the solution presented in Ch. (6) may be adapted to two further situations : i) Systems with gaps between juxtaposed coaxial tubular electrodes may be accommodated by representing the potential in the gap by a separate finite Fourier series, and the coefficients of the latter may be calculated by requiring that Laplace's equation is satisfied in the gap.

ii) Systems with space charge may be described by representing the volume charge density in the lens region (excluding the electrodes) by a separate Fourier-Bessel series.

Both these cases have been excluded from the present study, and will be investigated in the near future.

## 7. A STUDY OF ONE-FOIL LENSES

The solution of Ch. (6) is in a form which allows the charge distribution  $\sigma(r)$  on the foil of one-foil lenses to be calculated.

In Ch. (7) a discussion is found on the behaviour of weak one-foil lenses, in which the signs of the focal length and of  $C_s$  are related to the nature of  $\sigma(r)$ . In the graphs presented, the close relationship between  $\sigma(r)$  and the axial potential distribution is also illustrated. By means of the graphs a good insight may be gained into the electron optical behaviour of a wide variety of cathode lenses and immersion objectives and, in particular, the role played by Wehnelt electrodes.

It is also shown that weak one-foil lenses can be designed which have a negligible focussing effect on paraxial rays, but (e.g.) a large divergent effect on zonal rays. Such a lens can be used to reduce the spherical aberration of an existing system, without changing its focal length. By computer ray tracing the focal properties of some lenses of this type were determined and the results presented graphically.

This study was undertaken i) to determine the utility of the solution of Ch. (6), ii) to demonstrate the relationships between  $\sigma(r)$  and the focal properties of the lens in its weak form, and also between  $\sigma(r)$  and the axial potential distribution, iii) to relate the axial potential behaviour to the zonal "Wehnelt" voltages, and show how the latter determine the properties of cathode lenses and

immersion objectives; and iv) to investigate some properties of zero-convergence correcting lenses. It is hoped to carry out a more complete study of the latter group of lenses at a later stage.

8. CONFIGURATIONS ASSOCIATED WITH AXIAL POTENTIAL DISTRIBUTIONS –  
THE INVERSE INTERIOR DIRICHLET PROBLEM

Analytical axial potential functions have played an important role in the study of the paraxial focal properties of electron optical systems. Further progress has, however, been hampered by two aspects : i) the fact that the paraxial ray equation was used, excluded the investigation of zonal focal properties, and ii) the axial potential functions in common use did not lend themselves to simple optimization procedures. [Two exceptions were discussed in Section (5) of Ch. (1).]

In Section (6) of Ch. (1) it was suggested that open and closed electron optical systems can be optimized i.r.o. both zonal and paraxial focal properties, if the solution to the inverse interior Dirichlet problem is expressed in terms of a suitable Fourier-Bessel series. As a first step towards realizing the goal, various aspects of such solutions were investigated in Ch. (8).

It was shown how infinitely many solutions  $\Psi(r;z)$  can be found which approximate a given axial function  $f(z)$ . Restrictions may also be imposed so as to select solutions that can be approximated by physical electrodes in a practical way.

Whereas existing solutions to the inverse interior Dirichlet boundary value problem were limited to analytic axial functions, the solution given in Ch. (8) was shown to apply to a broader class of axial functions, namely continuous functions with piece-wise continuous  $z$ -derivatives. Preliminary results indicate that experimentally measured axial distributions can also be handled, but a complete report will be published elsewhere.

As an illustration of the electron optical use of the solution of Ch. (8), computer ray tracings were carried out for a one-foil lens very similar to that of Section (3.2.7) of Ch. (8). The results, presented in Appendix (4), show that for strong lenses of this type, the value of  $C_s$  depends strongly upon, i.a., the focal length of the lens, and the Lanczos smoothing factor introduced in the solution of the inverse problem. It is found that — in contrast to open lenses — the longitudinal spherical aberration  $\Delta J$  does not increase significantly if the focal length is increased. Therefore the circle of confusion  $\Delta r$  due to spherical aberration is approximately proportional to the inverse of the focal length, whereas open lenses usually reach low values of  $\Delta r$  at short focal lengths.

In Ch. (8) solutions were investigated for a variety of axial functions, and no indications were found that the series representation of Section (6.3) of Ch. (1) might be unsuitable for use in the suggested steepest descent method. Implementation of this method will require a comprehensive study of various factors, which will have to be reported elsewhere.



## 9. CONCLUDING REMARKS

It has been attempted to show that orthogonal functions can be used profitably in electron optical design. A few of the advantages are :

- i) Potentials and electric intensities can be calculated to a high degree of precision, and an estimate of the precision can easily be made.
- ii) Ray tracing is facilitated by the fact that the fields are known at all points; therefore no interpolation is required.
- iii) By means of the solutions presented, the precise calculation of charge distributions on electrodes is a straightforward procedure; this is useful in understanding the behaviour of, i.a., weak foil lenses.
- iv) Fourier techniques can be applied to find approximate solutions to the inverse interior Dirichlet boundary value problem, allowing a broader class of axial potential functions to be handled.
- v) If care is exercised in the choice of functions, it is possible to carry out a steepest descent procedure to optimize a system i.r.o. both paraxial and zonal focal properties.
- vi) The optimization procedure of Section (6.3.i) of Ch. (1)

may be carried out experimentally, by applying the specified potentials to a set of coaxial ring electrodes. This may, for instance, be practicable in attempting to reduce the image curvature in electrostatic image intensifiers. If the precision of the experimental procedure becomes inadequate, and the optimization must be continued by computer, the experimental result provides a suitable starting point for the computer simulation.

Many aspects of this study have been dealt with only very briefly, and some need further detailed investigation; there is also little doubt that some methods may be refined considerably in order to increase the computational efficiency. At the same time it is hoped that it has been shown that existing methods of electron optical design can be augmented by methods, particular to the use of orthogonal functions, which are versatile, simple to understand and easy to implement.

## A P P E N D I X 1

### SERIES EXPANSIONS AND TABLES OF INTEGRALS OF PRODUCTS OF SOME BESSEL FUNCTIONS

In the Fourier analysis performed when studying electrostatic electron-optical systems of rotational symmetry, evaluation of some integrals of products of both normal and modified Bessel functions of the first kind and of orders nought and one is required. In this appendix the computation of the integrals are discussed and tables of some integrals are given.

## 1. INTRODUCTION

In Chs. (2-9) the electrostatic fields of some electron-optical systems with rotational symmetry were described in terms of various Bessel functions and several papers have appeared recently [Read (1969a , 1969b and 1970), Read et. al. (1970), Werner (1971), Wittels et. al. (1976)] employing Fourier-analytical techniques involving Bessel functions. These procedures normally require the values of the integrals of the products of various Bessel functions, some of which are not found in existing tables.

The evaluation of the integrals by numerical integration is time consuming, especially if precise values are required (8 significant figures are normally adequate). Alternatively the Bessel functions can be series expanded and the resulting polynomials integrated analytically. This results in series expansions for the integrals themselves. If such a series is not alternating, its evaluation presents no problems, but the series of integrals involving the unmodified Bessel functions are found to alternate, and these would normally require excessive computer word lengths in their evaluation.

## 2. SERIES EXPANSIONS FOR THE BESSEL PRODUCT INTEGRALS

As an alternative to the evaluation of the integrals, defined later in this paragraph, by straight numerical integration, series expansions for the integrals can be derived which, in principle, allow the evaluation of the integrals with a minimal amount of computing.

In the integrals involving  $J_0$  or  $J_1$ , however, the series expansions are alternating series, which can oscillate excessively before converging. (The largest term may be  $10^{80}$  larger than the value of the series itself.) This calls for (i) a computer word length much in excess of the usual extended precision found on most digital computers, and (ii) the availability of the zero's of the Bessel functions to a very large number of significant figures. [Abramowitz (1970), for instance, gives the zero's of  $J_0$  to 12 significant figures only.]

The series expansions of the integrals are derived by making use of the following expansions for the Bessel functions :

$$J_g(z) = (0,5 z)^g \sum_{k=0}^{\infty} \frac{(-0,25 z^2)^k}{k! (g+k)!}$$

$$I_g(z) = (0,5 z)^g \sum_{k=0}^{\infty} \frac{(0,5 z)^{2k}}{k! (g+k)!}$$

2.1 The integral  $Q_{pq}$  of Eq.(5.15) of Ch. (5)

$$Q_{pq} = \int_0^1 J_1(Z_{0p}x) J_1(Z_{0q}x) dx$$

$$= \frac{Z_{0p} Z_{0q}}{4} \int_0^1 \left[ \sum_{i=1}^{\infty} c_i x^{2i} \right] \left[ \sum_{i=1}^{\infty} d_i x^{2i} \right] dx$$

with

$$c_j = \frac{(-1)^{j+1} (Z_{0p}/2)^{2(j-1)}}{j! (j-1)!}$$

$$d_i = \frac{(-1)^{i+1} (Z_{0q}/2)^{2(i-1)}}{i! (i-1)!}$$

Therefore

$$\begin{aligned} Q_{pq} &= \frac{Z_{0p}Z_{0q}}{4} \int_0^1 \left[ \sum_{i=1}^{\infty} K_i x^{2i} \right] dx \\ &= \frac{Z_{0p} Z_{0q}}{4} \sum_{i=1}^{\infty} \frac{K_i}{2i+1} \end{aligned}$$

with

$$K_i = \sum_{j=1}^i c_j d_{i+1-j}$$

Table 1 lists the values of  $Q_{pq} \forall p, q \leq 20$  (noting that  $Q_{pq} = Q_{qp}$ ).

2.2 The integral  $P_{ij} = \int_0^1 I_1(i\pi Ax/L) J_1(Z_{0j} x) dx$

In the process of performing the Fourier analysis of Eq.(5.20) of Par. (4.1.2) of Ch. (5), the integrals  $P_{ij}$  are required  $\forall j < j_1$  and  $\forall n < n_1$ , where  $j_1$  and  $n_1$  are constants determined by the nature of the problem to be solved. For a "typical" configuration and a relative precision of  $1:10^5$  required for the solution of the boundary value problem,  $n_1 \doteq 20$  and  $j_1 < 10$ .

$$\begin{aligned} P_{ij} &\equiv \int_0^1 I_1(i\pi Ax/L) J_1(Z_{0j}x) dx \\ &= \frac{1}{4} \int_0^1 \left[ \sum_{h=1}^{\infty} c_h x^{2h-1} \right] \left[ \sum_{k=1}^{\infty} d_k x^{2k-1} \right] dx \end{aligned}$$

With

$$c_h = \frac{(i\pi A/L)^{2h-1}}{h! (h-1)! 4^{h-1}}$$

$$d_k = \frac{(-1)^{k+1} Z_{0j}^{2k-1}}{k! (k-1)! 4^{k-1}}$$

Therefore

$$P_{ij} = \frac{1}{4} \int_0^1 \sum_{s=1}^{\infty} K_s x^{2s} dx$$

$$= \frac{1}{4} \sum_{s=1}^{\infty} \frac{K_s}{2s+1}$$

with

$$K_s = \sum_{p=1}^s c_p d_{s+1-p}$$

The constant  $c = A/L$  depends upon the physical dimensions of the configuration under investigation, and only the values  $c = 0,2$ ;  $0,5$  and  $1,0$  are represented in Table 2.

### 2.3 The integral $M_{hj}$

To evaluate the integrals of Eq.(5,23) of Ch. (5) we change to a variable

$$\rho = r/A$$

$$\int_0^A r I_0(h\pi r/L) J_0(\lambda_{0j} r) dr = A^2 \int_0^1 \rho I_0(h\pi A/L) J_0(Z_{0j} \rho) d\rho$$

$$= A^2 M_{hj}$$

$$M_{hj} = \int_0^1 \rho \sum_{k=0}^{\infty} c_k \rho^{2k} \sum_{m=0}^{\infty} d_m (-\rho^2)^m d\rho$$

$$= \sum_{s=1}^{\infty} \frac{K_s}{2s}$$

$$\text{with } c_k = \frac{(h\pi A/2L)^{2k-2}}{((k-1)!)^2}$$

$$d_m = \frac{(-1)^{m+1} (Z_{0j})^{2m-2}}{((m-1)!)^2}$$

$$\text{and } K_s = \sum_{p=1}^s c_p d_{s+1-p}$$

Due to the appearance of the constant  $c = A/L$  in the integrals  $M_{hj}$ , it can be seen that the integrals are specific to particular configurations; consequently the integrals  $M_{hj}$  are given for the values  $c = 0,2; 0,5$  and  $1,0$  in Table 3.

2.4 The integrals  $S_{pq} = \int_0^1 l_1(p c \pi \rho) l_1(q c \pi \rho) d\rho$

If it is attempted to eliminate the spherical aberration of all orders in weak electrostatic foil lenses, the integrals  $S_{pq}$  are required in the course of a Fourier analysis. In cases of practical interest the values of  $p$  and  $q$  would not exceed 10.



After substitution and simplification, the following series is obtained :

$$S_{pq} = \sum_{i=1}^{\infty} \frac{K_i}{2^{i+1}}$$

$$K_i = \sum_{j=1}^i c_j d_{i+1-j}$$

$$c_h = \frac{(pc\pi/2)^{2h-1}}{h! (h-1)!}$$

$$d_k = \frac{(qc\pi/2)^{2k-1}}{k! (k-1)!}$$

Investigation of the series expansion of  $I_1$  shows that the series is not alternating, so that the evaluation of the series for  $S_{pq}$  given above can be carried out without requiring an excessive computer word length. Consequently no tables for  $S_{pq}$  are given.

### 3. PRECISION

The integrals  $Q$ ,  $P$  and  $M$  were computed on an IBM System 3 computer, using extended precision (i.e. 16 significant figures). The Simpson integration limited the precision of the integrals to between 7 and 10 significant figures, depending upon the nature of the integrand. The evaluation of the Bessel function was carried out to 10 significant figures by means of the series expansions of §2, except where the nature of the series calls for a computer word length in excess of 16 decimal digits; in such

cases polynomial approximations [Abramowitz (1970)] were used for which the absolute errors do not exceed  $10^{-7}$ . Therefore some or all of the underlined digits in the tables may or may not be significant.

Table 1: The integral  $Q_{pq}(\rho)$

p	q	Q
1	1	0,203956288
1	2	0,050183900
1	3	0,014447945
1	4	0,009707157
1	5	0,004947832
1	6	0,004012868
1	7	0,002481780
1	8	0,002179629
1	9	0,001489648
1	10	0,001364649
1	11	0,000993071
1	12	0,000933999
1	13	0,000709335
1	14	0,000678963
1	15	0,000532031
1	16	0,000515647
1	17	0,000413857
1	18	0,000404800
1	19	0,000331139
1	20	0,000326183

p	q	Q
2	2	0,136483329
2	3	0,048114466
2	4	0,020738360
2	5	0,013527872
2	6	0,008515331
2	7	0,006454043
2	8	0,004639643
2	9	0,003784314
2	10	0,002920498
2	11	0,002488026
2	12	0,002007564
2	13	0,001760525
2	14	0,001464970
2	15	0,001311426
2	16	0,001116221
2	17	0,001014719
2	18	0,000878813
2	19	0,000808465
2	20	0,000709880

Table 1: The integral  $Q_{pq}(\rho)$  (cont.)

p	q	Q
3	3	0,103560275
3	4	0,043378537
3	5	0,021861214
3	6	0,014890175
3	7	0,010118745
3	8	0,007779021
3	9	0,005878313
3	10	0,004808256
3	11	0,003850724
3	12	0,003273215
3	13	0,002720625
3	14	0,002374120
3	15	0,002025386
3	16	0,001801528
3	17	0,001566908
3	18	0,001414116
3	19	0,001248498
3	20	0,001139712

p	q	Q
4	4	0,084344545
4	5	0,039077644
4	6	0,021551508
4	7	0,015234571
4	8	0,010841416
4	9	0,008490597
4	10	0,006612002
4	11	0,005464237
4	12	0,004472582
4	13	0,003824000
4	14	0,003232967
4	15	0,002830252
4	16	0,002448319
4	17	0,002181075
4	18	0,001919468
4	19	0,001733077
4	20	0,001545778

Table 1: The integral  $Q_{pq}(\rho)$  (cont.)

p	q	Q
5	5	0,071639130
5	6	0,035495077
5	7	0,020789606
5	8	0,015132208
5	9	0,011122050
5	10	0,008857123
5	11	0,007046870
5	12	0,005885501
5	13	0,004893437
5	14	0,004213413
5	15	0,003605776
5	16	0,003171976
5	17	0,002771097
5	18	0,002477003
5	19	0,002197928
5	20	0,001989231

p	q	Q
6	6	0,062551320
6	7	0,032530476
6	8	0,019901680
6	9	0,014823749
6	10	0,011165206
6	11	0,009019523
6	12	0,007295814
6	13	0,006152423
6	14	0,005178338
6	15	0,004489354
6	16	0,003878763
6	17	0,003429340
6	18	0,003019206
6	19	0,002709043
6	20	0,002419375

Table 1: The integral  $Q_{pq}(\rho)$  (cont.)

p	q	Q
7	7	0,055693849
7	8	0,030057012
7	9	0,019009097
7	10	0,014426091
7	11	0,011076787
7	12	0,009057551
7	13	0,007424997
7	14	0,006315098
7	15	0,005368678
7	16	0,004683800
7	17	0,004078717
7	18	0,003623486
7	19	0,003210620
7	20	0,002891627

p	q	Q
8	8	0,050315542
8	9	0,027956938
8	10	0,018157346
8	11	0,013993389
8	12	0,010915484
8	13	0,009017979
8	14	0,007475117
8	15	0,006405672
8	16	0,005491813
8	17	0,004818529
8	18	0,004224250
8	19	0,003769454
8	20	0,003358329

Table 1: The integral  $Q_{pq}(p)$  (cont.)

p	q	Q
11	11	0,039359744
11	12	0,023248178
11	13	0,015950032
11	14	0,012712329
11	15	0,010254343
11	16	0,008676151
11	17	0,007369930
11	18	0,006429691
11	19	0,005618150
11	20	0,004999066
12	12	0,036777320
12	13	0,022045976
12	14	0,015326463
12	15	0,012317705
12	16	0,010018949
12	17	0,008528976
12	18	0,007290037
12	19	0,006390324
12	20	0,005611288

p	q	Q
13	13	0,034542153
13	14	0,020975640
13	15	0,014751754
13	16	0,011943425
13	17	0,009785927
13	18	0,008376232
13	19	0,007199126
13	20	0,006337814
14	14	0,032586587
14	15	0,020016123
14	16	0,014221142
14	17	0,011589502
14	18	0,009557965
14	19	0,008221404
14	20	0,007101101

Table 1: The integral  $Q_{pq}(\rho)$  (cont.)

p	q	Q
9	9	0,045971237
9	10	0,026164417
9	11	0,017362326
9	12	0,013555810
9	13	0,010711696
9	14	0,008930554
9	15	0,007472190
9	16	0,006446191
9	17	0,005566409
9	18	0,004909318
9	19	0,004328671
9	20	0,003878568

p	q	Q
10	10	0,042381461
10	11	0,024609425
10	12	0,016627261
10	13	0,013126174
10	14	0,010487672
10	15	0,008812598
10	16	0,007433285
10	17	0,006450731
10	18	0,005605430
10	19	0,004966784
10	20	0,004401607



Table 1: The integral  $Q_{pq}(\rho)$  (cont.)

p	q	Q
15	15	0,030859727
15	16	0,019151351
15	17	0,013730178
15	18	0,011255288
15	19	0,009336648
15	20	0,008066795
16	16	0,029322490
16	17	0,018364826
16	18	0,013274825
16	19	0,010939861
16	20	0,009122849

p	q	Q
17	17	0,027944350
17	18	0,017648568
17	19	0,012851476
17	20	0,010642086
18	18	0,026701098
18	19	0,016992491
18	20	0,012456940
19	19	0,025573275
19	20	0,016388948
20	20	0,024545041

Table 2: The integral  $P_{jn}(\rho)$

j	n	c = 0,2	c = 0,5	c = 1,0
1	1	0,08202509700	0,23535777729	0,7518226022
1	2	0,00633312625	0,00760281460	-0,0713858737
1	3	0,00548231315	0,01619418917	0,0624865659
1	4	0,00165619138	0,00289335652	-0,0093122187
1	5	0,00174213404	0,00502173753	0,0183835473
1	6	0,00075415889	0,00145710677	-0,0024122383
1	7	0,00083708628	0,00237343687	0,0082909830
1	8	0,00043174972	0,00087691805	-0,0007890852
1	9	0,00048831619	0,00136840966	0,0046067584
1	10	0,00027914825	0,00058365073	-0,0002731707
1	11	0,00031886766	0,00088568075	0,0028943617
1	12	0,00019563528	0,00041748945	-0,0000702126
1	13	0,00022417788	0,00061833310	0,0019717583
1	14	0,00014478739	0,00031365063	0,0000155306
1	15	0,00016602493	0,00045532660	0,0014222080
1	16	0,00011154052	0,00024445916	0,0000530227
1	17	0,00012781026	0,00034885258	0,0010704169
1	18	0,00008858087	0,00019594578	0,0000684065
1	19	0,00010137096	0,00027556077	0,0008324737
1	20	0,00007207985	0,00016067739	0,0000736295

Table 2: The integral  $P_{jn}(\rho)$  (cont.)

j	n	c = 0,2	c = 0,5	c = 1,0
2	1	0,1775584802	0,7518226467	7,496749573
2	2	0,0090470319	-0,0713859029	-2,596078324
2	3	0,0120409000	0,0624865891	1,249272951
2	4	0,0027723830	-0,0093122386	-0,622583776
2	5	0,0037716567	0,0183835649	0,394901694
2	6	0,0013233916	-0,0024122543	-0,236814184
2	7	0,0017951512	0,0082909976	0,175471453
2	8	0,0007761750	-0,0007890989	-0,115968386
2	9	0,0010402340	0,0046067711	0,094575715
2	10	0,0005090513	-0,0002731827	-0,066276132
2	11	0,0006758662	0,0028943731	0,057525471
2	12	0,0003604093	-0,0000702234	-0,041786251
2	13	0,0004732927	0,0019717686	0,037986446
2	14	0,0002687516	0,0000155208	-0,028255085
2	15	0,0003493942	0,0014222174	0,026612429
2	16	0,0002082609	0,0000530137	-0,020114908
2	17	0,0002682532	0,0010704255	0,019494890
2	18	0,0001561714	0,0000683982	-0,014902212
2	19	0,0002122758	0,0008324816	0,014785022
2	20	0,0001357483	0,0000736218	-0,011389104

Table 2: The integral  $P_{jn}(\rho)$  (cont.)

j	n	c = 0,2	c = 0,5	c = 1,0
3	1	0,3031901998	2,300676827	95,26447399
3	2	0,0032249885	0,536295726	-46,24433154
3	3	0,0213104056	0,270293444	25,62103442
3	4	0,0025333924	0,105095215	-15,18197534
3	5	0,0065338038	0,079982323	9,68692356
3	6	0,0014233032	0,037189449	-6,49153596
3	7	0,0030625061	0,035152508	4,59621595
3	8	0,0008980598	0,017470488	-3,35031418
3	9	0,0017549236	0,018992718	2,54732390
3	10	0,0006132470	0,009699560	-1,96812531
3	11	0,0011304975	0,011627121	1,56979357
3	12	0,0004463226	0,005966583	-1,26272541
3	13	0,0007862734	0,007737449	1,04316250
3	14	0,0003394724	0,003947637	-0,86420603
3	15	0,0005771901	0,005464299	0,73293855
3	16	0,0002670710	0,002754424	-0,62087390
3	17	0,0004410569	0,004034752	0,53745613
3	18	0,0002156405	0,002002756	-0,46330589
3	19	0,0003476048	0,003083603	0,40758594
3	20	0,0001778893	0,001503213	-0,35625896

Table 2: The integral  $P_{jn}(\rho)$  (cont.)

j	n	c = 0,2	c = 0,5	c = 1,0
4	1	0,4824956303	7,496751669	1420,597962
4	2	-0,0190558051	-2,596079697	-785,643097
4	3	0,0362603946	1,249274045	491,299712
4	4	-0,0005471306	-0,622584712	-321,178995
4	5	0,0108619802	0,394902523	218,251580
4	6	0,0005236555	-0,236814935	-153,726843
4	7	0,0049943371	0,175472144	111,974452
4	8	0,0005432556	-0,115969029	-83,897246
4	9	0,0028199853	0,094576317	64,584731
4	10	0,0004475430	-0,066276699	-50,770430
4	11	0,0017954810	0,057526009	40,697476
4	12	0,0003626770	-0,041786762	-33,150992
4	13	0,0012369221	0,037986933	27,410822
4	14	0,0002956157	-0,028255550	-22,941457
4	15	0,0009007799	0,026612874	19,426748
4	16	0,0002442515	-0,020115335	-16,605190
4	17	0,0006836498	0,019495301	14,329007
4	18	0,0002045351	-0,014902607	-12,455740
4	19	0,0005356138	0,014785402	10,911466
4	20	0,0001736446	-0,011389470	-9,614713

Table 2 : The integral  $P_{jn}(\rho)$  (cont.)

j	n	c = 0,2	c = 0,5	c = 1,0
5	1	0,7518226467	26,04764488	23330,21030
5	2	-0,0713859029	11,15784741	-13723,00890
5	3	0,0624865891	5,72308062	9253,33001
5	4	-0,0093122386	-3,16932773	-6482,78438
5	5	0,0183835649	1,97631675	4656,58194
5	6	-0,0024122543	-1,27840414	-3423,71187
5	7	0,0082909976	0,90427288	2575,07715
5	8	-0,0007890989	-0,64280169	-1977,75215
5	9	0,0046067711	0,49288989	1550,62085
5	10	-0,0002731827	-0,37263576	-1236,96261
5	11	0,0028943731	0,30114028	1002,60334
5	12	-0,0000702234	-0,23719553	-824,28415
5	13	0,0019717686	0,19915020	686,34334
5	14	0,0000155208	-0,16150962	-577,99373
5	15	0,0014222174	0,13952487	491,70438
5	16	0,0000530137	-0,11562006	-422,12068
5	17	0,0010704255	0,10213358	365,39593
5	18	0,0000683982	-0,08605251	-318,64225
5	19	0,0008324816	0,07737019	279,74558
5	20	0,0000736218	-0,06603415	-247,10530

Table 2: The integral  $P_{jn}(\rho)$  (cont.)

j	n	c = 0,2	c = 0,5	c = 1,0
6	1	1,169578674	95,26454055	407913,8980
6	2	-0,177485172	46,24437515	-248122,6904
6	3	0,110497474	25,62106916	175328,8068
6	4	-0,029219517	15,18200504	-128936,8771
6	5	0,032277477	9,68694989	96741,1996
6	6	-0,009419158	-6,49155982	-73775,3438
6	7	0,014336335	4,59623790	57153,7324
6	8	-0,004090078	-3,35033461	-44949,7275
6	9	0,007852508	2,54734302	35908,4877
6	10	-0,002115120	-1,96814334	-29079,8626
6	11	0,004872041	1,56981064	23857,6313
6	12	-0,001209940	-1,26274164	-19808,7290
6	13	0,003282791	1,04317798	16627,2322
6	14	-0,000743189	-0,86422082	-14096,2421
6	15	0,002345028	0,73295272	12058,6054
6	16	-0,000479685	-0,62088750	-10400,8572
6	17	0,001749827	0,53746919	9038,8178
6	18	-0,000321355	-0,46331845	-7909,1151
6	19	0,001350350	0,40759804	6963,8513
6	20	-0,000220752	-0,35627062	-6166,9752

Table 2: The integral  $P_{jn}(\rho)$  (cont.)

j	n	c = 0,2	c = 0,5	c = 1,0
7	1	1,831675553	362,3614514	7449810,572
7	2	-0,378889118	-190,2610141	-4623735,626
7	3	0,199831594	112,7359972	3367754,201
7	4	-0,070676936	-70,4741582	-2562618,259
7	5	0,058704899	46,4027925	1987795,844
7	6	-0,024467617	-31,9205977	-1561994,491
7	7	0,025847171	22,8899561	1241665,170
7	8	-0,011310411	-16,9330242	-997949,427
7	9	0,014012392	12,9324878	811617,006
7	10	-0,006197015	-10,0904060	-667101,288
7	11	0,008509009	8,0541628	554062,831
7	12	-0,003764528	-6,5284605	-464744,259
7	13	0,005748813	5,3859132	393432,199
7	14	-0,002461108	-4,4917319	-335932,424
7	15	0,004073081	3,7993867	289110,881
7	16	-0,001697257	-3,2385059	-250646,935
7	17	0,003016613	2,7935154	218779,485
7	18	-0,001220055	-2,4226528	-192158,640
7	19	0,002311997	2,1224565	169746,391
7	20	-0,000905299	-1,8663549	-150750,463



Table 2: The integral  $P_{jn}(\rho)$  (conti.)

j	n	c = 0,2	c = 0,5	c = 1,0
8	1	2,897646412	1420,599842	140476694,3
8	2	-0,748326365	-785,644328	-88328564,5
8	3	0,366490414	491,300693	65666551,0
8	4	-0,153377937	-321,179834	-51203252,6
8	5	0,109508773	218,252324	40735619,9
8	6	-0,055251535	-153,727517	-32790840,8
8	7	0,048119240	111,975072	26641269,7
8	8	-0,026265022	-83,897823	-21826915,0
8	9	0,025940001	64,585271	18045937,4
8	10	-0,014715980	-50,770939	-15042836,1
8	11	0,015837277	40,697958	12644062,3
8	12	-0,009127846	-33,151450	-10713839,5
8	13	0,010510400	27,411259	9148381,8
8	14	-0,006085673	-22,941875	-7868954,7
8	15	0,007403083	19,427148	6814942,7
8	16	-0,004277338	-16,605574	-5940309,1
8	17	0,005452679	14,329376	5209316,1
8	18	-0,003131849	-12,456096	-4594026,8
8	19	0,004157450	10,911808	4072585,1
8	20	-0,002366846	-9,615042	-3628051,8

Table 2: The integral  $P_{jn}(\rho)$  (cont.)

J	n	c = 0,2	c = 0,5
9	1	4,635208378	5702,735785
9	2	-1,413102852	-3269,096859
9	3	0,676344042	2132,585857
9	4	-0,314319985	-1447,636665
9	5	0,207288517	1012,892366
9	6	-0,116583020	-729,448337
9	7	0,091409247	539,995629
9	8	-0,056370316	-409,661182
9	9	0,049198221	318,202688
9	10	-0,031962875	-251,965733
9	11	0,029944689	203,053451
9	12	-0,020029046	-166,158962
9	13	0,019802907	137,841233
9	14	-0,013474840	-115,719951
9	15	0,013898403	98,199263
9	16	-0,009550155	-84,119913
9	17	0,010200811	72,690197
9	18	-0,007047081	-63,290089
9	19	0,007751379	55,495227
9	20	-0,005365665	-48,962552

Table 3: The integral  $M_{jn}(\rho)$

j	n	c = 0,2	c = 0,5	c = 1,0
1	1	0,2225247720	0,2600778344	0,4369105974
1	2	-0,0670086744	-0,0980099347	-0,2550509822
1	3	0,0343602708	0,0521945899	0,1518214445
1	4	-0,0216469117	-0,0332929254	-0,1008334371
1	5	0,0152059134	0,0235160620	0,0725650547
1	6	-0,0114254259	-0,0177211601	-0,0552365288
1	7	0,0089868523	0,0139629554	0,0437849590
1	8	-0,0073070735	-0,0113657327	-0,0357797261
1	9	0,0060919191	0,0094826457	0,0299300192
2	1	0,2434236563	0,4369105974	2,4027332210
2	2	-0,0841263532	-0,2550509822	-2,3390394383
2	3	0,0440992092	0,1518214445	1,7892168731
2	4	-0,0279818302	-0,1008334371	-1,3375048809
2	5	0,0197182741	0,0725650547	1,0237253865
2	6	-0,0148407409	-0,0552365288	-0,8073196600
2	7	0,0116847750	0,0437849590	0,6541436396
2	8	-0,0095067831	-0,0357797261	-0,5423549239
2	9	0,0079291744	0,0299300192	0,4582282505

Table 3: The integral  $M_{jn}(\rho)$  (cont.)

j	n	c = 0,2	c = 0,5	c = 1,0
3	1	0,2816323892	0,9406428331	21,55014318
3	2	-0,1162661262	-0,7519415709	-25,71230955
3	3	0,0630723768	0,5102183932	23,43274832
3	4	-0,0404854821	-0,3584898114	-19,64481700
3	5	0,0286777041	0,2653028228	16,15459984
3	6	-0,0216435320	-0,2051285182	-13,33737694
3	7	0,0170687986	0,1641594656	11,14043127
3	8	-0,0139019155	-0,1349859004	-9,43242699
3	9	0,0116031201	0,1133981243	8,08888844
4	1	0,3429159683	2,4027332210	248,6875528
4	2	-0,1696865611	-2,3390394333	-325,1141014
4	3	0,0961414833	1,7892168731	329,0274243
4	4	-0,0626717501	-1,3375048809	-300,9875188
4	5	0,0447080837	1,0237253865	264,0427080
4	6	-0,0338700970	-0,8073196600	-228,3295020
4	7	0,0267715255	0,6541436396	197,1566531
4	8	-0,0218363329	-0,5423549239	-171,0150752
4	9	0,0182434085	0,4582282505	149,2984831

Table 3: The integral  $M_{jn}(\rho)$  (cont.)

j	n	c = 0,2	c = 0,5	c = 1,0
5	1	0,4369105974	6,902536383	3329,511229
5	2	-0,2550509822	-7,602749242	-4563,083110
5	3	0,1518214445	6,416058360	4918,708454
5	4	-0,1008334371	-5,093886741	-4785,031412
5	5	0,0725650547	4,041811318	4421,970435
5	6	-0,0552365288	-3,259409964	-3985,091136
5	7	0,0437849590	2,679622698	3552,741848
5	8	-0,0357797261	-2,243769693	-3158,532313
5	9	0,0299300192	1,908951120	2810,313010

Table 4: The coefficient  $G_{ij}$

$i \backslash j$	1	2	3	4	5
1	2,214274458	0	0	0	0
2	0,315389998	-2,838259214	0	0	0
3	0,108748839	-0,429912062	-3,399281264	0	0
4	0,083598168	-0,202562399	-0,477327200	-3,889316224	0
5	0,047407757	-0,151192025	-0,251406937	-0,503072468	-4,327160546
6	0,041992204	-0,100974442	-0,191227709	-0,280883635	-0,519222932
7	0,027993867	-0,084486147	-0,135853378	-0,217535964	-0,300574195
8	0,026245636	-0,063333382	-0,113716785	-0,159995930	-0,236182173
9	0,019002832	-0,055885577	-0,089025527	-0,134842415	-0,177694988
10	0,018334813	-0,044513349	-0,078043494	-0,108236202	-0,150881219

$i \backslash j$	6	7	8	9	10
1	0	0	0	0	0
2	0	0	0	0	0
3	0	0	0	0	0
4	0	0	0	0	0
5	0	0	0	0	0
6	-4,725876196	0	0	0	0
7	-0,530290039	-5,094108245	0	0	0
8	-0,314649691	-0,538454518	-5,438048446	0	0
9	-0,249989523	-0,325211347	-0,544387311	-5,761071013	0
10	-0,191233003	-0,260721801	-0,333441560	-0,549303188	-6,067699503

Table 5: The coefficients  $F_{ij}$

$i \backslash j$	1	2	3	4	5
1	2,214274458	0	0	0	0
2	0,698360016	-2,838259214	0	0	0
3	-0,059433617	1,220201872	-3,399281264	0	0
4	0,072017089	-0,00751095	1,622569407	-3,889316224	0
5	-0,021900472	0,126133493	0,038332896	1,95660791	-4,327160546
6	0,024973911	-0,010126469	0,174380258	0,076529583	2,246760986
7	-0,011268391	0,043116434	0,00484265	0,217377429	0,109197826
8	0,012503682	-0,00761959	0,060421048	0,019030989	0,256257467
9	-0,00686447	0,021245710	0,00104051	0,076579945	0,032232350
10	0,00742342	-0,00554125	0,029702150	0,00602770	0,091609770

$i \backslash j$	6	7	8	9	10
1	0	0	0	0	0
2	0	0	0	0	0
3	0	0	0	0	0
4	0	0	0	0	0
5	0	0	0	0	0
6	-4,725876196	0	0	0	0
7	2,506085073	-5,094108245	0	0	0
8	0,137582655	2,742945598	-5,438048446	0	0
9	0,291513980	0,163437026	2,960404570	-5,761071013	0
10	0,044345691	0,323755718	0,18709689	3,164603476	-6,067699503

THE METHOD OF AUXILIARY FOURIER-BESSEL SERIES

In Ch. (6) it is shown that the quality of modelling of open or semi-open electrostatic lenses can be improved by increasing the z-period  $L$  of the Fourier-Bessel series used to approximate the potential  $\phi(r;z)$  in the lens. The increase in  $L$  requires a corresponding increase in  $N$ , the number of terms included in the series, so as to limit the truncation error to an acceptably small value. An increase in  $N$  results in an increase in computer time, which makes high precision ray tracing a costly process. In this appendix the method of auxiliary series is discussed, a method which results in a significant reduction in the total number of terms to be evaluated.

The method is illustrated by discussing the Fourier-Bessel solution to the exterior Dirichlet boundary value problem, for which unacceptably large values of  $L$  may be required if only the basic series is used. It is shown that for a finite period  $L$ , the error of the approximation can be understood either in terms of induced charge distributions on two parallel planes, or by considering an infinity of image charge distributions at  $r=A$ . The error can be reduced by eliminating the image potential distributions, which is done numerically through the addition of suitably chosen auxiliary Fourier-Bessel series.

1. INTRODUCTION

The following boundary value problem with rotational symmetry is considered :



$$\phi(A; z) = 0 \text{ for } z \leq 0 \text{ and } z \geq L \quad (\text{A2.1a})$$

$$\phi(A; z) = F(z) \text{ for } 0 < z < L \quad (\text{A2.1b})$$

$$\text{and } \nabla^2 \phi(r; z) = 0 \text{ for } r \neq A \quad (\text{A2.1c})$$

where  $\phi(r; z)$  is the potential at a point  $(r; z)$ ,  $r$  and  $z$  being cylindrical polar coordinates.  $A$  and  $L$  are two given lengths and  $F(z)$  is a given nonsingular function with a finite number of discontinuities. Let the region  $r < A$  be  $\Omega_i$  and the region  $r > A$  be  $\Omega_e$ ; then finding  $\phi(r; z)$  in  $\Omega_i$  and  $\Omega_e$  constitutes the solution of an interior and exterior Dirichlet boundary value problem, respectively. The interior problem was discussed in Chs. (5) and (6), and this appendix gives a solution to the exterior problem in terms of a Fourier-Bessel series.

Although quite a few different numerical methods can in principle be applied to solve both the interior and exterior boundary value problems, it is found that some of the methods that are commonly used to solve the interior problem can only be applied to the exterior problem if special care is taken, or certain modifications made.

When, for instance, the finite difference method is used, Eqs. (A2.1a) and (A2.1b) provide boundary values on one side of, e.g., a square grid of infinite extent, and the values of  $\phi$  on the other three sides may be taken to be zero. Limiting the relaxation computation to a square of finite size (Evans, 1977), it is found that the boundary values on three sides will now be unknown, and approximate values will have to be supplied before iterative relaxation can

commence [Nedoma (1975a and 1975b)]. A possible approximation will be  $\phi=0$ ; or a better choice is  $\phi(\rho)=k/\rho$  where  $\rho$  is the distance between the boundary point and the "effective centre" of the source distribution, and  $k$  is a constant which can only be specified if the source of the potential distribution can be approximated (this information is normally only known after the boundary value problem has been solved). It is also possible to solve the problem for squares of various sizes (taking  $\phi=0$  on the three sides) and, by investigating the solutions, decide whether the error caused by using a finite boundary can be tolerated. [See Nedoma (1975b) for further references]. The finite element method is also hampered by the undefined finite boundaries, and several references on so-called boundary relaxation methods are given by McDonald et al. (1972). Computer experiments on the handling of boundaries have been described by Wood (1976) and a way to match a (two-dimensional) closed region containing the field sources, to a large annular region representing the surrounding empty space, has been discussed by Silvester et al. (1977).

A novel way of dealing with the infinite exterior region has been applied by Greenspan (1966) by converting the exterior problem to an interior one through inversion in the unit sphere, and then solving the resulting interior problem by a finite difference method.

Another way of avoiding the problem of infinite boundaries is to calculate the source distribution giving rise to the potential field [Harrington (1968), Singer et al. (1970), Birtles et al.

(1973), Du Toit (1976) and Geer (1976)]. This normally involves the solution of a system of linear algebraic equations with a large number of unknowns. The potential at any point in  $\Omega_i$  or  $\Omega_e$  can then be found by means of Coulomb's law. For fields with rotational symmetry this involves evaluating an integral (or sum) with an elliptic integral in the integrand. Although the interior problem can be solved to a high degree of accuracy, the author is not aware of reports on the accuracy of exterior solutions.

In contrast to most of the methods outlined above, which involve either iterative procedures or matrix inversion, the Fourier-Bessel solution to be described is arrived at by summing a series, a process which can be terminated when sufficient precision has been reached. In this sense the method is a direct one, and there does not seem to be any limit to the precision attainable.

## 2. FOURIER-BESSEL SOLUTIONS

In the case of rotational symmetry, Laplace's equation reduces to

$$\frac{1}{r} \frac{\partial}{\partial r} \left[ r \frac{\partial \phi}{\partial r} \right] + \frac{\partial^2 \phi}{\partial z^2} = 0 \quad (\text{A2.2})$$

and we investigate solutions of the form  $\phi(r,z)=R(r)Z(z)$ , where four families of functions may be of use :

$$\begin{aligned} &K_0(\alpha r) \sin(\alpha z), K_0(\alpha r) \cos(\alpha z); \\ &I_0(\beta r) \sin(\beta z), I_0(\beta r) \cos(\beta z); \\ &J_0(\gamma r) \sinh(\gamma z), J_0(\gamma r) \cosh(\gamma z); \quad \text{and} \\ &Y_0(\delta r) \sinh(\delta z), Y_0(\delta r) \cosh(\delta z) \end{aligned}$$

where  $J_n$  and  $Y_n$  represent the unmodified Bessel functions of first and second kinds, respectively, and  $I_n$  and  $K_n$  the modified Bessel functions of first and second kinds, respectively, all of order  $n$ . (Throughout this paper the arguments of Bessel functions are restricted to real values).

For the exterior problem, the function  $I_0$  is unsuitable, because  $I_0(z \rightarrow \infty) \rightarrow \infty$ , and the function  $J_0$  will be given preference over  $Y_0$  because the numerical evaluation of  $J_n$  is simpler than that of  $Y_n$ .

Two different types of solution are now discussed.

### 2.1 Use of subregions

The empty space  $\Omega_e$  can be subdivided into three regions,  $\Omega_{e1}$ ,  $\Omega_{e2}$  and  $\Omega_{e3}$ , defined by  $z \leq 0$ ,  $0 \leq z \leq L$  and  $z \geq L$ , respectively, and solutions  $\phi_I$ ,  $\phi_{II}$  and  $\phi_{III}$ , respectively, are defined in the three regions, choosing the form of the solutions in such a way that  $\phi_I = \phi_{II}$  at  $z=0$  and  $\phi_{II} = \phi_{III}$  at  $z=L$ :

$$\phi_I = \sum_{n=1}^{\infty} J_0(\lambda_{0n}r) \left\{ A_n \exp(\lambda_{0n}z) + C_n \exp[\lambda_{0n}(z-L)] \right\} \quad (A2.3a)$$

$$\begin{aligned} \phi_{II} = & \sum_{n=1}^{\infty} \left[ B_n \sin(n\pi z/L) K_0(n\pi r/L) / K_0(n\pi A/L) \right. \\ & \left. + J_0(\lambda_{0n}r) \left\{ A_n \exp(-\lambda_{0n}z) + C_n \exp[-\lambda_{0n}(L-z)] \right\} \right] \quad (A2.3b) \end{aligned}$$

$$\phi_{III} = \sum_{n=1}^{\infty} J_0(\lambda_{0n}r) \left\{ A_n \exp(-\lambda_{0n}z) + C_n \exp[-\lambda_{0n}(z-L)] \right\} \quad (A2.3c)$$

in which  $\lambda_{0n} = Z_{0n}/A$ ,  $Z_{0n}$  being the  $n$ -th zero of  $J_0$ .

The coefficients  $B_n$  are determined by performing a Fourier analysis at  $r=A$  in the region  $\Omega_{e2}$ , using Eq. (A2.1b) :

$$\sum_{n=1}^{\infty} B_n \sin(n\pi z/L) = F(z)$$

Determination of the coefficients  $A_n$  and  $C_n$  may be done by requiring that  $\partial\phi_I/\partial z = \partial\phi_{II}/\partial z$  at  $z=0$  and that  $\partial\phi_{II}/\partial z = \partial\phi_{III}/\partial z$  at  $z=L$ .

In Ch. (5) this approach has led, for the interior Dirichlet problem, to series with acceptable convergence in  $\Omega_i$  except at  $(r; z=0)$  and  $(r; z=L)$  and  $(r=A; z)$ . The same behaviour may be expected for the exterior problem, but the practical implementation may prove to be more involved, because the orthogonalization of the Bessel functions may be complicated.

## 2.2 Fourier integral approach

Consider the function  $G(z) = \phi(A; z)$ , i.e.

$$G(z) = 0 \text{ for } z \leq 0 \text{ and } z \geq L, \text{ and } G(z) = F(z) \text{ for } 0 < z < L \quad (A2.4)$$

Then  $G(z)$  can be represented by the Fourier integral

$$G(z) = \int_0^{\infty} B(\omega) \sin(\omega z) d\omega \quad (A2.5)$$

in which the amplitude function is given by

$$B(\omega) = \frac{\pi}{2} \int_0^{\infty} G(z) \sin(\omega z) dz \quad (\text{A2.6})$$

For  $\Omega_e$  the following then represents a solution :

$$\phi(r; z) = \int_0^{\infty} B(\omega) \sin(\omega z) \frac{K_0(\omega r)}{K_0(\omega A)} d\omega \quad (\text{A2.7})$$

As discussed in Ch. (6), the integral of Eq. (A2.5) can be calculated numerically to a high degree of precision, and for  $0 < z < L$  the quality of fit of the Fourier integral representation of  $G(z)$  is not fundamentally affected by the fact that the numerical process of evaluating the integral amounts to the summation of a finite series

$$\sum_{n=1}^N B(\omega_n) \sin(\omega_n z)$$

in which the values of  $\omega_n$  are determined by the nature of the numerical integration procedure.

For the region  $\Omega_e$  [and  $\Omega_i$ , as shown in Ch. (6)] the situation is different, since the Fourier-Bessel integral changes into a Fourier-Bessel series of which the period is related to the lowest non-zero frequency  $\omega_1$  found in the series. The nonperiodic function  $\phi(r; z)$  is represented symbolically by the nonperiodic function of Eq. (A2.7), but in practice is approximated by a periodic function. This periodicity has a detrimental effect on the quality of the approximation of  $\phi(r \neq A; z)$ , as will be shown in Section (2.3)

### 2.3 Fourier-Bessel series approach

Consider the following boundary value problem :

$$H(z) = \Psi(A; z) = F(z) \text{ for } 0 \leq z \leq L \quad (\text{A2.8a})$$

$$H(z) = \Psi(A; z) = 0 \text{ for } (L-L_+)/2 \leq z \leq 0 \quad (\text{A2.8b})$$

and for  $L \leq z \leq (L_+ + L)/2$

$$\Psi[r; (L-L_+)/2] = \Psi[r; (L_++L)/2] = 0 \quad \forall r \quad (\text{A2.8c})$$

$$\nabla^2 \Psi = 0 \text{ for } r > A, (L-L_+)/2 < z < (L_++L)/2 \quad (\text{A2.8d})$$

where  $A, L$  and  $F(z)$  have been defined in Section (1), and  $L_+ > L$  is an arbitrary length.

The solution is then given by

$$\Psi(r; z) = \sum_{n=1}^{\infty} B_n \sin(n\pi z/L_+) K_0(n\pi r/L_+) / K_0(n\pi A/L_+) \quad (\text{A2.9})$$

with

$$B_n = \frac{2}{L_+} \int_0^{L_+} H[\xi - (L_+ - L)/2] \sin(n\pi \xi/L_+) d\xi \quad (\text{A2.10})$$

It can be shown that, if  $L_+ \rightarrow \infty$ , the solution  $\Psi$  will be identical with the solution  $\phi$  of Eq. (A2.7). [For the one-dimensional case, see, e.g., Lanczos (1957) p. 252.] For finite  $L_+$  the infinite planes  $P_1$  and  $P_2$  at zero potential at  $z = (L-L_+)/2$  and  $z = (L_++L)/2$  affect the solution for the regions  $r \neq A$ , as can be shown in various ways :

2.3.1 Placing zero values along the planes  $P_1$  and  $P_2$  where the

values of  $\phi$  are not expected to be zero, amounts to using a grid of finite extent in finite difference or finite element solutions, as discussed in Section (1). (The boundary values on only two, not three sides are modified here, however).

2.3.2 Charge distributions  $\sigma_1(r)$  and  $\sigma_2(r)$  are induced on the earthed conducting plates at  $P_1$  and  $P_2$ . These distributions cause  $\Psi(r \neq A; z)$  to differ from  $\phi(r \neq A; z)$ , and the magnitude of the error introduced can be calculated by means of Coulomb's law if the functions  $\sigma_1$  and  $\sigma_2$  are known. The latter functions can be found from the normal derivatives of  $\Psi$  at the planes  $P_1$  and  $P_2$  :

$$\sigma(r) = -2\epsilon_0 \eta \frac{\partial \Psi}{\partial z} = \frac{-2\pi\epsilon_0 \eta}{L_+} \sum_{n=1}^{\infty} n B_n \eta^{n-1} U(r) \quad (\text{A2.11})$$

where  $\eta=1$  for  $\sigma_1$ ,  $\eta=-1$  for  $\sigma_2$ ,  $\epsilon_0$  = permittivity of free space,

$$U_n(r) = K_0(n\pi r/L_+) / K_0(n\pi A/L_+) \text{ for } r > A$$

$$\text{and } U_n(r) = I_0(n\pi r/L_+) / I_0(n\pi A/L_+) \text{ for } r < A$$

in which the field in  $\Omega_i$  has been approximated by

$$\Psi(r < A; z) = \sum_{n=1}^{\infty} B_n \sin(n\pi z/L_+) I_0(n\pi r/L_+) / I_0(n\pi A/L_+) \quad (\text{A2.12})$$

as in Ch. (6).

$Q_1$  and  $Q_2$ , the total induced charges on the two plates can be found by calculating



$$\begin{aligned}
Q_j &= \int_0^{\infty} 2\pi r \sigma_j(r) dr \quad \text{where } j=1 \text{ or } 2 \\
&= -4\pi\epsilon_0 A \sum_{n=1}^{\infty} (\eta)^{n-1} B_n [K_1(\theta)/K_0(\theta) \\
&\quad + I_1(\theta)/I_0(\theta)] \tag{A2.13}
\end{aligned}$$

using various integrals [Gradshteyn et al. (1965), p. 684, and Abramowitz et al. (1970), pp. 77 and 484];  $\theta = n\pi A/L_+$ .

This is an extension of the well known result [Scanio (1973), Pumplin (1969) and Fong et al. (1967)] that the charges induced by a point charge  $q$  (which is distances  $x$  and  $L-x$  from two infinite parallel conducting plates a distance  $L$  apart) are  $-q(L-x)/L$  and  $-qx/L$ . This fact can be used in an alternative calculation of the induced charges  $Q_1$  and  $Q_2$  of the present problem, by noting that the charge distribution  $\sigma_A(z)$  at  $r=A$  is known  $\forall z$ , in terms of the discontinuity in the derivative  $(\partial/\partial r)\Psi(A; z)$  :

$$\begin{aligned}
\sigma_A(z) &= 2\epsilon_0 \frac{\partial \Psi}{\partial r} (A; z) \\
&= 2\epsilon_0 (\pi/L_+) \sum_{n=1}^{\infty} n B_n \sin (n\pi z/L_+) [K_1(\theta)/K_0(\theta) \\
&\quad + I_1(\theta)/I_0(\theta)] \tag{A2.14}
\end{aligned}$$

A ring-like element at  $(A; z)$ , with charge density  $\sigma_A$  will induce a charge  $-2\pi A \sigma_A z/L_+$  in the plate  $P_2$ , giving

$$Q_2 = - \int_0^{L_+} \frac{2\pi A \sigma_A z}{L_+} dz$$

which gives the same expression as (Eq. (A 2.13)).

In spite of this detailed knowledge of the induced charge distributions, correction of  $\Psi(r;z)$  to find  $\phi(r;z)$  does not seem feasible. It will, however, be shown in Section (3) that the required correction is possible by exploiting certain properties of the image charge model.

2.3.3 Although the potential field of a point charge  $q$  located between two parallel grounded conducting plates can be calculated by taking into account  $q$  itself, and the induced distribution  $\sigma_i$  on the plates (involving the evaluation of an integral with an elliptic integral in the integrand), it is well known [Kellogg (1953)] that the potential between the plates can alternatively be found by considering an infinity of image charges of alternating signs, in each of the plates. This obviates the inconvenience of the elliptic integrals altogether, and the integration is now replaced by the evaluation of an infinite series. (The series converges very slowly, but since it alternates, efficient accelerating algorithms are available).

Some thought will show that it is possible to estimate to what extent the image charges affect the potential distri-

bution  $\Psi(r;z)$  [causing it to differ from  $\phi(r;z)$ ] by calculating the potential  $V_i(r;z)$  due to the image charges only, at points in  $\Omega_e$  (or  $\Omega_i$ ) and at points  $(r=A; 0 < z < L)$ . For points in  $\Omega_i$  the differences  $V_i(r \neq A; z) - V_i(A; z)$  for  $0 < z < L$  are small compared to the potential  $\Psi$  at the point, and it was seen in Ch. (6) that by simply taking  $L_+/L$  sufficiently large, the difference  $\Psi(r;z) - \phi(r;z)$  could be made acceptably small. For points in  $\Omega_e$ , especially for  $r \gg A$ , it is found that the differences are large, calling for an alternative form of correction.

The simplest way of reducing the effect of the induced charges (or image charges) is by taking  $L_+ \gg L$ , which effectively moves the induced charges further away and, as can be shown, tends to reduce the magnitudes of  $Q_1$  and  $Q_2$ . Fig. (A2.1) shows how an increase in  $L_+$  reduces the ratio

$$E_x = \frac{\Psi_x(r_0; z_0) + \Psi_{7290}(r_0; z_0)}{\Psi_{7290}(r_0; z_0)} \quad (\text{A2.15})$$

for two chosen functions  $F(z)$  and Eq. (A 2.1b). The functions  $F_1(z)$  and  $F_2(z)$  are zero everywhere, except in the following regions :

$$F_1(z) = 1 \quad \text{for } L/2 - 1 < z < L/2 + 1 \quad (\text{A2.16})$$

$$F_2(z) = -1 \quad \text{for } L/2 - 2 < z < L/2 - 1 \quad (\text{A2.17a})$$

$$F_2(z) = 1 \quad \text{for } L/2 + 1 < z < L/2 + 2 \quad (\text{A2.17b})$$

The subscript  $x$  in  $E_x$  refers to the value  $L_+$  used in calcu=

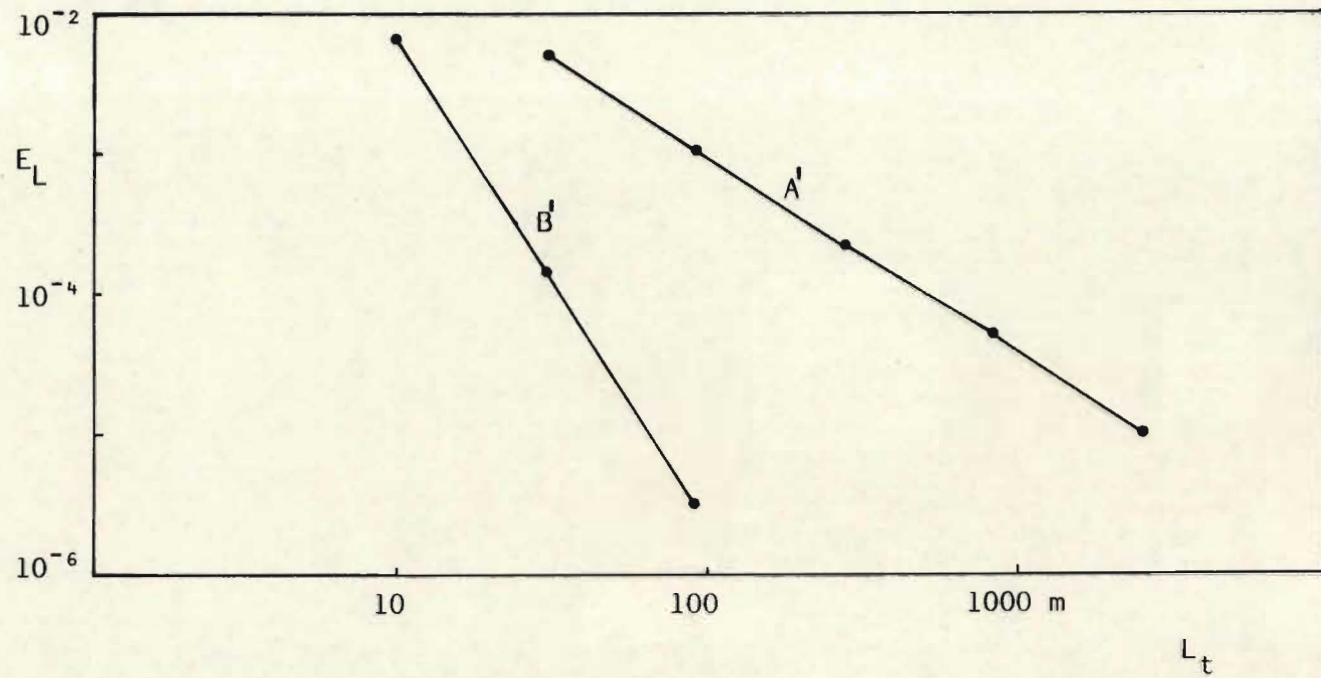


Fig. (A2.1) The ratio  $E_{L_t}$  of Eq.(A2.15) plotted against  $L_t$ . Lines A' and B' apply to  $\psi_{L_t}(5m; z_0)$  resulting from  $F_1$  and  $F_2$  resp., as evaluated at  $z_0=L/2$  and  $z_0=L/2+3$ , resp. The functions  $F_1$  and  $F_2$  are defined by Eqs.(A2.16) and (A2.17), resp.

lating  $\Psi_x$ . For  $F_1(z)$ ,  $\Psi$  is evaluated at the point  $(r_0; z_0) = (5m; L/2)$  and for  $F_2(z)$ ,  $\Psi$  is evaluated at  $(r_0; z_0) = (5m; L/2+3)$ . In both cases,  $A=1$  m.

The rapid decrease in  $E_x$  when increasing  $L_+$  in the case of  $\Psi$  of  $F_2$  is explained by noting that (especially when  $A \ll L$ ) the charge distribution giving rise to  $G(z)$  resembles that of a dipole, whereas with  $F_1(z)$  it resembles a monopole. The flux lines of a monopole terminate at infinity, whereas those of a dipole terminate at the negative pole of the dipole.

For functions like  $F_1(z)$  very large values of  $L_+$  would be required to obtain sufficiently precise solutions for points  $(r \gg A; z)$ , resulting in very slow convergence of the Fourier-Bessel series, as shown in Section (4). A more practical method in these cases is that of eliminating the images, as discussed in the next section.

### 3. ELIMINATION OF IMAGES

The principle of the method is illustrated in Fig. (A2.2). Suppose that the boundary value problem of Eq. (A2.1) must be solved, with  $F(z)=1$ . Then  $L_+$  is chosen large enough that the region in which  $\phi(r; z)$  is required, falls within the limits  $-(L_+-L)/2 < z < (L_++L)/2$ . The solution  $\Psi(r; z)$  of Eq. (A2.9) which is the solution of Eqs. (A2.8), is a periodic solution (period  $L_+$ ), and is therefore also the solution of the following boundary value problem :

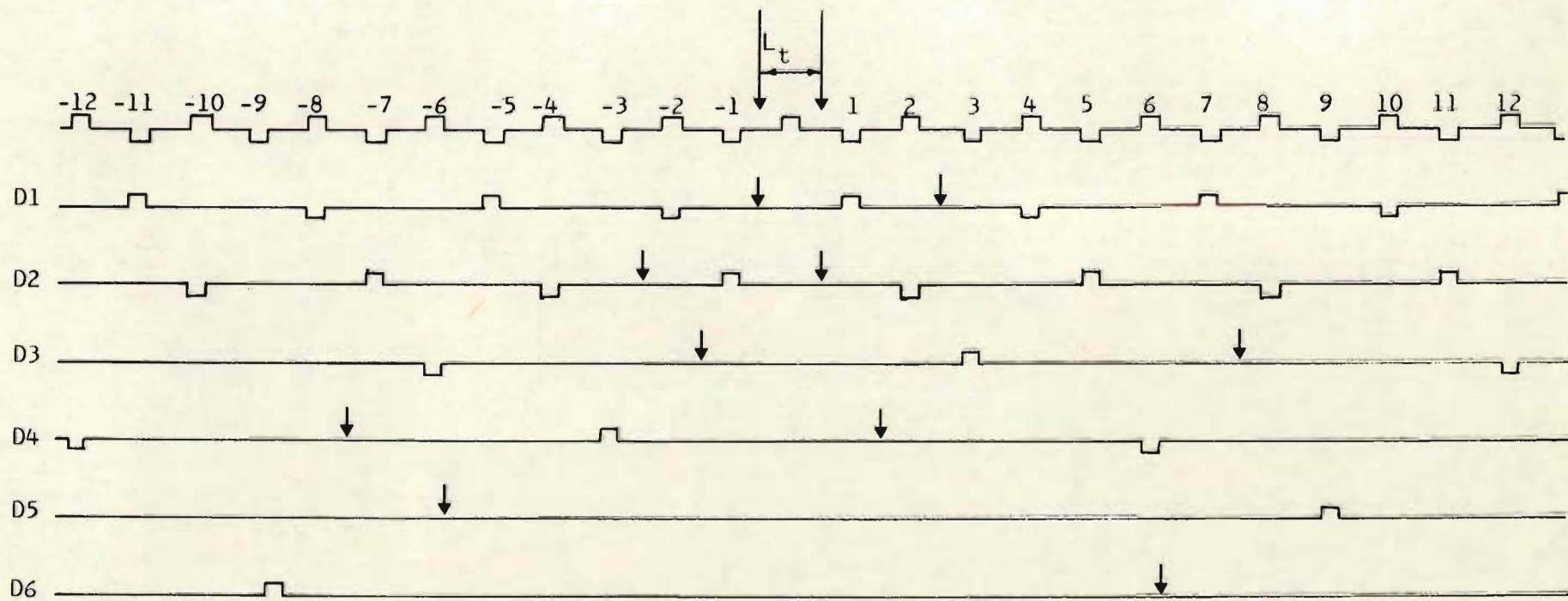


Fig. (A2.2) Diagram to illustrate the correction of the function  $H(z)$  of Eq.(A2.18), shown in the top graph, by superposing the functions appearing in Eq.(A2.20), shown by graphs  $D_1, D_2, \dots$ . The arrows indicate half-periods of the various periodic functions, and the numbers at the top show the positions of the images discussed in Section (3).

$$H_p(z) = \Psi(A; z) = F(z) \quad \text{for } sL_+ \leq z \leq sL_+ + L \quad (\text{A2.18a})$$

$$H_p(z) = \Psi(A; z) = -F(z) \quad \text{for } (s+1)L_+ \leq z \leq (s+1)L_+ + L \quad (\text{A2.18b})$$

$$H_p(z) = \Psi(A; z) = 0 \quad \text{for } sL_+ + (L_+ - L)/2 \leq z \leq sL_+ \quad (\text{A2.18c})$$

$$\text{and for } sL_+ + L \leq z \leq sL_+ + (L_+ + L)/2 \quad (\text{A2.18d})$$

$$\nabla^2 \Psi(r; A; z) = 0 \quad \forall z \quad (\text{A2.18e})$$

in which  $s = 0; \pm 2; \pm 4; \dots$

The behaviour of  $H(z) = \Psi(A; z)$  for the regions  $z < (L - L_+)/2$  and  $z > (L_+ + L)/2$  is in complete correspondence with the description in terms of images; we may even extend the idea of point charge images to that of images of potential distributions, stating that the potential  $\Psi(r; z)$  at any point between two parallel grounded conducting plates will give rise to an infinity of image potentials in each of the plates.

The method of elimination of images may be discussed by referring to Fig. (A2.2).  $\Psi(A; z)$  is shown as the top graph, and the region of interest is found between the two arrows. If the images marked  $1; 2; \dots$  and  $-1; -2; \dots$  can be eliminated,  $\Psi(A; z)$  of Eq. (A2.18) would be changed to  $\phi(A; z)$  of Eq. (A2.1), and the boundary value problem of Section (1) solved.

The elimination can be carried out as follows: to  $\Psi_{L_+}(r; z)$  is added a function  $-\Psi_{3L_+}(r; z; -2L_+)$ , shown by graph  $D_1$  (The variable  $d$  in  $\Psi_{nL_+}(r; z; d)$  indicates that the train of pulses is displaced towards the right by an amount  $d$ ). This eliminates images  $1; 4; 7, \dots$  and  $-2; -5; -8; \dots$ . Then  $-\Psi_{3L_+}(r; z; 2L_+)$  is added, elimina=

ting images 2;5;8,... and -1;-4;-7,... After this first stage of correction, the nearest images are nos. 3 and -3, giving the corrected function  $\psi^{C1}$  a period of  $T_1=6L_+$ . In the second stage of correction the functions  $-\psi_{9L_+}(r;z;-6L_+)$  and  $-\psi_{9L_+}(r;z;6L_+)$  are added, eliminating images 3;12;... and -6;15;... as well as 6;15;... and -9;-18;... so that the period of  $\psi^{C2}$  is now  $T_2=9L_+$ . (The arrows in graphs  $D_1, D_2, \dots$  show half-periods of the respective functions.) It can be seen that after  $M$  stages of correction the period of the corrected function  $\psi^{CM}$  will be  $T_M=3^M(2L_+)$  and for large values of  $M$  the distance to the nearest image will be approximately  $T_M/2$ .

Although the proposed method increases the period of  $\psi^{CM}$  in an exponential fashion, and we know that  $\psi^{CM} \rightarrow \phi$  for  $M \rightarrow \infty$ , it must still be established that the total computational effort required by this method is less than choosing  $L_+$  a sufficiently large value  $T_M$  in the first place. This is done in the next section by investigating the convergence of the series.

#### 4. CONVERGENCE OF THE FOURIER-BESSEL SERIES

Suppose that the series of Eq. (A2.9) is truncated after the  $N$ -th term, and that the truncation error is  $\epsilon_N(r;z)$ .

Then it can be shown that for a chosen point  $(r_0; z_0)$ ,  $\epsilon_N(r_0; z_0)$  increases rapidly with  $L_+$ , the chosen period.  $\epsilon_N(r; z_0)$  also depends strongly upon  $r$ ; [ due to the asymptotic behaviour of the  $I_0$  and  $K_0$  Bessel functions,  $\epsilon_N(r; z_0)$  decreases with an increase in



$|A-r| \ll r$ ]. If, for  $r_0$ , a chosen value of  $r$ , it is found that  $\epsilon_N(r_0, z)$  is approximately constant for  $0 < z < L$ , then the proposed method will not bring about any reduction in computer time, but possibly even an increase. Fig. (A2.3) shows that except if  $N$  is taken quite large (e.g.  $N = 120$ ), the use of the method of Section (3) will only be profitable if the convergence is accelerated.

Investigating the series of Eq. (A2.9), as modified by the introduction of Lanczos  $\sigma$ -factors [Lanczos (1957)] by writing

$$\Psi_{\text{Lanc}, L_+} = \sum_{n=1}^N B_n \left\{ \frac{\sin [\pi n / (N+1)]}{n\pi / (N+1)} \right\} \sin(n\pi z / L_+) \frac{K_0(n\pi r / L_+)}{K_0(n\pi A / L_+)} \quad (19)$$

it is seen that, although the convergence of  $\Psi_{\text{Lanc}, L_+}$  is slower than that of  $\Psi_{L_+}$  near  $z = L/2$ , its convergence for low values of  $N$  is considerably better for  $(L-L_+)/2 < z < (L-L_+)/3$ . The Lanczos  $\sigma$ -factors, shown in braces in Eq. (A2.19) are derived by performing a spatial averaging process, and the property of  $H(z)$  of Eq. (A2.8) of being zero in the regions specified by Eqs. (A2.8b) and (A2.8c) allows the function  $\Psi_{\text{Lanc}, L_+}(r_0, z)$  to approximate  $\phi(r_0; z)$  very well in the outer regions  $L_+/3 < |z - L/2| < L_+/2$  as long as  $r_0/A \ll L_+$ . Due to the smoothing action,  $\Psi_{\text{Lanc}, L_+}$  is not useful for  $0 < z < L$ .

If we now investigate the convergence of

$$\begin{aligned} \Psi_{\text{corr}}(r_0; z) = & \Psi_{L_+}(r_0; z) - \Psi_{\text{Lanc}, 3L_+}(r_0; z; z_1) - \Psi_{\text{Lanc}, 3L_+}(r_0; z; z_2) \\ & \Psi_{\text{Lanc}, 9L_+}(r_0; z; z_3) + \dots \end{aligned} \quad (A2.20)$$

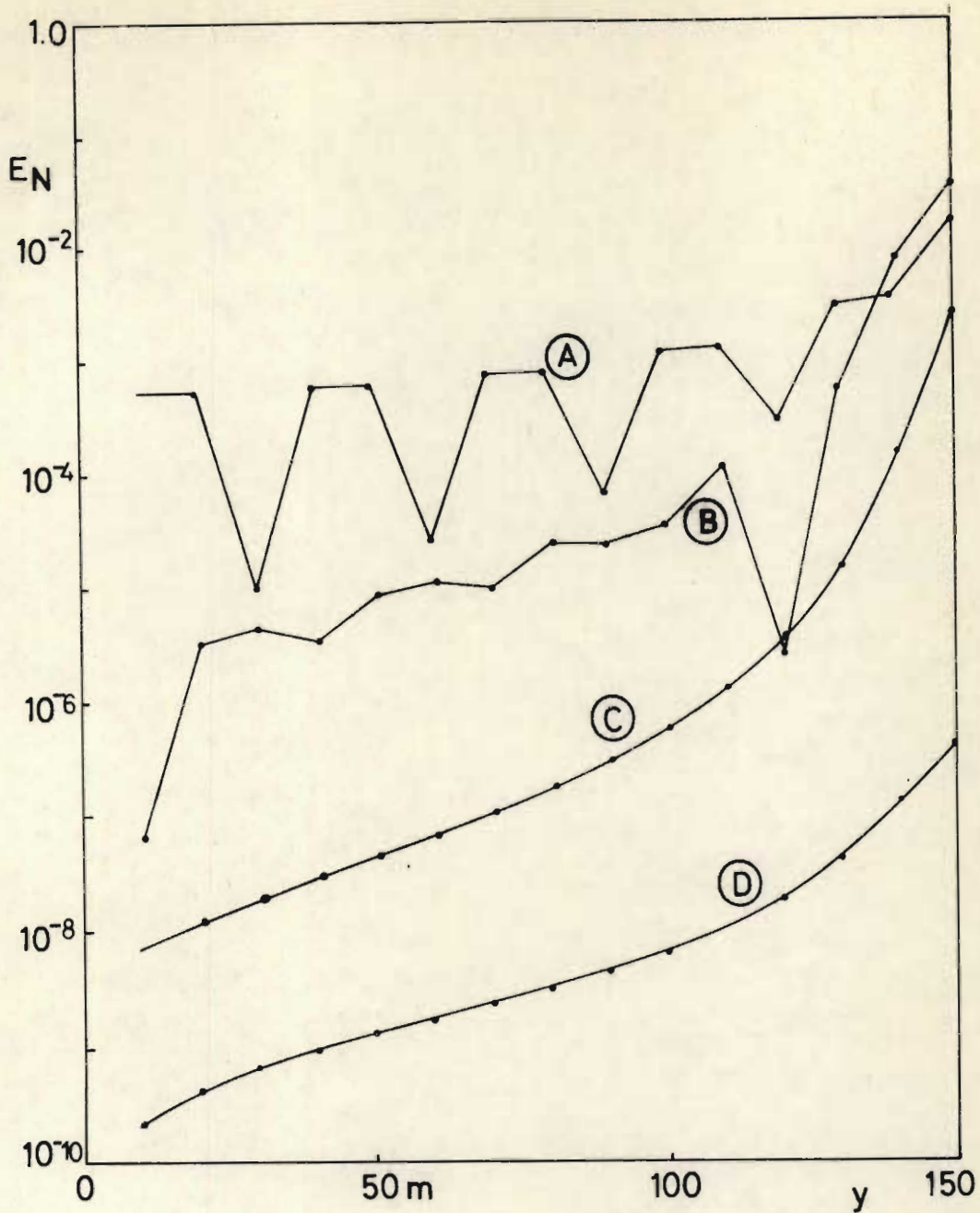


Fig. (A2.3) The truncation error  $\epsilon_N$  of Section (4) is plotted against  $y \equiv z + L_t/4 - L/2$   $L=2$  and  $L_t=300$ . Let  $W$  be an estimate of  $\psi_{L_t}(5m; z)$  of Eq.(A2.9), due to a boundary function  $F(z)$  given by Eq.(A2.16). Then curves B and C show  $\epsilon_N = |\psi_{Lanc, L_t}(5m; z) - W|$  with  $\psi_{Lanc, L_t}$  calculated by means of Eq.(A2.19) with  $N=20$  and  $N=120$ , resp. Curves A and D show  $\epsilon_N = |\psi_{L_t}(5m; z) - W|$ , with  $\psi_{L_t}$  given by Eq.(A2.9), as summed to 20 and 120 terms, resp.

in which  $z_1, z_2, \dots$  are defined by Section (3) and illustrated in Fig. (A2.2), then the series representing each function of Eq. (A2.20) may be truncated after approximately the same number of terms. By way of illustration the values of the terms appearing in the above equation are given for the point (5m; 1,5m) :

$$\begin{aligned} \Psi_{\text{corr}}(5\text{m}; 1,5\text{m}) &= 0,0818005 + 0,00399316 + 0,000172 + 0,000042 + 0,000010 \\ &= 0,0868203 \end{aligned}$$

in which the terms have been calculated by truncating the series at  $N = 40, 40, 40, 20$  and  $20$  respectively.

The result obtained may be compared with the value  $\Psi_{7290} = 0,0868222$  which has been found by calculating  $\Psi$  without Lanczos acceleration for  $L_{\dagger} = 7290\text{m}$  and  $N = 5500$ . (The truncation error for this value is  $1 \times 10^{-6}$  and the error due to the remaining image charges is  $3 \times 10^{-6}$ .) Since the method of elimination of images has required only 160 terms for the same precision, it can be seen that the method allows a significant reduction in computing time.

This can be stated more generally by noting that every correcting stage requires a further  $2N$  Fourier-Bessel terms to be evaluated, whereas the calculation by means of a straightforward threefold increase in  $L_{\dagger}$  would have required  $3N$  terms. For  $M$  stages, the proposed method would require  $2MN$  evaluations, as compared to  $3^M N$  evaluations. For calculations of high precision,  $M$  may, for instance, be 8, in which case the ratio of the number of evaluations required by the two methods is 0,0024, a saving which is significant enough to warrant the additional programming to evaluate the expression of

Eq. (A2.20).

In Fig. (A2.4) a cross section of part of the field is shown for  $\phi(r;z)$  due to  $F(z)$  of Eq. (A2.16). The solution for  $r < A$  has been found by means of Eq. (A2.12); see Ch. (6). An equipotential diagram for  $\phi(r;z)$  due to  $F(z) = \exp(-Az^2)$  is given in Ch. (6), as well a table comparing the convergence of the  $I_0$  Fourier-Bessel series for rectangular, spline and exponential functions, showing that for the smoother functions the convergence is considerably faster than for functions with discontinuities. The same behaviour can be expected for the  $K_0$  Fourier-Bessel Series.

## 5. CAPACITANCE

Normally the calculation of capacitance is either an aim or a by-product of the solution of the exterior Dirichlet boundary value problem. In the present case the capacitance of an electrode ( $A; 0 < z < L$ ) at an applied potential  $V_0$  can be found by means of Eq. (A2.14) if small gaps are allowed between this electrode and the earthed electrodes ( $A; z < 0$ ) and ( $A; z < L$ ). The potentials in the gaps are, however, unknown, and special care must be taken [Read (1969a, 1969b and 1970), Wittels et al. (1976) and Natali (1972)] if assumptions are to be made [Anicin (1976), Saito et al. (1977), Cook et al. (1976), Bertram (1940 and 1942), El-Kareh et al. (1970a), Heerens et al. (1975) and Heerens (1976)] about the potential distributions in the gaps. For thin, tubular electrodes, the assumption of linear distributions in the

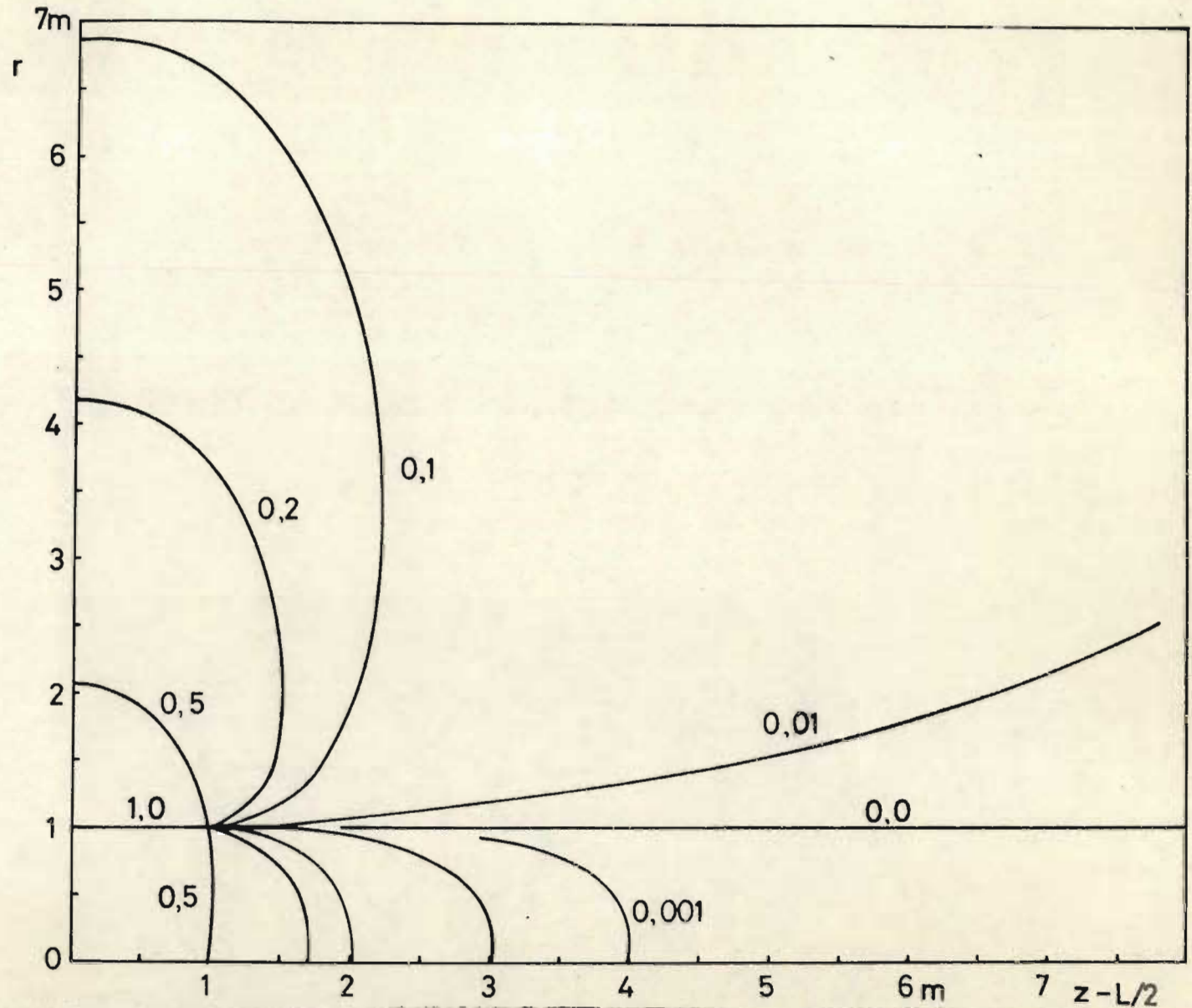


Fig. (A2.4) Equipotential diagram for  $\phi(r;z)$  due to  $F(z)$  of Eq.(A2.16), showing part of the region  $z>L/2, r>0$ . The equipotential values are indicated by the figures in the diagram. The solution for  $r<A$  has been calculated from Eq.(A2.12)  $A=1$  m;  $L=2$  m and  $L_t=320$  m.

gaps will not be justified, and a Fourier-Bessel method of handling boundary value problems with gaps is being developed at the moment. It is expected that the precise calculation of capacitances will be made possible by this method.

## 6. CONCLUSION

A Fourier-Bessel integral representation is given for the potential field of rotational symmetry in a region exterior to a cylindrical surface on which the potential is specified :

$\phi(A; z < 0) = \phi(A; z > L) = 0$  and  $\phi(A; 0 < z < L) = F(z)$ , a given function.

When the integral is evaluated numerically, the discretization of the amplitude function introduces an error which can be described in terms of potential fields of induced or image charge distributions. It is shown how the error may be reduced by superposing Fourier-Bessel series of different periods. The method is a direct one, involving no iterations or matrix inversions. Programming is simple, requiring only a few tens of statements in the BASIC language. Computer requirements are very modest, allowing implementation on a small desk-top computer. There does not seem to be a limit to the precision attainable, and the proposed method is applicable to the corresponding interior Dirichlet boundary value problem of Ch. (6) as well. Whether the method can be applied profitably to the inverse interior Dirichlet problem of Ch. (8) will only be known after a detailed study has been completed.

A P P E N D I X (3)

SOME PROPERTIES OF BESSEL FUNCTIONS

The information in this appendix is taken from Ch. (9) of Abramowitz et al. (1970) and is provided for quick reference only.

i) Series expansions for integer values of n

$$J_n(z) = (0,5z)^n \sum_{k=0}^{\infty} \frac{(-0,25 z^2)^k}{k! (n+k)!}$$

$$I_n(z) = (0,5z)^n \sum_{k=0}^{\infty} \frac{(0,25 z^2)^k}{k! (n+k)!}$$

$$K_n(z) = 0,5(0,5z)^{-n} \sum_{k=0}^{n-1} \frac{(n-k-1)! (-0,25 z^2)^k}{k!}$$

$$+ (-1)^{n+1} \log_e (0,5z) I_n(z)$$

$$+ (-1)^n 0,5 (0,5z)^n \sum_{k=0}^{\infty} \left\{ \Psi(k+1) + \Psi(n+k+1) \right\} \cdot \frac{(0,25 z^2)^k}{k! (n+k)!}$$

in which  $\Psi$  is the  $\Psi$ -function

$$\Psi(1) = -\gamma \text{ and } \Psi(n \geq 2) = -\gamma + \sum_{k=1}^{n-1} k^{-1}$$

in which  $\gamma$  is Euler's constant

ii) Derivatives

$$(\partial/\partial z) J_0(z) = -J_1(z)$$

$$(\partial/\partial z) I_0(z) = I_1(z)$$

$$(\partial/\partial z) K_0(z) = -K_1(z)$$



## A P P E N D I X 4

### SOME ELECTRON OPTICAL PROPERTIES OF THE "ZERO SPHERICAL ABERRATION ONE-FOIL LENS".

#### 1. INTRODUCTION

In this appendix some electron optical properties are given of a one-foil lens similar to the one discussed in Section (3.2.7) of Ch. (8). This lens has a charge distribution on the foil which is such that the lens can be expected to show negligible spherical aberration to particles entering the lens parallel to the axis at sufficient speed.

The lens was represented by the Fourier-Bessel series of Eq. (8.15) by means of which ray tracings were carried out by computer. The number of terms,  $N$ , was taken large enough that the potential gradients for  $z > L/2$  could be neglected, and different values of  $P$  were chosen in order to investigate the effect of smoothing on the Gaussian focal distance,  $z_d$ , and the spherical aberration. Ray tracings were carried out for weak and strong lenses, and the results are presented in Table (A4.1). The spherical aberration coefficients given, are  $c = \Delta J / r^2$  and  $C_s = c f^2 = c z_d^2$ , in which  $\Delta J$  is the longitudinal spherical aberration experienced by a ray entering the lens at  $(r; 0)$

#### 2. DISCUSSION OF THE RESULTS.

a. For a chosen value of  $N$ , a larger amount of smoothing (i.e.

a higher value of  $P$ ) tends to cause a slight increase in  $z_d$ , as shown by entries (1) to (6) and (7) to (8).

For fast particles — entries (9) and (10) — the change in  $z_d$  produced by increased smoothing is much smaller, probably because of  $O_r$ - and  $O_z$ - effects of Section (2) of Ch. (7) are much smaller than the  $F$ -effect in these cases.

b. Larger  $P$ -values reduce the aberration  $c$  and  $C_s$  up to a point — entries (1) to (5) — but a further increase in  $P$  causes an increase in  $c$  and  $C_s$ .

c. Comparing entries (2) and (3) with entries (7) and (8), resp., shows that their electron optical properties are virtually identical, in spite of differences in  $N$  and  $P$ .

d. Entries (11) — (13) are included in the table to allow an estimate to be made of the precision of the results, by comparing these entries with numbers (9) and (7).

e. Entries (9) and (10) show that their  $c$ -values are not much larger for weak lenses than for strong lenses. Considering the circle of confusion  $\Delta r \doteq r^3 c / z_d$  in the Gaussian focal plane, it is seen that a parallel beam of radius  $r$  is focused to a value  $r \propto 1/z_d$ . This is in marked contrast to, e.g. 3-aperture open lenses for which, in their weak forms,  $C_s \propto f^3$  and  $c \propto f$  [see e.g., Klemperer (1971), Fig. (6.12)]. For strong open lenses of this type,  $C_s \propto f^b$ , where

$b < 3$ , and  $\Delta r \propto f^d$ , where  $d < 0$ ; consequently low  $\Delta r$  values are obtained by increasing the strength of the open lens.

f. The  $C_5/z_d$  values for the stronger one-foil lenses of Table (A4.1) appear to be slightly superior to open lenses of the same strength, and the weak one-foil lenses of the table have  $C_5/z_d$  values which may be 2 orders of magnitude lower than open lenses of the same strength.

g. It has been shown that for the one-foil lens under discussion,  $\Delta J$  is almost constant for a large range of focal lengths. An explanation may be arrived at by considering a zonal curve of Fig. (8.7) to be a superposition of a piece-wise linear graph and a perturbation. The piece-wise linear potential field produces a deflection of a particle which results in zero spherical aberration [see Section (2.2) of Ch. (7) and Section (3.2.7) of Ch. (9)], but the perturbation corresponds to an open Einzel type lens. Use of relationships shown in Figs. (2.2) and (2.3) allows the invariance of  $\Delta J$  to be explained in mathematical terms; this will be published elsewhere.

Table (A4.1) : Some focal properties of a one-foil lens defined by the following points on the  $[z=\phi(0,z)]$  diagram : (0 m; 0 V), (1 m; 1 V) and (3 m; 1V). N and P are parameters appearing in Eq. (8.15) and L=6 m.  $v_p$  is proportional the speed of the particle when entering the lens, and the number of steps in the ray tracing between  $z=0$  and  $z=L/2$  is proportional to  $N_2$

No.	N	P	$v_p$	$N_2$	$z_g$	c	$C_s$
1	40	1	2	8	5,1578	3,511	93,40
2	40	2	2	8	5,2082	2,727	73,97
3	40	4	2	16	5,28083	2,0210	56,36
4	40	8	2	32	5,390266	1,44082	41,86
5	40	16	2	32	5,553414	1,13786	35,09
6	40	32	2	32	5,902153	1,18465	41,26
7	80	8	2	16	5,2026	2,8724	77,75
8	80	16	2	16	5,2826	2,0280	56,595
9	40	4	20	16	797,2884	2,1491	$1,3661 \times 10^6$
10	40	8	20	16	797,40669	1,55754	$0,9037 \times 10^6$
11	40	4	20	32	797,28790	2,13951	$1,3600 \times 10^6$
12	80	8	2	32	5,2011	2,89478	78,30
13	80	8	2	64	5,20073	-	-

## A P P E N D I X 5

### NOTATION

$a_r, a_z$  : radial and transverse acceleration.

A: expansion radius.

C: S.I. unit

$C_C$ : chromatic aberration coefficient; Section (2.2) of Ch. (2).

$C_S$ : spherical aberration coefficient; Section (2.4) of Ch. (2).

$C(n)$ : Fourier-Bessel basis fields Section (2.1) of Ch. (2).

$A_n, B_n, C_n, D_n, E_n$ : Fourier coefficients.

F-effect: Section (2) of Ch. (7).

$F_{ij}, G_{ij}, H_i$ : coefficients used in orthonormalisation of Bessel functions.

$i$ :  $(-1)^{0,5}$

$I_n$ : modified Bessel function of first kind and order  $n$ .

$J_n$ : unmodified Bessel function of first kind and order  $n$ .

$K_n$ : modified Bessel function of second kind and order  $n$ .

L: half-period of Fourier expansions.

$L_a$ :  $L/A$

$L_e$ : lens length; Section (5) of Ch. (6)

m: S.I. unit

N: number of terms included in finite Fourier series.

$O_r$ -and  $O$ -effects; Section (2) of Ch. (7).

P: power to which Lanczos sigma-factor is raised.

$q_m$ : charge to mass ratio of particle.

r: cylindrical polar coordinate.

s: S.I. unit.

S: ratio of Einzel saddle potential to kinetic energy of particle

$S(r)$ : spherical aberration; Eq. (7.4).

$t$ : time variable.

$\underline{v}$ : velocity.

$v_{re}$ : radial speed of particle at exit plane.

$z$ : cylindrical polar coordinate

$z_d$ : focal distance; Section (2.2) of Ch. (2).

$z_f$ : focal length; Fig. (2.1).

$Z_{mn}$ :  $n$ -th zero of  $J_m$

$z_p$ : principal plane position, see Fig. (2.1)

$\Delta J$ : longitudinal spherical aberration.

$\epsilon_0$ : permittivity of free space.

$\epsilon$ : truncation error.

$\pi$ : numerical constant, 3,1415...

$\rho$ : volume charge density.

$\sigma$ : surface charge density.

$\theta_i$ : angle between  $i$ -th ray at exit, and optical axis; Fig. (2.1)

$\phi$ : electric potential.

$\underline{\nabla}$ : nabla operator

## A P P E N D I X 6

### SUMMARY

The feasibility of utilizing Fourier-Bessel functions and Fourier techniques in the analysis and design of electrostatic electron optical systems with rotational symmetry, is investigated. Various approaches are followed, and open systems as well as systems closed off by one or two plane conducting foils, are included in the study. It is assumed that relativistic effects may be disregarded, and that the systems are free of space charge.

In one approach the electron optical properties of various "fundamental" fields are investigated, and syntheses found (superpositions of relatively small numbers of fields) which show reduced spherical aberration. Such syntheses correspond to lenses which are closed off by two plane foils. A steepest descent optimization method is also suggested, which can optimize two-foil lenses i.r.o. zonal as well as paraxial focal properties.

Fourier-Bessel series representations are given for the potential and electric intensity fields of open and one-foil configurations, and it is also shown how the total amount of computing can be reduced by defining auxiliary Fourier-Bessel series which are derived by means of the model of electrostatic images.

Fourier-Bessel series can also be found which represent the surface charge densities on electrodes in the system, and as an application an analysis is given which relates the behaviour of various classes of one-foil lenses to the charge distribution induced on the foil.

A discussion is given of Fourier-Bessel series which approximate a given axial potential function  $\phi(0;z)$ . There are infinitely many approximate solutions to such an inverse interior Dirichlet boundary value problem, and the roles played by various parameters in the solution are investigated. It is shown that certain piece-wise linear axial functions can be expected to render fields  $\phi(r;z)$  that have interesting electron optical properties, and ray tracing results are given for some one-foil lenses of this type.

The solutions to the inverse problem can represent two-foil, one-foil and open systems, and an optimization method is suggested which is applicable to all three these categories of lenses.

A few outstanding features of the Fourier-Bessel approaches discussed are the high precision with which electric potential, intensity and charge distributions can be calculated (resulting in the precise determination of focal properties), the modest computer memory requirements, and the ease of programming.



A P P E N D I X (7)

REFERENCES

- ABRAMOWITZ, M. and STEGUN, I.A. (1970). Handbook of Mathematical Functions (Dover, New York)
- APPELT, W. (1973a). ZAMM 53, T 177
- APPELT, W. (1973b). Berichte der Gesellschaft für Mathematik und Datenverarbeitung (Bonn) no. 68, 1
- ADAMS, A. and READ, F.H. (1972a). J. Phys. E 5, 150
- ADAMS, A. and READ, F.H. (1972b). J. Phys. E 5, 156
- ANICIN, B., TERZIĆ, I., VUKANIĆ, J. and BABOVIĆ, V. (1976). J. Phys. E 9, 837
- BERNARD, M. (1951a). Compt. Rend. Acad. Sci. (Paris) 233, 298
- BERNARD, M. (1951b). Compt. Rend. Acad. Sci. (Paris) 233, 1354
- BERNARD, M. (1952). Compt. Rend. Acad. Sci. (Paris) 235, 1115
- BERNARD, M.Y. (1953a). J. Physique Rad. 14, 381
- BERNARD, M.Y. (1953b). J. Physique Rad. 14, 451
- BERNARD, M.Y. (1967). Particles and Fields : Fundamental Equations, in Septier, A. (Ed.), Focussing of Charged Particles, Vol. 1 (Academic Press, New York).
- BERTRAM, S. (1940). Proc. I.R.E. 28, 418
- BERTRAM, S. (1942). J. Appl. Phys. 13, 496
- BERZ, F. (1950). Phil. Mag. 41, 209
- BINNS, K.J. and LAWRENSEN, P.J. (1973). Analysis and computation of electric and magnetic field problems (Pergamon, New York)
- BIRTLES, A.B., MAYO, B.J. and BENNET, A.W. (1973). Proc. I.E.E. 120, 213
- BOBYKIN, B.V., ZHDANOV, V.S., ZERNOV, A.A., LYUBOV, S.K., MALKA, V.I. and NEVINNYI, Yu.A. (1976). Sov. Phys. Tech. Phys. 21, 766

- BRÜCHE, E. and SCHERZER, O. (1934). Geometrische Elektronenoptik (Springer, Berlin).
- CARLSLAW, H.S. (1930). Introduction to the Theory of Fourier's Series and Integrals (Dover, New York)
- CARRÉ, B.A. and WREATHALL, W.M. (1964). *Radio and Electron. Eng.* 27, 446
- CHORLTON, F. (1968). Boundary Value Problems in Physics and Engineering (Dover, New York)
- ĆIRIĆ, D., TERZIC, I. and VUKANIC, J. (1976). *J. Phys. E: Sci. Instrum.* 9, 839
- CLEAVER, J.R.A., (1975). *Int. J. Electronics* 38, 513
- COOK, R.D. and HEDDLE, D.W.O. (1976). *J. Phys. E: Sci. Instrum.* 9, 279
- COSSLETT, V.E. (1946). Introduction to Electron Optics (University Press, Oxford)
- CREWE, A.V. (1977). *Ultramicroscopy* 2, 281
- CROITORU, P. (1965/66). *Optik* 23, 610
- CRUISE, D.R. (1963). *J. Appl. Phys.* 34, 3477
- DER-SHVARTS, G.V. and MAKAROVA, I.S. (1966). *Radio Engineering and Electronic Physics (U.S.A.)* 11, 1581
- DICHIO, D., NATALI, S.V., KUYATT, C.E. and GALEJS, A. (1974). *Rev. Sci. Instrum.* 45, 566
- DICHIO, D., NATALI, S.V., and KUYATT, C.E. (1975). *Rev. Sci. Instrum.* 46, 71
- DIRMIKIS, D. and BIRTLES, A.B. (1975). *Int. J. Electronics* 39, 441
- DOMMASCHK, W. (1965/66). *Optik* 23, 472
- DU TOIT, A.G. (1976). *Adv. Electronics Electron Phys.* 40A, 485

- EINARSSON, B. (1968). BIT 8, 279
- EINARSSON, B. (1971). Information Processing 71, Proceedings of IFIP Congress 1971 in Ljubljana (North Holland, Amsterdam)
- EINARSSON, B. (1972). Comm. A.C.M. 15, 47
- EINARSSON, B. (1976). J. Comput. Phys. 21, 365
- EL-KAREH, A.B. and EL-KAREH, J.C.J. (1970a). Electron Beams, Lenses and Optics, Vol. I (Academic Press, New York)
- EL-KAREH, A.B., and EL-KAREH, J.C.J. (1970b). Electron Beams, Lenses and Optics, Vol. II (Academic Press, New York)
- EL-KAREH, A.B. and STURANS, M.A. (1971). J. Appl. Phys. 42, 1870.
- EL-KAREH, A.B. and STURANS, M.A. (1972). IEEE Trans. El. Devices ED-19, 1075
- EVANS, D.J. (1977). J. Inst. Maths. Applics. 19, 399
- FIRESTEIN, F. and VINE, J. (1963). Brit. J. Appl. Phys. 14, 449
- FONG, C.Y. and KITTEL, C. (1967). Amer. J. Phys. 35, 1091
- FRANCKEN, J.C. (1967). Analogical Methods for Resolving Laplace's and Poisson's Equations, in Septier, A. (Ed.), Focussing of Charged Particles, Vol. I (Academic Press, New York)
- GABOR, D. (1942). Nature 150, 650
- GALEJS, A. and ROSE, P.H. (1967). Optics of Electrostatic Accelerator Tubes, in Septier, A., Focussing of Charged Particles, Vol. II (Academic Press, New York).
- GEER, J.F. (1976). J. Appl. Phys. 47, 5313
- GIANOLA, U.F. (1950). Proc. Phys. Soc. 63, 1037
- GLASER, W. (1933). Z. f. Phys. 81, 647
- GLASER, W. (1956). Elektronen- und Ionenoptik. In Flügge, S. (Ed.), Encyclopedia of Physics (Springer, Berlin).

- GLIKMAN, L.G., KEL'MAN, V.M. and NURMANOV, M. Sh. (1974a). Sov. Phys. Tech. Phys. 18, 1441
- GLIKMAN, L.G., KEL'MAN, V.M. and NURMANOV, M.Sh. (1974b). Sov. Phys. Tech. Phys. 19, 680
- GLIKMAN, L.G. and NURMANOV, M.Sh. (1976 ). Sov. Phys. Tech. Phys. 21, 911
- GRADSTEYN, I.S. and RYZHIK, I.M. (1965). Tables of Integrals, Series and Products (Academic Press, New York)
- GRAY, F. (1939). The Bell System Technical Journal 18, 1
- GRIVET, I. (1965). Electron Optics (Pergamon, New York)
- GRIVET, P. and BERNARD, M. (1952). Annales de Radioelectricite 7, 3
- GREENSPAN, D. (1966). Can. J. Phys. 44, 2605
- HANSZEN, K.J. (1958). Z. f. Naturforschung 13a, 409
- HANSZEN, K.J. and LAUER, R. (1967). Electrostatic Lenses. In Septier, A., Focussing of Charged Particles, Vol. I (Academic Press, New York)
- HARMAN, W.W. (1953). Fundamentals of Electronic Motion (McGraw-Hill, New York).
- HARRINGTON, R.F. (1968). Field Computation by Moment Methods. (Macmillan, New York)
- HARTING, E. and READ, F.H. (1976). Electrostatic Lenses (Elsevier, Amsterdam)
- HAWKES, P.W. (1967). Lens Aberrations, in Septier, A. (Ed.), Focussing of Charged Particles, Vol. I (Academic Press, New York)
- HAWKES, P.W. (1973). Optik 38, 589
- HEDDLE, D.W.O. (1969). J. Phys. E: Sci. Instrum. 2 1046
- HEDDLE, D.W.O. (1971). J. Phys. E: Sci. Instrum. 4, 981

- HEDDLE, D.W.O. and KUREPA, M.V. (1970). J. Phys. E: Sci. Instrum. 3, 552
- HEERENS, W.C. (1976). J. Appl. Phys. 47, 3740
- HEERENS, W.C. and VERMEULEN, F.C. (1975). J. Appl. Phys. 46, 2486
- HEINEMANN, K. and LENZ, F. (1968). Optik 27, 454
- HEISE, F. and RANG, O. (1949). Optik 5, 201
- HENKELMAN, R.M. and OTTENSMEYER, F.P. (1974). J. Phys. E: Sci. Instrum. 7, 176
- HEYNICK, L.N., WESTERBERG, E.R., HARTELIUS, C.C. and LEE, R.E. (1975) I.E.E.E. Trans. Electron Devices ED-22, 400
- HIBINO, M. and MARUSE, S. (1976). J. Electron Microscopy 25, 229
- HIBINO, M., SUGIYAMA, S., HANAI, T., and MARUSE, S. (1977). Proc. Fifth Int. Conf. on High Voltage Electron Microscopy (Kyoto), 49
- HUBERT, P. (1949). Compt. Rend. Acad. Sci. Paris 228, 233
- ICHIHASHI, M. and MARUSE, S. (1971). J. Electron Microscopy 20, 167
- ICHIHASHI, M. and MARUSE, S. (1973). J. Electron Microscopy 22, 321
- IMHOF, R.E. and READ, F.H. (1968). J. Phys. E: Sci. Instrum. 1, 859
- HOCH, H., KASPER, E. and KERN, D. (1976). Optik 46, 463
- JOHNSON, C.H. (1975). Nucl. Instr. Meth. 127, 163
- KANAYA, K. and BABA, N. (1978). J. Phys. E: Sci. Instrum. 11, 265
- KANAYA, K., KAWAKATSU, H., YAMAZAKI, H. and SIBATA, S. (1966). J. Sci. Instrum. 43, 416
- KANAYA, K., KAWAKATSU, H. and MIYA, T. (1972). J. Electron Microscopy 21, 261
- KELLOGG, O.D. (1953). Foundations of Potential Theory (Dover, New York)
- KLEMPERER, O. and BARNETT, M.E. (1971). Electron Optics, (University Press, Cambridge)

- KOMPFNER, R. (1941). *Phil. Mag.* 32, 410
- KURODA, K., EBISUI, H. and SUZUKI, T. (1974). *J. Appl. Phys.* 45, 2336
- KUYATT, C.E., DICHIO, D. and NATALI, S.V. (1974). *Rev. Sci. Instrum.* 45, 1275
- LANCZOS, C. (1957). *Applied Analysis* (Pitman, London)
- LEBEDEV, N.N. and SKAL'SKAYA, I.P. (1960). *Zhurnal Tekhnicheskoi Fisiki* 30, 472
- LENZ, F. (1973). *Computer-aided Design of Electron-optical Systems*, in Hawkes, P.W. (Ed.), *Image Processing and Computer-aided Design in Electron-optics* (Academic Press, London).
- LENZ, F. and WILSKA, A.P. (1966/67). *Optik* 24, 383
- LEWIS, H.R. (1966). *J. Appl. Phys.* 37, 2541
- LIEBL, H. (1972). *Vacuum* 22, 619
- LIEBMAN, G. (1949). *Proc. Phys. Soc.* 62, 213
- LIPPERT, W. and Pohlit, W. (1952). *Optik* 9, 456
- LIPPERT, W. and POHLIT, W. (1953). *Optik* 10, 447
- MALOFF, I.G. and EPSTEIN, D.W. (1938). *Electron Optics in Television* (McGraw-Hill, New York)
- MARUSE, S., HIRATAKE, S. and ICHIHASHI, M. (1970a). *Japan. J. Appl. Phys.* 9, 1549
- MARUSE, S., ICHIHASHI, M. and HIRATAKE, S. (1970b). *Septieme Congres International de Microscopie Electronique, Grenoble, 1.*
- MAUTZ, J.R. and HARRINGTON, R.F. (1970). *Proc. I.E.E.* 117, 850
- MAYO, B.J. and BENNETT, A.W. (1972). *Adv. Electronics and Electron Optics* 33A, 571
- MCDONALD, B.H. and WEXLER, A. (1972). *I.E.E.E. Trans. Microwave Theory Tech.* MTT-20, 841

- MEL/NIKOV, S.L. (1971). Sov. Phys. Tech. Phys. 16, 127
- MILLER, G.F. (1974). Fredholm equations of the first kind, in Delves, L.M. and Walsh, J. (Eds.) Numerical solution of integral equations (Clarendon, Oxford).
- MÖLLENSTEDT, G. and SCHWARZER, R. (1973). Beitr. elektronenmikroskop. Direktabb. Oberfl. 6, 495
- MOSES, R.W. (1973). Lens optimization by direct application of the calculus of variations, in Hawkes, P.W. (Ed.), Image processing and computer-aided design in electron optics (Academic Press, London)
- MOTZ, H. and KLANFER, L. (1946). Proc. Phys. Soc. 58, 30
- MULVEY, T. and WALLINGTON, M.J. (1973). Rep. Prog. Phys. 36, 347
- MUNRO, E. (1973). Computer-aided design of electron lenses by the finite element method, in Hawkes, P.W. (Ed.), Image processing and computer-aided design in electron optics (Academic Press, London).
- MUNRO, E. (1975). J. Vac. Sci. Technol. 12, 1146
- MUNRO, E. and WITTELS, N.D. (1977). Optik 47, 25
- MYERS, L.M. (1939). Electron Optics (Chapman and Hall)
- NATALI, S., DI CHIO, D. and KUYATT, C.E. (1972a). J. Research, National Bureau of Standards - A Physics and Chemistry 76A, 27
- NATALI, S., DI CHIO, D., UVA, E. and KUYATT, C.E. (1972b). Rev. Sci. Instrum. 43, 80
- NEDOMA, J. (1975a). Studia Geoph. et Geod. 19, 85
- NEDOMA, J. (1975b). Studia Geoph. et Geod. 19, 226
- OLSEN, B., PETTERSON, G. and SCHNEIDER, W. (1966). Nucl. Instr. Meth. 41, 325
- ORLOV, B.I. (1967/68). Optical Design, 554
- PLASS, G.N. (1942). J. Appl. Phys. 13, 49

- PUMPLIN, J. (1969). Amer. J. Phys. 37, 737
- RAMBERG, E.G. (1942). J. Appl. Phys. 13, 582
- RANG, O. (1948). Optik 4, 251
- READ, F.H. (1969a). J. Phys. E 2, 165
- READ, F.H. (1969b). J. Phys. E 2, 679
- READ, F.H. (1970). J. Phys. E 3, 127
- READ, F.H. (1971). J. Phys. E 4, 562
- READ, F.H., ADAMS, A. and SOTO-MONTIEL, J.R. (1970). J. Phys. E 4,  
625
- REGENSTREIF, E. (1951). Annales de Radioelectricité 6, 51
- RIDDLE, G.H.N. (1978). J. Vac. Sci. Technol. 15, 857
- SAITO, T., KUBOTA, S. and MIYAOKA, S. (1973). J. Appl. Phys. 44, 4505
- SAITO, T. and SOVERS, O. (1977). J. Appl. Phys. 48, 2306
- SCANIO, J.J.G. (1973). Amer. J. Phys. 41, 415
- SCHERZER, O. (1933). Z. f. Phys. 80, 193
- SCHERZER, O. (1936a). Z. f. Phys. 101, 23
- SCHERZER, O. (1936b). Z.f. Phys. 101, 593
- SCHERZER, O. (1947). Optik 2, 115
- SCHERZER, O. (1949). J. Appl. Phys. 20, 20
- SCHWARZER, R. (1975). Optik 44, 61
- SCHWARZER, R. (1976). Optik 44, 121
- SEPTIER, A. and RUYTOOR, M. (1959). Comptes Rendus 249, 2746
- SEPTIER, A. (1966). Adv. Optical and Electron Microscopy 1, 204
- SHIMIZU, K and KAWAKATSU, H. (1974). J. Phys. E: Sci. Instrum. 7, 472
- SILVERSTER, P.P., LOWTHER, D.A., CARPENTER, C.J. and WYATT, E.A. (1977).  
Proc. I.E.E. 124, 1267



- SINGER, B. and BRAUN, M. (1970). I.E.E.E. Trans. Electron Devices, ED-17, 926
- SKÖLLERMO, A. (1976a). Nucl. Instr. and Meth. 137, 339
- SKÖLLERMO, A. (1976b). Nucl. Instr. and Meth. 137, 363
- SPANGENBERG, K. and FIELD, L.M. (1943). Elec. Comm. 21, 194
- SZILÁGYI, M. (1977). Optik 48, 215
- SZILÁGYI, M. (1978). Optik 50, 35
- TONOMURA, A. (1973). Japan. J. Appl. Phys. 12, 1065
- TYPKE, D. (1966/67). Optik 24, 1
- TYPKE, D. (1968). Optik 28, 488
- TYPKE, D. (1972a). Optik 34, 573
- TYPKE, D. (1972b). Optik 36, 124
- VARAKIN, G.K. (1974). Pribory i Tekhnika Eksperimenta 1, 211
- VENEKLASSEN, L.H. and SIEGEL, B.M. (1972). J. Appl. Phys. 43, 4989
- VERSTER, J.L. (1963). Philips Res. Rep. 18, 465
- VILJOEN, E. (1976). The Numerical Solution of a Fredholm Integral Equation of the First Kind arising in Electron Optics, CSIR Special Report, WISK 236.
- VITKOVICH, D. (Ed.) (1966). Field Analysis (Van Nostrand, London)
- WEBER, C. (1967). Numerical Solution of Laplace's and Poisson's Equations and the Calculation of Electron Trajectories and Electron Beams, in Septier, A. (Ed.), Focussing of Charged Particles, Vol. I (Academic Press, New York).
- WEBER, E. (1950). The Electromagnetic Field (John Wiley, New York)
- WENDT, G. (1951). Z. f. angew. Phys. 3, 219
- WERNER, D. (1971). Optik 32, 320

WILHELMSON, R.B. and ERICKSEN, J.H. (1977). J. Comput. Phys. 25,  
319

WITTELS, N.D. (1975). J. Vac. Sci. Technol. 12, 1165

WITTELS, N.D. and JACOBSEN, E.H. (1976). J. Appl. Phys. 47, 2716

WOOD, W.L. (1976). Int. J. Num. Meth. Eng. 10, 885

YAMAMOTO, T. (1974). Optik 41, 256

YAMAZAKI, H. (1973). Optik 38, 9

YAMAZAKI, H. (1977). Optik 48, 357

YEH, H.C. (1975). J. Appl. Phys. 46, 4431

YEH, H.C. (1976). J. Appl. Phys. 47, 2923

YEH, H.C. (1977). J. Appl. Phys. 48, 4423

YEH, H.C. and YANG, W.J. (1969). J. Appl. Phys. 40, 3687

YOUNG, C.E. (1975). Rev. Sci. Instrum. 46, 296

ZASHKVARA, V.V., IL'IN, A.M. and KRYUCHKOV, V.F. (1977). Sov. Phys.  
Tech. Phys. 22, 909

THE ANALYSIS AND OPTIMIZATION OF ELECTROSTATIC ELECTRON OPTICAL  
LENSES WITH ROTATIONAL SYMMETRY, THROUGH THE USE OF ORTHOGONAL  
FUNCTIONS.

by

JOHANNES PETRUS VAN DER MERWE

Submitted in partial fulfilment of the requirements for the degree of  
Doctor of Philosophy, in the department of Physics, University of Natal.

Durban.

1978